Exhibit GMP-RH-2

Evidence linking Arctic amplification to extreme weather in mid-latitudes

Jennifer A. Francis[1] and Stephen J. Vavrus[2]

Received 17 January 2012; revised 20 February 2012; accepted 21 February 2012; published 17 March 2012.

[1] Arctic amplification (AA) – the observed enhanced warming in high northern latitudes relative to the northern hemisphere – is evident in lower-tropospheric temperatures and in 1000-to-500 hPa thicknesses. Daily fields of 500 hPa heights from the National Centers for Environmental Prediction Reanalysis are analyzed over N. America and the N. Atlantic to assess changes in north-south (Rossby) wave characteristics associated with AA and the relaxation of poleward thickness gradients. Two effects are identified that each contribute to a slower eastward progression of Rossby waves in the upper-level flow: 1) weakened zonal winds, and 2) increased wave amplitude. These effects are particularly evident in autumn and winter consistent with sea-ice loss, but are also apparent in summer, possibly related to earlier snow melt on high-latitude land. Slower progression of upper-level waves would cause associated weather patterns in mid-latitudes to be more persistent, which may lead to an increased probability of extreme weather events that result from prolonged conditions, such as drought, flooding, cold spells, and heat waves. **Citation:** Francis, J. A., and S. J. Vavrus (2012), Evidence linking Arctic amplification to extreme weather in mid-latitudes, *Geophys. Res. Lett.*, *39*, L06801, doi:10.1029/2012GL051000.

1. Introduction

[2] During the past few decades the Arctic has warmed approximately twice as rapidly as has the entire northern hemisphere [*Screen and Simmonds*, 2010; *Serreze et al.*, 2009], a phenomenon called Arctic Amplification (AA). The widespread warming resulted from a combination of increased greenhouse gases and positive feedbacks involving sea ice, snow, water vapor, and clouds [*Stroeve et al.*, 2012]. The area of summer sea ice lost since the 1980s would cover over 40% of the contiguous United States. As autumn freeze-up begins, the extra solar energy absorbed during summer in these vast new expanses of open water is released to the atmosphere as heat, thus raising the question of not *whether* the large-scale atmospheric circulation will be affected, but *how*? While global climate models project that the frequency and intensity of many types of extreme weather will increase as greenhouse gases continue to accumulate in the atmosphere [*Meehl et al.*, 2007], this analysis presents evidence suggesting that enhanced Arctic warming is one of the causes.

[1]Institute of Marine and Coastal Sciences, Rutgers University, New Brunswick, New Jersey, USA.
[2]Center for Climatic Research, University of Wisconsin-Madison, Madison, Wisconsin, USA.

This paper is not subject to U.S. copyright.
Published in 2012 by the American Geophysical Union.

[3] Exploration of the atmospheric response to Arctic change has been an active area of research during the past decade. Both observational and modeling studies have identified a variety of large-scale changes in the atmospheric circulation associated with sea-ice loss and earlier snow melt, which in turn affect precipitation, seasonal temperatures, storm tracks, and surface winds in mid-latitudes [e.g., *Budikova*, 2009; *Honda et al.*, 2009; *Francis et al.*, 2009; *Overland and Wang*, 2010; *Petoukhov and Semenov*, 2010; *Deser et al.*, 2010; *Alexander et al.*, 2010; *Jaiser et al.*, 2012; *Blüthgen et al.*, 2012]. While it is understood that greenhouse-gas-induced tropospheric warming will cause an increase in atmospheric water content that is expected to fuel stronger storms and flooding [*Meehl et al.*, 2007], individual extreme weather events typically have a dynamical origin. Many of these events result from persistent weather patterns, which are typically associated with blocking and high-amplitude waves in the upper-level flow. Examples include the 2010 European and Russian heat waves, the 1993 Mississippi River floods, and freezing conditions in Florida during winter 2010–11. This study focuses on evidence linking AA with an increased tendency for a slower progression of Rossby waves in 500-hPa height fields that favor the types of extreme weather caused by persistent weather conditions, such as drought, flooding, heat waves, and cold spells in the northern hemisphere mid-latitudes.

2. Analysis and Results

[4] How does Arctic Amplification promote higher amplitude and slower moving waves? To address this question, output from the National Center for Environmental Prediction (NCEP)/National Center for Atmospheric Research (NCAR) Reanalysis (NRA) data set [*Kalnay et al.*, 1996] is used to assess changes in the atmosphere related to enhanced Arctic warming, and to investigate the effects of high-latitude change on mid-latitude patterns in 500 hPa heights. While direct comparisons of reanalysis to observations is problematic owing to a lack of independent measurements, *Archer and Caldeira* [2008] found that the upper-level circulation in the NRA is very similar to that of the European Centre for Medium-Range Weather Forecasts (ECMWF) Reanalysis (ERA-40), and *Bromwich et al.* [2007] found excellent agreement between surface pressure fields from these reanalyses in the Arctic after 1979, when assimilation of satellite data began. To reduce the possibility of spurious variability owing to differing data sources assimilated by the reanalysis, only fields from the post-satellite era are used.

[5] Following summers during recent decades with diminished Arctic sea ice, large fluxes of heat and moisture enter the lower atmosphere during fall and winter, which together with enhanced poleward fluxes of latent heat [*Alexeev*

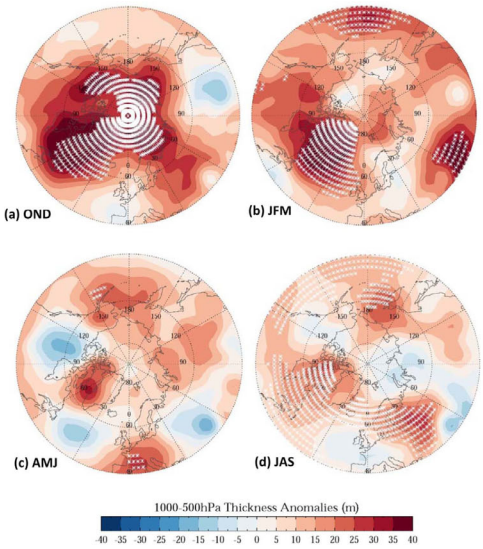

Figure 1. Seasonal anomalies in 1000-500 hPa thicknesses (m) north of 40°N during 2000–2010 relative to 1970–1999: (a) autumn (OND), (b) winter (JFM), (c) spring (AMJ), and (d) summer (JAS). White asterisks indicate significance with $p < 0.05$. Data are from the NCEP/NCAR Reanalysis.

et al., 2005], contribute to AA. This warming is clearly observable during autumn in near-surface air temperature anomalies in proximity to the areas of ice loss [*Serreze et al.*, 2009]. The integrated lower-tropospheric warming is apparent in widespread anomalies in the vertical thickness of the layer between 1000 and 500 hPa, illustrated in Figure 1 for each season during 2000 to 2010 relative to the previous 30 years. During fall (Oct.–Dec.) statistically significant anomalies are apparent over much of the Arctic region, and during winter (Jan.–Mar.) a strong anomaly persists in the N. Atlantic and west of Greenland, along with positive areas at lower latitudes over Russia and the N. Pacific. Strong positive values during summer (Jun.–Sep.) occur mainly over high-latitude land areas, consistent with warmer, drier soils resulting from earlier snow melt [*Brown et al.*, 2010]. Significant anomalies are absent in spring during recent years because heating that results from a reduced summer ice cover has dissipated and because high-latitude soils have not yet dried following snow melt.

[6] The differential warming of the Arctic relative to mid-latitudes is the key linking AA with patterns favoring persistent weather conditions in mid-latitudes. Two separate effects on upper-level characteristics are anticipated: weaker poleward thickness gradients cause slower zonal winds, and enhanced high-latitude warming causes 500 hPa heights to rise more than in mid-latitudes, which elongates the peaks of ridges northward and increases wave amplitude. Both of these effects should slow eastward wave progression. Wave features in 500 hPa fields are analyzed from 1979 through 2010. The study focuses on the mid-latitudes of N. America and the N. Atlantic (140°W to 0°, Figure 2a), north of which the ice-loss has been substantial and atmospheric heating has been statistically significant (Figure 1). Fields of 500 hPa heights are selected for this analysis because they are constrained by observations from numerous radiosondes and satellite retrievals, they are relatively free from surface effects, and they capture upper-level wave patterns.

[7] Evidence supporting the first effect – zonal wind reduction – was identified in a previous study by *Francis et al.* [2009], who found that poleward thickness gradients were weaker over the N. Atlantic and N. Pacific in summers with less sea ice than normal, and that the weakening persisted well into the following spring. This tendency is also clearly evident over the present study region, as shown in the time series of 1000-500 hPa thickness differences between a high-latitude region (80–60°N) and low-latitude region (50–30°N) for each season (Figure 3, left). Since the late 1980s when rapid ice loss and enhanced warming began, poleward thickness differences have decreased in all seasons, especially during fall and winter (~10% with > 95% confidence in fall trend).

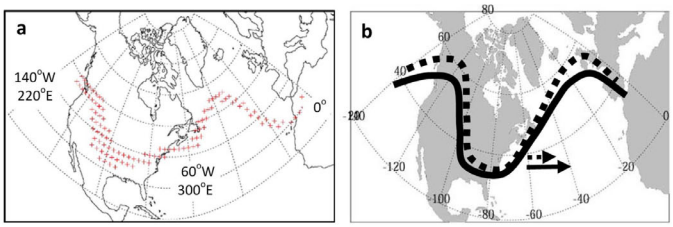

Figure 2. Region of study: 140°W to 0°. (a) Asterisks illustrate an example of a selected range of 500 hPa heights used in the analysis. (b) Schematic of ridge elongation (dashed vs. solid) in upper-level heights caused by enhanced warming in Arctic relative to mid-latitudes. Higher amplitude waves progress eastward more slowly, as indicated by arrows.

[8] The strength of the poleward thickness gradient determines the speed of upper-level zonal winds. As the gradient has decreased with a warming Arctic, the upper-level zonal winds during fall have also weakened since 1979 (Figure 3, right), with a total reduction of about 14% (>95% confidence). Winter winds are more variable but exhibit a steady decline since the early 1990s. When zonal wind speed decreases, the large-scale Rossby waves progress more slowly from west to east, and weaker flow is also associated with higher wave amplitudes [*Palmén and Newton*, 1969]. Slower progression of upper-level waves causes more persistent weather conditions that can increase the likelihood of certain types of extreme weather, such as drought, prolonged precipitation, cold spells, and heat waves. Previous studies support this idea: weaker zonal-mean, upper-level wind is associated with increased atmospheric blocking events in the northern hemisphere [*Barriopedro and Garcia-Herrera*, 2006] as well as with cold-air outbreaks in the western U.S. and Europe [*Thompson and Wallace*, 2001; *Vavrus et al.*, 2006].

[9] The second effect – ridge elongation – is also expected in response to larger increases in 500-hPa heights at high latitudes than at mid-latitudes. This effectively stretches the peaks of ridges northward, as illustrated schematically in Figure 2b, and further augments the wave amplitude. Higher amplitude waves also tend to progress more slowly. Evidence of this mechanism is investigated by selecting a narrow range of 500 hPa heights for each season that captures the daily wave pattern in the height field. The following ranges were used for fall: 5600 m ± 50 m, winter: 5400 m ± 50 m, and summer: 5700 m ± 50 m. The example in Figure 2a illustrates an "isoheight" represented by the selected gridpoints over the study region on a typical day, which are then analyzed to reveal changes in 500 hPa patterns over time.

[10] First row of Figures 4a–4c presents time series of the seasonally averaged maximum latitude of daily isoheights (corresponding to peaks of ridges) for fall, winter, and summer. Spring is not shown because high-latitude thickness anomalies are not statistically different from mean conditions. The steady northward progression of ridge peaks supports the hypothesis that AA is contributing to ridge elongation; confidence in these trends exceeds 99%. The fall plot also presents the time series of September sea ice extent (reversed scale, Spearman's correlation = −0.71) derived from passive microwave satellite information (obtained from the National Snow and Ice Data Center, http://nsidc.org/data/docs/noaa/g02135_seaice_index/ [*Fetterer et al.*, 2002]). The winter

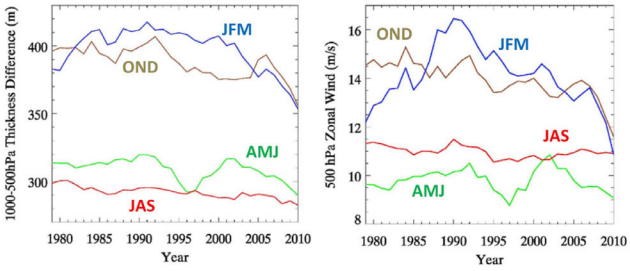

Figure 3. (left) Time series of seasonal 1000–500 hPa thickness differences between 80–60°N and 50–30°N over the study region (140°W to 0°). (right) Seasonal zonal mean winds at 500 hPa between 60–40°N over the study region. Seasons are labeled. Data obtained from the NCEP/NCAR reanalysis, http://www.esrl.noaa.gov/psd.

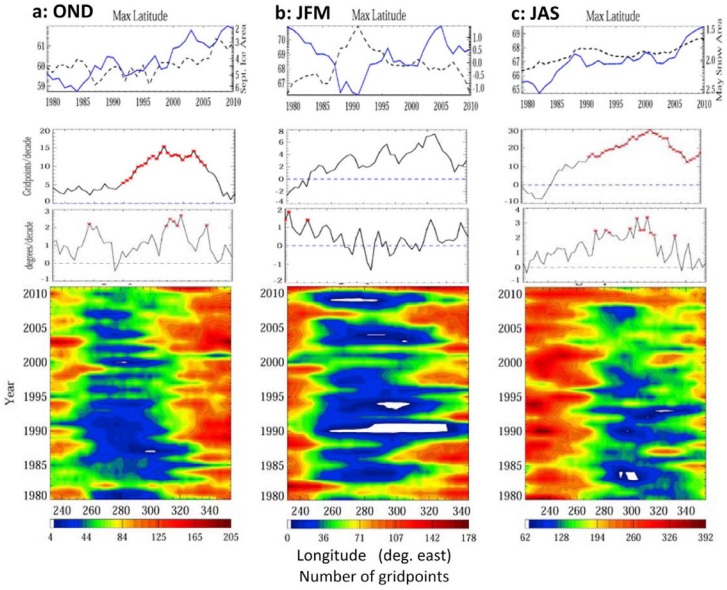

Figure 4. First row shows time series of maximum latitude of ridge peaks during (a) fall, (b) winter, and (c) summer from 1979 to 2010. A running 5-year box-car smoother was applied. The dotted line in fall is the time series of September-mean sea ice area (reversed axis, $\times 10^6$ km^2); in winter the JFM Arctic Oscillation Index, and in summer the northern hemisphere snow cover for May (reversed axis, $\times 10^7$ km^2). Second row is trends in the number of gridpoints that are located north of 50°N (60°N for winter) vs. longitude for each season. Red asterisks indicate significance at a 90% confidence level, the zero line is dashed blue. Third row is the same as the second row, but for wave amplitude (deg./decade). Fourth row (Hovmöller diagrams) presents time/longitude variations in the numbers of gridpoints located north of 50°N (60°N winter) with 500 hPa heights in the ranges of 5600, 5400, and 5700 m (±50 m) for each season, respectively. See text for details.

Arctic Oscillation index [*Thompson and Wallace*, 2001] appears in the winter panel, with a correlation of −0.65. Along with the summer panel is plotted the time series for the northern hemisphere snow cover for May (obtained from the Rutgers University Global Snow Lab, http://climate.rutgers.edu/snowcover [*Ghatak et al.*, 2010]). The two curves are strongly correlated with r = −0.88, suggesting the northward elongation of ridge peaks may be a response to enhanced warming over high-latitude land owing to earlier snow melt and warming soil [*Jaeger and Seneviratne*, 2011].

[11] Could this poleward shift be explained by the observed migration of the entire height field, rather than only the ridge peaks, in response to increasing greenhouse gases, as reported by *Seidel and Randel* [2007]? The analysis presented in the fourth row of Figures 4a–4c sheds light on this question. Hovmöllor diagrams present time/longitude contours that illustrate the preferred locations and time evolution of the number of gridpoints in each selected 500 hPa isopleth that are located north of 50°N (i.e., peaks of ridges) during autumn and summer, and north of 60°N during winter. Related to these Hovmöllors is the second row of Figure 4, which displays trends in the number of these gridpoints, indicating which longitudes have experienced a change in ridging over the past three decades. Finally, the third row of plots presents the corresponding trends in wave amplitude, calculated as the difference between the maximum and minimum latitude of the isopleths along each longitude for each season and year. This difference calculation also helps mitigate any systematic bias in the reanalysis height field. While the significance of the trends in ridge points or wave amplitude at any one longitude often falls short of a 90% confidence level (marked with red asterisks), the probability is near zero ($p < 10^{-5}$) that the population of positive trends in ridging and amplitudes for all longitudes can be random.

[12] The Hovmöllor diagrams exhibit the clear geographic preferences of ridge axes during each season. In fall they tend to align over western N. America and the eastern

N. Atlantic. Trends in ridge gridpoints (second row) are positive across the region, with largest values over the entire N. Atlantic. Corresponding trends in wave amplitude (third row) are also positive at most longitudes, with the largest increases in the central U.S. and central N. Atlantic. These tendencies favor warmer, more persistent conditions along the N. American east coast and in the N. Atlantic, and may have contributed to the dramatic increase in maximum temperature extremes in those areas during fall, as shown in the Climate Extreme Index (available from NOAA's National Climate Data Center, http://www.ncdc.noaa.gov/extremes/cei/ [*Gleason et al.*, 2008]).

[13] During winter the preferred longitudinal positioning of ridges is similar to those in autumn, and ridging trends are again positive at most longitudes. While wave amplitude trends are less uniform, significant increases appear particularly over the Rocky Mountains, which is consistent with more persistent patterns that may have contributed to reduced mountain snowpacks in recent decades [*Mote*, 2006]. The Hovmöllor plot for summer shows that ridging occurs predominantly over central and western N. America, but the largest increases in ridge gridpoints (second row) have occurred over the eastern N. Atlantic. Trends in wave amplitude are positive nearly everywhere, particularly from the east coast of N. America across the N. Atlantic. Increased ridging and higher wave amplitudes over the Atlantic may have contributed to unprecedented surface melt in Greenland during recent years [*Tedesco et al.*, 2011] as well as to recent heat-waves in western Europe [*Jaeger and Seneviratne*, 2011].

3. Conclusions

[14] In summary, the observational analysis presented in this study provides evidence supporting two hypothesized mechanisms by which Arctic amplification – enhanced Arctic warming relative to that in mid-latitudes – may cause more persistent weather patterns in mid-latitudes that can lead to extreme weather. One effect is a reduced poleward gradient in 1000-500 hPa thicknesses, which weakens the zonal upper-level flow. According to Rossby wave theory, a weaker flow slows the eastward wave progression and tends to follow a higher amplitude trajectory, resulting in slower moving circulation systems. More prolonged weather conditions enhance the probability for extreme weather due to drought, flooding, cold spells, and heat waves. The second effect is a northward elongation of ridge peaks in 500 hPa waves, which amplifies the flow trajectory and further exacerbates the increased probability of slow-moving weather patterns. While Arctic amplification during autumn and winter is largely driven by sea-ice loss and the subsequent transfer of additional energy from the ocean into the high-latitude atmosphere, the increasing tendency for high-amplitude patterns in summer is consistent with enhanced warming over high-latitude land caused by earlier snow melt and drying of the soil. Enhanced 500-hPa ridging observed over the eastern N. Atlantic is consistent with more persistent high surface pressure over western Europe. This effect has been implicated as contributing to record heat waves in Europe during recent summers [*Jaeger and Seneviratne*, 2011].

[15] Can the persistent weather conditions associated with recent severe events such as the snowy winters of 2009/2010 and 2010/2011 in the eastern U.S. and Europe, the historic drought and heat-wave in Texas during summer 2011, or record-breaking rains in the northeast U.S. of summer 2011 be attributed to enhanced high-latitude warming? Particular causes are difficult to implicate, but these sorts of occurrences are consistent with the analysis and mechanism presented in this study. As the Arctic sea-ice cover continues to disappear and the snow cover melts ever earlier over vast regions of Eurasia and North America [*Brown et al.*, 2010], it is expected that large-scale circulation patterns throughout the northern hemisphere will become increasingly influenced by Arctic Amplification. Gradual warming of the globe may not be noticed by most, but everyone – either directly or indirectly – will be affected to some degree by changes in the frequency and intensity of extreme weather events as greenhouse gases continue to accumulate in the atmosphere. Further research will elucidate the types, locations, timing, and character of the weather changes, which will provide valuable guidance to decision-makers in vulnerable regions.

[16] **Acknowledgments.** The Editor and the authors thank the two anonymous reviewers for their assistance in evaluating this paper.

References

Alexander, M. A., R. Tomas, C. Deser, and D. M. Lawrence (2010), The atmospheric response to projected terrestrial snow changes in the late 21st century, *J. Clim.*, *23*, 6430–6437, doi:10.1175/2010JCLI3899.1.

Alexeev, V. A., P. L. Langen, and J. R. Bates (2005), Polar amplification of surface warming on an aquaplanet in ghost forcing experiments without sea ice feedbacks, *Clim. Dyn.*, *24*, 655–666, doi:10.1007/s00382-005-0018-3.

Archer, C. L., and K. Caldeira (2008), Historical trends in the jet streams, *Geophys. Res. Lett.*, *35*, L08803, doi:10.1029/2008GL033614.

Barriopedro, D., and R. Garcia-Herrera (2006), A climatology of Northern Hemisphere blocking, *J. Clim.*, *19*, 1042–1063, doi:10.1175/JCLI3678.1.

Blüthgen, J., R. Gerdes, and M. Werner (2012), Atmospheric response to the extreme Arctic sea ice conditions in 2007, *Geophys. Res. Lett.*, *39*, L02707, doi:10.1029/2011GL050486.

Bromwich, D. H., R. L. Fogt, K. I. Hodges, and J. E. Walsh (2007), A tropospheric assessment of the ERA-40, NCEP, and JRA-25 global reanalyses in the polar regions, *J. Geophys. Res.*, *112*, D10111, doi:10.1029/2006JD007859.

Brown, R., C. Derksen, and L. Wang (2010), A multi-dataset analysis of variability and change in Arctic spring snow cover extent, 1967–2008, *J. Geophys. Res.*, *115*, D16111, doi:10.1029/2010JD013975.

Budikova, D. (2009), Role of Arctic sea ice in global atmospheric circulation: A review, *Global Planet. Change*, *68*(3), 149–163, doi:10.1016/j.gloplacha.2009.04.001.

Deser, C., R. Tomas, M. Alexander, and D. Lawrence (2010), The seasonal atmospheric response to projected Arctic sea ice loss in the late 21st century, *J. Clim.*, *23*, 333–351, doi:10.1175/2009JCLI3053.1.

Fetterer, F., K. Knowles, W. Meier, and M. Savoie (2002), Sea ice index, digital media, Natl. Snow and Ice Data Cent., Boulder, Colo.

Francis, J. A., W. Chan, D. Leathers, J. R. Miller, and D. E. Veron (2009), Winter Northern Hemisphere weather patterns remember summer Arctic sea ice extent, *Geophys. Res. Lett.*, *36*, L07503, doi:10.1029/2009GL037274.

Ghatak, D., A. Frei, G. Gong, J. Stroeve, and D. Robinson (2010), On the emergence of an Arctic amplification signal in terrestrial Arctic snow extent, *J. Geophys. Res.*, *115*, D24105, doi:10.1029/2010JD014007.

Gleason, K. L., J. H. Lawrimore, D. H. Levinson, T. R. Karl, and D. J. Karoly (2008), A revised U.S. climate extremes index, *J. Clim.*, *21*, 2124–2137, doi:10.1175/2007JCLI1883.1.

Honda, M., J. Inoue, and S. Yamane (2009), Influence of low Arctic sea-ice minima on anomalously cold Eurasian winters, *Geophys. Res. Lett.*, *36*, L08707, doi:10.1029/2008GL037079.

Jaeger, E. B., and S. I. Seneviratne (2011), Impact of soil moisture-atmosphere coupling on European climate extremes and trends in a regional climate model, *Clim. Dyn.*, *36*, 1919–1939, doi:10.1007/s00382-010-0780-8.

Jaiser, R., K. Dethloff, D. Handorf, A. Rinke, and J. Cohen (2012), Impact of sea ice cover changes on the Northern Hemisphere atmospheric winter circulation, *Tellus, Ser. A*, *64*, 11595, doi:10.3402/tellusa.v64i0.11595.

Kalnay, E., et al. (1996), The NCEP/NCAR 40-year reanalysis project, *Bull. Am. Meteorol. Soc.*, *77*, 437–471, doi:10.1175/1520-0477(1996)077<0437:TNYRP>2.0.CO;2.

Meehl, G. A., et al. (2007), Global climate projections, in *Climate Change 2007: The Physical Science Basis. Contribution of Working Group I to the Fourth Assessment Report of the Intergovernmental Panel on Climate Change*, edited by S. Solomon et al., pp. 747–845, Cambridge Univ. Press, Cambridge, U. K.

Mote, P. W. (2006), Climate-driven variability and trends in mountain snowpack in western North America, *J. Clim.*, *19*, 6209–6220, doi:10.1175/JCLI3971.1.

Overland, J. E., and M. Wang (2010), Large-scale atmospheric circulation changes are associated with the recent loss of Arctic sea ice, *Tellus, Ser. A*, *62*, 1–9, doi:10.1111/j.1600-0870.2009.00421.x.

Palmén, E., and C. W. Newton (1969), *Atmospheric Circulation Systems*, *Int. Geophys. Ser.*, vol. 13, Academic, New York.

Petoukhov, V., and V. A. Semenov (2010), A link between reduced Barents-Kara sea ice and cold winter extremes over northern continents, *J. Geophys. Res.*, *115*, D21111, doi:10.1029/2009JD013568.

Screen, J. A., and I. Simmonds (2010), The central role of diminishing sea ice in recent Arctic temperature amplification, *Nature*, *464*, 1334–1337, doi:10.1038/nature09051.

Seidel, D. J., and W. J. Randel (2007), Recent widening of the tropical belt: Evidence from tropopause observations, *J. Geophys. Res.*, *112*, D20113, doi:10.1029/2007JD008861.

Serreze, M. C., A. P. Barrett, J. C. Stroeve, D. N. Kindig, and M. M. Holland (2009), The emergence of surface-based Arctic amplification, *Cryosphere*, *3*, 11–19, doi:10.5194/tc-3-11-2009.

Stroeve, J. C., M. C. Serreze, M. M. Holland, J. E. Kay, J. Maslanik, and A. P. Barrett (2012), The Arctic's rapidly shrinking sea ice cover: A research synthesis, *Clim. Change*, *110*, 1005–1027, doi:10.1007/s10584-011-0101-1.

Tedesco, M., X. Fettweis, M. R. van den Broeke, R. S. W. van de Wal, C. J. P. P. Smeets, W. J. van de Berg, M. C. Serreze, and J. E. Box (2011), Record summer melt in Greenland in 2010, *Eos Trans. AGU*, *92*(15), 126, doi:10.1029/2011EO150002.

Thompson, D. W., and J. M. Wallace (2001), Regional climate impacts of the Northern Hemisphere annular mode, *Science*, *293*, 85–89, doi:10.1126/science.1058958.

Vavrus, S., J. E. Walsh, W. L. Chapman, and D. Protis (2006), The behavior of extreme cold air outbreaks under greenhouse warming, *Int. J. Climatol.*, *26*, 1133–1147, doi:10.1002/joc.1301.

J. A. Francis, Institute of Marine and Coastal Sciences, Rutgers University, 71 Dudley Rd., New Brunswick, NJ 08901, USA. (francis@imcs.rutgers.edu)
S. J. Vavrus, Center for Climatic Research, University of Wisconsin-Madison, 1225 West Dayton St., Madison, WI 53706, USA.

Environmental Research Letters

LETTER • **OPEN ACCESS**

Evidence for a wavier jet stream in response to rapid Arctic warming

To cite this article: Jennifer A Francis and Stephen J Vavrus 2015 *Environ. Res. Lett.* **10** 014005

View the article online for updates and enhancements.

Related content

- Changes in meandering of the Northern Hemisphere circulation
  Giorgia Di Capua and Dim Coumou
- The Arctic matters: extreme weather responds to diminished Arctic Sea ice
  J A Francis
- Persistent cold air outbreaks over North America in a warming climate
  Yang Gao, L Ruby Leung, Jian Lu et al.

Recent citations

- Recent Trends in the Near-Surface Climatology of the Northern North American Great Plains
  Gabriel T. Bromley *et al*
- Maureen McCue
- TwentyFirstCentury Changes in the Eastern Mediterranean Etesians and Associated Midlatitude Atmospheric Circulation
  Stella Dafka *et al*

This content was downloaded from IP address 96.89.211.73 on 26/12/2019 at 20:40

Environmental Research Letters

LETTER

Evidence for a wavier jet stream in response to rapid Arctic warming

Jennifer A Francis[1] and Stephen J Vavrus[2]

[1] Institute of Marine and Coastal Sciences, Rutgers University, New Brunswick, New Jersey, USA
[2] Center for Climatic Research, University of Wisconsin-Madison, Madison, Wisconsin, USA

E-mail: francis@imcs.rutgers.edu

Keywords: jet stream, Arctic amplification, extreme weather

OPEN ACCESS

RECEIVED
4 November 2014

ACCEPTED FOR PUBLICATION
11 December 2014

PUBLISHED
6 January 2015

Content from this work may be used under the terms of the Creative Commons Attribution 3.0 licence.

Any further distribution of this work must maintain attribution to the author (s) and the title of the work, journal citation and DOI.

Abstract

New metrics and evidence are presented that support a linkage between rapid Arctic warming, relative to Northern hemisphere mid-latitudes, and more frequent high-amplitude (wavy) jet-stream configurations that favor persistent weather patterns. We find robust relationships among seasonal and regional patterns of weaker poleward thickness gradients, weaker zonal upper-level winds, and a more meridional flow direction. These results suggest that as the Arctic continues to warm faster than elsewhere in response to rising greenhouse-gas concentrations, the frequency of extreme weather events caused by persistent jet-stream patterns will increase.

This paper builds on the proposed linkage between Arctic amplification (AA)—defined here as the enhanced sensitivity of Arctic temperature change relative to mid-latitude regions—and changes in the large-scale, upper-level flow in mid-latitudes [1, 2]. Widespread Arctic change continues to intensify, as evidenced by continued loss of Arctic sea ice [3]; decreasing mass of Greenland's ice sheet [4], rapid decline of snow cover on Northern hemisphere continents during early summer [5], and the continued rapid warming of the Arctic relative to mid-latitudes. While these events are driven by AA, they also amplify it: melting ice and snow expose the dark surfaces beneath, which reduces the surface albedo, further enhances the absorption of insolation, and exacerbates melting. Expanding ice-free areas in the Arctic Ocean also lead to additional evaporation that augments warming and Arctic precipitation [6].

Traditionally AA is measured as the change in surface air temperature in the Arctic relative to either the Northern hemisphere or the globe [7]. It arises owing to a variety of factors, including the loss of sea-ice and snow, increased water vapor, a thinner and more fractured ice cover, and differences between the Arctic and lower latitudes in the behavior of lapse-rate and radiative feedbacks [8–13]. Here we do not address the relative importance of various factors causing AA, but it is clear from the height-latitude anomalies of air temperature, geopotential, and zonal wind (figure 1) that AA results in large part from near-surface heating, although contributions from poleward heat transport may also play a role [14].

Seasonal time series and trends in AA based on two metrics and varying initial years are presented in figure 2. The more traditional method of assessing AA is to subtract changes in near-surface (1000 hPa) air temperature anomalies in mid-latitudes (60–30°N) from those in the Arctic (left side of figure 2). A positive value of AA indicates that the Arctic is warming faster than mid-latitudes. Both the time series and progressive 15 year trends (figure 2, bottom) indicate an increasingly positive AA in all seasons, particularly in fall and winter, in agreement with previous analyses [8]. Starting in the 1990s, coincident with an accelerated decline in Arctic sea-ice extent [3], AA values and trends became positive in all four seasons for the first time since the beginning of the modern data record in the late 1940s, illustrating the Arctic's enhanced sensitivity to global warming.

The right side of figure 2 presents an alternative metric for AA based on the difference in the 1000–500 hPa thickness change in the Arctic relative to that in mid-latitudes (same zones as for the traditional method). Arguably the thickness difference is more relevant for assessing the effects of AA on the large-scale circulation, as it represents differences in warming over a deeper layer of the atmosphere that should more directly influence winds at upper levels. Several recent autumns have exhibited strong warming anomalies in some mid-latitude areas, contributing to the weakened positive trend after 2007. It is

© 2015 IOP Publishing Ltd

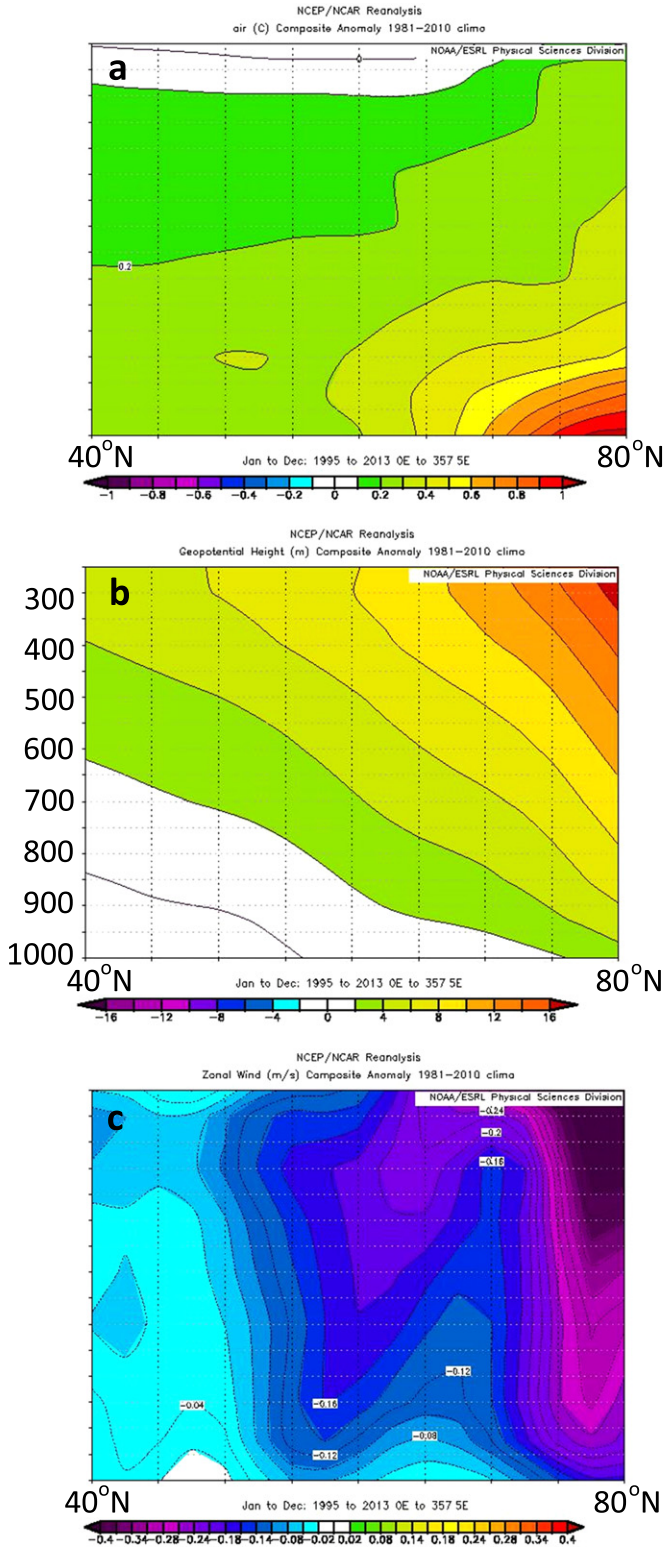

Figure 1. Annual-mean anomalies in air temperature (left), geopotential (middle), and zonal winds (right) during 1995–2013 relative to 1981–2010 for 40–80°N and 1000–250 hPa. Data were obtained from the NCEP/NCAR Reanalysis at http://www.esrl.noaa.gov/psd/.

important to note the recent emergence of the signal of AA from the noise of natural variability: since ~1995 near the surface and since ~2000 in the lower troposphere. This short period presents a substantial challenge to the detection of robust signals of atmospheric response amid the noise of natural variability [15, 16]. Thus for this study we define the period from 1995 to 2013 as the 'AA era.' While this demarcation is consistent with previous studies [17], we also investigate the effects of choosing different commencement years on detecting changes in the frequency of high-amplitude jet-stream configurations.

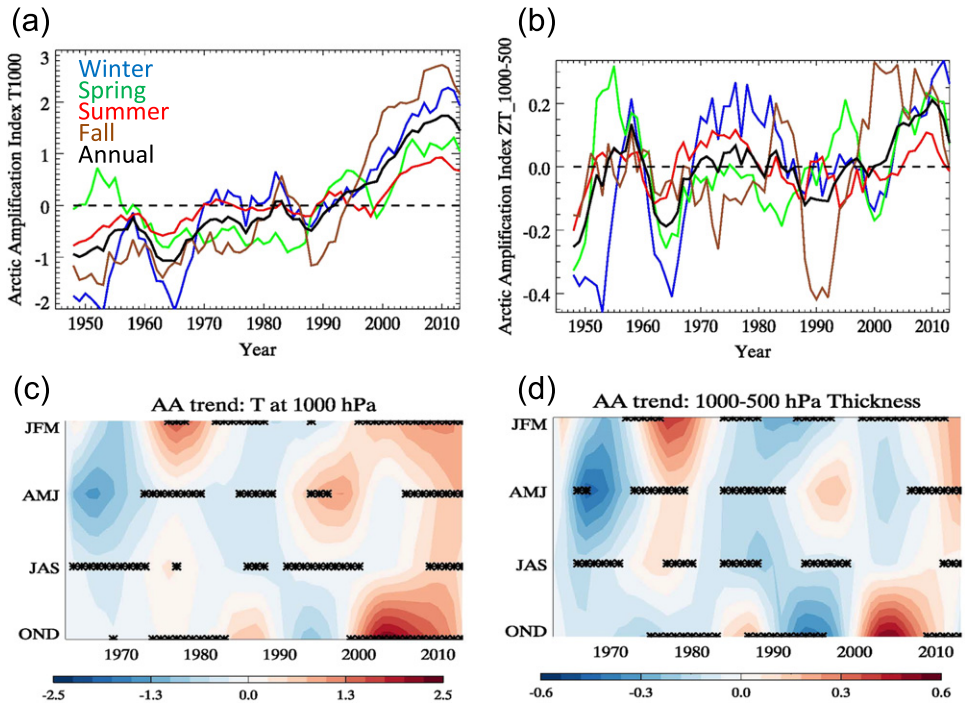

Figure 2. Arctic amplification seasonal time series (a), (b) and trends (c), (d) based on two metrics: (left) differences in 1000 hPa temperature anomalies (relative to 1948–2013 mean, °C) between the Arctic (70–90°N) and mid-latitudes (30–60°N); (right) differences in 1000–500 hPa thickness anomalies (percent of mean for each zone) between the two zones. Contoured colors in c,d indicate moving 15 year trends (C/decade for T1000 and percent of mean per decade) for each season. The *x*-axis indicates the ending year of each 15 year period between 1949 and 2013, and asterisks indicate ending year of periods with significant trends (confidence >95%, assessed using an F-test goodness of fit). Data were obtained from the NCEP/NCAR Reanalysis at http://www.esrl.noaa.gov/psd/.

The following linkage between AA and mid-latitude weather patterns has been hypothesized [1]. Increasing AA weakens the poleward temperature gradient—a fundamental driver of zonal winds in upper levels of the atmosphere—which causes zonal winds to decrease, following the thermal wind relationship [18]. A weaker poleward temperature gradient is also a signature of the negative phase of the so-called Arctic oscillation/Northern annular mode (AO/NAM), in which weaker zonal winds are associated with a tendency for a more meridional flow, blocking, and a variety of extreme weather events in much of the extratropics [19]. Disproportionate Arctic warming and sea-ice loss favor a negative AO/NAM aloft [1, 2, 20, 21] and a Northward migration of ridges in the upper-level flow [1], further contributing to an increased meridional pattern. As the wave amplitude and/or frequency of amplified flow regimes increases, the incidence of blocking becomes more likely [2], which reduces the Eastward propagation speed of the pattern. Consequently, the associated weather systems persist longer in a particular area. Extreme weather events caused by prolonged weather conditions (such as cold spells, stormy periods, heat waves, and droughts), therefore, should also become more likely, as illustrated by recent studies linking these events to high-amplitude planetary waves [22–24].

Because AA is strongest in fall and winter (figure 2), the atmospheric response is expected to be largest and observed first in these seasons. Results corroborate this expectation [1], showing a marked reduction in the poleward thickness gradient and weaker zonal winds at 500 hPa during fall (OND) and winter (JFM) since 1979 over the North America/North Atlantic study region. Others find statistically significant decreases in zonal-mean zonal winds in the fall but not in winter [15].

Marked spatial and seasonal variability in the changing poleward thickness gradient dictates patterns of change in zonal winds. While hemisphere-mean, mid-latitude, zonal winds at 500 hPa have decreased by about 10% since 1979 during fall [23], no robust hemispheric trends are apparent in other seasons owing to the spatial variability of the AA signal.

The objectives of the present study are to examine regional and seasonal expressions of AA that produce changes in poleward thickness gradients, corresponding effects on zonal wind speeds, and the hypothesized increase in highly amplified jet-stream regimes. Recent studies have presented a mixed picture regarding this atmospheric response to AA. Some observational analyses find evidence of increased wave amplitude in certain locations and seasons, but statistical significance is often lacking [1, 15, 16], likely owing to the recent emergence of AA from natural

variability. Analyses based on climate model simulations are challenged by the sometimes unrealistic representations of complex Arctic physics and nonlinear atmospheric dynamics. Nevertheless, they, too, suggest a more meridional flow (often resembling the negative phase of the AO/NAM) in response to sea-ice loss [25], and none suggests that the flow will become more zonal or that planetary waves will decrease in amplitude. Measuring changes in the strength of the zonal wind is straightforward, whereas quantifying the 'waviness' of the circulation is not. We therefore aim to shed further light on this critical aspect of the linkage by using new techniques to measure the waviness of the upper-level flow, and we also comment on the results of previous efforts to diagnose changes in wave amplitude.

Seasons are defined as follows: winter (JFM), spring (AMJ), summer (JAS), and fall (OND). These definitions are selected to coincide with the summer minimum and winter maximum of Arctic sea-ice extent, as well as the onset times of freeze and melt. All data are from the NCEP/NCAR Reanalysis (NRA) [26] obtained at http://www.esrl.noaa.gov/psd/.

Analysis of 500 hPa height contours

A simple new method was introduced to assess the daily meridional amplitude of waves in the upper-level flow [1]. A single contour in the 500 hPa height field was selected based on its climatological position within the strongest gradient, thus representing the path of the polar jet stream on any individual day. The planetary wave locations and shapes depicted by height fields at 500 hPa and those at typical heights of the jet stream maximum (~250 hPa) are very similar. The selected heights of individual contours vary slightly with season to match climatological jet-stream locations: within 50 m of 5600 m during the cool/cold seasons (JFM, AMJ, OND), and 5700 m during summer months (JAS). Daily height contours are subsetted from daily mean 500 hPa fields from the NRA. Correlations of 500 hPa height anomalies between NRA and either the NCEP Climate Forecast System Reanalysis or the European Centre for Medium-Range Forecasts Interim values are over 0.99 in all seasons (not shown), suggesting that mid-tropospheric height fields in NRA are nearly identical to those of other reanalyses. Small differences in blocking statistics among various reanalyses have also been reported [27].

The selection of particular 500 hPa height contours used for analysis of wave amplitude [1] has been questioned by assertions that the proper contours to use should be those exhibiting the greatest degree of waviness [15]. This study reproduced the increased wave amplitude in the 5600 m contour from 1979 to 2010, but the same analysis based on the contour identified as the waviest (5300 m) exhibited no increase in amplitude. As illustrated in figures 3(a) and (b), however, the mean latitude of the 5300 m contour during fall (1980–2011) is nearly 15° of latitude farther North than the mean latitude of the 5600 m contour. Moreover, its more Northerly position is far from the core of strongest upper-level winds and thus its location differs substantially from the path of the jet stream. Winds well North of the jet are substantially weaker (figures 3(a) and (c)), consequently is it not surprising that the flow is wavier. Arguably, the analysis of the more Northerly 5300 m contour does not capture the location and evolution of the polar jet stream, while the 5600 m contour more closely tracks the shape of planetary waves in the strongest upper-level flow. Note that the mean latitude of the strongest zonal 500 hPa winds is nearly identical in both the AA era (figure 3(a)) and in earlier years (figure 3(c)), suggesting that contours used here and previously [1] represent the jet-stream location throughout the satellite record (since 1979).

Meridional circulation index (MCI)

A key outstanding question in the proposed linkage between AA and jet-stream behavior is whether weakened poleward thickness gradients are causing the upper-level flow to become wavier. One measure of flow waviness is the ratio of the meridional (North/South) wind component to the total wind speed. We propose a simple metric to assess this characteristic of the flow: the MCI:

$$\mathrm{MCI} = \frac{v * |v|}{u^2 + v^2},$$

where u and v are the zonal and meridional components of the wind. When MCI = 0, the wind is purely zonal, and when MCI = 1 (−1), the flow is from the South (North). We note that a more meridional flow can result from either a stronger v and/or weaker u wind component through simple vector geometry. Whatever the cause, an increase in |MCI| indicates a wind vector aligned more North–South and reflects a changed flow direction. The speed of the meridional (v) wind may not change, as it is associated with East–West temperature gradients, but if the total wind vector becomes more meridional, then the flow is by definition 'wavier'. For example, a Northwesterly wind could shift to a North–Northwesterly wind solely through a reduction of the Westerly wind component. For this analysis, MCI is calculated from daily 500 hPa wind components between 20°N and 80°N at each gridpoint in NCEP Reanalysis fields.

Coincident anomalies in thickness, zonal winds, and MCI

In an effort to assess the effects of AA on waviness of upper-level winds, we compare coincident seasonal

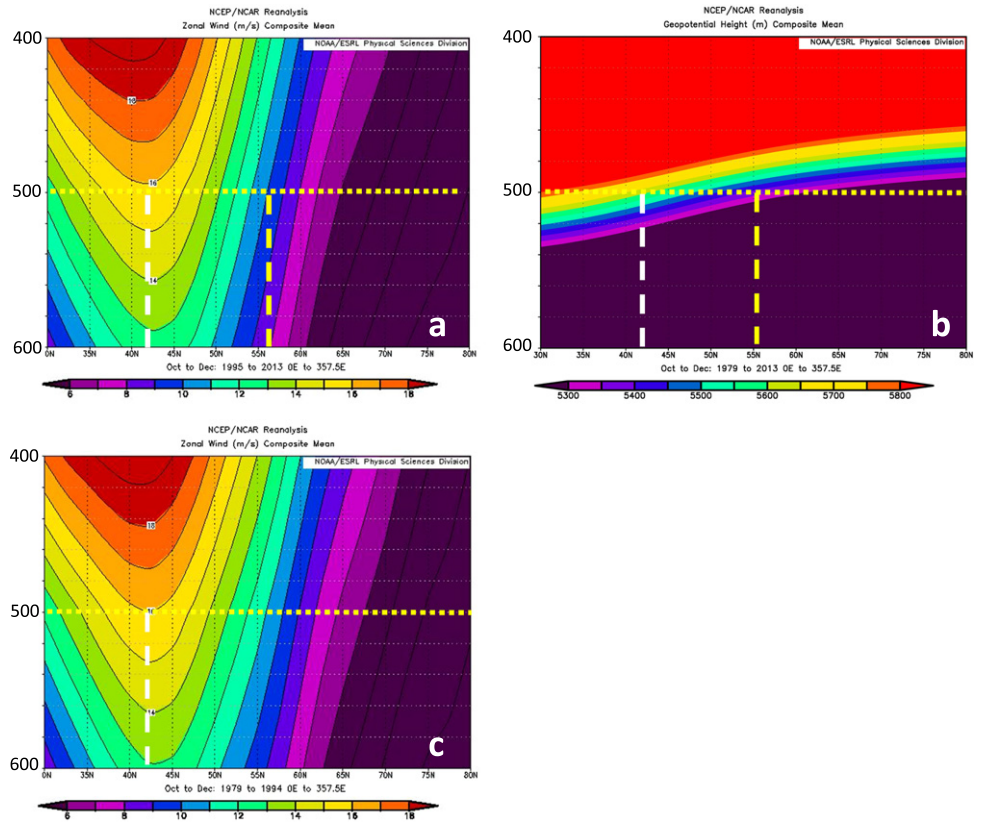

Figure 3. Zonal-mean zonal winds for fall (OND) from 1995 to 2013 (a) and from 1979 to 1995 (c). Corresponding zonal-mean geopotential heights for 1979–2013 are shown in (b). Dotted horizontal lines highlight the 500 hPa level, white dashed vertical lines indicate the latitude of maximum mean zonal winds at 500 hPa, and yellow dashed lines are the latitude of the waviest 500 hPa contour, as identified in [15].

anomalies during the AA era relative to the period from 1981–2010. Anomalies in the 1000–500 hPa thicknesses are presented in the top panels of figures 4–7. During fall (OND, figure 7(a)), when sea-ice loss exerts its largest direct impact, the pattern of AA extends across much of the Central Arctic, while during spring (AMJ, figure 5(a)) and summer (JAS, figure 6(a)) the areas of positive thickness differences occur primarily over high-latitude land, likely in response to earlier snow melt [5]. In all seasons, positive thickness differences are evident in the Northwest Atlantic. This substantial regional and seasonal variability illustrates the challenge in detecting robust hemispheric-mean atmospheric responses to AA, resulting in the low statistical significance reported in some previous studies [15, 16, 28].

The middle panels of figures 4–7 present anomalies in zonal wind speeds at 500 hPa corresponding to anomalies in the poleward gradient of 1000–500 hPa thicknesses (top panels). Anomalies in |MCI| are shown in the bottom panels. Immediately obvious is the close association between the spatial patterns of weakened poleward gradients (regions where positive anomalies occur Northward of weaker or negative anomalies) and areas where zonal winds are weaker.

During winter and autumn (figures 4 and 7) a broad area of substantially weakened poleward gradient is evident across much of the Northern hemisphere mid-latitudes, particularly in the N. Atlantic and Northern Eurasia. These areas are closely matched by the spatial pattern of slower zonal winds, as would be expected according to the thermal wind relationship. Widespread positive anomalies in |MCI| also correspond to these regions. Changes in the meridional wind speed, however, are not correlated with either the changes in poleward gradient or zonal winds, suggesting that changes in |MCI| arise mostly because of changes in the zonal wind speed. These findings support the hypothesis that AA causes a more meridional character to the upper-level wind flow, but this change is achieved primarily via a reduction in Westerly winds rather than through an increase in meridional wind speeds.

Relationships between these variables on a gridpoint-by-gridpoint basis are illustrated in scatterplots (figure 8). Gridpoints with weaker (stronger) poleward gradients tend to have larger (smaller) |MCI| values (red scatter-plots), particularly for gridpoints with the strongest (top decile) total winds, indicative of the jet stream. In all seasons, robust relationships between anomalies in the poleward gradient, zonal winds, and |MCI| are evident. Moreover, in spring, summer, and fall, the anomaly in 500 hPa zonal winds accounts for a much larger fraction of the variance in

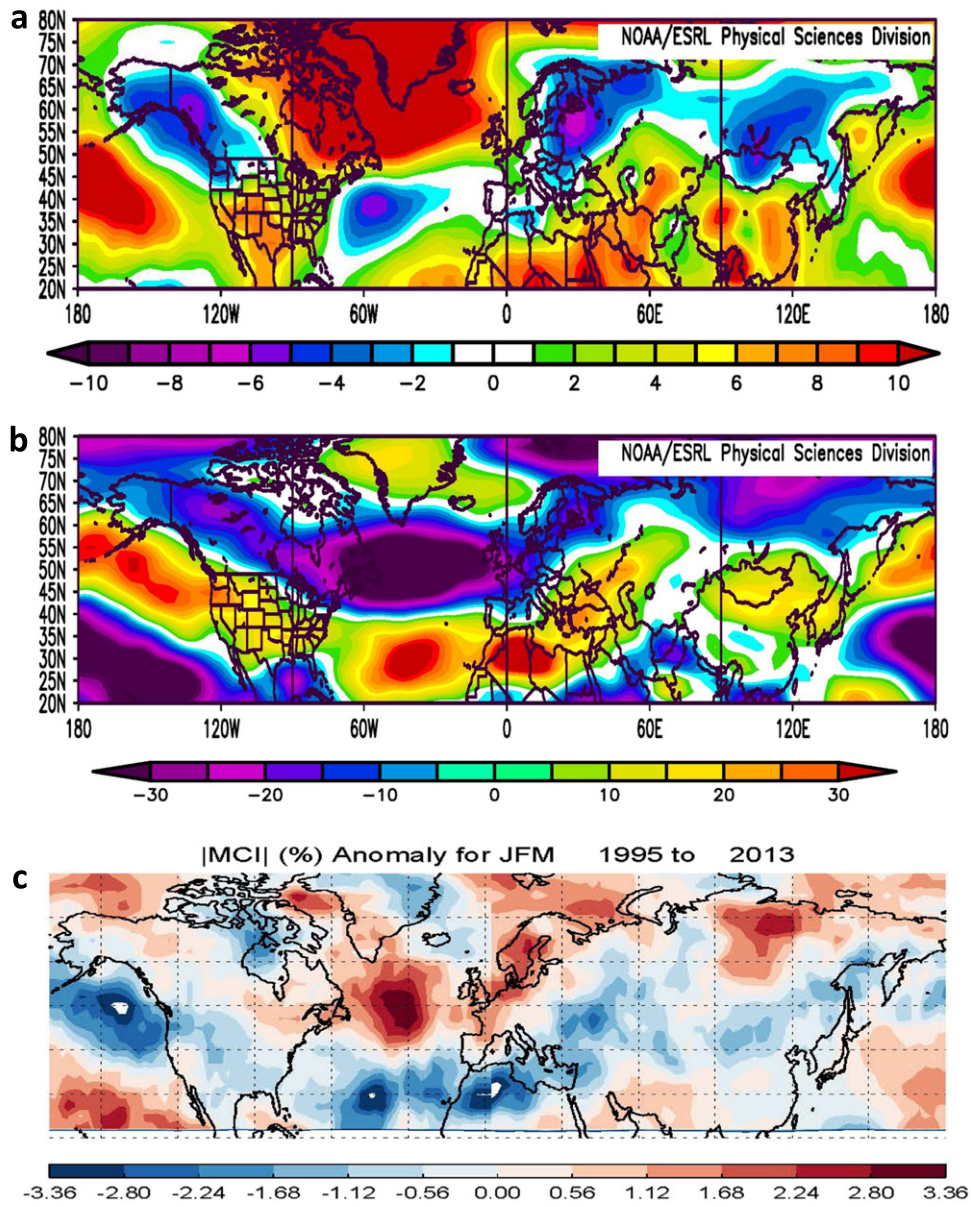

Figure 4. Anomalies in winter (JFM) (a) 1000–500 hPa thickness (m), (b) zonal wind at 500 hPa (m s^{-1}), and (c) the absolute value of the MCI during 1995–2013 relative to 1981–2010. Data were obtained from NOAA/ESRL at http://www.esrl.noaa.gov/psd/.

|MCI| than does the anomaly in the meridional wind component (variance explained by U500 in JFM, AMJ, JAS, OND = 0.42, 0.33, 0.61, 0.38; by V500 = 0.59, 0.02, 0.07, 0.001), suggesting that weakened zonal winds due to AA are the main factor driving the more meridional flow in these seasons. We also note that correlations between differences in 500 hPa meridional wind speeds with either the differences in poleward thickness gradient or zonal wind speed were small and insignificant, suggesting that changes in the |MCI| arise primarily because of changes in zonal wind speeds.

Extreme wave frequency

One aspect of the proposed linkage [1] that heretofore has been difficult to assess is whether the amplitude of planetary waves is increasing in response to strengthening AA. An alternative metric that we pursue here is the frequency of highly amplified jet-stream configurations. Single contours of daily mean 500 hPa height fields are used to identify 'extreme waves' in the jet stream. Representative contours (5600 m ± 50 m, except 5700 m ± 50 m in JAS) are selected to represent the streamline of the strongest 500 hPa winds as discussed previously, and we note that the selected contours shift little in latitude with time (figure 3). Data are analyzed in various longitude zones to identify days in which the difference between the maximum and minimum latitudes (ridges and troughs) of the contour within a region exceeds 35° of latitude. The threshold of 35° was selected to achieve a frequency of approximately 20 days per season (~20%). Note that individual high-amplitude events,

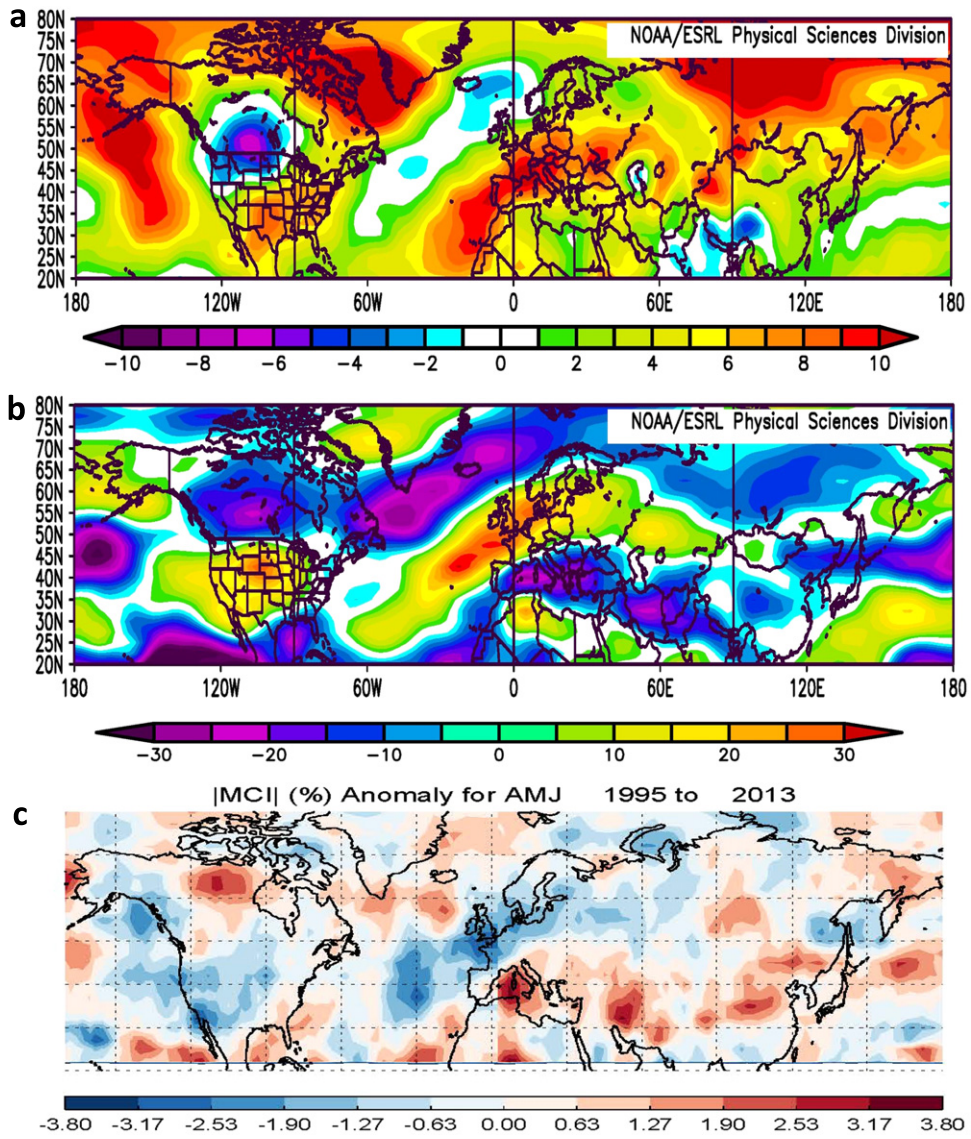

Figure 5. Same as figure 4 but for spring (AMJ).

such as blocks and cut-off lows, often persist for several days, thus the frequency of events < frequency of high-amplitude days.

The frequency of occurrence of high-amplitude days is assessed in each season and for the AA era (1995–2013) relative to the pre-AA period (1979–1994). We repeat the analysis using two additional definitions of the AA era—1990–2013 and 2000–2013—to determine the sensitivity of differences in high-amplitude days to the time period selected for the AA era. The mean differences in frequency between these periods for each season and in selected regions are presented in table 1. Changes in frequency are expressed as a percentage relative to the pre-AA period. We also assess the choice of comparative years by randomly selecting 100 sets of a number of years from the pre-AA period corresponding to the length of each AA era, then calculating the standard deviation of the extreme-wave frequency in each set. Changes in frequency from the pre-AA period to the AA era that exceed one (two) standard deviation(s) are indicated by an underscore (asterisk).

The changes in frequency are predominantly positive, indicating more frequent occurrences of highly amplified jet-stream configurations in the AA era. Seasonal and regional variations are generally consistent with the spatial patterns of anomalies in poleward thickness gradients shown in figures 4–7, particularly the most robust positive trends in extreme waves over the Atlantic and North American regions. We find a statistically significant negative correlation (Spearman's correlation = −0.30, >90% confidence) between the seasonal, regional-mean change in thickness gradient and the change in extreme-wave frequency. The autumn particularly stands out in table 1, with increases in extreme waves in all of the categories representing the post-AA period (1995–2013 and 2000–2013), as would be expected because fall exhibits the largest and most regionally consistent signal of AA. The Atlantic and North American regions also stand

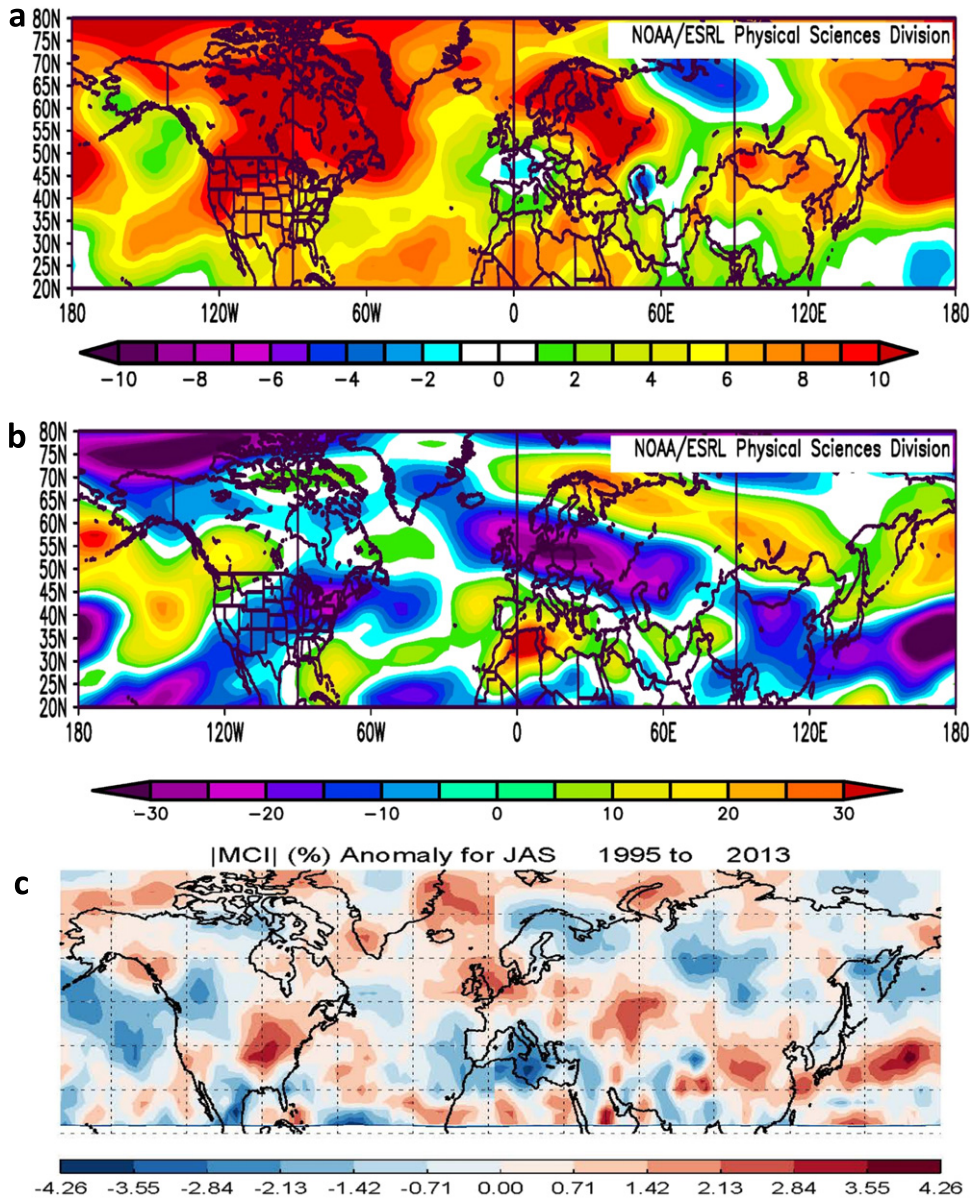

Figure 6. Same as figure 4 but for summer (JAS).

out, with increased frequencies in all post-AA categories. Decreased frequencies during Asian summer are consistent with recent cooling in North-Central Asia (figure 6), which strengthens the poleward gradient, drives stronger zonal winds, and results in a decreased |MCI|. Overall, the pattern of frequency change is consistent with expectations of a more amplified jet stream in response to rapid Arctic warming. Amplified jet-stream patterns are associated with a variety of extreme weather events (i.e., persistent heat, cold, wet, and dry) [22], thus an increase in amplified patterns suggests that these types of extreme events will become more frequent in the future as AA continues to intensify in all seasons. These results may also provide a mechanism to explain observed associations between sea-ice loss and continental heat waves [23, 29], cold spells [24, 30, 31], heavy snowfall [2], and anomalous summer precipitation patterns in Europe [32].

Discussion and conclusions

The Arctic has warmed at approximately twice the rate of the Northern mid-latitudes since the 1990s owing to a variety of positive feedbacks that amplify greenhouse-gas-induced global warming. This disproportionate temperature rise is expected to influence the large-scale circulation, perhaps with far-reaching effects. The North/South temperature gradient is an important driver of the polar jet stream, thus as rapid Arctic warming continues, one anticipated effect is a slowing of upper-level zonal winds. It has been

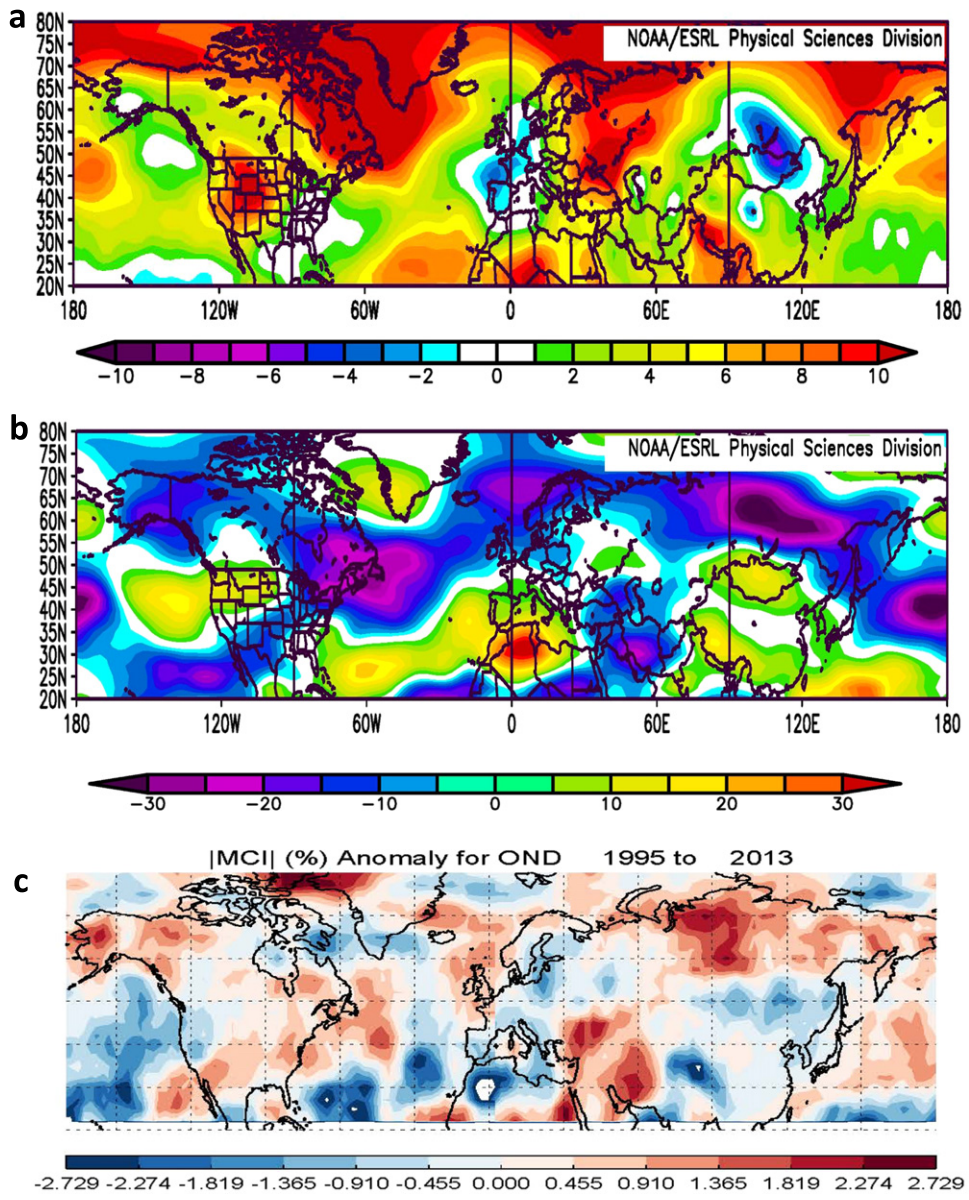

Figure 7. Same as figure 4 but for fall (OND).

hypothesized that these weakened winds would cause the path of the jet stream to become more meandering, leading to slower Eastward progression of ridges and troughs, which increases the likelihood of persistent weather patterns and, consequently, extreme events [1]. While weaker zonal winds have been observed in response to reduced poleward temperature gradients, the link to a wavier upper-level flow has not yet been confirmed [31, 33], although recent studies provide strong support of a mechanism linking sea-ice loss in the Barents/Kara Sea with amplified patterns over Eurasia during winter [24, 34] and summer [23]. We also note that the annual-mean NOAA-tabulated climate extreme index for the US [35] has increased by approximately one-third in the AA era relative to pre-AA years, though it is presently unknown whether rapid Arctic warming is a contributing factor.

Here we provide evidence demonstrating that in areas and seasons in which poleward gradients have weakened in response to AA, the upper-level flow has become more meridional, or wavier. Moreover, the frequency of days with high-amplitude jet-stream configurations has increased during recent years. These high-amplitude patterns are known to produce persistent weather patterns that can lead to extreme weather events [22, 23]. Notable examples of these types of events include cold, snowy winters in Eastern North America during winters of 2009/10, 2010/11, and 2013/14; record-breaking snowfalls in Japan and SE Alaska during winter 2011/12; and Middle-East floods in winter 2012/2013, to name only a few.

We assess anomalies in the poleward 1000–500 hPa thickness gradient during the AA era (since the mid-1990s) relative to climatology (1981–2010), along with corresponding changes in the

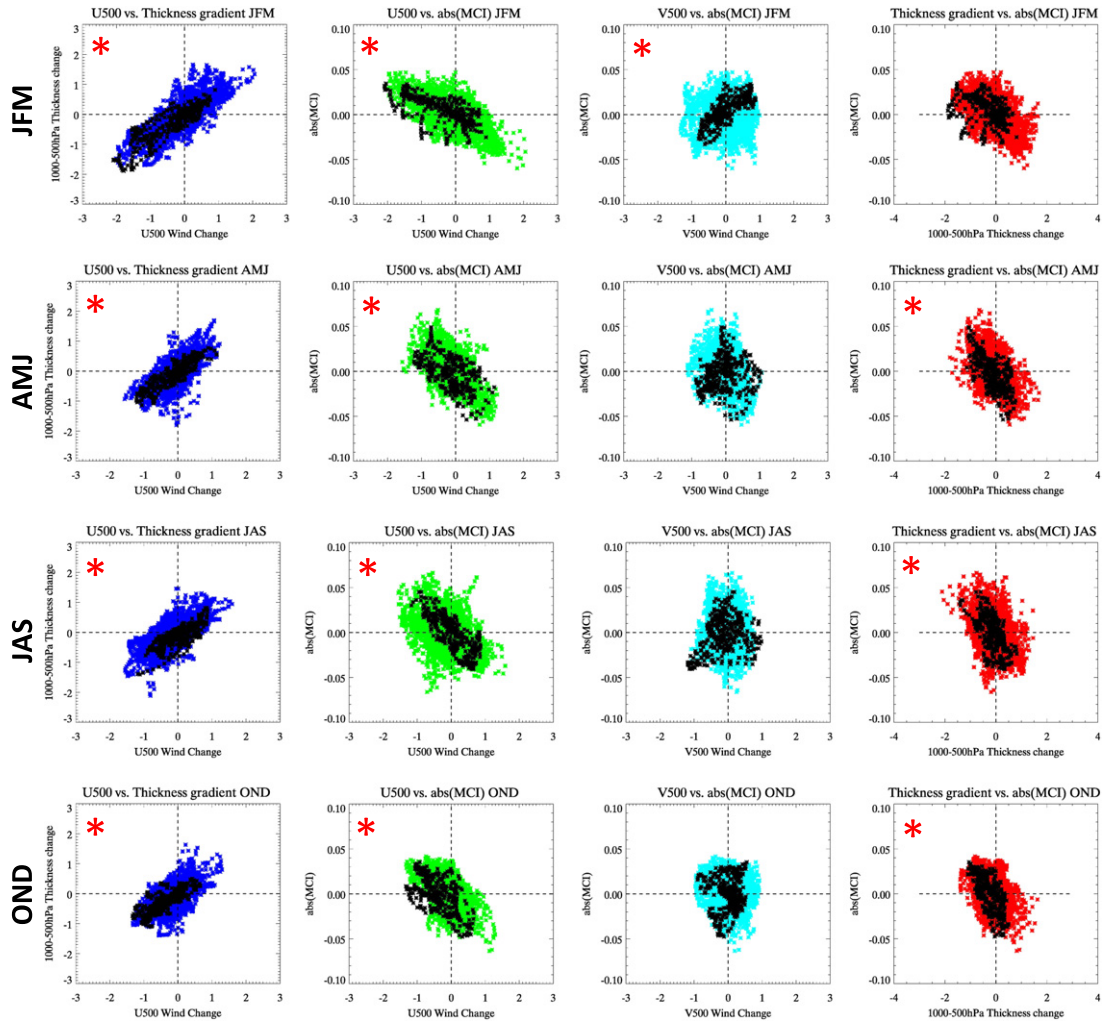

Figure 8. Seasonal scatterplots relating individual gridpoint values of anomalies during 1995–2013 for zonal and meridional winds at 500 hPa (U500, V500; m s^{-1}), poleward gradients in 1000–500 hPa thickness (m deg^{-1}), and |MCI| (unitless). Black asterisks indicate gridpoints corresponding to the highest 10% of total wind speed during 1995–2013 at 500 hPa, a proxy for the jet stream. Red asterisks indicate correlations between black points that exceed 50% and $p \ll .001$.

zonal winds at 500 hPa and the waviness of the 500 hPa flow (|MCI|). While these time periods are short and certainly include effects of other natural fluctuations in the climate system, the conspicuous emergence of AA since the mid-1990s dictates this focused temporal analysis to identify responses of the large-scale circulation to this 'new' forcing. Future work will analyze climate model projections of a future with greater global warming and intensified AA. A recent study [36] documents a reduction in the frequency of atmospheric fronts under strong greenhouse forcing, particularly in high latitudes where the meridional temperature gradient relaxes the most, suggestive of more persistent weather patterns.

We find that in all seasons, the regions in which the poleward gradient weakens also exhibit weaker zonal winds (as expected via the thermal wind relationship) and consequently a more meridional, or wavier, flow character. This localized response is corroborated by seasonally varying, regional-scale increases in the frequency of amplified jet-stream configurations. The strongest response occurs during fall, when sea-ice loss and increased atmospheric water vapor augment Arctic warming, and a robust response is also evident during summer over North America and the Atlantic sectors, when the observed rapid decline of early-summer snow cover and the lower heat capacity of land promote a drying and warming of high-latitude land areas. Significant increases are observed in winter and spring, as well. These results reinforce the hypothesis that a rapidly warming Arctic promotes amplified jet-stream trajectories, which are known to favor persistent weather patterns and a higher likelihood of extreme weather events. Based on these results, we conclude that further strengthening and expansion of AA in all seasons, as a result of unabated increases in greenhouse gas emissions, will contribute to an increasingly wavy character in the upper-level winds, and consequently, an increase in extreme weather events that arise from prolonged atmospheric conditions.

Table 1. Percentage change in seasonal frequency of high-amplitude days from the pre-AA period to the AA-era assessed using three different initial years to define the AA-era: 1990–2013 (left column under each seasonal heading), 1995–2013 (middle column), and 2000–2013 (right column). High-amplitude days are identified when the difference between the maximum and minimum latitude of the selected daily 500 hPa height contour within a specified region exceeds 35° latitude (see text for contour selections). Underlined values indicate changes that exceed one standard deviation of wave frequencies during the pre-AA period as determined from 100 sets of randomly selected groups of years of the same number as the corresponding AA era (i.e., 24, 19, and 14 years beginning in 1979). Underlined and asterisked values exceed two standard deviations.

Region	JFM			AMJ			JAS			OND		
Atlantic 285 – 60E	16	19	30	10	5	15	25	57*	58*	23	47*	70*
North America 220 – 290E	14	18	27	13	12	18	33	59*	65*	-5	23	20
Europe -15 – 45E	3	1	-3	7	3	14	-8	6	0	1	17	40*
Asia 30 – 150E	4	4	5	12	1	18	-15	-15	-24*	15	65*	103*
Pacific 150 – 240E	-4	-18	-14	18*	12	24*	-3	-3	-9	2	25	13
Northern Hemisphere	4	-6	-5	3	1	3	-7	-5	-11	7	16	25*

< -40%	-39 to -30%	-29 to -20%	-19 to -10%	-9 to 0%
0 to 9%	10 to 19%	20 to 29%	30 to 39%	> 40%

Acknowledgments

The authors are grateful for funding provided by the National Science Foundation's Arctic System Science Program (NSF/ARCSS 1304097), to programming assistance from R Kyle Zahn, and for helpful suggestions from Dr John Walsh and two anonymous reviewers.

References

[1] Francis J A and Vavrus S J 2012 Evidence linking Arctic amplification to extreme weather in mid-latitudes *Geophys. Res. Lett.* **39** L06801
[2] Liu J, Curry J A, Wang H, Song M and Horton R M 2012 Impact of declining Arctic sea ice on winter snowfall *Proc. Natl Acad. Sci. USA* **109** 4074–9
[3] Simmonds I 2015 Comparing and contrasting the behaviour of Arctic and Antarctic sea ice over the 35 year period 1979–2013 *Ann. Glaciol.* **56** 2015
[4] Tedesco M, Fettweis X, Mote T, Wahr J, Alexander P, Box J E and Wouters B 2013 Evidence and analysis of 2012 Greenland records from spaceborne observations, a regional climate model and reanalysis data *Cryosphere* **7** 615–30
[5] Derksen C and Brown R 2012 Spring snow cover extent reductions in the 2008–2012 period exceeding climate model projections *Geophys. Res. Lett.* **39** L19504
[6] Brintanja R and Selten F M 2014 Future increases in Arctic precipitation linked to local evaporation and sea ice retreat *Nature* **509** 479–82
[7] Holland M M and Bitz C 2003 Polar amplification of climate change in coupled models *Clim. Dyn.* **21** 221–32
[8] Screen J A and Simmonds I 2010 The central role of diminishing sea ice in recent Arctic temperature amplification *Nature* **464** 1334–7
[9] Alexeev V A, Langen P L and Bates J R 2005 Polar amplification of surface warming on an aquaplanet in 'ghost forcing' experiments without sea ice feedbacks *Clim. Dyn.* **24** 655–66
[10] Pithan F and Mauritsen T 2014 Arctic amplification dominated by temperature feedbacks in contemporary climate models *Nat. Geosci.* **7** 181–4
[11] Graversen R G, Langen P L and Mauritsen T 2014 Polar amplification in CCSM4: contributions from the lapse rate and surface Albedo feedbacks *J. Clim.* **27** 4433–50
[12] Thomson J and Rogers W E 2014 Swell and sea in the emerging Arctic ocean *Geophys. Res. Lett.* **41** 3136–40
[13] Khon V C, Mokhov I I, Pogarskiy F A, Babanin A, Dethloff K, Rinke A and Matthes H 2014 Wave heights in the 21st century Arctic ocean simulated with a regional climate model *Geophys. Res. Lett.* **41** 2956–61
[14] Porter D F, Cassano J J and Serreze M C 2012 Local and large-scale atmospheric responses to reduced Arctic sea ice and ocean warming in the WRF model *J. Geophys. Res.* **117** D11115
[15] Barnes E A 2013 Revisiting the evidence linking Arctic amplification to extreme weather in midlatitudes *Geophys. Res. Lett.* **40** 1–6
[16] Screen J A and Simmonds I 2013 Exploring links between Arctic amplification and mid-latitude weather *Geophys. Res. Lett.* **40** 959–64
[17] Barnes E A, Dunn-Sigouin E, Masato G and Woollings T 2014 Exploring recent trends in Northern hemisphere blocking *Geophys. Res. Lett.* **41** 638–44
[18] Wallace J M and Hobbs P V 1977 *Atmospheric Science, An Introductory Survey* (New York: Academic)
[19] Thompson D W J and Wallace J M 2001 Regional climate impacts of the Northern hemisphere annular mode *Science* **293** 85–9
[20] Feldstein S B and Lee S 2014 Intraseasonal and interdecadal jet shifts in the Northern hemisphere: the role of warm pool tropical convection and sea ice *J. Clim.* **27** 6497–518
[21] Francis J A, Chan W, Leathers D J and Miller J R 2009 Winter Northern hemisphere weather patterns remember summer Arctic sea-ice extent *Geophys. Res. Lett.* **36** L07503

[22] Screen J A and Simmonds I 2014 Amplified mid-latitude planetary waves favour particular regional weather extremes *Nat. Clim. Change* **4** 704–9
[23] Coumou D, Petoukhov V, Rahmstorf S, Petri S and Schellnguber H J 2014 Quasi-resonant circulation regimes and hemispheric synchronization of extreme weather in boreal summer *Proc. Nat. Acad. Sci.* 12331–6
[24] Kim B-M, Son S-W, Min S-K, Jeong J-H, Kim S-J, Zhang X, Shim T and Yoon J-H 2014 Weakening of the stratospheric polar vortex by Arctic sea ice loss *Nat. Commun.* **4** 4646
[25] Vihma T 2014 Effects of Arctic sea ice decline on weather and climate *Surv. Geophys.* **35** 1175–214
[26] Kalnay E *et al* 1996 The NCEP/NCAR 40 year realanysis project *Bull. Am. Meteorol. Soc.* **77** 437–71
[27] Davini T D 2013 Atmospheric blocking and mid-latitude climate variability *PhD Dissertation, Programme in Science and Management of Climate Change* University of Foscari, Italy
[28] Screen J A, Deser C, Simmonds I and Tomas R 2014 Atmospheric impacts of Arctic sea-ice loss, 1979–2009: separating forced change from atmospheric internal variability *Clim. Dyn.* **43** 333–44
[29] Tang Q, Zhang X and Francis J A 2014 Extreme summer weather in Northern mid-latitudes linked to a vanishing cryosphere *Nat. Clim. Change* **4** 45–50
[30] Tang Q, Zhang X, Yang X and Francis J A 2013 Cold winter extremes in Northern continents linked to Arctic sea ice loss *Environ. Res. Lett.* **8** 014036
[31] Cohen J *et al* 2014 Recent Arctic amplification and extreme mid-latitude weather *Nat. Geosci.* **7** 627–37
[32] Screen J A 2013 Influence of Arctic sea ice on European summer precipitation *Environ. Res. Lett.* **8** 044015
[33] Hall R, Erdelyi R, Hanna E, Jones J M and Scaife A A 2014 Review: drivers of North Atlantic polar front jet stream variability *Int. J. Climatol.* doi:10.1002/joc.4121
[34] Mori M, Watanabe M, Shiogama H, Inoue J and Kimoto M 2014 Robust Arctic sea-ice influence on the frequent Eurasian cold winters in past decades *Nat. Geosci.* **7** 869–73
[35] Karl T R, Knight R W, Easterling D R and Quayle R G 1996 Indices of climate change for the United States *Bull. Am. Meteorol. Soc.* **77** 279–92
[36] Catto J L, Nicholls N, Jackob C and Shelton K L 2014 Atmospheric fronts in current and future climates *Geophys. Res. Lett.* **41** 7642–50

Changes in North American Atmospheric Circulation and Extreme Weather: Influence of Arctic Amplification and Northern Hemisphere Snow Cover

STEPHEN J. VAVRUS AND FUYAO WANG

Nelson Institute Center for Climatic Research, University of Wisconsin–Madison, Madison, Wisconsin

JONATHAN E. MARTIN

Department of Atmospheric and Oceanic Sciences, University of Wisconsin–Madison, Madison, Wisconsin

JENNIFER A. FRANCIS

Department of Marine and Coastal Studies, Rutgers, The State University of New Jersey, New Brunswick, New Jersey

YANNICK PEINGS

Department of Earth Systems Science, University of California, Irvine, Irvine, California

JULIEN CATTIAUX

Centre National de Recherches Météorologiques, UMR 3589 CNRS/Meteo-France, Toulouse, France

(Manuscript received 21 October 2016, in final form 17 February 2017)

ABSTRACT

This study tests the hypothesis that Arctic amplification (AA) of global warming remotely affects midlatitudes by promoting a weaker, wavier atmospheric circulation conducive to extreme weather. The investigation is based on the late twenty-first century over greater North America (20°–90°N, 50°–160°W) using 40 simulations from the Community Earth System Model Large Ensemble, spanning 1920–2100. AA is found to promote regionally varying ridging aloft (500 hPa) with strong seasonal differences reflecting the location of the strongest surface thermal forcing. During winter, maximum increases in future geopotential heights are centered over the Arctic Ocean, in conjunction with sea ice loss, but minimum height increases (troughing) occur to the south, over the continental United States. During summer the location of maximum height inflation shifts equatorward, forming an annular band across mid-to-high latitudes of the entire Northern Hemisphere. This band spans the continents, whose enhanced surface heating is aided by antecedent snow-cover loss and reduced terrestrial heat capacity. Through the thermal wind relationship, midtropospheric winds weaken on the equatorward flank of both seasonal ridging anomalies—mainly over Canada during winter and even more over the continental United States during summer—but strengthen elsewhere to form a dipole anomaly pattern in each season. Changes in circulation waviness, expressed as sinuosity, are inversely correlated with changes in zonal wind speed at nearly all latitudes, both in the projections and as observed during recent decades. Over the central United States during summer, the weaker and wavier flow promotes drying and enhanced heating, thus favoring more intense summer weather.

1. Introduction

Numerous studies have suggested a relationship between midlatitude weather and Arctic amplification (AA) of global climate change (e.g., Newson 1973; Honda et al. 2009; Petoukhov and Semenov 2010; Liu et al. 2012; Cohen et al. 2014; Coumou et al. 2015). Francis and Vavrus (2012, hereinafter FV12) and Overland et al. (2015) described a proposed chain of causality, linking AA to a reduced meridional geopotential height gradient aloft, which leads to weaker upper-air extratropical westerlies, a wavier circulation, and the promotion of more frequent and persistent circulation patterns that favor extreme weather. Empirical evidence demonstrates a strong relationship between

Supplemental information related to this paper is available at the Journals Online website: http://dx.doi.org/10.1175/JCLI-D-16-0762.s1.

Corresponding author e-mail: Stephen Vavrus, sjvavrus@wisc.edu

DOI: 10.1175/JCLI-D-16-0762.1

© 2017 American Meteorological Society. For information regarding reuse of this content and general copyright information, consult the AMS Copyright Policy (www.ametsoc.org/PUBSReuseLicenses).

extreme weather events and slow-moving, high-amplitude wave patterns (Thompson and Wallace 2001; Meehl and Tebaldi 2004; Petoukhov et al. 2013; Screen and Simmonds 2014), but whether AA actually forces such remote circulation changes remains in question (Vihma 2014; Walsh 2014; Cohen et al. 2014). Moreover, this hypothesized correlation is complicated by recent studies showing that expressions of Arctic–midlatitude teleconnections are probably regionally dependent (Overland et al. 2015; Kug et al. 2015). Furthermore, while the connection between a reduced meridional pressure gradient and a weaker zonal wind stems directly from thermal wind considerations, the subsequent linkage between a weaker zonal wind promoting enhanced meridional flow is harder to establish. In part this difficulty arises because different metrics have been used to quantify waviness, which has led to varying conclusions about recent trends in blocking and other high-amplitude patterns (Screen and Simmonds 2013; Barnes et al. 2014; Kennedy et al. 2016; Francis and Vavrus 2015, hereinafter FV15).

The purpose of this study is to test the FV12 hypothesis under very strong greenhouse forcing, over a single geographic domain, and using multiple model realizations to improve the signal-to-noise ratio, which is relatively weak in observational studies that span only the recent short period of enhanced Arctic warming (since the mid-to-late 1990s). We focus on the projected late twenty-first-century climate change over greater North America (20°–90°N, 50°–160°W) using 40 realizations from the Community Earth System Model Large Ensemble (LENS; Kay et al. 2015). For comparison, we also analyze observed trends using the NCEP–NCAR Reanalysis-1 (NNR; Kalnay et al. 1996) from 1948 to 2014. A similar methodology has recently been applied to analyze the strength and waviness of the midlatitude circulation on a hemispheric scale using LENS Peings et al. 2017, manuscript submitted to *J. Climate*, hereinafter PCVM), reanalyses (Di Capua and Coumou 2016), and a combination of data from reanalyses and phase 5 of the Coupled Model Intercomparison Project (CMIP5; Cattiaux et al. 2016). All of these studies identified changes in midlatitude circulation that varied seasonally and regionally, but their focus was not exclusively North America. In addition, their reference location for representing the extratropics was fixed at a single latitude, which is a useful approach for succinctly characterizing aggregate circulation but potentially limiting in capturing variations within geographic sectors. A similar regionally averaged perspective using CMIP5 output was provided by Barnes and Polvani (2015), who described projected midlatitude circulation changes over the North America–Atlantic region based on the average response from 30° to 70°N.

In this study, we extend these prior findings by revealing a more complete spatial picture of greenhouse-forced climate changes within the North American region. As in prior studies, our analysis considers changes in both the speed and waviness of the atmospheric circulation and their implications for extreme weather. Following Cattiaux et al. (2016) and PCVM), we quantify waviness using the metric of sinuosity (SIN), a common metric in geomorphology to measure the waviness of streams that was described by J. E. Martin et al. (2017, unpublished manuscript, hereinafter MVWF) as a way to characterize midtropospheric atmospheric circulation. Di Capua and Coumou (2016) employed a similar metric called the meandering index *M*. Strongly zonal flow patterns result in low values of SIN and *M*, whereas very meridional patterns yield high SIN and *M*. Based on the FV12 hypothesis, we expect that Arctic amplification will contribute to a weaker and more sinuous circulation in midlatitudes.

Here we extend these related recent studies by presenting SIN as a function of latitude to identify potentially distinct responses in the behavior of the circulation across the vast expanse of the extratropics (20°–90°N) over greater North America. Rather than considering the entire Northern Hemisphere, we adopt a regional focus for several reasons. First, shrinking the domain reduces the risk of diluting the signal when combining sectors whose flow becomes more zonal with sectors trending toward more meridional circulation. Second, extreme weather has been increasing in recent years over this region, based on the U.S. climate extremes index (Gleason et al. 2008), featuring many high-profile events such as Superstorm Sandy in 2012 and the so-called polar vortex in 2014. Third, this region experiences the clearest dipole pattern of projected future changes in zonal winds aloft and thus serves as a useful test bed for the expected relationship between waviness and circulation strength. Fourth, the North American domain encompasses a distinct climatological ridge–trough couplet from west to east (Singh et al. 2016), providing a clearly defined wave structure for computing sinuosity. Fifth, recent research has found a strong regional dependence on the teleconnections between Arctic change and midlatitude weather (e.g., Overland et al. 2015 and references therein).

2. Data and methods

We utilize 500-hPa daily geopotential heights and zonal wind speeds from both atmospheric reanalysis and global climate model simulations. The reanalysis data are from NNR (Kalnay et al. 1996), with horizontal resolution of 2.5° × 2.5° and spanning 1948–2014. Similar results are obtained using data from the 40-yr

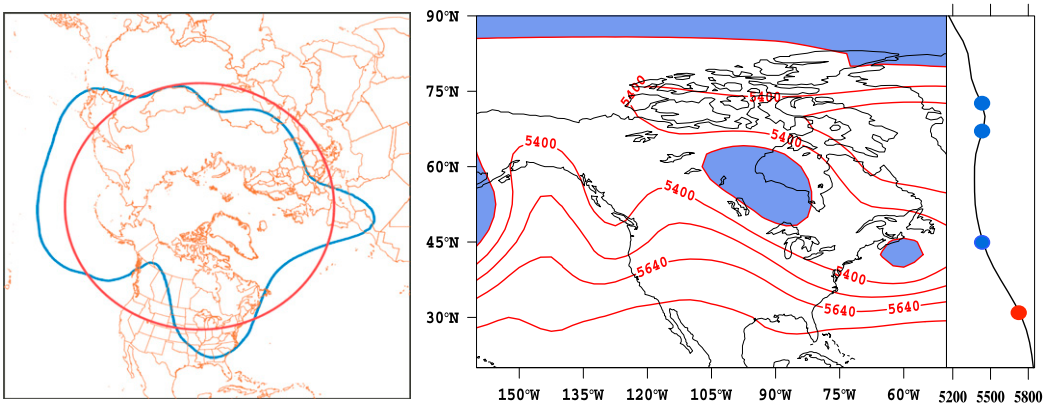

FIG. 1. Example of sinuosity calculations for simple hemispheric and complex regional cases. (left) Blue line is a geopotential height contour at 500 hPa. The area enclosed poleward of that contour is equal to the area within the red circle, the equivalent latitude. Sinuosity equals the ratio of the length of the blue curve to the length of the red circle. (right) Example of regional sinuosity in a flow with multiple features. Using the most complex case of the 5280-m isohypse as an example, sinuosity is based on the combined length of all 5280-m isohypse segments bounding the blue shading. This sum is divided by the arclength of the equivalent latitude determined by the sum of all shaded areas. See text for additional explanation.

European Centre for Medium-Range Weather Forecasts (ECMWF) Re-Analysis (ERA-40) data and ERA-Interim, so only the findings from NNR are shown here. The simulated atmospheric data from both historical and projected [representative concentration pathway 8.5 (RCP8.5)] LENS simulations are from the Community Earth System Model, version 1 (Community Atmosphere Model, version 5) [CESM1(CAM5)], which produces one of the most realistic climatologies in the CMIP5 suite of models (Knutti et al. 2013). Furthermore, the projected changes in upper-air circulation in LENS closely resemble the average CMIP5 pattern, suggesting that the findings identified here are representative. Each of the 40 ensemble members within LENS uses historical radiative forcing from 1920 to 2005 and RCP8.5 radiative forcing thereafter until 2100. Each model realization differs from one another by only small round-off level variations in their atmospheric initial conditions. The CESM1(CAM5) version used here is the 1° latitude–longitude configuration (0.9 × 1.25_gx1v6). The large size of the ensemble helps to distinguish signals of change from internal noise.

The strength of the circulation is defined as the speed of the zonal wind aloft, taken at a standard midtropospheric reference level of 500 hPa, while the more challenging description of circulation waviness is achieved through the SIN metric. As described in Cattiaux et al. (2016), SIN is defined as the ratio of the curvilinear length of a 500-hPa geopotential height contour (isohypse) to the perimeter of its equivalent latitude, where the contour and the equivalent latitude enclose the same area within the regional boundaries (Fig. 1). Relating its usage here to the more common application of sinuosity in geomorphology, the length of an isohypse is analogous to the length of a stream, while the perimeter of its equivalent latitude is akin to the shortest distance between the starting and ending points of that stream. SIN thus quantifies atmospheric waviness by representing the departure of 500-hPa height contours (isohypses) from a purely zonal orientation, and it accounts for closed circulation systems such as blocking highs and cutoff lows.

As noted in MVWF, other metrics have also been used to characterize the waviness of the large-scale circulation, such as the zonal index (Rossby et al. 1939), the circularity ratio (Rohli et al. 2005), high-amplitude wave frequency (FV15), effective diffusivity (Nakamura 1996), meandering index (Di Capua and Coumou 2016), and various versions of wave activity (Nakamura and Solomon 2010; Huang and Nakamura 2016; Chen et al. 2015). Although each of these measures provides particular insights into the waviness of the flow, sinuosity applied to large-scale geopotential height fields offers an attractively intuitive description of the circulation compared with related metrics.

To create a single value of SIN that characterizes waviness in midlatitudes, we follow MVWF by computing an aggregate sinuosity (ASIN) as a weighted average by using a set of five 500-hPa isohypses (576, 564, 552, 540, and 528 dam) representative of the midlatitude circulation:

$$\mathrm{ASIN} = \frac{(L_{576} + L_{564} + L_{552} + L_{540} + L_{528})}{(\mathrm{EL}_{576} + \mathrm{EL}_{564} + \mathrm{EL}_{552} + \mathrm{EL}_{540} + \mathrm{EL}_{528})},$$

where L represents the length and EL the equivalent length of the isohypse within the greater North American

domain. By boiling down the entire regional circulation into a single index, the purpose of aggregate sinuosity is similar to that of Cattiaux et al. (2016) and PCVM), who represented the whole midlatitude circulation from 30° to 70°N by calculating SIN at the approximate midpoint (~50°N). Likewise, Di Capua and Coumou (2016) applied their meandering index to the latitude of maximum daily waviness, around 60°N, but their index does not account for closed circulation features.

To obtain more information on the spatial variations of waviness within the domain, we also apply a more comprehensive method by expressing SIN as a function of latitude rather than particular geopotential heights. We first calculate daily SIN for individual geopotential height contours from 4600 to 6050 m in 10-m increments to obtain a quasi-continuous magnitude of sinuosity across a span of geopotential heights characteristic of the extratropics. This geopotential height range covers all values in both the historical and future climates. The second step is to compute the zonally averaged geopotential height across each latitude band on every day, as illustrated in Fig. 1, right. We then assign to each latitude the SIN corresponding to the height contour representing that latitude. For example, the zonally averaged height at 30°N is 5730 m (red dot in Fig. 1), and thus 30°N is assigned the sinuosity of the 5730-m isohypse. If a zonally averaged height occurs at more than one latitude, then the SIN at each of these latitudes is identical, as shown for the 5430-m isohypse, whose sinuosity is assigned to 45°, 67°, and 73°N (blue dots). Expressing SIN as a function of latitude accounts for the confounding effect of inflating geopotential heights in a warming climate (Barnes 2013) and identifies potentially different subregional changes in the magnitude of SIN, such as those hypothesized to occur between places experiencing zonal wind increases versus decreases in the future.

3. Results

a. *Recent past*

To illustrate how sinuosity can quantify exceptional circulation states, we show the lowest and highest values of daily ASIN during the study period (Figs. 2a,b). A very zonally oriented flow with aggregate sinuosity of 1.04 occurred on 24 December 1951, associated with an extremely positive Arctic Oscillation (AO) index of +3.47. In contrast, the remarkably muddled circulation pattern of 13 May 1993 yielded a record high ASIN of 2.64, coincident with an extremely negative −2.92 AO index. Many extreme weather events coincide with high values of ASIN, such as the extreme cold-air outbreak in the United States in January 2014 and Superstorm Sandy in October 2012 (Figs. 2c,d), both of which occurred amid highly negative AO phases that are conducive to meridionally oriented circulation patterns and anomalously weak zonal flow across much of the midlatitudes (Thompson and Wallace 2001).

The mean annual cycle of ASIN in reanalysis exhibits a pronounced seasonal migration, ranging from a broad wintertime minimum around 1.3 to a somewhat narrower peak just above 1.6 during late spring and early summer (Fig. 3a). This cycle over the greater North American domain is similar to the hemispheric average obtained in MVWF, while the alternative sinuosity definition used in Cattiaux et al. (2016) results in a somewhat earlier annual maximum during spring. The higher waviness during warmer months is consistent with the observed maxima in blocking frequency during springtime (Barriopedro et al. 2006), cutoff lows during summer (Price and Vaughan 1992; Kentarchos and Davies 1998), and atmospheric wavenumber in summer (Willson 1975). Throughout the year there is a strongly inverse relationship between ASIN and zonal wind speed, such that waviness is higher (lower) when westerlies aloft are weaker (stronger), conforming with empirical evidence (Walsh 2014) and theory (Chen et al. 2015; Wang and Nakamura 2015; Huang and Nakamura 2016). The correlation coefficient between aggregate sinuosity and zonal wind speed is −0.61 for all days in the time series and −0.93 based on the climatological annual cycle shown in Fig. 3a.

The annual cycle of aggregate sinuosity can be explained by the seasonality of the individual isohypses that constitute ASIN (Fig. 3b). The more southerly isohypses (552, 564, and 576 dam) exhibit a peak during summer, indicating their dominant role in shaping ASIN. By contrast, the remaining isohypses (528 and 540 dam) feature a double peak, one in spring and one in fall, which coincides with the prevalence of cutoff lows in more northerly locations across the domain (MVWF). During summer, these isohypses migrate so far poleward that their meridional wave amplitude is constrained. LENS reproduces these major circulation features in the ensemble mean and shows a relatively small ensemble range (Figs. 3c,d), closely simulating the phasing of the annual cycle but with a somewhat sharper and elevated summer maximum. Likewise, the model reproduces the major features of individual isohypses, although it simulates a more distinct summertime sinuosity peak of the southernmost contour (576 dam).

Annually averaged ASIN exhibits an upward trend over the course of the study period that is significant at the 99% level, based on the Sen–Kendall method (Sen 1968) and a Mann–Kendall test (Mann 1945). Embedded within this positive tendency is pronounced

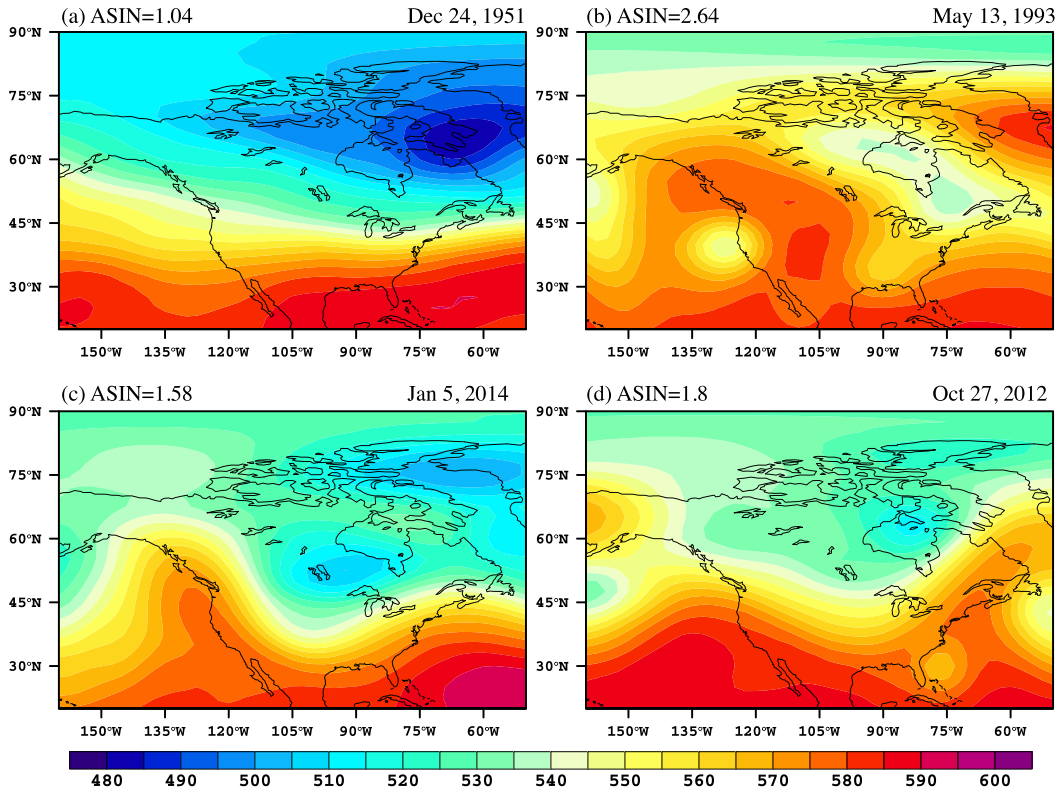

FIG. 2. Examples of noteworthy circulation states, illustrated by 500-hPa geopotential heights [dekameter (dam)]. (a) Lowest ASIN on record (1.04), (b) highest ASIN (2.64), (c) extreme cold-air outbreak in January 2014 (ASIN = 95th percentile for January), and (d) Superstorm Sandy (ASIN = 98th percentile for October).

interannual variability (Fig. 4) related closely to the annual AO index ($r = -0.51$; 99% significance level). This relationship is apparent in the two highest ASIN years (2009 and 2010) that coincide with very negative AO indices during winter 2009/10 (Cohen et al. 2010), as well as the lowest annual ASIN in more than 40 years occurring during the most positive AO year (1990). Daily variations in ASIN are significantly associated with the AO throughout the year, ranging from correlations of −0.40 (November) to −0.53 (March), in agreement with MVWF, Cattiaux et al. (2016), and Di Capua and Coumou (2016). The strongly inverse relationship between ASIN and the AO on daily–annual time scales indicates that sinuosity represents variations of circulation waviness prevailing across the midlatitudes as the polar vortex weakens and strengthens.

A potential problem with interpreting the long-term behavior of ASIN is that a warming climate inflates geopotential height contours, thus causing the reference isohypses to shift poleward and possibly confounding comparisons over time, as demonstrated by Barnes (2013). To circumvent this complication, we also examined trends in sinuosity by latitude during winter and summer (Fig. 5), whose intraseasonal trends are much more consistent than those in spring and autumn (not shown). The long-term behavior of SIN, as expressed by moving linear trends, varies with time and season, but a noteworthy feature is the consistently positive trends during winter and summer beginning around 1980 in mid-to-high latitudes that largely account for the increasing annual ASIN. Interestingly, this timing coincides with the start of reliable satellite records of Arctic sea ice and certain reanalysis products, such as ERA-Interim (Dee et al. 2011), that have been used to diagnose recent Arctic climate change. These recent upward trends in SIN generally align with downward trends in zonal wind speed aloft (Fig. 5), particularly during winter, reflecting their inverse relationship over the annual cycle shown in Fig. 3 and interannually (Cattiaux et al. 2016; PCVM).

b. Simulated future changes

Driven by strong greenhouse forcing, the simulated extratropical climate warms significantly in the future and features major circulation changes by late century. As shown in Fig. 6, the 40-member LENS average produces two general patterns of 500-hPa geopotential height anomalies: one that occurs during winter (November–March), exemplified by January, and the other during

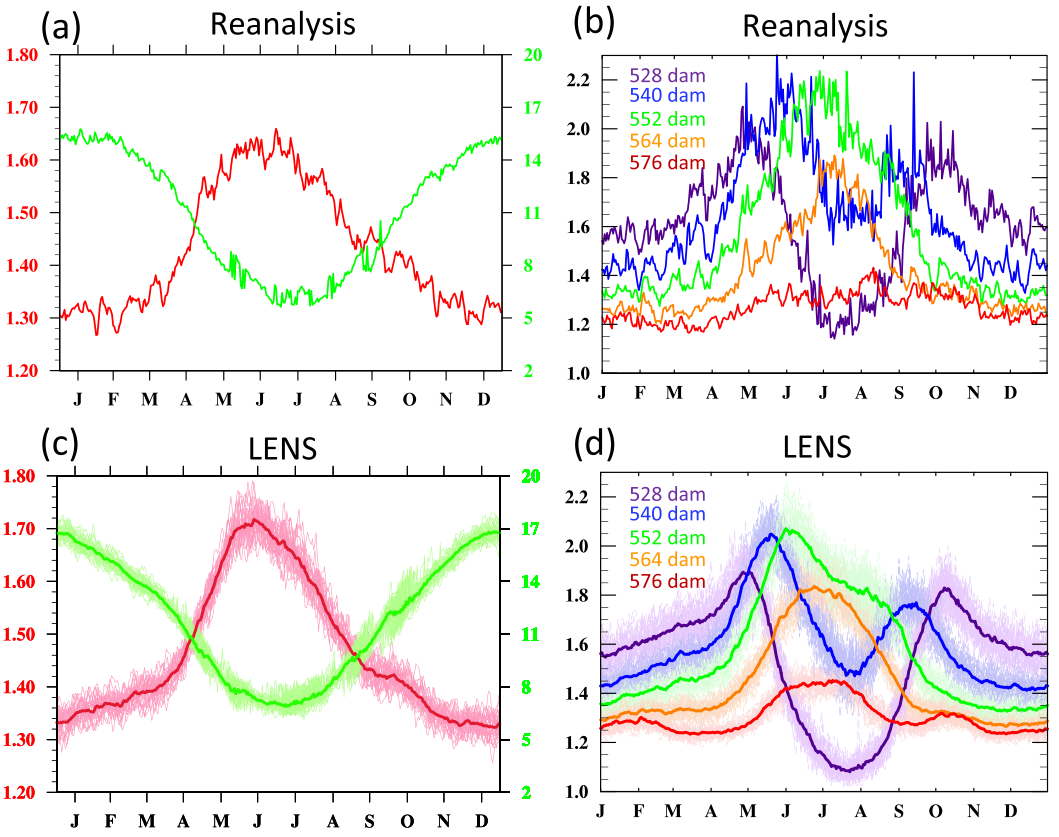

FIG. 3. Annual cycle of sinuosity and zonal wind speed (m s^{-1}) at 500 hPa. Aggregate SIN from 1948 to 2014 in red and zonal wind speed in green from (a) reanalysis and (c) LENS. The zonal wind curve was calculated in the same weighted manner as aggregate SIN, based on the zonally averaged westerly wind speed across each isohypse. Zonally averaged sinuosity at individual isohypses comprising aggregate SIN from (b) reanalysis and (d) LENS. Individual ensemble members are shown in light shading, and ensemble means are represented by dark lines.

summer (June–September), represented by August (individual months are presented in Figs. S1–S3 in the supplemental material). The winter pattern is characterized by exceptionally strong surface heating in the Arctic, particularly over the Arctic Ocean (Fig. 6a), which experiences dramatic reductions in sea ice extent and thickness (not shown). Remarkably, near-surface temperatures rise by up to 25 K in January and promote major positive midtropospheric height anomalies aloft over most of the Arctic, as well as across most of the Eurasian midlatitudes. By contrast, heights fall in a relative sense to the south of the Arctic-based ridging anomaly, extending from the North Pacific to northern Europe and bearing some resemblance to the negative phase of the Arctic Oscillation (Fig. 6c). The associated changes in zonal winds are dictated by these pressure redistributions through the thermal wind relationship, such that weaker westerlies aloft across North America (centered mainly over Canada) are sandwiched between the anomalous ridging over the Arctic and anomalous troughing to the south, with maximum wind increases impinging on the Southern California coast (Fig. 6e). Conversely, the pressure redistribution over the Eastern Hemisphere causes a very different zonal wind response, featuring stronger speeds over most of western Europe but a widespread band of weaker westerlies across the entire southernmost part of the extratropics from the prime meridian to the date line.

The summertime climate changes (Figs. 6b,d) are very different from those during winter. There is a more uniform warming pattern over mid-to-high latitudes, with some of the most pronounced temperature increases occurring farther south, over midlatitude continents (Fig. 6b). Warming over western North America is particularly strong, reminiscent of recent years. This widespread surface warming is associated with very large geopotential height increases across the entire extratropics (Fig. 6d), indicative of the overall warmer Northern Hemisphere during boreal summer. A more important seasonal difference is the configuration of

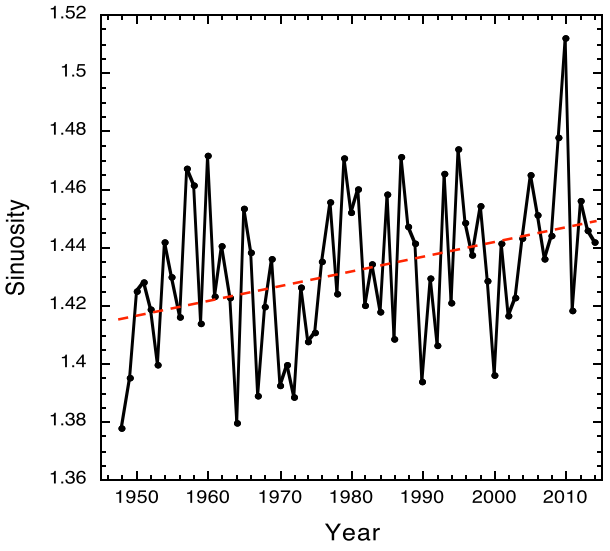

FIG. 4. Mean annual aggregate SIN and linear trend line from 1948 to 2014 using reanalysis data.

maximum height increases, which in summer are oriented in an annular pattern approximately centered around the location of greatest ridging over the central Arctic during winter. This summertime shift causes fairly coherent spatial changes in the speed of the zonal winds, which weaken over the entire Northern Hemisphere around 40°N and strengthen over most of the hemisphere around 60°N (Fig. 6f). The weakening of the westerlies is especially pronounced over North America, reaching 3–4 $m\,s^{-1}$ over the central United States, attributable to the enhanced ridging anomaly over western Canada that extends across the continent (Fig. 6d). This synoptic pattern is highly conducive to extreme heat and drought over the central United States (Chang and Wallace 1987; Mo et al. 1997; Rowell 2009) and is consistent with the documented weakening of midlatitude storm tracks and zonal wind in CMIP5 models (Chang et al. 2012; Lehmann et al. 2014; Coumou et al. 2015; Brewer and Mass 2016). In fact, the circulation changes in LENS during both winter and summer stem from geopotential height responses that are strikingly similar to those in CMIP5 (Fig. S4 in the supplemental material).

Despite the very different circulation responses between summer and winter, one commonality is the dipole pattern of zonal wind changes that emerges in both seasons, indicative of meridional shifts in the mean jet stream. This response is more complex than a general weakening of the extratropical circulation induced by AA, as hypothesized by FV12, but it closely conforms to the proposed mechanisms via the loss of sea ice and snow cover. Consistent with expectations, the simulated AA in these experiments promotes marine-based ridging over high latitudes during winter and terrestrial-based ridging over the northern extratropics during summer, both of which cause weaker westerlies aloft on their equatorward flanks. FV12 further hypothesized that the weaker circulation would lead to a wavier flow, a prediction that can be tested using the sinuosity metric. PCVM report that late twenty-first-century sinuosity in LENS decreased during winter and increased during summer (JJA) across the Northern Hemisphere overall, but opposite seasonal changes occurred in the North American sector. Because of the distinctly dipole response of the simulated zonal wind changes over North America, we opt here for an alternative to either using sinuosity or calculating sinuosity at a fixed latitude, as in PCVM. Instead, we calculate SIN at each latitude band to capture the potentially variable response of circulation waviness across greater North America.

The response of SIN and zonal wind is found to be highly inversely correlated, both in winter and summer (Fig. 7 and Fig. S5 in the supplemental material). The ensemble-mean sinuosity during winter is consistently lower south of 40°N, where the zonal wind strengthens by up to 2 $m\,s^{-1}$. Poleward of 40°N the zonal wind slackens by up to 2 $m\,s^{-1}$, while SIN increases at almost all latitudes by approximately the same amount (0.05–0.10) and by nearly the same magnitude as the maximum decrease south of 40°N. Inversely related changes in zonal wind and SIN also occur during summer and feature higher SIN between 35° and 50°N, in concert with weakened westerlies of up to 2 $m\,s^{-1}$. A striking feature is the pronounced peak increase in sinuosity of around 0.8 at 42°N that is consistent with the sharp jump in climatological summertime SIN between 50° and 40°N in the twentieth century (Fig. S6 in the supplemental material), characterized by more closed highs aloft when the circulation weakens during late summer. Sinuosity is sensitive to the presence of closed cyclones and anticyclones, whose isohypse length is extensive relative to equivalent length, and thus these features are exceptionally wavy by our metric (MVWF). In high latitudes the westerlies strengthen during August by up to 1.5 $m\,s^{-1}$ at 60°N, collocated with a maximum SIN reduction of nearly 0.2, but then exhibit no significant changes poleward of 70°N, where SIN declines modestly. In both seasons, the changes in SIN south of 30°N are less reliable, owing to difficulties in calculating this circulation metric where the wave structure becomes less coherent outside of the climatological westerlies. This increased uncertainty is illustrated by the large scatter among ensemble members in SIN changes at low latitudes during January, whereas the sign of the sinuosity changes is generally consistent among ensemble members at other latitudes in both seasons.

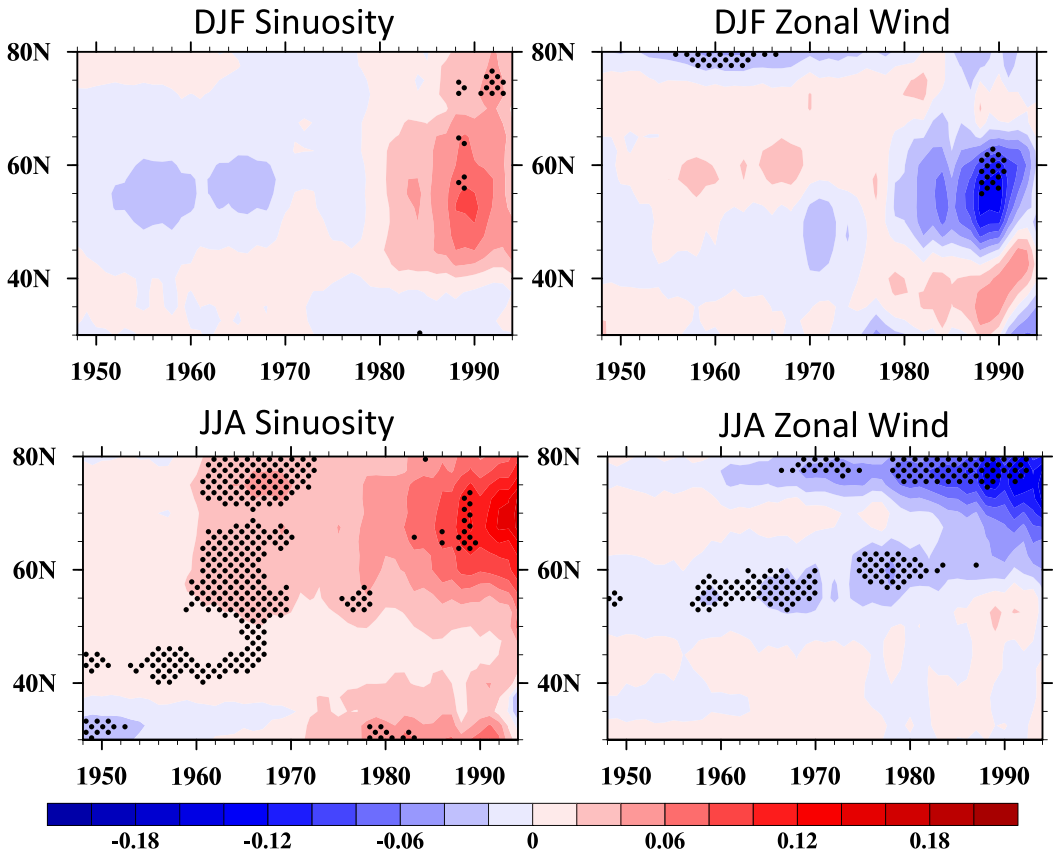

FIG. 5. Moving linear trends of (left) sinuosity (decade^{-1}) and (right) 500-hPa zonal wind speed (m s^{-1} yr^{-1}) from reanalysis during (top) DJF and (bottom) JJA. The trends begin in a given year on the x axis and end in 2014. Stippling denotes significant trends at the 90% confidence level using a least squares regression.

c. *Relationship with extreme weather*

Our findings from LENS demonstrate that significant but spatially variable changes in the strength and waviness of the circulation over North America can be expected in the future. Because a sluggish, sinuous flow is often associated with extreme weather (Screen and Simmonds 2014; FV12), our results suggest that conditions will become more favorable for such anomalies over Canada and Alaska during winter and over much of the continental United States during summer. In particular, the very large sinuosity increase and weaker winds centered over the middle of the United States during summer warrants closer examination. The circulation change in this season should promote excess heat and drought, consistent with evidence of reduced cyclone activity (Lehmann et al. 2014; Coumou et al. 2015). Indeed, LENS simulates that interior North America will receive up to 1–2 mm day^{-1} less August rainfall (30%–50%) in the future (Fig. 8), roughly collocated with enhanced surface warming evident in Fig. 6b. The combination of these two changes promotes a strong loss of soil moisture that favors extreme heat and severe aridity in this region (Teng et al. 2016; Douville et al. 2016). Many climate model simulations have produced accentuated summer rainfall reductions in the Great Plains, including CMIP5 (Maloney et al. 2014), although there is not a consensus on the cause(s).

Our results suggest that the mean change in the large-scale circulation promotes enhanced heating and rainfall reductions, but the mean does not reveal the synoptic-scale expression of this climate change in terms of daily weather. To gain insight on that question, we first show the relationship in LENS between the strength of the flow aloft and the associated daily near-surface temperature and rainfall during August, averaged over the box of maximum drying in Fig. 8 (35°–45°N, 105°–100°W) that also encompasses the core of maximum zonal wind speed reduction. Simulated daily anomalies are a strong function of zonal wind speed, such that days with the weakest westerlies (or even easterlies) aloft are the warmest and driest (Figs. 9a–d). This relationship becomes especially strong and virtually monotonic in the future and features a particularly

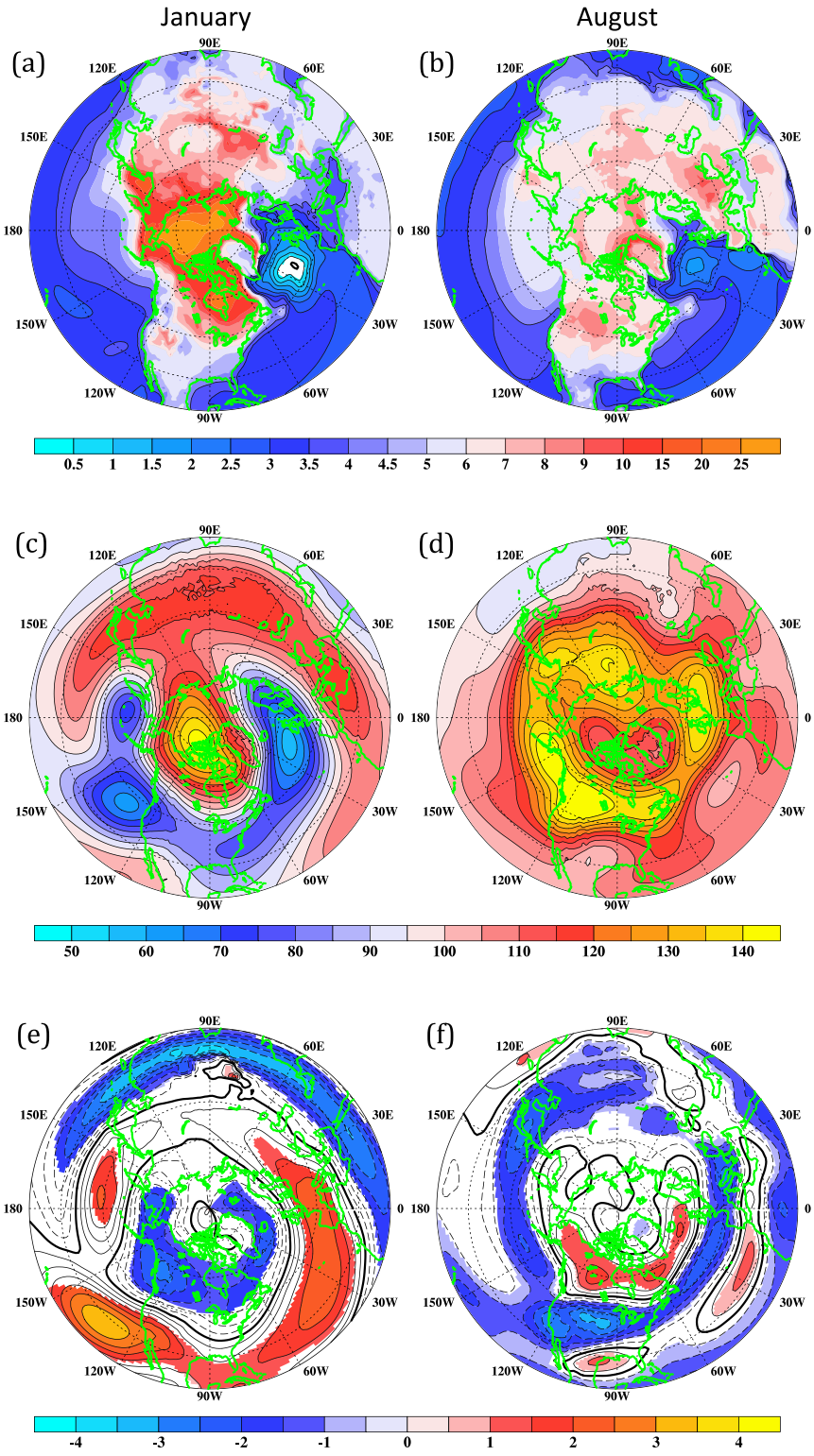

FIG. 6. Future changes (2081–2100 vs 1981–2000) in (a),(b) 2-m air temperature (K), (c),(d) 500-hPa heights (m), and (e),(f) 500-hPa zonal wind speed ($m\,s^{-1}$) during (left) January and (right) August. Shaded regions denote where the ensemble-mean changes are larger than the standard deviation of the intraensemble changes. Dashed contours indicate where wind speed changes are negative.

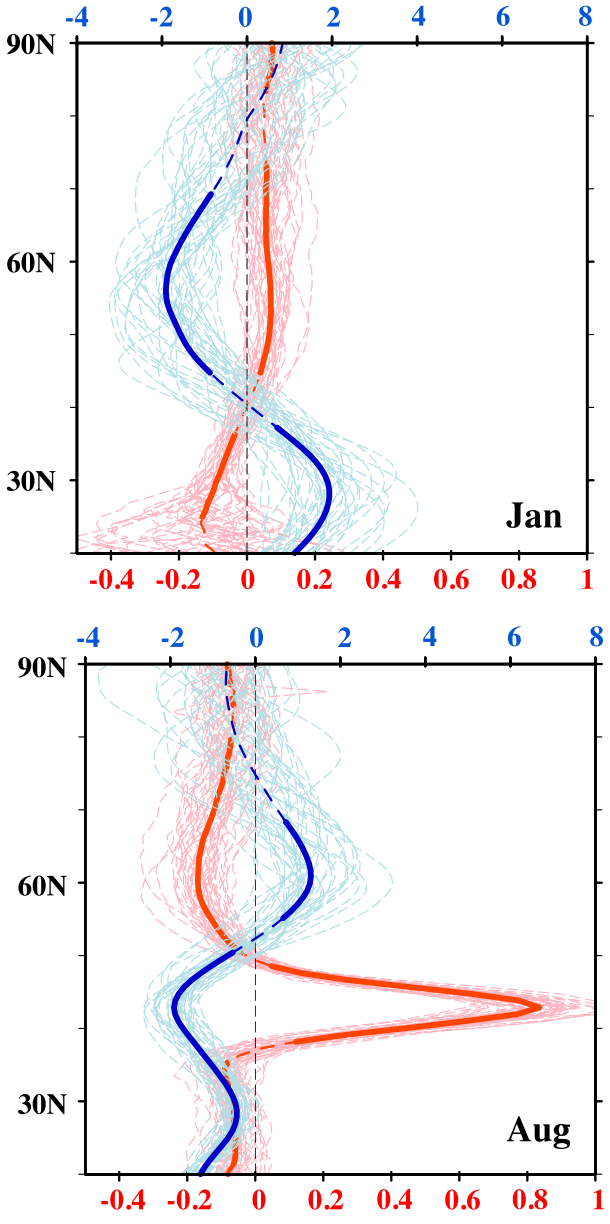

FIG. 7. Future changes (2081–2100 vs 1981–2000) in zonal wind speed ($m\,s^{-1}$; blue; upper x axis) and sinuosity (unitless; red; bottom x axis) during (top) January and (bottom) August over the greater North American domain. Thin lines denote individual ensemble members, and thick lines are the ensemble average. Solid thick lines indicate where the ensemble-mean change exceeds the standard deviation of changes among all ensemble members.

large drop-off in rainfall at the far-left tail of the distribution that represents light easterly winds aloft. These results are consistent with prior studies that demonstrated a highly inverse relationship between summer temperature and rainfall over the Midwest (Madden and Williams 1978; Chang and Wallace 1987; Trenberth and Shea 2005).

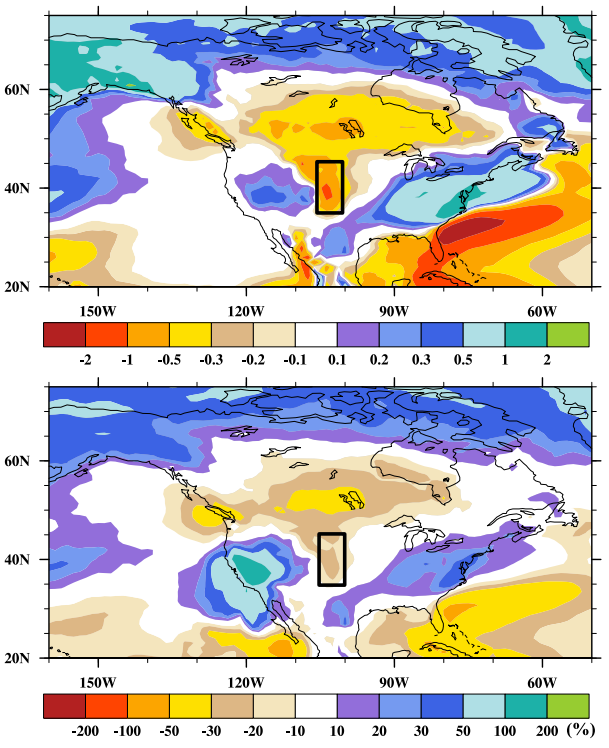

FIG. 8. Future changes (2081–2100 vs 1981–2000) in August precipitation expressed as (top) absolute difference ($mm\,day^{-1}$) and (bottom) percentage difference. The box over the plains denotes the reference region of especially pronounced drying and heating.

This linkage between large-scale circulation and extreme weather means that the overall weakening and amplification of the summertime flow aloft over interior North America favors hotter and drier weather, but the breakdown of projected changes in the distribution of wind speeds yields additional information (Figs. 9e,f). The average weakening of the zonal circulation aloft is expressed as fewer days with strong flow and more days with weak flow. This change is especially pronounced for days with easterly winds, which occur less than 2% of the time in the late twentieth century but approximately 15% in the future simulation. A cleaner comparison between the two time periods can be made by calculating the percentage change in the frequency of wind speeds across the distribution, using equal-sized bins that each occupies 5% of the total (Fig. 9f). The shift in the distribution produces highly asymmetric changes, such that the frequency of days with easterlies or the lightest westerlies increases much more (up to 375%) than the decline of the strongest westerlies. Because days with light winds are coincident with the driest and warmest conditions during both time periods (Figs. 9a–d), their spike in the future implies that circulation changes will contribute strongly to increased extreme summertime weather in this region.

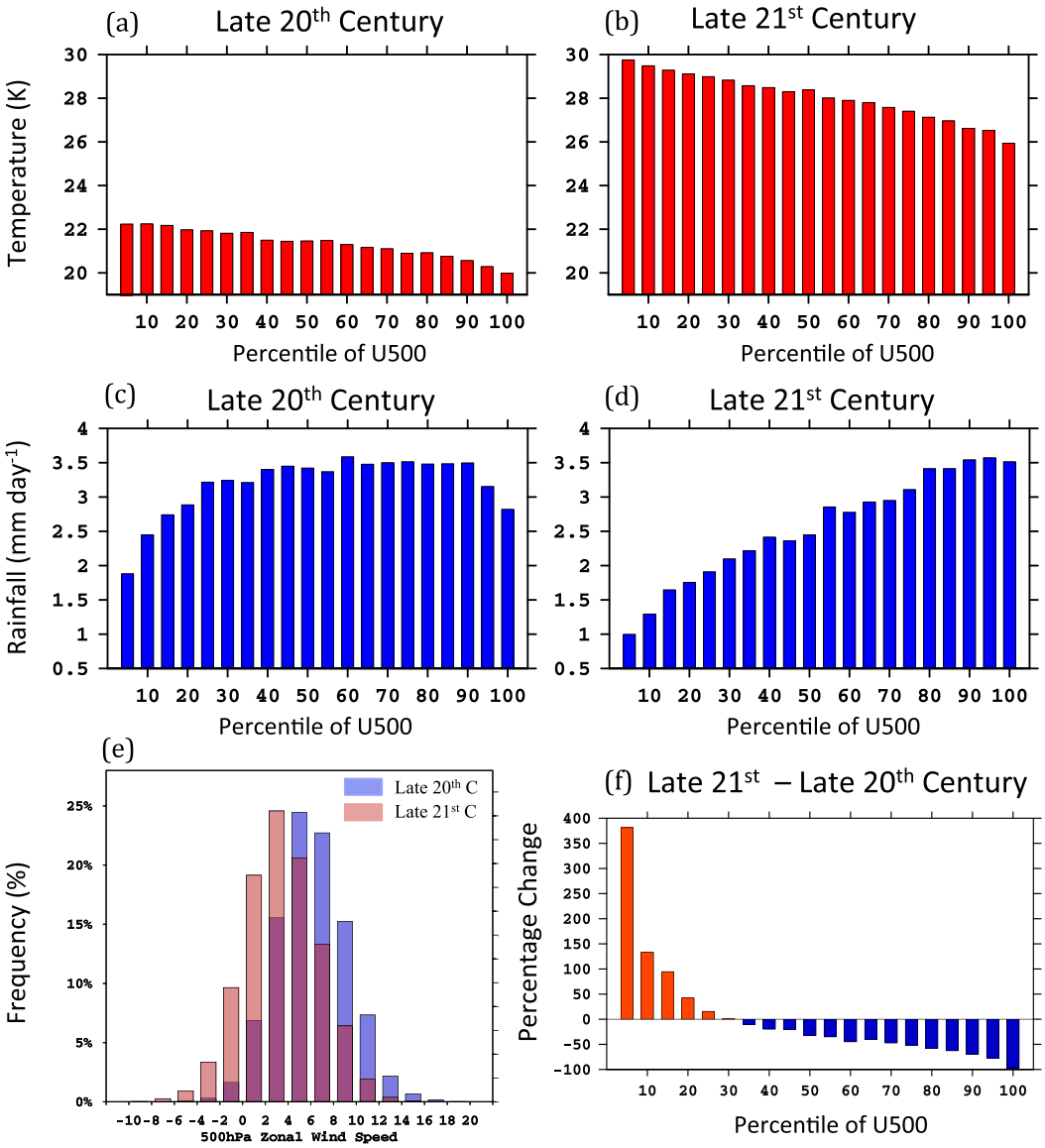

FIG. 9. Daily mean 2-m air temperatures and rainfall over the midcontinental box (see Fig. 8) for all August days as a function of the 500-hPa zonal wind speed (percentile) during the (a),(c) late twentieth century and (b),(d) late twenty-first century. High percentiles indicate a strong westerly wind aloft, and low percentiles represent either a weak westerly wind or an easterly wind. (e) Histogram of daily August wind speeds ($m\,s^{-1}$) in the late twentieth and late twenty-first century. (f) Percentage change in August wind speed frequency during the late twenty-first century relative to the late twentieth century.

Further insight into the relationship between large-scale circulation and weather impacts is found by compositing the large-scale circulation anomalies on the driest August months within the same box described above (Fig. 10). During these extremely dry months, the simulated circulation consists of an anomalous ridge to the north of the maximum midcontinental drying with anomalous easterly flow. The strength of the ridge also builds in the future and reaches up to a 30-m anomaly, compared with 20 m in the late twentieth century. These characteristic drought circulation patterns in both time periods resemble the mean summertime circulation change (Fig. 6d) and the observed pattern during mid-western droughts and heat waves (Mo et al. 1997; Lau and Nath 2012). This agreement provides further evidence that the mean shift toward a weaker, wavier summertime circulation favors drier, warmer conditions that promotes extreme aridity over the central United States. This dynamical signature further suggests that the excessive future drying and heating in this region is

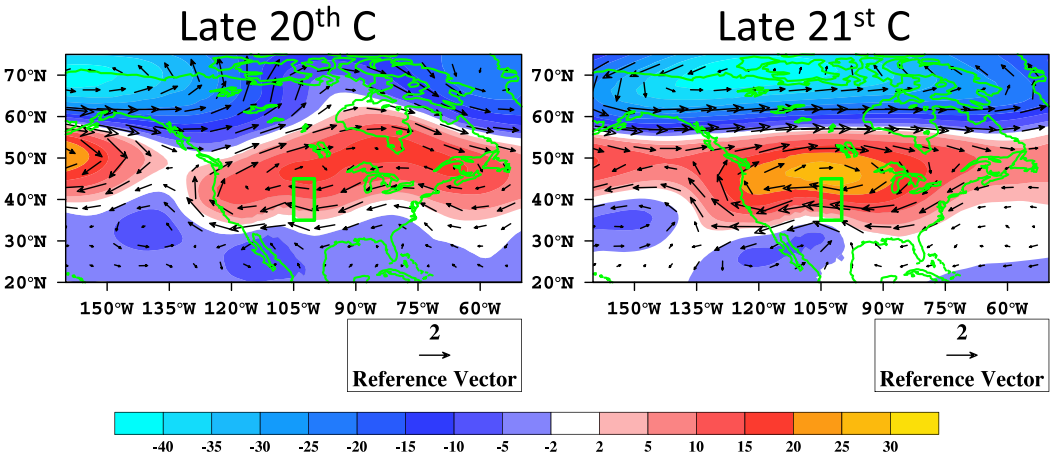

FIG. 10. The 500-hPa geopotential height (m) and wind velocity ($m\,s^{-1}$) anomalies in LENS on the driest 5% of August months during the (left) late twentieth century and (right) late twenty-first century, relative to each time period's climatology. The box corresponds to the region of enhanced drying and heating shown in Fig. 8.

unlikely to be caused exclusively by local soil-moisture feedbacks but rather that this aridity signal is significantly influenced by large-scale circulation changes.

d. Role of higher latitudes

A central open question is whether the projected summertime midlatitude circulation changes are a direct consequence of AA. Although the traditional perspective is that the dynamical contribution to midcontinental drying stems from a poleward expansion of the Hadley circulation and eddy-driven jet (Lu et al. 2007; Rivière 2011) and thus is somewhat independent of high-latitude changes, an alternative explanation is that AA also plays a significant role by promoting the annular band of maximum ridging (Fig. 6d) through enhanced heating of mid-to-high-latitude continents.

Several lines of reasoning support this interpretation of an Arctic influence. First, simulated greenhouse warming causes a large reduction in continental snow cover during spring and early summer (Fig. 11), which promotes warming by lowering surface albedo and soil moisture (Matsumura and Yamazaki 2012; Crawford and Serreze 2015). Second, this enhanced surface warming is most pronounced in mid-to-high latitudes, where hemispheric land cover is most prevalent (between 45° and 70°N, peaking around 65°N). Third, the much lower heat capacity of land versus water causes continents to warm more than adjacent oceans during summer, as is apparent in LENS (Fig. 6b). Alexander et al. (2010) showed that imposed snow-cover reductions in the CAM3 AGCM caused mid-to-high-latitude ridging during spring and summer, while observations demonstrate a similar relationship from interannual snow-cover anomalies (Matsumura and Yamazaki 2012). In addition, an experiment using the CCSM3 GCM with all terrestrial snow cover eliminated (Vavrus 2007) produced amplified summertime surface warming locally and an annular band of ridging aloft that resembles the pattern produced in LENS (Fig. 12, left, and Fig. S7 in the supplemental material). Furthermore, these terrestrially based heating sources can generate standing Rossby waves that are advected downstream by adiabatic warming from descending air masses and the prevailing westerlies aloft (Rowell 2009; Matsumura and Yamazaki 2012; Matsumura et al. 2014). Indeed, the strongest 500-hPa zonal winds during summer in the late twenty-first-century LENS simulations (Fig. S8 in the supplemental material) are closely aligned with the band of maximum 500-hPa height increases (Fig. 6d), particularly over the oceans. In this manner, enhanced terrestrial warming during summer over mid-to-high latitudes can initiate the annular band of maximum ridging simulated by LENS, very similar to the circumhemispheric band of 500-hPa height anomalies found to be most highly correlated with projected summer rainfall reductions over western North America and Europe from greenhouse forcing (Rowell 2009). Over North America, the location of the band of inflated heights that peaks over western Canada (Fig. 6d) is highly conducive to the simulated rainfall reductions in the plains.

An Arctic-oriented remote influence may exacerbate known factors related to local soil-moisture feedbacks (Wetherald and Manabe 1999; Gregory et al. 1997; Su et al. 2014) and an expanded subtropical aridity belt (Lu et al. 2007; Scheff and Frierson 2012) as sources of midcontinental drying during summer, and it could be an important contributor to promoting the ridging pattern favorable for drought that is also simulated in the

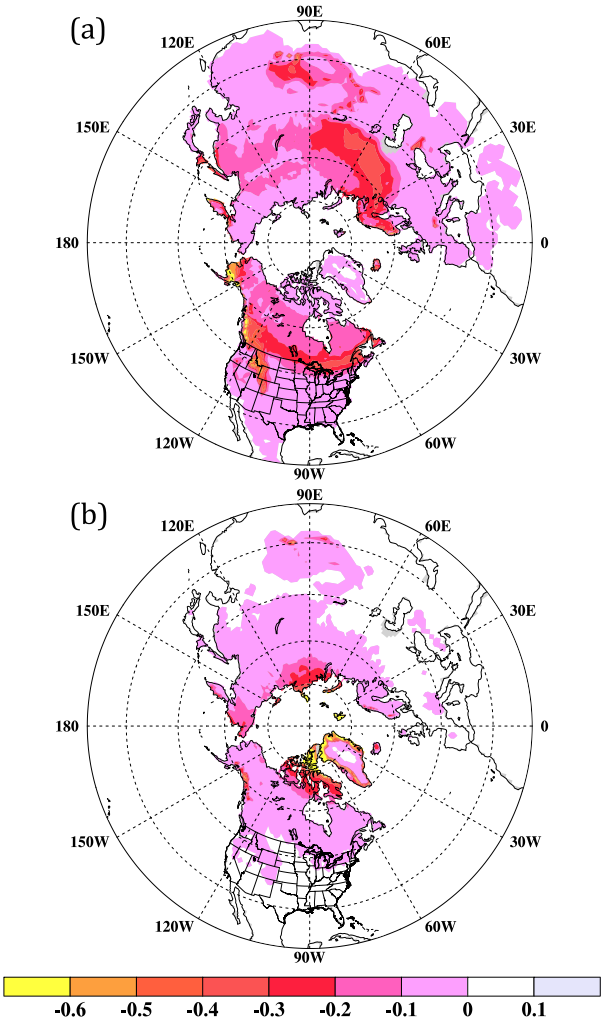

FIG. 11. Future changes (2081–2100 vs 1981–2000) in (a) MAM and (b) JJA snow fraction averaged among all ensemble members in LENS.

CMIP5 ensemble (Fig. S4; Maloney et al. 2014; Brewer and Mass 2016). Evidence from other studies also allows for nontraditional sources of possible teleconnective drivers, as in Rowell (2009) and Rowell and Jones (2006), who determined that remote circulation anomalies originating in the tropics contribute little to projected continental drying in Europe and North America. Similarly, Lu et al. (2007) concluded that future Hadley cell expansion and the associated poleward shift of the subtropical dry zone is unlikely to originate from tropical processes but rather is highly correlated with the extratropical tropopause height. The annular pattern of ridging anomalies identified here is different from the circumglobal teleconnection (CGT; Yang et al. 2009) because the ridging band in LENS is much farther north and there is no characteristic ridge to the northwest of India in LENS (a key feature of the monsoon-driven CGT). Also, the CGT structure is equivalent barotropic, but the LENS response over land is a mix of barotropic and baroclinic (not shown).

Further support for a terrestrially driven, high-latitude circulation contribution comes from a CCSM4 paleoclimate simulation of 6000 years ago, when differences in Earth's orbital configuration caused much more summertime insolation in the Northern Hemisphere, especially in high latitudes (Otto-Bliesner et al. 2006). As with greenhouse forcing, the strongest summer warming occurred on mid-to-high-latitude land and was also associated with a circumhemispheric band of 500-hPa height increases that resembles the LENS response, despite widespread tropical cooling (Fig. 12, right). Moreover, the teleconnection identified by Meehl and Tebaldi (2004) of enhanced Indian monsoon rainfall driving a mid-to-high-latitude band of ridging under greenhouse forcing does not explain the hemispheric-scale response in LENS. Although LENS also simulates greater monsoonal rainfall in the future, summers with more (less) rainfall are instead associated with lower (higher) geopotential heights aloft in a band stretching from Asia to North America (Fig. S9 in the supplemental material). By contrast, the strength of the zonal wind over the North American sector was found by PCVM to have a strong negative correlation with the magnitude of AA among LENS ensemble members. Deciphering the definitive role of higher latitudes in the summertime circulation changes described here requires additional investigation and will benefit from further modeling experiments.

4. Discussion and conclusions

Our study leads to the following conclusions regarding atmospheric circulation changes over North America and their possible connection with the Arctic:

- We find evidence for an increasing trend in mean annual waviness during the past several decades, superimposed on strong interannual variations associated with the phase of the AO, in agreement with Francis and Skific (2015), FV15, and Di Capua and Coumou (2016).
- There is a strong inverse relationship between projected changes in zonal wind speed and waviness, consistent with the intermodel CMIP5 and intraensemble LENS correlations identified in Cattiaux et al. (2016) and PCVM.
- This negative correlation occurs in both winter and summer, but the alignment of the circulation changes across the domain nearly reverses between seasons. A dipole pattern of weaker (stronger) westerlies arises in low to midlatitudes during summer (winter), and generally stronger (weaker) westerlies develop in higher latitudes during summer (winter).

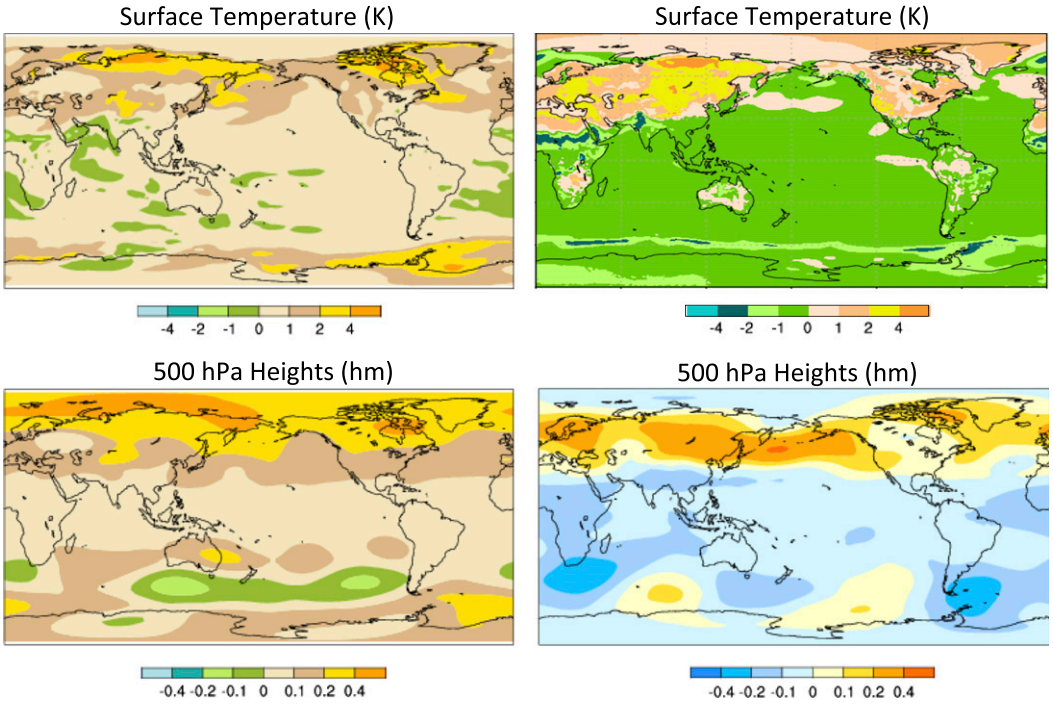

FIG. 12. Simulated changes in 2-m air temperature and 500-hPa geopotential heights [hectometer (hm)] during June–August in two climate model simulations that produced amplified high-latitude warming. (left) CCSM3 driven by contemporary greenhouse forcing (year 1990) but with all terrestrial snow cover eliminated (from Vavrus 2007). (right) CCSM4 paleoclimate simulation of 6000 years ago minus year 1850 driven by differences in Earth's orbital configuration between the two time periods.

- Simulations suggest a trend toward a future circulation pattern conducive to extreme drying and heating in central North America during summer, particularly in association with greater instances of easterly flow aloft.
- This circulation change appears to be fostered by the enhanced summertime heating of continents in mid-to-high latitudes, which promotes an annular band of maximum height increases across the entire Northern Hemisphere. The amplified warmth over land and its remote influence are favored by diminishing snow cover and low terrestrial heat capacity in latitudes where land is especially prevalent.

Our analysis focuses on greater North America because its projected response to greenhouse forcing is considerably different from elsewhere in the Northern Hemisphere (Fig. 6; Cattiaux et al. 2016; PCVM). A distinguishing finding of this study is the latitudinally varying response of projected seasonal circulation changes, which reveal dipole changes in circulation vigor and waviness from north to south that are related to meridional shifts in jet stream location. This differentiation contrasts with the "block" approach taken by Barnes and Polvani (2015), who concluded that CMIP5 models generally simulate a weak Arctic influence on future circulation characteristics over the greater North American–Atlantic region, based on domain averages from 30° to 70°N. Our study also refines recent findings by Cattiaux et al. (2016) and PCVM, whose conclusions of future circulation changes in the CMIP5 and LENS simulations, respectively, were based on sinuosity centered at a fixed latitude (~50°N). Both of these studies identified a future increase (decrease) in sinuosity during winter (summer) over the North American sector, but our results demonstrate that this average response is the result of opposing changes in different zones within the domain.

One motivation for this work was to test the hypothesis of FV12 that Arctic amplification would lead to a weaker and wavier midlatitude circulation that is more conducive to prolonged extreme weather events. Our results provide partial support for this hypothesis but reveal that the extratropical response is more geographically varied than implied by that study. FV12's central physical mechanism is supported by our results, in that simulated AA promotes ridging in mid-to-high latitudes that weakens the zonal wind on the equatorward flank and leads to a wavier (more sinuous) flow. However, this response is not uniform across the entire extratropical domain; instead, we find that some areas exhibit the opposite pattern of troughing, stronger zonal winds, and reduced waviness.

An open question is the extent to which the enhanced westerlies around 30°N during winter (Fig. 6e) originate from a tropically induced strengthening of the meridional height gradient, as opposed to a direct mass-compensation response to AA itself (Fig. 6c). For example, during a negative AO phase the characteristic high-latitude ridging anomaly is offset by a midlatitude troughing anomaly (Thompson and Wallace 1998) associated with stronger westerlies on its equatorward flank that resembles the atmospheric response to tropical warming during El Niños. Because greenhouse forcing causes warming and height inflation in upper levels of the tropical troposphere as well as in the lower polar troposphere (Held 1993; Barnes and Screen 2015; Cattiaux et al. 2016), isolating the Arctic contribution to the strengthened westerlies during winter in the LENS simulations is difficult. Further complicating this issue is the fact that Arctic warming is associated with temperature increases elsewhere, thus leading indirectly to tropical heating anomalies. However, some resolution of these competing influences is found in the CCSM4 experiments with prescribed future reductions in Arctic sea ice by Deser et al. (2015), which showed that the induced Arctic warming from ice loss alone caused additional warming in the upper-troposphere tropics along with significantly stronger westerlies between 30° and 40°N—even excluding SST changes elsewhere in the world—suggesting that the additional tropical heating in their fully coupled simulation further strengthened the zonal winds in this band.

Although our study does not provide a conclusive answer to the role of the Arctic in affecting midlatitude atmospheric circulation and weather extremes, it does augment the body of evidence suggesting that AA exerts a remote climatic influence that is highly variable by both latitude and season. In particular, our findings point to a potentially important contribution from enhanced terrestrial Arctic warming during spring–summer, a piece of the story that has been overshadowed by the widespread research focus on wintertime heating from sea ice loss. However, the recent decline in hemispheric spring snow-cover extent has actually outpaced the corresponding reduction in sea ice coverage in both absolute and relative terms (Derksen and Brown 2012). Assuming that spring snow extent will continue its downward trend, the results from LENS suggest that this change may have important repercussions beyond the Arctic by influencing the large-scale extratropical circulation in a way that helps to explain the commonly simulated drying and enhanced heating of interior North America.

Acknowledgments. This project has been supported by NSF Grants PLR-1304398, PLR-1304097, AGS-1407360, AGS-1203430, and AGS-1602771. Computing resources on the Yellowstone supercomputer were provided by NCAR's Computational and Information Systems Laboratory, sponsored by the National Science Foundation.

REFERENCES

Alexander, M. A., R. Tomas, C. Deser, and D. M. Lawrence, 2010: The atmospheric response to projected terrestrial snow changes in the late twenty-first century. *J. Climate*, **23**, 6430–6437, doi:10.1175/2010JCLI3899.1.

Barnes, E. A., 2013: Revisiting the evidence linking Arctic amplification to extreme weather in midlatitudes. *Geophys. Res. Lett.*, **40**, 4734–4739, doi:10.1002/grl.50880.

——, and L. M. Polvani, 2015: CMIP5 projections of Arctic amplification, of the North American/North Atlantic circulation, and of their relationship. *J. Climate*, **28**, 5254–5271, doi:10.1175/JCLI-D-14-00589.1.

——, and J. A. Screen, 2015: The impact of Arctic warming on the midlatitude jet-stream: Can it? Has it? Will it? *Wiley Interdiscip. Rev.: Climate Change*, **6**, 277–286, doi:10.1002/wcc.337.

——, E. Dunn-Sigouin, G. Masato, and T. Woolings, 2014: Exploring recent trends in Northern Hemisphere blocking. *Geophys. Res. Lett.*, **41**, 638–644, doi:10.1002/2013GL058745.

Barriopedro, D., R. García-Herrera, A. R. Lupo, and E. Hernandez, 2006: A climatology of Northern Hemisphere blocking. *J. Climate*, **19**, 1042–1063, doi:10.1175/JCLI3678.1.

Brewer, M. C., and C. F. Mass, 2016: Projected changes in western U.S. large-scale summer synoptic circulations and variability in CMIP5 models. *J. Climate*, **29**, 5965–5978, doi:10.1175/JCLI-D-15-0598.1.

Cattiaux, J., Y. Peings, D. Saint-Martin, N. Trou-Kechout, and S. J. Vavrus, 2016: Sinuosity of midlatitude atmospheric flow in a warming world. *Geophys. Res. Lett.*, **43**, 8259–8268, doi:10.1002/2016GL070309.

Chang, E. K. M., Y. Guo, and X. Xia, 2012: CMIP5 multimodel ensemble projection of storm track change under global warming. *J. Geophys. Res.*, **117**, D23118, doi:10.1029/2012JD018578.

Chang, F.-C., and J. M. Wallace, 1987: Meteorological conditions during heat waves and droughts in the United States Great Plains. *Mon. Wea. Rev.*, **115**, 1253–1269, doi:10.1175/1520-0493(1987)115<1253:MCDHWA>2.0.CO;2.

Chen, G., J. Lu, D. A. Burrows, and L. R. Leung, 2015: Local finite-amplitude wave activity as an objective diagnostic of midlatitude extreme weather. *Geophys. Res. Lett.*, **42**, 10 952–10 960, doi:10.1002/2015GL066959.

Cohen, J., J. Foster, M. Barlow, K. Saito, and J. Jones, 2010: Winter 2009–2010: A case study of an extreme Arctic Oscillation event. *Geophys. Res. Lett.*, **37**, L17707, doi:10.1029/2010GL044256.

——, and Coauthors, 2014: Recent Arctic amplification and extreme mid-latitude weather. *Nat. Geosci.*, **7**, 627–637, doi:10.1038/ngeo2234.

Coumou, D., J. Lehmann, and J. Beckmann, 2015: The weakening summer circulation in the Northern Hemisphere mid-latitudes. *Science*, **348**, 324–327, doi:10.1126/science.1261768.

Crawford, A., and M. Serreze, 2015: A new look at the summer Arctic frontal zone. *J. Climate*, **28**, 737–754, doi:10.1175/JCLI-D-14-00447.1.

Dee, D. P., and Coauthors, 2011: The ERA-Interim reanalysis: Configuration and performance of the data assimilation system. *Quart. J. Roy. Meteor. Soc.*, **137**, 553–597, doi:10.1002/qj.828.

Derksen, C., and R. Brown, 2012: Spring snow cover extent reductions in the 2008–2012 period exceeding climate model projections. *Geophys. Res. Lett.*, **39**, L19504, doi:10.1029/2012GL053387.

Deser, C., R. A. Tomas, and L. Sun, 2015: The role of ocean–atmosphere coupling in the zonal-mean atmospheric response to Arctic sea ice loss. *J. Climate*, **28**, 2168–2186, doi:10.1175/JCLI-D-14-00325.1.

Di Capua, G., and D. Coumou, 2016: Changes in meandering of the Northern Hemisphere circulation. *Environ. Res. Lett.*, **11**, 094028, doi:10.1088/1748-9326/11/9/094028.

Douville, H., J. Colin, E. Krug, J. Cattiaux, and S. Thao, 2016: Midlatitude daily summer temperatures reshaped by soil moisture under climate change. *Geophys. Res. Lett.*, **43**, 812–818, doi:10.1002/2015GL066222.

Francis, J. A. and S. J. Vavrus, 2012: Evidence linking Arctic amplification to extreme weather in mid-latitudes. *Geophys. Res. Lett.*, **39**, L06801, doi:10.1029/2012GL051000.

——, and N. Skific, 2015: Evidence linking rapid Arctic warming to mid-latitude weather patterns. *Philos. Trans. Roy. Soc. London*, **373A**, 20140170, doi:10.1098/rsta.2014.0170.

——, and S. Vavrus, 2015: Evidence for a wavier jet stream in response to rapid Arctic warming. *Environ. Res. Lett.*, **10**, 014005, doi:10.1088/1748-9326/10/1/014005.

Gleason, K. L., J. H. Lawrimore, D. H. Levinson, T. R. Karl, and D. J. Karoly, 2008: A revised U.S. climate extremes index. *J. Climate*, **21**, 2124–2137, doi:10.1175/2007JCLI1883.1.

Gregory, J. M., J. F. B. Mitchell, and A. J. Brady, 1997: Summer drought in northern midlatitudes in a time-dependent CO_2 climate experiment. *J. Climate*, **10**, 662–686, doi:10.1175/1520-0442(1997)010<0662:SDINMI>2.0.CO;2.

Held, I., 1993: Large-scale dynamics and global warming. *Bull. Amer. Meteor. Soc.*, **74**, 228–241, doi:10.1175/1520-0477(1993)074<0228:LSDAGW>2.0.CO;2.

Honda, M., J. Inoue, and S. Yamane, 2009: Influence of low Arctic sea-ice minima on anomalously cold Eurasian winters. *Geophys. Res. Lett.*, **36**, L08707, doi:10.1029/2008GL037079.

Huang, C. S., and N. Nakamura, 2016: Local finite-amplitude wave activity as a diagnostic of anomalous weather events. *J. Atmos. Sci.*, **73**, 211–229, doi:10.1175/JAS-D-15-0194.1.

Kalnay, E., and Coauthors, 1996: The NCEP/NCAR 40-Year Reanalysis Project. *Bull. Amer. Meteor. Soc.*, **77**, 437–471, doi:10.1175/1520-0477(1996)077<0437:TNYRP>2.0.CO;2.

Kay, J. E., and Coauthors, 2015: The Community Earth System Model (CESM) Large Ensemble Project: A community resource for studying climate change in the presence of internal climate variability. *Bull. Amer. Meteor. Soc.*, **96**, 1333–1349, doi:10.1175/BAMS-D-13-00255.1.

Kennedy, D., T. Parker, T. Woolings, B. Harvey, and L. Shaffrey, 2016: The response of high-impact blocking weather systems to climate change. *Geophys. Res. Lett.*, **43**, 7250–7258, doi:10.1002/2016GL069725.

Kentarchos, A. S., and T. D. Davies, 1998: A climatology of cut-off lows at 200 hPa in the Northern Hemisphere, 1990–1994. *Int. J. Climatol.*, **18**, 379–390, doi:10.1002/(SICI)1097-0088(19980330)18:4<379::AID-JOC257>3.0.CO;2-F.

Knutti, R., D. Masson, and A. Gettelman, 2013: Climate model genealogy: Generation CMIP5 and how we got there. *Geophys. Res. Lett.*, **40**, 1194–1199, doi:10.1002/grl.50256.

Kug, J.-S., J.-H. Jeong, Y.-S. Jang, B.-M. Kim, C. K. Folland, S.-K. Min, and S.-W. Son, 2015: Two distinct influences of Arctic warming on cold winters over North America and East Asia. *Nat. Geosci.*, **8**, 759–762, doi:10.1038/ngeo2517.

Lau, N.-C., and M. J. Nath, 2012: A model study of heat waves over North America: Meteorological aspects and projections for the twenty-first century. *J. Climate*, **25**, 4761–4784, doi:10.1175/JCLI-D-11-00575.1.

Lehmann, J., D. Coumou, K. Frieler, A. V. Eliseev, and A. Levermann, 2014: Future changes in extratropical storm tracks and baroclinicity under climate change. *Environ. Res. Lett.*, **9**, 084002, doi:10.1088/1748-9326/9/8/084002.

Liu, J., J. A. Curry, H. Wang, M. Song, and R. M. Horton, 2012: Impact of declining Arctic sea ice on winter snowfall. *Proc. Natl. Acad. Sci. USA*, **109**, 4074–4079, doi:10.1073/pnas.1114910109.

Lu, J., G. A. Vecchi, and T. Reichler, 2007: Expansion of the Hadley cell under global warming. *Geophys. Res. Lett.*, **34**, L06805, doi:10.1029/2006GL028443.

Madden, R. A., and J. Williams, 1978: The correlation between temperature and precipitation in the United States and Europe. *Mon. Wea. Rev.*, **106**, 142–147, doi:10.1175/1520-0493(1978)106<0142:TCBTAP>2.0.CO;2.

Maloney, E. D., and Coauthors, 2014: North American climate in CMIP5 experiments: Part III: Assessment of twenty-first-century projections. *J. Climate*, **27**, 2230–2270, doi:10.1175/JCLI-D-13-00273.1.

Mann, H. B., 1945: Nonparametric tests against trend. *Econometrica*, **13**, 245–259, doi:10.2307/1907187.

Matsumura, S., and K. Yamazaki, 2012: Eurasian subarctic summer climate in response to anomalous snow cover. *J. Climate*, **25**, 1305–1317, doi:10.1175/2011JCLI4116.1.

——, X. Zhang, and K. Yamazaki, 2014: Summer Arctic atmospheric circulation response to spring Eurasian snow cover and its possible linkage to accelerated sea ice decrease. *J. Climate*, **27**, 6551–6558, doi:10.1175/JCLI-D-13-00549.1.

Meehl, G. A., and C. Tebaldi, 2004: More intense, more frequent, and longer lasting heat waves in the 21st century. *Science*, **305**, 994–997, doi:10.1126/science.1098704.

Mo, K. C., J. N. Paegle, and R. W. Higgins, 1997: Atmospheric processes associated with summer floods and droughts in the central United States. *J. Climate*, **10**, 3028–3046, doi:10.1175/1520-0442(1997)010<3028:APAWSF>2.0.CO;2.

Nakamura, N., 1996: Two-dimensional mixing, edge formation, and permeability diagnosed in an area coordinate. *J. Atmos. Sci.*, **53**, 1524–1537, doi:10.1175/1520-0469(1996)053<1524:TDMEFA>2.0.CO;2.

——, and A. Solomon, 2010: Finite-amplitude wave activity and mean flow adjustments in the atmospheric general circulation. Part I: Quasigeostrophic theory and analysis. *J. Atmos. Sci.*, **67**, 3967–3983, doi:10.1175/2010JAS3503.1.

Newson, R. L., 1973: Response of a general circulation model of the atmosphere to removal of the Arctic ice cap. *Nature*, **241**, 39–40, doi:10.1038/241039b0.

Otto-Bliesner, B. L., E. C. Brady, G. Clauzet, R. Tomas, S. Levis, and Z. Kothavala, 2006: Last Glacial Maximum and Holocene climate in CCSM3. *J. Climate*, **19**, 2526–2544, doi:10.1175/JCLI3748.1.

Overland, J. E., J. A. Francis, R. Hall, E. Hanna, S.-J. Kim, and T. Vihma, 2015: The melting Arctic and midlatitude weather patterns: Are they connected? *J. Climate*, **28**, 7917–7932, doi:10.1175/JCLI-D-14-00822.1.

Petoukhov, V., and V. Semenov, 2010: A link between reduced Barents-Kara sea ice and cold winter extremes over northern continents. *J. Geophys. Res.*, **115**, D21111, doi:10.1029/2009JD013568.

——, S. Rahmstorf, S. Petri, and H. J. Schellnhuber, 2013: Quasiresonant amplification of planetary waves and recent

Northern Hemisphere weather extremes. *Proc. Natl. Acad. Sci. USA*, **110**, 5336–5341, doi:10.1073/pnas.1222000110.

Price, J. D., and G. Vaughan, 1992: Statistical studies of cutoff-low systems. *Ann. Geophys.*, **10**, 96–102.

Rivière, G., 2011: A dynamical interpretation of the poleward shift of the jet streams in global warming scenarios. *J. Atmos. Sci.*, **68**, 1253–1272, doi:10.1175/2011JAS3641.1.

Rohli, R. V., K. M. Wrona, and M. J. McHugh, 2005: January Northern Hemisphere circumpolar vortex variability and its relationship with hemispheric temperature and regional teleconnections. *Int. J. Climatol.*, **25**, 1421–1436, doi:10.1002/joc.1204.

Rossby, C.-G., and Coauthors, 1939: Relation between variations in the intensity of the zonal circulation of the atmosphere and the displacements of the semi-permanent centers of action. *J. Mar. Res.*, **2**, 38–54.

Rowell, D. P., 2009: Projected midlatitude continental summer drying: North America versus Europe. *J. Climate*, **22**, 2813–2833, doi:10.1175/2008JCLI2713.1.

——, and R. G. Jones, 2006: Causes and uncertainty of future summer drying over Europe. *Climate Dyn.*, **27**, 281–299, doi:10.1007/s00382-006-0125-9.

Scheff, J., and D. M. W. Frierson, 2012: Robust future precipitation declines in CMIP5 largely reflect the poleward expansion of model subtropical dry zones. *Geophys. Res. Lett.*, **39**, L18704, doi:10.1029/2012GL052910.

Screen, J. A., and I. Simmonds, 2013: Exploring links between Arctic amplification and mid-latitude weather. *Geophys. Res. Lett.*, **40**, 959–964, doi:10.1002/grl.50174.

——, and ——, 2014: Amplified mid-latitude planetary waves favour particular regional weather extremes. *Nat. Climate Change*, **4**, 704–709, doi:10.1038/nclimate2271.

Sen, P. K., 1968: Estimates of the regression coefficient based on Kendall's tau. *J. Amer. Stat. Assoc.*, **63**, 1379–1389, doi:10.1080/01621459.1968.10480934.

Singh, D. S., D. L. Swain, J. S. Mankin, D. E. Horton, L. N. Thomas, B. Rajaratnam, and N. S. Diffenbaugh, 2016: Recent amplification of the North American winter temperature dipole. *J. Geophys. Res. Atmos.*, **121**, 9911–9928, doi:10.1002/2016JD025116.

Su, H., Z.-L. Yang, R. E. Dickinson, and J. Wei, 2014: Spring soil moisture–precipitation feedback in the Southern Great Plains: How is it related to large-scale atmospheric conditions? *Geophys. Res. Lett.*, **41**, 1283–1289, doi:10.1002/2013GL058931.

Teng, H., G. W. Branstator, G. A. Meehl, and W. M. Washington, 2016: Projected intensification of subseasonal temperature variability and heat waves in the Great Plains. *Geophys. Res. Lett.*, **43**, 2165–2173, doi:10.1002/2015GL067574.

Thompson, D. W. J., and J. M. Wallace, 1998: The Arctic Oscillation signature in the wintertime geopotential height and temperature fields. *Geophys. Res. Lett.*, **25**, 1297–1300, doi:10.1029/98GL00950.

——, and ——, 2001: Regional climate impacts of the Northern Hemisphere annular mode. *Science*, **293**, 85–88, doi:10.1126/science.1058958.

Trenberth, K. E., and D. J. Shea, 2005: Relationships between precipitation and surface temperature. *Geophys. Res. Lett.*, **32**, L14703, doi:10.1029/2005GL022760.

Vavrus, S., 2007: The role of terrestrial snow cover in the climate system. *Climate Dyn.*, **29**, 73–88, doi:10.1007/s00382-007-0226-0.

Vihma, T., 2014: Effects of Arctic sea ice decline on weather and climate: A review. *Surv. Geophys.*, **35**, 1175–1214, doi:10.1007/s10712-014-9284-0.

Walsh, J. E., 2014: Intensified warming of the Arctic: Causes and impacts on middle latitudes. *Global Planet. Change*, **117**, 52–63, doi:10.1016/j.gloplacha.2014.03.003.

Wang, L., and N. Nakamura, 2015: Covariation of finite-amplitude wave activity and the zonal mean flow in the midlatitude troposphere: 1. Theory and application to the Southern Hemisphere summer. *Geophys. Res. Lett.*, **42**, 8192–8200, doi:10.1002/2015GL065830.

Wetherald, R. T., and S. Manabe, 1999: Detectability of summer dryness caused by greenhouse warming. *Climatic Change*, **43**, 495–511, doi:10.1023/A:1005499220385.

Willson, M. A. G., 1975: A wavenumber-frequency analysis of large-scale tropospheric motions in the extratropical Northern Hemisphere. *J. Atmos. Sci.*, **32**, 478–488, doi:10.1175/1520-0469(1975)032<0478:AWFAOL>2.0.CO;2.

Yang, J., Q. Liu, Z. Liu, L. Wu, and F. Huang, 2009: Basin mode of Indian Ocean sea surface temperature and Northern Hemisphere teleconnection. *Geophys. Res. Lett.*, **36**, L19705, doi:10.1029/2009GL039559.

NASA Public Access
Author manuscript
US CLIVAR Rep. Author manuscript; available in PMC 2019 October 19.

Published in final edited form as:
US CLIVAR Rep. 2018 March ; N/A: . doi:10.5065/D6TH8KGW.

ARCTIC CHANGE AND POSSIBLE INFLUENCE ON MID-LATITUDE CLIMATE AND WEATHER:

A US CLIVAR White Paper

J. Cohen[1], **X. Zhang**[2], **J. Francis**[3], **T. Jung**[4], **R. Kwok**[5], **J. Overland**[6], **T. Ballinger**[7], **R. Blackport**[8], **U.S. Bhatt**[2], **H. Chen**[9], **D. Coumou**[10], **S. Feldstein**[9], **D. Handorf**[4], **M. Hell**[11], **G. Henderson**[12], **M. Ionita**[4], **M. Kretschmer**[10], **F. Laliberte**[13], **S. Lee**[9], **H. Linderholm**[14], **W. Maslowski**[15], **I. Rigor**[16], **C. Routson**[17], **J. Screen**[8], **T. Semmler**[4], **D. Singh**[18], **D. Smith**[19], **J. Stroeve**[20], **P.C. Taylor**[21], **T. Vihma**[22], **M. Wang**[16], **S. Wang**[23], **Y. Wu**[24], **M. Wendisch**[25], **J. Yoon**[26]

[1]Atmospheric and Environmental Research, Inc.

[2]University of Alaska Fairbanks.

[3]Rutgers University.

[4]Alfred Wegener Institute Helmholtz Centre for Polar and Marine Research.

[5]Jet Propulsion Laboratory.

[6]NOAA/PMEL.

[7]Department of Geography, Texas State University.

[8]University of Exeter.

[9]Pennsylvania State University.

[10]Potsdam Institute for Climate Impact Research / VU Amsterdam.

[11]Scripps Institute of Oceanography/UCSD.

[12]United States Naval Academy.

[13]Environment and Climate Change Canada.

[14]University of Gothenburg.

[15]Naval Postgraduate School.

[16]University of Washington.

[17]Northern Arizona University.

[18]Lamont-Doherty Earth Observatory, Columbia University.

[19]Met Office Hadley Center.

[20]University College London.

[21]NASA Langley Research Center.

[22]Finnish Meteorological Institute.

NASA Author Manuscript
NASA Author Manuscript
NASA Author Manuscript

NASA Author Manuscript NASA Author Manuscript NASA Author Manuscript

[23]Utah Climate Center/Dept. PSC/Utah State Univ.

[24]Purdue University.

[25]University of Leipzig.

[26]Gwangju Institute of Science and Technology.

EXECUTIVE SUMMARY

The Arctic has warmed more than twice as fast as the global average since the mid 20th century, a phenomenon known as Arctic amplification (AA). These profound changes to the Arctic system have coincided with a period of ostensibly more frequent events of extreme weather across the Northern Hemisphere (NH) mid-latitudes, including extreme heat and rainfall events and recent severe winters. Though winter temperatures have generally warmed since 1960 over mid-to-high latitudes, the acceleration in the rate of warming at high-latitudes, relative to the rest of the NH, started approximately in 1990. Trends since 1990 show cooling over the NH continents, especially in Northern Eurasia.

The possible link between Arctic change and mid-latitude climate and weather has spurred a rush of new observational and modeling studies. A number of workshops held during 2013–2014 have helped frame the problem and have called for continuing and enhancing efforts for improving our understanding of Arctic-mid-latitude linkages and its attribution to the occurrence of extreme climate and weather events. Although these workshops have outlined some of the major challenges and provided broad recommendations, further efforts are needed to synthesize the diversified research results to identify where community consensus and gaps exist.

Building upon findings and recommendations of the previous workshops, the US CLIVAR Working Group on Arctic Change and Possible Influence on Mid-latitude Climate and Weather convened an international workshop at Georgetown University in Washington, DC, on February 1–3, 2017. Experts in the fields of atmosphere, ocean, and cryosphere sciences assembled to assess the rapidly evolving state of understanding, identify consensus on knowledge and gaps in research, and develop specific actions to accelerate progress within the research community. With more than 100 participants, the workshop was the largest and most comprehensive gathering of climate scientists to address the topic to date. In this white paper, we synthesize and discuss outcomes from this workshop and activities involving many of the working group members.

Workshop findings

Rapid Arctic change – Emergence of new forcing (external and internal) of atmospheric circulation: Rapid Arctic change is evident in the observations and is simulated and projected by global climate models. AA has been attributed to sea ice and snow decline (regionally and seasonally varying). However this cannot explain why AA is greatest in winter and weakest in summer. It was argued at the workshop that other factors can also greatly contribute to AA including: increased downwelling longwave radiation from greenhouse gases (including greater water vapor concentrations from local and remote sources); increasing ocean heat content, due to local and remote processes; regional and hemispheric atmospheric circulation changes; increased poleward heat transport in the atmosphere and ocean; and cloud radiative forcing. In particular, there is emerging observational evidence that an enhanced poleward transport of sensible and

NASA Author Manuscript NASA Author Manuscript NASA Author Manuscript

latent heat plays a very important role in the AA of the recent decades, and that this enhancement is mostly fueled by changes in the atmospheric circulation. We concluded that our understanding of AA is incomplete, especially the relative contributions from the different radiative, thermodynamic, and dynamic processes.

Arctic mid-latitude linkages – Focusing on seasonal and regional linkages and addressing sources of inconsistency and uncertainty among studies: The topic of Arctic mid-latitude linkages is controversial and was vigorously debated at the workshop. However, we concluded that rapid Arctic change is contributing to changes in mid-latitude climate and weather, as well as the occurrence of extreme events. But how significant the contribution is and what mechanisms are responsible are less well understood. Based on the synthesis efforts of observational and modeling studies, we identified a list of proposed physical processes or mechanisms that may play important roles in linking Arctic change to mid-latitude climate and weather. The list, ordered from high to low confidence, includes: increasing geopotential thickness over the polar cap; weakening of the thermal wind; modulating stratosphere-troposphere coupling; exciting anomalous planetary waves or stationary Rossby wave trains in winter and modulating transient synoptic waves in summer; altering storm tracks and behavior of blockings; and increasing frequency of occurrence of summer wave resonance. The pathway considered most robust is the propagation of planetary/Rossby waves excited by the diminished Barents-Kara sea ice, contributing to a northwestward expansion and intensification of the Siberian high leading to cold Eurasian winters.

Opportunities and recommendations—An important goal of the workshop was achieved: to hasten progress towards consensus understanding and identification of knowledge gaps. Based on the workshop findings, we identify specific opportunities to utilize observations and models, particularly a combination of them, to enable and accelerate progress in determining the mechanisms of rapid Arctic change and its mid-latitude linkages.

Observations: Due to the remoteness and harsh environmental conditions of the Arctic, *in situ* observational time series are highly limited spatially and temporally in the region.

Six recommendations to expand approaches using observational datasets and analyses of Arctic change and mid-latitude linkages include:

1. Synthesize new Arctic observations;
2. Create physically-based sea ice–ocean surface forcing datasets;
3. Systematically employ proven and new metrics;
4. Analyze paleoclimate data and new longer observational datasets;
5. Utilize new observational analysis methods that extend beyond correlative relationships; and
6. Consider both established and new theories of atmospheric and oceanic dynamics to interpret and guide observational and modeling studies.

Model experiments: We acknowledge that models provide the primary tool for gaining a mechanistic understanding of variability and change in the Arctic and at mid-latitudes. Coordinated modeling studies should include approaches using a hierarchy of models from conceptual, simple component, or coupled models to complex atmospheric climate models or fully

NASA Author Manuscript NASA Author Manuscript NASA Author Manuscript

coupled Earth system models. We further recommend to force dynamical models with consistent boundary forcings.

Three recommendations to advance modeling and synthesis understanding of Arctic change and mid-latitude linkages include:

1. Establish a Modeling Task Force to plan protocols, forcing, and output parameters for coordinated modeling experiments (Polar Amplification Model Intercomparison Project; PAMIP);
2. Furnish experiment datasets to the community through open access (via Earth System Grid); and
3. Promote analysis within the community of the coordinated modeling experiments to understand mechanisms for AA and to further understand pathways for Arctic mid-latitude linkages.

1 The character and mechanisms of Arctic Amplification

In light of recent scientific advances, the community should quantify the relative importance of processes that give rise to rapid Arctic warming and determine in what measure each process modulates how Arctic warming influences mid-latitude weather and climate variability.

The Arctic has warmed more than twice as fast as the global average since the mid 20th century (e.g., Blunden and Arndt 2012), a phenomenon referred to as Arctic Amplification (AA). In particular, AA was further enhanced during 1998–2012, showing a warming rate more than six times the global average (Huang et al. 2017). The high sensitivity of the Arctic climate change has been known for some time (Manabe and Wetherald 1975). Beginning with this early paper and reiterated recently, the high sensitivity of the Arctic climate to external forcing has been largely attributed to the reduction in the Arctic surface albedo. Our understanding of the mechanisms contributing to the enhanced Arctic warming, however, has significantly evolved in the last couple of decades, finding that other mechanisms may be more important, thus altering the currently accepted chain of causality.

Observed Arctic changes

For brevity, we limit the discussion of recent Arctic climate changes to surface temperature and sea ice, even though there are other notable changes (e.g., Greenland Ice Sheet and permafrost degradation). Figure 1a shows Arctic averaged surface air temperature (SAT) trends between 1981–2014. Arctic warming is evident in these datasets, with strongest warming during fall and weakest during summer. The vertical distribution of Arctic temperature trends, as reconstructed by reanalyses, shows warming that extends throughout the troposphere but strongest near the surface (Figure 1b–e).

Arctic climate change manifests visibly in the declining perennial sea ice cover (Kwok et al. 2009; Lang et al. 2017), which has intensified over the last few decades, resulting in a record minimum sea ice extent in September 2007 and a new record in 2012 (Figure 2; e.g., Comiso et al. 2008; Zhang et al. 2008). Seasonally, sea ice decline is most prominent over

NASA Author Manuscript NASA Author Manuscript NASA Author Manuscript

the western Arctic Ocean in summer and over the Nordic/Barents/Kara seas in winter (Figure 2). Additionally, the time between the spring melt and the fall freeze-up increased by roughly 5–11 days per decade. This lengthening of the sea ice-free season has been shown to influence the interactions between the Arctic atmosphere and surface (Stroeve et al. 2014).

Despite robust observed signals of AA, our knowledge of the mechanisms contributing to AA and their seasonal dependence remains incomplete. At the workshop, we agreed that the nature of AA, including its magnitude and mechanisms, likely influences the temporal and spatial character of Arctic and mid-latitude climate and weather linkages.

Arctic amplification mechanisms

The mechanisms of AA can be divided into two groups: local forcing and remote forcing. The local forcing group includes radiative forcing (from both greenhouse gases and cloudiness), sea ice-albedo feedback, lapse rate feedback, and surface turbulent heat fluxes from the Arctic Ocean. The conventional viewpoint places local forcing mechanisms as the trigger in the causal chain leading to AA (Manabe and Wetherald 1975). Mechanisms in the remote forcing group represent newer research, including forcing from the mid-latitudes and tropics, which are subsequently amplified by various feedback processes.

It can often be challenging to distinguish between the local and remote forcing. For example, an increase in Arctic clouds and atmospheric water vapor could result from a local forcing if cloud properties change in response to reduced sea ice cover. Alternatively, remote forcing can alter clouds through a change in moisture transport from lower latitudes. In either case, any increase in Arctic heating will be magnified owing to a variety of positive feedbacks involving ice, snow, and particular characteristics of the Arctic atmosphere.

Perhaps the best-known sensitivity in the Arctic is the sea ice albedo feedback (Perovich et al. 2008), owing its existence to the stark difference in albedo between open water and snow-covered sea ice surfaces (cf. ~7% with ~80% reflectance, respectively). The sea ice albedo feedback links the disappearance of sea ice to Arctic lower tropospheric warming and the subsequent melting of sea ice, and it has become common practice to conflate the two on climatological time scales (Screen and Simmonds 2010). However, modeling studies indicate that AA can occur in the absence of the sea ice albedo feedback (Alexeev et al. 2005), even though changes in sea ice have certainly altered the Arctic surface energy budget (Pistone et al. 2014). Recent research has forced us to question the role of sea ice albedo feedback in the causal chain driving AA. One outcome of the workshop was the need to disentangle the contributions of local and remote forcing on AA as a way to better guide scientific efforts on the issue of Arctic and mid-latitude linkages.

Surface turbulent fluxes of sensible and latent heat represent an important medium of transferring local forcing due to increasingly exposed warm ocean water into a mechanism for AA. Declining sea ice cover and extent (Figure 2) have enabled enhanced air-sea energy exchanges in recent years (Figure 3; Boisvert et al. 2015; Taylor et al. 2018).

Regional and seasonal variations in surface turbulent flux trends (Figure 3, top panels) may be important characteristics of AA and potential Arctic and mid-latitude linkages (Honda

NASA Author Manuscript NASA Author Manuscript NASA Author Manuscript

2009; Peings and Magnusdottir 2014; Feldstein and Lee 2014; Cohen et al. 2014; Kim et al. 2014). The largest increases in surface turbulent heat fluxes from the ocean to the atmosphere are found in the Chukchi and Kara seas. It is important to note that not all trends are positive. For instance, over the Bering Sea, Barents Sea, and the waters surrounding Greenland, both sensible (not shown) and latent heat flux trends are from the atmosphere into the ocean (negative in Figure 3 top left panel). However, over most of the Arctic, sensible and latent heat flux trends are small. An additional mechanism is that anomalous warmth in the lower atmosphere and surface are maintained longer into the early winter season, which supports larger geopotential thickness values (Figure 1, right) that, in turn, reduce poleward gradients and ultimately feed back into wind fields.

An equal, or possibly more important, sensitivity relates to the role of clouds in the surface energy budget. Arctic clouds warm the surface via enhanced downwelling longwave radiation for much of the year, except during June and July when the shortwave cloud radiative effect dominates, cooling the surface (Kay and L'Ecuyer 2013). The shortwave cloud effect is further complicated by the seasonal evolution of surface albedo. During summer, for instance, the surface albedo decreases owing to increased open ocean areas and melt pond fraction (Intrieri et al. 2002). The surface energy budget in climate models is also very sensitive to clouds. For example, small errors in simulating cloud amount and the cloud liquid/ice water optical path may be sufficient to perturb the surface energy balance and greatly influence sea ice concentrations simulated by climate models. Results presented at the workshop indicate that the Fifth Coupled Model Intercomparison Project (CMIP5) climate models disagree about whether Arctic cloud changes dampen or amplify AA (Taylor et al. 2017). This lack of consensus among models could be due to a number of factors discussed later.

The importance of downward longwave radiation on AA and sea ice has been identified by a number of studies (Uttal et al. 2002; Francis et al. 2005; Screen 2017). With respect to sea ice cover, emerging evidence suggests that anomalous cloud cover and downward longwave radiation during winter can hinder sea ice growth, thus impacting Arctic sea ice cover the following summer (Liu and Key 2014; Lee 2014; H.-S. Park et al. 2015b). As presented at the workshop, the CMIP5 climate models indicate that changes in the downwelling clear-sky longwave flux from the atmosphere, rather than the surface albedo feedback, are the largest contributing factor to simulated AA (Taylor et al. 2017), depending on partitioning of downward longwave and shortwave radiation due to cloud effects. The downward longwave radiation trend is positive almost everywhere over the Arctic Ocean for all seasons (Figure 3, bottom panel). The spatial trend patterns are substantially different from the corresponding surface heat flux, which exhibits both positive and negative signs (Figure 3, top panels). This dissonance in their trend patterns is consistent with the importance of the remote driving of the downward longwave radiation trends. During the period when AA has occurred and Arctic sea ice decrease has accelerated, it has been found that poleward atmospheric heat and moisture transport has been enhanced (Zhang et al. 2008; 2013), which acts as a remote driving of formation of clouds and increase in downward longwave radiation. Based on *in situ* measurements over Eureka, Canada (80°N, 86°W), Doyle et al. (2011) also report that warm, moist air intrusion events and attendant cloud radiative forcing regularly occur in Arctic winter (Kapsch et al. 2016). It was found that extreme warm and moist air intrusion

NASA Author Manuscript NASA Author Manuscript NASA Author Manuscript

from the North Atlantic into the Arctic can cause extreme warming event (Kim et al. 2017). This extreme intrusion occurs associated with poleward propagation of intense storms, which could be a manifestation of a long-term poleward shift of storm tracks (e.g., Zhang, et al. 2004; Serreze and Barrett 2008; Sepp and Jaagus 2011). Other recent studies have also highlighted the importance of spring extreme moisture transport into the Arctic in controlling the minimum sea-ice extent in the following September (Kapsch et al. 2013, Yang and Magnusdottir 2017, Yang and Magnusdottir 2018). Moisture transport is most pronounced through the N. Atlantic pathway and is favored during the Atlantic blocking weather regime (Yang and Magnusdottir 2017).

A comprehensive mechanistic understanding of AA requires knowledge of the source of increased Arctic heat and water vapor, as local sensible heat flux and evaporation versus remote transport have different implications to the causal chain of events leading to AA. The primary source of the Arctic atmospheric water is currently unclear. From the local process perspective, fluxes from the Arctic Ocean are obvious candidates. But with a global reanalysis dataset, it has been shown that over the past several decades horizontal moisture transport from lower latitudes has been a predominant source (Zhang et al. 2013), which could be a significant contributor to AA in the western Arctic during both winter (D.-S. Park et al. 2015a; Gong et al. 2017) and summer (Laliberté and Kushner 2014; Ding et al. 2017).

Tropical convection may also play an important role in forcing AA via heat and moisture transports during the cold season when the strong subtropical jet provides fertile grounds for a convection-driven Rossby wave source. Tropical convection can excite moisture intrusion events and Arctic warming on inter-decadal timescales (Lee et al. 2011; Cvijanovic et al. 2017) and in association with ENSO (Lee 2012). Furthermore, intraseasonal tropical convection also appears to influence daily Arctic surface temperature and sea ice concentration via the Madden Julian Oscillation (MJO) phase 5 in both summer and winter (Yoo et al. 2012a,b; Henderson et al. 2014). These heat and moisture transports are enhanced by poleward propagating Rossby waves, excited by the tropical convection, that constructively interfere with the climatological stationary eddies (Lee 2014; Goss et al. 2016; Cvijanovic et al 2017). Energetically, the convectively generated Rossby waves can warm the Arctic by releasing the mostly untapped zonal available potential energy, a process very effective at driving AA (Lee 2014).

Inter-model spread in AA

Despite unanimous agreement for the existence of AA, current-generation models strongly disagree on the overall strength and individual process contributions to rapid Arctic warming (Figure 4). The causes of this large inter-model spread in Arctic warming relate to many possible limitations in our modeling capabilities. In particular, uncertainties in model parameterizations hinder our ability to predict/project future Arctic sea ice extent and its potential interaction with mid-latitudes. Cloud microphysics, convection, boundary layer processes, and surface turbulent flux parameterizations primarily developed to ensure accurate forecasts in the tropics and the mid-latitudes are inadequate at high-latitudes (Bourassa et al. 2013). In fact, because tropical convective heating also triggers Arctic warming through Rossby wave propagation, inaccuracies outside of the Arctic, such as

NASA Author Manuscript

NASA Author Manuscript

NASA Author Manuscript

tropical convective parameterizations, could contribute to the uncertainty in the large-scale circulation (Stevens and Bony 2013; Sohn et al. 2016), hence Arctic warming. Deficiencies have also been identified in how models approximate the surface mass and momentum budget, including: surface albedo parameterizations (Dorn et al. 2009); sea ice rheology (Girard et al. 2009); fluxes across the atmosphere-ice-ocean boundary layer (Dorn et al. 2009; Hunke 2010); cloud radiative properties and simulation (Bromwich et al. 2009), and numerical techniques (Losch et al. 2010). This wide range of relevant processes speaks to the need for coupled models to realistically represent Arctic sea ice (Deser et al. 2015). Given these limitations, perhaps it is not surprising that the current generation of models disagree on the strength of the AA (Figure 4).

Improving our understanding of AA

Improving our understanding of AA requires increased accuracy of climate models and, therefore, improved process-level understanding. One major barrier to the development of the parameterizations specific to high-latitudes is the sparsity of observations, especially during the polar night. The logistics of cold and remote places demand that in situ data collection occur in short-lived and/or spatially concentrated field campaigns (Perovich et al. 1999; Wullschleger et al. 2011). Processes on scales of 1–10 km and 10 minutes to 6 hours are seldom resolved in the observational record, yet observational and modeling evidence indicates the importance of fine-scale features, especially in understanding Arctic interactions with the larger scales (Overland et al. 1995; Weiss and Marsan 2004). Moisture intrusions into the Arctic are often realized through atmospheric rivers (Liu and Barnes 2015; Baggett et al. 2016), yet they are not well represented by the current conventional climate models (Shields and Kiehl 2016). To address model deficiencies, we need ongoing and future field campaigns in all seasons that resolve key Arctic processes, including cloud-aerosol interactions, surface energy fluxes, sea ice processes, and snow on sea ice. We expect that progress on the polar atmospheric physics will be made possible through the assimilation of observations obtained during the Year of Polar Prediction and through other targeted field campaigns (e.g., MOSAiC and airborne Arctic cloud-aerosol measurements).

It has been well investigated that changes in the atmospheric circulation and resulting enhancement of poleward heat and moist air transport into the Arctic Ocean play an important role in causing Arctic warming and sea ice decrease (Rigor et al. 2002; Zhang et al. 2003). Recently studies further examined the observed structure of atmospheric warming. Although sea ice decline is found to be responsible for the recent Arctic warming (Screen and Simmonds 2010), it has recently been shown that remotely forced warming can also generate a bottom-heavy warming structure (Zhang et al. 2008; Yoo et al. 2013; Woods and Caballero 2016; Kim et al. 2017). Therefore, at least one symptom that had been perceived as key evidence of sea ice melting influencing AA could also be a consequence of warm, moist air intrusions. Whether the frequency and amplitude of moisture intrusions into the Arctic are changing remains an open question. Wood and Caballero (2016) find an increased frequency of moisture intrusions in the Barents and Kara seas, which would be attributed to changes in transient storm track dynamics (e.g. Zhang et al. 2004; Yin 2005; Villamil-Otero et al. 2018). Further research on this question is recommended.

NASA Author Manuscript NASA Author Manuscript NASA Author Manuscript

A more realistic simulation of time-dependent conditions of the Arctic sea ice cover and its effect on air-sea interactions is needed and requires coupled models. In addition, seasonal space-time variability in the extent of snow cover over Arctic land areas, land surface water, and energy budgets of seasonal permafrost melt are not well represented in most coupled land-atmosphere-sea ice models (Vaganov et al. 2000). Disentangling the relative importance of these and other sources of uncertainty in modeling Arctic sea ice and climate presents a major challenge. Part of the solution rests in improving the representation of processes within models through increased resolution and improved parameterizations. Another part lies in increasing the number of Arctic processes included in models. There is growing interest in the combined use of global Earth system models with regional models to better characterize uncertainty and improve probabilistic projections (Giorgi 2005). We argue that it is critical to advance hierarchical climate modeling (Maslowski et al. 2012) coordinated with the future Arctic observing system.

Beyond model improvements, we recommend analyses of the chain of events leading to AA in the current generation of models. Such analyses would identify dynamical and process differences between models and observations, helping to pinpoint processes that require further observational constraint. Dynamical differences, associated with too much or too little Arctic warming, could also help the community understand the large inter-model spread. These dynamical analyses require the use of high-frequency data (daily or less; Laliberté and Kushner 2014; D.-S. Park et al. 2015; Gong et al. 2017) and/or a careful analysis of monthly changes (Krikken and Hazeleger 2015). Due to the large data volume associated with high-frequency data, the working group is aware that such an approach would likely require a sustained focus on the development of shared diagnostic tools that could easily be ported from models to reanalyses and vice versa. We support continued efforts to archive model output at daily and subdaily scales — enabling process-level model evaluation — and recommend a focused MIP) aimed at resolving the process contributions to AA in climate models. It would be further be beneficial to the community to make the model data publicly available and preferably allow users to create web-based plotting of the archived data.

2 Arctic and mid-latitude linkage physics

Understanding Arctic and mid-latitude linkages is a societally important topic but difficult given its complexity. Arctic impacts on mid-latitudes are increasing, but they are mediated by chaotic jet stream dynamics. As noted in Section I, Arctic temperatures have experienced dramatic increases with new record highs in the winters of 2015–16 and 2016–17, with a potential to modify tropospheric and stratospheric jet streams. Such impacts will play a role in future subseasonal-to-seasonal (S2S) forecasts across the mid-latitudes. The issue is difficult as mid-latitude S2S conditions are also affected by large internal variability and mid-latitude and equatorial sea surface temperature anomalies. It appears that Arctic impacts will be regional and intermittent, clouding the identification of cause-and-effect and raising the issue of how to effectively communicate potential Arctic impacts.

Figure 5 illustrates the pathways of potential linkages from global change, through AA, to large-scale atmospheric wind patterns and finally to regional weather and extreme events.

NASA Author Manuscript

NASA Author Manuscript

NASA Author Manuscript

Tropospheric and stratospheric jet stream responses largely characterized by internal variability, which injects intermittency into linkage pathways, are particularly uncertain.

A well-predicted response of global climate change is the amplified Arctic warming, or AA, for the reasons noted in Section I. There is a greater thermodynamic connection of the surface with the overlying atmosphere due to extensive new sea ice-free areas in autumn and thinner sea ice in early winter months. This first link is through the thermal/geostrophic wind relationship that relates horizontal temperature gradients to vertical shear of the wind. A recent study using a regional reanalysis with the highest spatial resolution to date has revealed the complex, fine-scale relationships between winds, sea ice, and sea surface temperature, indicating an increase in surface wind towards the ice edge from both open water and thick sea ice areas (Zhang et al. 2018).

More complexity is introduced at the next stage where thermodynamic forcing and thermal wind modification in the Arctic interact with the internal variability of the tropospheric jet stream (white band in Figure 6) in the sub-Arctic, given by the gradient in the geopotential height field (Shepherd 2016). The tropospheric polar vortex structure is quasi-stable but can, chaotically to some degrees, shift between pattern shapes (such as in Figure 6a,b).

The physics driving changes in geopotential heights are described by the geopotential tendency equation (Holton 1979). Geopotential heights can change and, thus, modify wind fields by i) horizontal propagation of existing jet stream features that can be considered primarily a random part of atmospheric dynamics, ii) transport of low-level, warm air into a region, or iii) warming a region locally. Part of the difficulty with linkage research is quantifying the influence of thermal heating from Arctic sources relative to the other two contributions to geopotential height changes.

A final difficulty in the linkage chain (Figure 5) is the relationship of the large-scale atmospheric circulation patterns (Figure 6), which can last for weeks or can quickly break down, affecting local weather that can lead to extreme events. For example, the low geopotential height regions in Figure 6b can spawn local weather events regimes that travel eastward slowly, on timescales of days.

Possible links between how AA manifests and mid-latitude weather

A host of mechanisms and processes influence the surface and atmospheric temperatures in the Arctic and potentially contribute to AA as discussed in Section I. In recent years, significant attention has been given to the potential influence of AA on mid-latitude weather through its influence on the background temperature gradient and possible effects on the polar jet stream and storm track. For instance, enhanced surface turbulent fluxes from the surface to the atmosphere due to reduced sea ice cover represents a possible mechanism linking AA to mid-latitude weather. However, a probability distribution of Arctic sensible and latent heat fluxes reveals that at most times the fluxes are near zero, punctuated by significant episodic heat exchange events where surface turbulent fluxes exceed 100 W m^{-2} (Taylor et al. 2018). Therefore, the spatial variability and episodic nature of surface turbulent fluxes must be considered.

NASA Author Manuscript NASA Author Manuscript NASA Author Manuscript

This has two very important implications for AA and its linkages to mid-latitude weather. The first, and the most important, is that the exchange of sensible and latent heat fluxes from the surface is not constant in time but state-dependent. As indicated in previous studies (e.g., Rigor et al. 2002; Zhang et al. 2003; Zhang et al. 2008), there are strong heat and moisture transport from lower latitudes into the Arctic associated with the positive phase of the Arctic Oscillation (AO) or negative phase of the Arctic rapid change pattern. Under these conditions, very little exchange of heat and moisture occurs between the surface and the atmosphere owing to the associated weak vertical gradients in temperature and moisture. The lateral influx of heat and moisture due to changes in the atmospheric circulation, however, restricts sea ice growth and in some cases melts sea ice during winter (e.g., Rigor et al. 2002; Zhang et al. 2003; Zhang et al. 2008; Park et al. 2015a). However, when there is a flow of colder, drier air from the continent or solid ice pack associated with a particular atmospheric circulation pattern, such as the negative AO, an intense flux of heat and moisture occurs from the surface to the atmosphere. These conditions favor a strong forcing of the atmosphere by an ocean with no or thin ice cover, representing a state-dependent forcing. The second implication is that there is also a strong spatial variability in this forcing such that it is most prevalent in the marginal sea ice areas, such as the Barents and Kara seas.

We can also argue that hypothesized pathways linking the Arctic to mid-latitudes rely on a warming over the Arctic and not necessarily the disappearance of the sea ice. As described above, previous studies have indicated that changes in the atmospheric circulation, and their resultant poleward heat and moisture transport, play important driving role in Arctic warming and sea ice retreat (e.g., Rigor et al. 2002; Zhang et al. 2003; Zhang et al. 2008). Recent studies further suggest that a warming of the atmosphere over the Arctic through warm, moist air intrusions is an important contributor to sea ice loss (D.-S. Park et al. 2015; Woods and Caballero 2016), and these intrusions are caused by changes in the hemispheric atmospheric circulation in lower latitudes, rather than changes in the specific humidity (Lee et al. 2011; Zhang et al. 2013; Gong et al. 2017). Intruding mid-latitude warm, moist air leads to increased infrared radiation both upward and downward, the latter hindering sea ice growth (H.-S. Park et al. 2015a). This increase in downward infrared radiation arises from multiple factors, including the presence of warmer air due to both warm advection and latent heat release that results during cloud formation, as well as the increase in all three phases of water (Gong et al. 2017). This effect on sea ice is noticeable within several days of the intrusion (H.-S. Park et al. 2015a; Kapsch et al. 2016). Furthermore, studies such as D.-S. Park et al. (2015) and Gong et al. (2017) find that upward turbulent heat fluxes at the surface arise after the intrusions of warm, moist air. Therefore, even if this mechanism only partially accounts for the warming, it could have important implications for understanding linkages between the Arctic and mid-latitudes. For example, in climate model experiments that specify sea ice concentration and/or sea surface temperature anomalies, it is the upward turbulent heat fluxes from the surface that drive the Arctic and mid-latitude circulation (Deser et al. 2007). However, the aforementioned observational evidence suggests that the imposed negative sea ice concentration and positive sea surface temperature anomalies could in fact be caused by warm, moist intrusions from lower latitudes, which would result in a

NASA Author Manuscript

NASA Author Manuscript

NASA Author Manuscript

downward heat flux. If this is indeed correct, the causal chain of events is misrepresented in the model experiment, likely misrepresenting turbulent heat fluxes.

Hemispheric-wide response of AA

A key area of research for Arctic and mid-latitude linkages is to understand the two-way interactions between the tropospheric and stratospheric polar vortex. The jet stream from autumn to early winter is largely characterized by i) non-linear interactions between enhanced atmospheric planetary waves, such as in Figure 6, ii) irregular transitions between predominantly zonal and meridional flows, and iii) the maintenance of atmospheric blocking (near-stationary large-amplitude atmospheric waves) — all of which are not well understood or predicted by operational forecast models. The surface warming over the Arctic Ocean during the delayed re-freezing in autumn — along with increased heat fluxes and reduced vertical stability — may fuel strong storm systems to develop over the Arctic (Jaiser et al. 2012; Semmler et al. 2016; Basu et al. 2018). The non-linear interaction between storm systems and planetary-scale waves contributes to changes in atmospheric circulation, which allows enhanced upward propagation of energy in early- to mid-winter to weaken the stratospheric polar vortex. The conditions that trigger this interaction (e.g., wave structure and number: how many wavelengths there are around a latitude circle) are hard to predict, as they have a large chaotic component. Arctic and mid-latitude linkages may also be state-dependent, i.e., linkages may be more favorable in one atmospheric wave pattern than another, creating intermittency (Overland et al. 2016). The impact of anomalous transient storm systems on the growth and phasing of planetary waves, the onset and maintenance of blocks, and the strength and location of the Siberian high may be preconditioned by the state of the hemispheric atmospheric background flow.

While linkages in early winter have received the most attention by researchers owing to their influence on extreme winter weather, progress has also been made in understanding summer linkages. Here, there is an interaction of newly open water areas, atmospheric and oceanic frontal features, and phasing with high-amplitude/high-wavenumber atmospheric circulation features (Overland et al. 2012; Coumou et al. 2014). The summer season has seen an overall weakening of storm tracks over the last decades (Coumou et al. 2015), and this is also projected by future model projections (Lehmann et al, 2014). How a weakened flow might affect weather systems and especially their frequency is not fully understood (Coumou et al. 2017).

Though one might think that the concept of wavy versus zonal circulation patterns is straightforward, we have found challenges in quantifying these states. Approaches can be roughly separated into geometric and dynamic methods. The former focuses on the geometry of the circulation to characterize the departure of the flow from zonality in terms of wave amplitude, sinuosity, or circularity (Francis and Vavrus 2012; Cattiaux et al. 2016; Rohli et al. 2005; Di Capua and Coumou 2016). These metrics have the advantage of being intuitive and readily visualized from geopotential height contours, but they have been criticized for lacking a firm physical basis. By contrast, dynamically based waviness metrics, such as effective diffusivity of potential vorticity and finite-amplitude wave activity (Nakamura and Solomon 2010), are derived from first-order energy conservation principles.

NASA Author Manuscript NASA Author Manuscript NASA Author Manuscript

These measures provide a theoretical basis for relating changes in zonal wind speed to accompanying changes in wave amplitude, at least under idealized conditions. Such approaches are being applied in climatological studies of circulation trends and extreme weather events related to amplified flow patterns (Chen et al. 2015), but their derivation is more technical and their application more involved than recent geometric methods. An example of the results from sinuosity is shown in Figure 7. The time series for the North Atlantic (top) shows a weak trend and highlights year-to-year internal variability in such indices. The bottom diagram highlights the regional and seasonal nature of long-term positive trends.

At this point, there is no scientific consensus on which waviness metric or even category of methods is preferable. Our field may benefit from the variety of approaches to sort the most useful measures of waviness. In the meantime, the diversity of employed metrics complicates direct comparisons and conclusions drawn among studies. For example, Francis and Vavrus (2012) reported increasing wave amplitudes over the North American-Atlantic region during recent decades, whereas Barnes and Polvani (2015) applied a different wave-amplitude definition over the same domain and generally did not find increases observed in the past or projected into the future. More recent studies suggest complex circulation behavior, consisting of opposing trends in waviness depending on season, longitude, and latitude. For instance, future climate projections exhibit a trend towards increased sinuosity over the North American sector only, while other sectors exhibit unchanged or decreased waviness/blockings (Cattiaux et al. 2016, Di Capua and Coumou 2016; Peings et al. 2017; Vavrus et al. 2017). However, these changes are subject to high uncertainties due to internal variability and competing effect of low-latitude versus high-latitude warming on the response of the mid-latitude atmospheric dynamics (Peings et al. 2017, Deser et al. 2015, Blackport and Kushner 2017).

Regional Analyses

Asia—It has been well understood that AO modulates Asia surface air temperatures through altering warm and moist air transport (e.g., Thompson and Wallace 1998). Associated with positive (negative) AO, warm (cold) winter occurs in Eurasia and the Arctic and sea ice extent decreases (increases) (e.g., Rigor et al. 2002; Zhang et al. 2003). Honda et al. (2009) specifically examined a tropospheric dynamical pathway in which negative sea ice and positive air temperature anomalies over the Barents-Kara seas during autumn cause cold Eurasia-Far East temperatures in mid-to-late winter. In the troposphere, persistent constructive interference of lower-atmospheric warming with atmospheric Rossby waves into December/January may induce a negative AO-like pattern, which may continue into February/March. Kim et al. (2014) investigated the stratosphere pathway from both observational analysis and modeling experiments and found that sea ice loss can induce vertical propagation of planetary wave energy, which weakens the stratospheric polar vortex and then propagates wave energy downward into the troposphere, maintaining an amplified jet-stream pattern into mid-to-late winter (Figure 8).

In December and January, the additional oceanic heat and moisture release to the Arctic atmosphere can increase Siberian snow cover (Wegmann et al. 2015). The increased snow

NASA Author Manuscript NASA Author Manuscript NASA Author Manuscript

cover may enhance continental cooling and troughing over East Asia while strengthening the Siberian high upstream over northwest Eurasia. A ridge over northwestern Eurasia with a trough over northeastern Eurasia is favorable for the direct forcing of planetary waves with enhanced vertical propagation of wave energy into the stratosphere (Cohen et al. 2007; Nakamura et al. 2015). This can lead to wave breaking and disruption of the stratospheric polar vortex (Jaiser et al. 2016).

Such a negative AO-like circulation tends to produce atmospheric blocking over the Ural regions with an enhanced Siberian high (Hopsch et al. 2012; Mori et al. 2014). Such dynamically forced links can be extracted from observational data using causal discovery algorithms (Figure 9; from Kretschmer et al. 2016), indicating that these are real pathways and not spurious correlations. Figure 9 illustrates that low sea ice concentrations over the Barents-Kara seas lead to high pressure over Ural mountains, which leads to upward wave propagation (“v-flux”) and weakening of the stratospheric polar vortex. The anticyclonic anomaly first occurs over the Barents-Kara seas and Ural regions, bringing cold air from the Arctic to central Asia, which extends southeastward owing to a strengthened Siberian high. This southward flow of Arctic air has been implicated in more frequent or intensified cold surges over East Asia (Overland et al. 2015; Zuo et al. 2016). These processes are complicated by Arctic sea ice feedbacks (Li and Wang 2014; Luo et al. 2016; McCusker et al. 2016). While model simulations exhibit uncertainties in the Siberian high response, there is increasing evidence for the aforementioned processes taking place in recent decades.

North America—Potential connections between the North American Arctic and mid-latitudes depend on the constructive or destructive interactions with locations of existing large-scale waves in the jet stream. Climatological waves during winter usually consist of a ridge of higher geopotential heights over the northeastern Pacific and/or Greenland along with a trough of lower heights over central and eastern North America (Figure 6b), although a great deal of interannual variability is common. Of particular interest is the winter cooling trend in eastern North America since 1990 (Cohen et al. 2014). Although this trend coincides with Arctic warming (Kug et al. 2015; Lee et al. 2015; Cohen 2016), studies have also pointed to internal variability (Baxter and Nigam 2015) and influences from the tropical Pacific (Basu et al. 2013; Sun et al. 2016). Very recent work suggests a tropical response to Arctic warming that feeds back to the Arctic (Cvanovic et al 2017). Furthermore, Ayarzagüena and Screen (2016) and Trenary et al. (2016) do not see an increase in the number of cold events in data or future model projections.

The potential for the Arctic to influence eastern North America involves a modification and added persistence to the existing long-wave pattern. Figure 10 (left) shows the pattern of near-surface air temperatures that occurs during eastern North America cold events (note the warm Arctic/cold continent type pattern with positive temperature anomalies near southern Baffin Bay and in Alaska/East Siberia). Figure 10 (right) is the corresponding 250 hPa geopotential height anomaly field for cold events in eastern North America. Higher anomalies are collocated with the two regions of positive temperature anomalies, suggesting a surface/geopotential thickness connection. Higher regional Arctic geopotential heights increase the likelihood of Alaskan and/or Greenland blocks; further analyses suggest that these regional blocks are independent features. The geopotential height ridge along the US

NASA Author Manuscript NASA Author Manuscript NASA Author Manuscript

West Coast and the low heights over eastern North America are an amplification of the climatological late-autumn/early-winter wave pattern. The anomaly pattern over the North Atlantic Ocean exhibits a strong downstream storm track coincident with eastern North America cold events. While these historical teleconnections in Figure 10 do not necessarily involve Arctic change, Kug et al. (2015) suggest a recent (1980–2014) winter connection between warm temperatures in the Chukchi Sea and cold spells in eastern North America. Further, extreme sea ice loss and warm temperatures in the Chukchi region during November 2016 were consistent with this pattern, including a northward extension of the western ridge into the central Arctic along with an eastern cold event in early December 2016. Likewise, Ballinger et al. (2017) and Chen and Luo (2017) found variations in sea ice freeze onset in Baffin Bay and regional positive sea surface temperature anomalies were linked to 500-hPa blocking patterns and years of extreme late freeze conditions since 2006. Thus, it is overly simplistic to say that the Arctic could cause eastern North American cold spells, but near-future Arctic change has the potential to reinforce such cold events through tendencies to trigger the formation of Alaskan and Greenland blocks.

Europe—As is the case everywhere, potential linkages between Arctic warming and weather in Europe are complex in the sense that severe weather involves multiple causes. Greenland blocking tends to be associated with an abnormally southerly latitude of the storm track across the eastern Atlantic, which favors cold winters in northwestern Europe (Woollings et al. 2010). Evidence of connectivity between Barents-Kara sea ice loss and winter weather in northern Europe has been reported (Petoukhov and Semenov 2010; Orsolini et al. 2012; Liptak and Strong 2014), although variability in Europe's weather is principally associated with the North Atlantic Oscillation (NAO) and high-pressure cold air masses from the east. Over the North Atlantic, understanding NAO variability is complicated by differing factors that affect the strength and location of the Aleutian Low and Bermuda/Azores high, which, in turn, affect the strength and position of the eddy-driven jet. Further complexity is introduced by factors affecting the east Atlantic pattern, which is related to blocking over the eastern North Atlantic (Handorf and Dethloff 2012; Hall et al. 2015). Changes in the NAO and east Atlantic indices explain about 60% of the variability in the jet stream shift and strength. The primary influence of the North Atlantic eddy-driven jet stream on climate variability in northern and central Europe — together with the multitude of potential drivers for the variability of the eddy-driven jet, including North Atlantic SST, ENSO, quasi-biennial oscillation, and the highly non-linear intractions between the synoptic and planetary waves — point to large uncertainty in detecting robust impacts of Arctic climate changes on weather and climate over the North Atlantic-European region. Modeling experiments show a diversity of NAO and stratospheric polar vortex response to reduced Arctic sea ice. The atmospheric response is dependent on the pattern (Sun et al. 2015; Screen 2017), on the amplitude (Pethoukov and Semenov 2010, Peings and Magnusdottir 2014, Semenov and Latif 2015, Chen et al. 2016), and even in certain studies on the sign of sea ice anomalies (Liptak and Strong 2014). Dedicated multimodel experiments with coordinated protocol in sea ice prescription are needed to reconcile model results, as discussed in Section 3.

NASA Author Manuscript NASA Author Manuscript NASA Author Manuscript

Tropical influences

Observational studies suggest that tropical intraseasonal variations (e.g., MJO) may modulate Arctic temperature and atmospheric circulation (Yoo et al. 2013). Tropical influences stem from converging northward heat and moisture fluxes into the sub-Arctic, as well as through a stratospheric pathway from which anomalously warm Pacific sea surface temperatures during El Niño affect sub-Arctic weather conditions. Positive Pacific and/or Atlantic Ocean sea surface temperature anomalies can influence high-amplitude, stationary jet stream pattern anomalies (Basu et al. 2013; Sato et al. 2014; Cohen 2016). For example, Lee et al. (2015) found that the anomalously cold North American winter of 2013–14 was a result of the combination of anomalously warm sea surface temperatures in the tropical western Pacific, anomalously warm sea surface temperatures in the extratropical Pacific, and low sea ice concentration on the North Pacific side of the Arctic.

Cold Arctic outflows often intensify cyclonic disturbances that originate in mid-latitudes. The combination of extremely cold air with tropical inflow that occurs in typical/extratropical storms created recent severe weather events, such as Snowmaggedon in 2010, Superstorm Sandy in 2012, and the eastern North American cold outbreaks in January 2014 and February 2015. In early 2016, an extreme Arctic warming episode occurred concurrently with several extreme events worldwide, including heavy snow in the southwestern and northeastern US and over portions of Europe, as well as flooding in Great Britain and Ireland. These events also coincided with the near-record El Niño in 2016, which had a strong teleconnection influence conflating the impacts of Arctic influence, complicating attribution (Wang et al. 2017). Future progress on Arctic linkages and mid-latitude weather cannot remain an Arctic-only activity. The combination of Arctic forcing of mid-latitude weather linkages, combined with internal variability and equatorial and mid-latitude sea surface temperature forcings, provide a clear pathway forward for improving S2S weather outlooks.

Attribution of extreme weather events

The literature suggests that most linkages are regional and episodic, with timescales of weeks to a few months (Overland et al. 2016). As noted in earlier sections, the jet stream can act as a bridge between AA forcing and mid-latitude weather events. However, as noted earlier, there are many influences competing to modify mid-latitude weather including internal variability, and sometimes these other competing factors constructively and destructively interfere with Arctic forcing. A case for a potential linkage was December 2010, when a late freeze-up in Baffin Bay caused warm regional temperature anomalies and the dilation of upper-level atmospheric pressure surfaces (Ballinger et al. 2017). This contributed to the formation of a block in the geopotential height field, which in turn resulted in cold temperature anomalies in the eastern US. Rather than extremely cold temperatures, the main impact of this event was to increase the duration of the cold spell (Francis et al. 2017). Taken over a timescale of a whole season, however, there is less evidence for linkage impacts. Screen and Simmonds (2014) note the lack of changes in cold seasons during the last three decades and discount Arctic impacts based on seasonal and large-domain statistics, which may actually obscure the response as patterns align differently from one year to the next. Furthermore, Screen et al. (2015) and Ayarzaguena and Screen

NASA Author Manuscript

NASA Author Manuscript

NASA Author Manuscript

(2016) show future decreases in the frequency of occurrence of record-breaking cold seasons.

Often two or more weather events occur simultaneously owing to an amplified ridge/trough pattern across a continent. One example was the blizzard of February 2010 in the Washington, DC-region, referred to as Snowmageddon, in which cold air from the north met unusually warm, moist air from the south boosted by the coincident El Niño. A second example is hurricane Sandy in October 2012, one of the costliest hurricanes in US history. An extratropical weather system from the west merged with hurricane Sandy as it moved north, creating an intense, hybrid storm. Sandy tracked westward instead of a more normal track out to sea, owing to an atmospheric block southwest of Greenland. The storm surge, augmented by sea level rise, flooded about 1000 km of the eastern seaboard, including the New York subway system. It has been suggested that the exceptionally warm Arctic may have strengthened the blocking high that steered Sandy on its unusual path at the time (Greene et al. 2013).

Potential linkage pathways and confidence

Future progress on Arctic linkages to mid-latitude weather cannot remain an Arctic-only activity. The combination of Arctic forcing of mid-latitude weather linkages, combined with internal variability and equatorial and mid-latitude sea surface temperature forcings, provide a clear pathway forward for improving S2S weather outlooks.

Based on results from observational and modeling studies, physical processes or mechanisms have been proposed that may explain linkages between Arctic amplification and changes in mid-latitude climate and weather patterns. This list is not exhaustive and is ordered from high to low confidence based on the consensus of the scientists attending the workshop:

1. Low Barents-Kara sea ice favors a northwestward expansion and intensification of the Siberian high, contributing to cold Asian winters
2. Arctic warming causes increased geopotential thickness over the polar cap or regionally, leading to an equatorward shifted jet stream across the mid-latitude, which may have constructive/destructive interference with climatological ridging, and associated weather anomalies (e.g., colder temperatures, increased snowfall).
3. Weakening of horizontal temperature gradients and the thermal wind, working in opposition to prevailing wind direction
4. Modulating stratosphere-troposphere coupling
5. Exciting anomalous planetary waves or stationary Rossby waves in winter, weaker transient synoptic waves in summer and occurrence of blocks in all seasons.
6. Altering storm tracks and changes in the latitude of jet stream flow
7. Increasing frequency of occurrence of wave resonance

NASA Author Manuscript NASA Author Manuscript NASA Author Manuscript

3 Next steps and recommendations

An important goal of the workshop was achieved: to hasten progress towards consensus understanding and identification of knowledge gaps. Based on the workshop findings, we identify specific opportunities to utilize observations and models, particularly a combination of them, to enable and accelerate progress in determining the mechanisms of rapid Arctic change and its mid-latitude linkages.

Observations and reanalyses recommendations

Improvement of observational information concerning the Arctic can be achieved via i) better identification of datasets and assimilation of existing *in situ* and remote sensing observations into atmospheric and oceanic reanalyses, ii) increasing the spatial and temporal coverage of observations, and iii) developing new observational methods.

Forcing datasets available to investigate Arctic and mid-latitude linkages—To analyze the atmospheric response to changes in the Arctic, accurate data are needed for Arctic surface air pressure, atmospheric temperature profiles, sea ice concentration and thickness, snow extent and thickness, and soil moisture (e.g., Figure 11). These data will aid in assessing the realism of reanalysis fields as well as output from numerical weather prediction and climate models. They can also provide lower boundary conditions for atmospheric models and be assimilated into reanalyses.

Information on surface air pressure and air temperature profiles is vital for the analyses of Arctic and mid-latitude linkages. The surface air pressure field in the Arctic was considered to be reasonably well captured by atmospheric reanalyses already a decade ago (Bromwich and Fogt 2007). However, Inoue et al. (2009) found that poor coverage of drifting buoy data prior to 1979 led to inaccuracies in reanalyses and numerical forecasts. Inoue et al. (2009) further pointed out that the observational record may deteriorate in the future due to fewer opportunities for buoy deployments over the sea ice. The global surface temperature field is relatively accurate during the satellite era, and observations are available from various government centers (e.g., Operational Sea Surface Temperature and Sea Ice Analysis (OSTIA)). Although the effects of sea surface temperature changes on mid-latitude weather has been studied (Screen et al. 2012), the importance of the accuracy of the sea surface temperature datasets has not received much attention, but it is probably not a major issue in studies addressing the satellite era.

To assess the response of the Arctic atmosphere to changes in sea ice cover, a realistic representation of its temporal evolution is crucial. In general, the state is characterized by the sea ice concentration, thickness distribution, and snow depth. Since the advent of satellite multi-channel passive microwave observation systems in 1979, it has been possible to monitor the sea ice extent with a temporal resolution of less than a day and spatial resolution of about 25 km. Changes in the multi-year ice coverage (frequently used as a proxy for ice thickness) can also be estimated using passive and active microwave instruments on satellite platforms (Comiso 2012). During the ice growth season, estimates of monthly fields of sea ice thickness can now be derived from satellite altimeters (lidar and radar) at a fairly coarse resolution of about 25 km (Kwok et al. 2009).

NASA Author Manuscript NASA Author Manuscript NASA Author Manuscript

Not only is the abundance of open water important for assessing the atmospheric response, but also the thin ice (less than ~0.5 m) coverage within each grid element is essential. Available large-scale datasets are not tailored to provide this portion of the ice thickness distribution, thus it is essential that a 'realistic' dataset is synthesized using available observations for use in simulations. In parallel, an understanding of the sensitivity of the atmospheric responses to time-varying ice conditions should be developed, such that the shortcomings of available datasets could be better identified. There is an urgent need for more accurate information on sea ice and snow properties in conditions of compact ice cover (> 90% ice concentration) in winter and for better distinguishing between melt ponds and leads in summer.

Large-scale anomalies in soil moisture may generate surface temperature anomalies, which in turn effect planetary wave patterns and associated teleconnections. In addition, soil moisture may serve as an indicator of the Arctic's influence on the hydroclimate in different regions. One of the only long-term observational datasets of global surface soil moisture is assembled from multiple active and passive remote sensors by the European Space Agency (ESA), covering the period from 1978–2015 with 0.25° resolution (Liu et al. 2012). From 2002 to present, the Gravity Recovery and Climate Experiment (GRACE) satellite provides estimates of drought, through measurements of total terrestrial water storage in addition to surface soil moisture (Houborg et al. 2012). One of the limitations of such datasets is that they are only available at the monthly resolution. Soil moisture data with a higher temporal resolution (i.e., 3 hours) are available through data assimilation products like the Global Land Data Assimilation System (GLDAS), allowing more detailed investigations of the links between Arctic and mid-latitude extreme events that occur on sub-monthly timescales. Finally, more recent satellite missions, including ESA's Soil Moisture and Ocean Salinity (SMOS) launched in 2009 and NASA's Soil Moisture Active Passive (SMAP) launched in 2015, are aimed at providing high-resolution soil moisture measurements with global coverage in the near future.

High-quality observations of terrestrial snow cover are needed, as snow insulates the atmosphere from the ground heat source in autumn, insulates the ground from cold winter air, reflects most of spring insolation, and may contribute to the intensification of extended Ural and Siberian high pressure systems. Spring snow melt is important for the transition towards summer, controlling the strength and timing of processes involving the albedo feedback. Different datasets give contrasting results for the trend of Eurasian snow cover in autumn, and a recent study suggests that there are large spatial variations among datasets (Wegmann et al. 2017). The spring and early summer decline of terrestrial snow cover is evident, being twice as fast in June as the Arctic sea ice decline in September (Derksen et al. 2015). Long-term observations on snow water equivalent are limited in the high Arctic. Even GlobSnow, considered the most reliable snow water equivalent dataset, is inadequate for identifying the exact date of snowmelt. Snow products need to be improved in the Arctic for use in understanding climate trends and mechanisms. Observations of permafrost temperature and its relationship with snow depth have become available in recent decades (Romanovsky et al. 2010).

NASA Author Manuscript NASA Author Manuscript NASA Author Manuscript

New observational datasets and reanalyses that span most of the 20th century—Most of the research on past linkages between the Arctic and mid-latitudes is restricted to the period since 1979. To extend the time series and to investigate the effects of AA prior to the satellite era, additional sources of information are needed. For example, Walsh et al. (2015) have estimated the Arctic sea ice concentration from 1850 to 1979 based on ship observations, compilations by naval oceanographers, and analyses by national ice services. Monthly data are available in 0.25° × 0.25° resolution. Information on long-term snow, lake ice, and river ice data from the Eurasian Arctic exist at least in written archives, if not in digital format. Digitally available data include several long time series from the Scandinavian Arctic, ice breakup data from the Torne River since 1693, and snow cover data from Abisko, Sweden, since 1913, among others. A climatology of visually observed cloudiness over the Norwegian, Barents, and Kara seas is available since the late 19th century (Chernokulsky et al. 2017).

The reanalyses data starting from the late 1800s or 1900 are summarized in Table 1, along with information on spatial resolution and respective references. Two atmosphere-only reanalyses are available: the NOAA 20th century reanalysis (20CR) and the ECWMF's atmospheric reanalysis of the 20th century (ERA-20C). These reanalyses are generated by forcing the models with historical, time-varying sea surface temperature, sea ice concentration, and radiative fluxes, while assimilating surface air pressure observations. The 20CR reanalysis has a longer temporal coverage and provides a 56-member ensemble. The ERA-20C does not include an ensemble but has a higher horizontal (Table 1), vertical (91 levels relative to 28 levels in 20CR), and time (3-hourly compared to 6-hourly for 20CR) resolution. Both reanalyses are influenced by changes in the observational network of different variables. Due to its ensemble, the 20CR allows for a comprehensive examination of uncertainties. However, the higher resolution in the ERA-20C provides opportunities to study finer-scale processes. A coupled atmosphere-ocean reanalysis has been produced by the ECMWF, covering the same period as ERA-20C. In addition, two long-term ocean reanalyses are available. Using reanalyses in studies of AA and Arctic mid-latitude interactions, one should be aware of their errors and uncertainties, which are largest for clouds (Liu and Key 2016), Arctic boundary layer variables (Jakobson et al. 2012), as well as radiative and turbulent surface fluxes (Tastula et al. 2013). Fortunately the synoptic- and large-scale atmospheric circulation is better represented, although the products for years prior to 1979 suffer from the lack of assimilation of satellite data.

Paleoclimate perspective—Paleoclimate data offer centennial- to millennial-scale perspectives on environmental changes. Key intervals in Earth's past provide potential analogues to assess the impacts of Arctic warming on the mid-latitudes. For example, the early Holocene (~10,000 – 8,000 years ago) is one such interval when the Arctic and high-latitudes received enhanced average annual insolation with respect to the equator relative to the present, reducing the latitudinal temperature gradient. Also, on more recent timescales (e.g., over the past two millennia) variations in the mid-latitude and Arctic temperature gradient have occurred.

Paleoclimate archives include tree rings, sediments (lake, marine, and peat), speleothems, and glacier ice cores. Lake and marine sediments, as well as glacier ice cores, provide

NASA Author Manuscript NASA Author Manuscript NASA Author Manuscript

records of climate (e.g., temperature, moisture, and sea ice) over timescales from centuries to millennia. Annually resolved records, such as tree rings, provide high-resolution information, usually over shorter timescales of several parameters, including temperature, precipitation, and atmospheric circulation. The increasing number of gridded tree ring reconstructions facilitate detailed studies of Arctic impacts on mid-latitude climate during the last two millennia. Recent and ongoing paleoclimate data synthesis efforts give a unique opportunity to address the impacts of the Arctic on mid-latitude climate on a hemispheric scale: The Past Global Changes (PAGES) 2k project has synthesized over 600 global high-resolution temperature reconstructions. Presently, several regional, highly resolved (in time and space) reconstructions of drought and temperature exist for North America, Europe, and Asia, as well as for the whole Northern Hemisphere (Anchukaitis et al. 2017). Such products, together with reconstructions of Arctic climate conditions including sea ice changes (Kinnard et al. 2011), provide excellent means for fingerprinting regional mid-latitude impacts on Arctic climate change (Figure 12). Also, on longer timescales, such comparisons will soon become feasible. Preliminary global Holocene paleoclimate datasets have been published for temperature reconstructions (Marcott et al. 2013), and more comprehensive efforts to synthesize Holocene temperature and moisture records are underway.

Together, paleoclimate archives and recent data compilations will enable us to characterize past climate variability including Arctic sea ice extent and the Northern Hemisphere latitudinal temperature gradient, and to test if these changes had an impact on circulation and mid-latitude drought on timescales from centuries to millennia.

Process-level observations and new methods—Process-level observations from the Arctic originate from a limited number of partly permanent ground-based stations in the terrestrial Arctic (e.g., the International Arctic Systems for Observing the Atmosphere (IASOA)) and measurement campaigns (e.g., ship, aircraft) over the Arctic Ocean, mainly during spring and summer. Additional observations are needed of interactions between the open sea and atmosphere, sea ice and atmosphere, as well as terrestrial snow/ice and atmosphere. Among the key processes are the local and regional atmospheric responses to surface heating (e.g., due to loss of sea ice or snow), which depends on the physics of the boundary layer, cloud formation and persistence, vertical and horizontal distribution of radiative and turbulent energy fluxes, and baroclinicity around the lateral boundaries of the surface heat source. The observations should include solar (0.2–5 μm, shortwave) and terrestrial/thermal-infrared (3–50 μm, longwave) radiative fluxes; turbulent fluxes of momentum, heat, and moisture; and the effects of the fluxes on cloud formation and lifetime, air temperature, humidity, and wind in local and regional scales.

Recent advances in observation technology provide improved opportunities to quantify the state of the atmosphere, cryosphere, and the ocean. There is potential for a more extensive application of unmanned aerial vehicles (UAVs) in local and regional scales. Vertical profiles of air temperature, as well as wind speed and direction up to roughly 2 km, can be measured using small, cost-effective UAVs (Jonassen et al. 2015), and activities are ongoing to assimilate the data into numerical weather prediction models. Regional-scale UAV measurements are possible by using long-range aircraft, some of which can also release

NASA Author Manuscript NASA Author Manuscript NASA Author Manuscript

dropsondes (Intrieri et al. 2014). Further, controlled meteorological balloons have a high potential to contribute to regional wind and temperature observations from the Arctic. The balloons can drift for a few thousand kilometers horizontally, taking vertical soundings of wind and temperature (Hole et al. 2016). We have already developed the technology to extensively use UAVs and balloons for observing the Arctic atmosphere, but the actual advance is hampered by limited financial resources and various legal regulations. Furthermore, the instrumentation and operation range of manned research aircraft have improved, allowing studies covering wider regions, but also faces the same limitations.

Major advances have also been made in ground/ship/ice-based remote sensing of the Arctic atmosphere. High-resolution vertical profiling of air temperature, humidity, and cloud ice and water content is now possible using scanning multi-wavelength microwave radiometers and Doppler cloud radars, as well as wind profiling using sodars, lidars, radars, and passive solar sensors. The new methods for *in situ* observations and surface-based remote sensing will be important in filling the existing major gap of data on the vertical profiles throughout the Arctic troposphere. Developments in autonomous buoys, floats, and platforms to observe the ocean (Lee et al. 2016) and sea ice (Jackson et al. 2013) yield possibilities to better quantify i) the instantaneous lower boundary conditions for the Arctic and mid-latitude atmosphere, and ii) the heat capacity of the ocean and sea ice, which is important for seasonal forecasts.

To best utilize the existing and new observational methods, data should be collected during dedicated field campaigns, by regular observations at well-instrumented super sites (such as the IASOA observatories), and by satellites. Field campaigns should be performed in different seasons, as the surface thermal forcing to the Arctic atmosphere strongly depends on the season, as also does the atmospheric response to surface forcing. Surface–based measurements should be carried out in different conditions over various surface types with a focus on vertical profiles of mean variables, as well as turbulent and radiative fluxes, and airborne measurements are needed to observe the spatial variability. The observations should be supplemented by process model experiments to i) evaluate the model performance, ii) evaluate the factors controlling the fluxes, and iii) improve flux parameterizations. The year-round drifting ice station MOSAiC — planned from autumn 2019 to autumn 2020 — supported by research aircraft observations (e.g., planned activities in the framework of the $(AC)^3$ project, Wendisch et al. (2017)), other research vessel cruises, enhanced activities at IASOA stations, and various model experiments are expected to advance understanding of local and remote drivers of the AA and the processes that result in teleconnections from the Arctic to mid-latitudes.

Metrics to identify Arctic and mid-latitude linkages—Different metrics, applied to observations, reanalyses, and climate model output, can be used to analyze the relationships between conditions in the Arctic and mid-latitudes, and the mechanisms potentially responsible for these relationships. Among the most direct measures of the Arctic effects on mid-latitudes are the occurrence, duration, and intensity of cold-air outbreaks. AA tends to reduce their intensity but simultaneously favor more meridional circulation patterns, which may favor their increased frequency and persistence. Metrics applied to quantify the meridionality of the jet stream include the meridional circulation index, the frequency of

NASA Author Manuscript NASA Author Manuscript NASA Author Manuscript

occurrence of high-amplitude wave patterns, the meandering index, and sinuosity (Francis and Vavrus 2015; Di Capua and Coumou 2016; Cattiaux et al. 2016).

Developments in novel analysis methods have resulted in application of new metrics. Clustering of patterns of different variables, for example applying self-organizing maps (SOMs), yields information on their relationships, which can be further quantified — by dividing temporal changes into contributions due to changes in a) frequency of occurrence of patterns, b) intensity of patterns (e.g., warming or decrease in sea ice or snow cover), and c) both of them (Francis and Skific, 2015). To test for conditionally dependent relationships, we can apply a multivariate approach called causal effect networks (CEN). The CEN algorithm distinguishes between spurious correlations and causal relationships. Kretschmer et al. (2016) applied the method to test the hypothesis about Arctic-induced drivers of the wintertime stratospheric polar vortex. They concluded that the reduction in Barents-Kara sea ice in autumn causes an increased surface air pressure over the Ural Mountains, followed by an increased vertical wave activity flux and a weakened stratospheric polar vortex (Figure 9). The CEN algorithm has limitations: the causal interpretations are only possible with respect to the time series included in the analysis, whereas the excluded external drivers may affect the network structure. Hence, a more sophisticated method, the response-guided causal precursor detection (RG-CPD), has been developed. Also, the maximum covariance analysis (MCA) method has been applied to evaluate climate model output using a reanalysis as a reference. It revealed that atmosphere-only simulations of ECHAM6 climate model did not reproduce the negative AO/NAO response to Arctic sea-ice loss seen in ERA-Interim reanalysis (Handorf et al. 2015).

To progress, we need a standardization of metrics so that various studies can be better inter-compared. We also need to more extensively apply promising novel methods, such as CEN, RG-CPD, MCA, SOM, and evolutionary algorithms, some of which can distinguish between forced signals and natural variability. In particular, novel metrics that are found to be applicable in reanalysis studies should be used to evaluate climate and weather prediction model performance.

Recommendations—Six recommendations to expand the observational datasets and analyses approaches of change and mid-latitude linkages include:

1. Synthesize new Arctic observations to provide the best high-resolution estimate of the atmospheric state for better understanding sea ice and ocean surface processes;
2. Assess physically-based sea ice/ocean surface forcing data sets available to investigate Arctic mid-latitude linkages and provide improvements;
3. Systematically employ proven and new metrics to identify forced signals of atmospheric circulation from natural variability;
4. Analyze paleoclimate data and new observational datasets that span most of the past century, including reanalysis and sea ice;

NASA Author Manuscript NASA Author Manuscript NASA Author Manuscript

5. Utilize new observational analysis methods (e.g., fluctuation dissipation analysis, causal effect networks) that extend beyond correlative relationships to establish causal links between forcing and response; and

6. Consider both established and new theories of atmospheric and oceanic dynamics to interpret and guide observations and modeling studies.

Modeling recommendations

Modeling experiments are needed to establish the causality of linkages between the Arctic and mid-latitudes. This is illustrated in Figure 13, which compares the winter mean sea level response to reduced Arctic sea ice inferred from lagged regression with the simulated response obtained in model experiments driven by changes in sea ice (Smith et al. 2017). Lagged regression shows a pattern that projects onto a negative NAO, in both the observations and in atmosphere model experiments. The regressions imply a negative NAO response to reduced Arctic sea ice (e.g., Liu et al. 2012). However, the actual response to reduced Arctic sea ice determined from these model experiments is a weak positive NAO. Hence, although statistical analysis can provide useful insights, the results can sometimes be misleading and need to be supported by dedicated modeling experiments.

Modeling uncertainties—Many modeling experiments have been carried out to try to determine the atmospheric response to Arctic sea ice loss, but the results are inconclusive. For example, a key question is how the NAO responds, since this major teleconnection pattern is related to winter climate in North America, Europe, and parts of Asia. However, studies show a full range of responses, including negative NAO (e.g., Deser et al. 2015), positive NAO (e.g., Screen et al. 2014), very little response (e.g., Petrie et al. 2015; Blackport and Kushner 2016), and a response that depends on the details of the forcing (Petoukhov and Semenov 2010; Sun et al. 2015; Chen et al. 2016). It could also be that the NAO is not an optimal response index, as the two features that determine its sign — strength of the Icelandic low and Azores/Bermuda high — can be affected by independent factors, leading to sign variations that are difficult to interpret. Moreover, the centers of action characterized by the Icelandic low and Azores/Bermuda high could be also shifted as revealed by previous studies (Jung et al. 2003; Zhang et al. 2008; Wang and Magnusdottir 2012). In particular, Screen et al. (2018) reviewed the existing fully coupled climate model experiment results and found consistent atmospheric circulation responses to Arctic sea ice across the models resembling the negative phase of Arctic rapid change pattern, which is characterized by the strengthening of two different centers of action from NAO, corresponding to the Siberian high and Aleutian low (Zhang et al. 2008).

There are many potential reasons for the different responses found in modeling studies, including:

- Differences in the magnitude of the forcing. Some studies have investigated the response to sea ice perturbations typical of the present day and near future (e.g., Chen et al. 2016; Smith et al. 2017), while others have investigated the impact of larger changes expected towards the end of the century (e.g,. Deser et al. 2016; Blackport and Kushner 2016). Furthermore, interpreting the impact of

NASA Author Manuscript

NASA Author Manuscript

NASA Author Manuscript

differences in the magnitude of the forcing is particularly difficult because the relationship could be non-linear (Petoukhov and Semenov 2010; Peings and Magnusdottir 2014; Chen et al. 2016). It has also been shown that sea ice variability alone captures only a fraction of total Arctic amplification (e.g., Perlwitz et al. 2015, thus the response signal is weaker than in the real world.

- Differences in the pattern of forcing. Studies have demonstrated that the response is sensitive to the pattern of sea ice anomalies. For example, Sun et al. (2015) obtained opposite responses in the northern polar vortex to sea ice forcing from the Pacific and Atlantic sectors. Furthermore, the responses to regional sea ice anomalies do not add linearly (Screen 2017), complicating their interpretation.
- Atmosphere/ocean coupling. Although many studies have used atmosphere-only models, changes in Arctic sea ice can influence sea surface temperatures surrounding the ice pack and also in remote regions, including the tropics (e.g., Smith et al. 2017). Coupled models are essential to simulate these effects and have been found to amplify the winter mid-latitude wind response to Arctic sea ice (Deser et al. 2016).
- How the forcing is applied. Changes in sea ice can be imposed in different ways in coupled models, for example by nudging the model to the required state (e.g., Smith et al. 2017) or by changing the fluxes of energy in order to melt some of the sea ice (e.g., Deser et al. 2016; Blackport and Kushner 2016). The latter approach appears to induce a “mini-global warming” signal with enhanced warming in the tropical upper troposphere that could affect mid-latitude winds, whereas the former approach could potentially induce undesired ocean circulation changes in response to the nudging increments. Hence, the different approaches could lead to different atmospheric responses even if the sea ice changes are similar.
- Different models. The response can be very sensitive to the model used. For example, Sun et al. (2015) obtained opposite responses in the winter polar vortex in identical forcing experiments with two different models.
- Background state. Identical forcing experiments — with the same model but with different background states induced by different sea surface temperature biases — can produce opposite NAO responses (Smith et al. 2017). Furthermore, responses may not be robust across experiments due to strong nonlinearities in the system, which can depend on the background state (Chen et al. 2016).
- Low signal to noise ratio. The atmospheric response to Arctic sea ice simulated by models is typically small compared to internal variability so that a large ensemble of simulations is required to obtain robust signals (e.g., Mori et al. 2014). Some of the different responses reported in the literature could therefore arise from sampling errors. If the low signal-to-noise ratio in models is correct, then the response to Arctic sea ice could be swamped by internal variability (McCusker et al. 2016). However, the signal-to-noise ratio in seasonal forecasts

NASA Author Manuscript

NASA Author Manuscript

NASA Author Manuscript

of the NAO is too small in models (Eade et al. 2014), suggesting that the magnitude of the simulated response to sea ice could also be too small.

Coordinated experiments—At the workshop, the modeling breakout group proposed the creation of a modeling task force to coordinate modeling experiments. Given the variety of different factors that can influence the simulated response to Arctic sea ice loss, there is a clear need for coordinated modeling experiments so that these factors can be controlled, allowing the different model responses to be better understood. This will be addressed by a new CMIP6 Polar Amplification MIP (PAMIP), which will investigate the causes and consequences of polar amplification.

Coordinated modeling experiments are currently being designed and will investigate several of the factors listed above, including the roles of coupling, the background state, and the pattern of forcing. Tier one experiments would consist of two fast-track sets of atmosphere MIP (AMIP)-like simulations that can be conducted by different groups and made available to the community for analysis relatively quickly. Fast-track #1 would exploit the CMIP6 AMIP (from 1979-present) as the control run, and modeling groups would then execute two sets of sensitivity experiments — one with climatological sea ice and the other with climatological sea surface temperatures — to evaluate the atmospheric response to recent AA. For fast-track #2, modeling groups would run AMIP-like control simulations with observed climatological sea ice and sea surface temperature, and then three different time slice experiments using modeled sea ice and sea surface temperature patterns from the past (pre-industrial), the present (transient runs), and future (pattern under +2°C warming). Protocols for these fast-track experiments have been determined in autumn 2017. In addition, atmosphere-ocean coupled models will be forced with pre-industrial, the present, and future Arctic and Antarctic sea ice. It is planned to make the model simulation outputs from the experiments accessible through the Earth System Grid to allow the broader community to evaluate the proposed mechanisms linking changes in the Arctic to mid-latitudes.

Analysis of these experiments will seek to exploit the different model responses to obtain the real-world response using an “emergent constraint.” In this constraint, a relationship is sought between the different simulated responses and an observable parameter that is related to the underlying physical cause of the simulated differences. For example, Smith et al. (2017) found that changes in mid-latitude winds in response to reduced Arctic sea ice are sensitive to the refraction of anomalous planetary waves. By relating the simulated response to the observed atmospheric refractive index, they obtained an emergent constraint that suggests a weakening of the Atlantic jet (a negative NAO response) (Figure 14). However, this result is based on just three sets of simulations with a single model. PAMIP will provide a much larger sample of model responses, potentially providing more robust emergent constraints. Furthermore, we anticipate that a hierarchy of models, ranging from simplified dry dynamical cores to fully coupled general circulation models, will participate in the PAMIP, enabling the physical processes involved in the atmospheric response to Arctic sea ice to be explored in detail.

NASA Author Manuscript NASA Author Manuscript NASA Author Manuscript

An initial proposal for coordinated modeling experiments to be carried out at multiple modeling centers for PAMIP is shown in Table 2. An update of the proposed PAMIP experiments can be found in Smith et al. (2018). These multi-tiered set of MIP experiments draw from the initial planning and discussions of the US CLIVAR Working Group and planned modeling elements of the European Horizon 2020 projects (APPLICATE, Blue Action, and PRIMAVERA). Twenty-two modeling centers and groups in the US, Canada, Europe, and Asia have expressed interest in conducting the experiments.

Recommendations—Three recommendations to advance modeling and synthesis understanding of Arctic change and midlatitude linkages include:

1. Establish a Modeling Task Force to plan protocols, forcing, and output parameters for coordinated modeling experiments (PAMIP);
2. Furnish experiment datasets to the community through open access (via Earth System Grid); and
3. Promote analysis within the community of simulations to understand mechanisms for AA and to further understand pathways for Arctic mid-latitude linkages.

4 References

Alexeev VA, Langen PL, and Bates JR, 2005: Polar amplification of surface warming on an aquaplanet in “ghost forcing” experiments without sea ice feedbacks. Climate Dyn., 24, 655–666, doi:10.1007/s00382-005-0018-3.

Anchukaitis KJ, and Coauthors, 2017: Last millennium Northern Hemisphere summer temperatures from tree rings: Part II, spatially resolved reconstructions. Quat. Sci. Rev, 163, 1–22, doi:10.1016/j.quascirev.2017.02.020.

Ayarzagüena B, and Screen JA, 2016: Future Arctic sea-ice loss reduces severity of cold air outbreaks in midlatitudes. Geophys. Res. Lett, 43, 2801–2809, doi:10.1002/2016GL068092.

Baggett C, Lee S, and Feldstein SB, 2016: An investigation of the presence of atmospheric rivers over the North Pacific during planetary-scale wave life cycles and their role in Arctic warming. J. Atmos. Sci, 73, 4329–4347, doi:10.1175/JAS-D-16-0033.1.

Ballinger T, Hanna E, Hall RJ, Miller J, Ribergaard MH, and Hoyer JL, 2017: Greenland coastal air temperatures linked to Baffin Bay and Greenland Sea ice conditions during autumn through regional blocking patterns. Climate Dyn, doi:10.1007/s00382-017-3583-3.

Barnes EA, and Polvani LM, 2015: CMIP5 projections of Arctic amplification of the North American/North Atlantic circulation and of their relationship. J. Climate, 28, 5254–5271, doi:10.1175/JCLI-D-14-00589.1.

Basu S, Zhang X, Polyakov I, and Bhatt US, 2013: North American winter-spring storms: Modeling investigation on tropical Pacific sea surface temperature impacts. Geophys. Res. Lett, 40, 5228–5233, doi:10.1002/grl.50990.

Basu S, Zhang X, and Wang Z, 2018: Eurasian winter storm activity at the end of the century: A CMIP5 multi-model ensemble projection. Earth’s Future, 6, 61–70, doi:10.1002/2017EF000670.

Baxter S, and Nigam S, 2015: Key role of North Pacific Oscillation/West Pacific pattern in generating the extreme 2013–2014 North American winter. J. Climate, 28, 8109–8117, doi:10.1175/JCLI-D-14-00726.1.

Blackport R, and Kushner P, 2016: The transient and equilibrium climate response to rapid summertime sea ice loss in CCSM4. J. Climate, 29, 401–417, doi:10.1175/JCLI-D-15-0284.1.

Blackport R, and Kushner PJ, 2017: Isolating the Atmospheric Circulation Response to Arctic Sea Ice Loss in the Coupled Climate System. J. Climate, 30, 2163–2185, doi:10.1175/JCLI-D-16-0257.1.

NASA Author Manuscript NASA Author Manuscript NASA Author Manuscript

Blunden J and Arndt DS, 2012: State of the climate in 2011. Bull. Am. Meteorol. Soc, 93, S1–S264, doi:10.1175/2012BAMSStateoftheClimate.1.

Boisvert LN, Wu DL, and Shie C-L, 2015: Increasing evaporation amounts seen in the Arctic between 2003 and 2013 from AIRS data. J. Geophys. Res, 120, 6865–6881, doi:10.1002/2015JD023258.

Boisvert LN, and Stroeve JC, 2015: The Arctic is becoming warmer and wetter as revealed by the Atmospheric Infrared Sounder. Geophys. Res. Lett, 42, 4439–4446, doi:10.1002/2015GL063775.

Bourassa MA, and Coauthors, 2013: High-latitude ocean and sea ice surface fluxes: challenges for climate research. Bull. Amer. Meteorol. Soc, 94, doi:10.1175/BAMS-D-11-00244.1.

Bromwich DH, Fogt RL, Hodges KI, and Walsh JE, 2007: A tropospheric assessment of the ERA-40, NCEP, and JRA-25 global reanalyses in the polar regions, J. Geophys. Res, 112, doi: 10.1029/2006JD007859.

Bromwich DH, Hines KM, and Bai L, 2009: Development and testing of Polar Weather Research and Forecasting model: 2. Arctic Ocean. J. Geophys. Res, 114, doi:10.1029/2008jd010300.

Carton JA, and Giese BS, 2008: A reanalysis of ocean climate using Simple Ocean Data Assimilation (SODA). Mon. Wea. Rev, 136, 2999–3017, doi:10.1175/2007MWR1978.1.

Cattiaux J, Peings Y, Saint-Martin D, Trou-Kechout N, and Vavrus SJ, 2016: Sinuosity of midlatitude atmospheric flow in a warming world. Geophys. Res. Lett, 43, 8259–8268, doi: 10.1002/2016GL070309.

Chen X, and Luo D, 2017: Arctic sea ice decline and continental cold anomalies: Upstream and downstream effects of Greenland blocking. Geophys. Res. Lett, 44, 3411–3419, doi: 10.1002/2016GL072387.

Chen G, Lu J, Burrows DA, and Leung LR, 2015: Local finite-amplitude wave activity as an objective diagnostic of midlatitude extreme weather. Geophys. Res. Lett, 42, 10,952–10,960, doi: 10.1002/2015GL066959.

Chen HW, Zhang F, and Alley RB, 2016: The robustness of midlatitude weather pattern changes due to Arctic sea ice loss. J. Climate, 29, 7831–7849, doi:10.1175/JCLI-D-16-0167.1.

Chernokulsky AV, Esau I, Bulygina ON, Davy R, Mokhov II, Outten S, and Semenov VA, 2017: Climatology and interannual variability of cloudiness in the Atlantic Arctic from surface observations since the late nineteenth century. J. Climate, 30, 2103–2020, doi:10.1175/JCLI-D-16-0329.1.

Cohen J, 2016: An observational analysis: Tropical relative to Arctic influence on midlatitude weather in the era of Arctic amplification. Geophys. Res. Lett, 43, 5287–5294, doi: 10.1002/2016GL069102.

Cohen J, Barlow M, Kushner PJ, and Saito K, 2007: Stratosphere-troposphere coupling and links with Eurasian land surface variability. J. Climate, 20, 5335–5343, doi:10.1175/2007JCLI1725.1.

Cohen J, Screen JA, Furtado JC, Barlow M, Whittleston D, Coumou D, Francis J, Dethloff K, Entekhabi D, Overland J, and Jones J, 2014: Recent Arctic amplification and extreme mid-latitude weather. Nat. Geosci, 7, 627–637, doi:10.1038/ngeo2234.

Comiso JC, 2012: Large decadal decline in the Arctic multiyear ice cover. J. Climate, 25, 1176–1193, doi:10.1175/JC-LI-D-11-00113.1.

Compo GP, and Coauthors, 2011: The Twentieth Century Reanalysis Project. Quart. J. Roy. Meteorol. Soc, 137, 1–28, doi:10.1002/qj.776.

Comiso JC, Parkinson CL, Gersten R, and Stock L, 2008: Accelerated decline in the Arctic sea ice cover, Geophys. Res. Lett, 35, L01703, doi:10.1029/2007GL031972.

Coumou D, Lehmann J, and Beckmann J, 2015: The weakening summer circulation in the Northern Hemisphere mid-latitudes. Science, 348, 324–327, doi:10.1126/science.1261768. [PubMed: 25765067]

Coumou D Kornhuber K, Lehmann J, and Petoukhov V, 2017: Weakened flow, persistent circulation, and prolonged weather extremes in boreal summer Climate Extremes: Patterns and Mechanisms, Geophys. Monogr 226, Wang S-Y, Yoon J-H, Funk CC, and Gilles RR, Eds., Amer. Geophys. Union, 61–74, ISBN:978119067849.

Coumou D, Petoukhov V, Rahmstorf S, Petri S, and Schellnhuber HJ, 2014: Quasi-resonant circulation regimes and hemispheric synchronization of extreme weather in boreal summer. Proc. Nat. Acad. Sci, 111, 12331–12336, doi:10.1073/pnas.1412797111. [PubMed: 25114245]

NASA Author Manuscript NASA Author Manuscript NASA Author Manuscript

Cvijanovic I, Santer BD, Bonfils C, Lucas DD, Chiang JCH, and Zimmerman S, 2017: future loss of Arctic sea-ice cover could drive a substantial decrease in California's rainfall. Nat. Comm, doi: 10.1038/s41467-017-01907-4.

Derksen C, Brown R, Mudryk L, and Luojus K, 2015: Arctic: terrestrial snow State of the Climate in 2014. Blunden J and Arndt DS, Eds., Bull. Amer. Meteorol. Soc., 96, 133–135, doi: 10.1175/2015BAMSStateoftheClimate.1.

Deser C, Tomas RA, and Peng S, 2007: The transient atmospheric circulation response to North Atlantic SST and sea ice anomalies. J. Climate, 20, 4751–4767, doi:10.1175/JCLI4278.1.

Deser C, Tomas RA, and Sun L, 2015: The role of ocean-atmosphere coupling in the zonal-mean atmospheric response to Arctic sea ice loss. J. Climate, 28, 2168–2186, doi:10.1175/JCLI-D-14-00325.1.

Deser C, Sun L, Tomas RA, and Screen J, 2016: Does ocean-coupling matter for the northern extra-tropical response to projected Arctic sea ice loss? Geophys. Res. Lett, 43, 2149–2157, doi: 10.1002/2016GL067792.

Di Capua G, and Coumou D, 2016: Changes in meandering of the Northern Hemisphere circulation. Enviro. Res. Lett, 11, doi:10.1088/1748-9326/11/9/094028.

Ding Q, Wallace JM, Battisti DS, Steig EJ, Galland AJE, Kim H-J, and Geng L, 2014: Tropical forcing of the recent rapid Arctic warming in northeastern Canada and Greenland. Nature, 509, 209–212, doi:10.1038/nature13260. [PubMed: 24805345]

Ding Q, and Coauthors, 2017: Influence of high-latitude atmospheric circulation changes on summertime Arctic sea ice. Nature Climate Change, 7, 289–295, doi:10.1038/NCLIMATE3241.

Dorn W, Dethloff K, and Rinke A, 2009: Improved simulation of feedbacks between atmosphere and sea ice over the Arctic Ocean in a coupled regional climate model. Ocean Model, 29, 103–114, doi:10.1016/J.Ocemod.2009.03.010.

Doyle JG, Lesins G, Thackray CP, Perro C, Nott GJ, Duck TJ, Damoah R, and Drummond JR, 2011: Water vapor intrusions into the high Arctic during winter. Geophys. Res. Lett, 38, doi: 10.1029/2011GL047493.

Eade R, Smith DM, Scaife AA, Wallace E, Dunstone N, Hermanson L, and Robinson N, 2014: Do seasonal to decadal climate predictions underestimate the predictability of the real world? Geophys. Res. Lett, 41, 5620–5628, doi:10.1002/2014GL061146. [PubMed: 25821271]

Feldstein S, and Lee S, 2014: Intraseasonal and interdecadal jet shifts in the Northern Hemisphere: the role of warm pool tropical convection and sea ice. J. Climate, 27, 6497–6518, doi:10.1175/JCLI-D-14-00057.1.

Francis JA, and Vavrus SJ, 2012: Evidence linking Arctic amplification to extreme weather in mid-latitudes. Geophys. Res. Lett, 39, doi:10.1029/2012GL051000.

Francis J, and Vavrus S, 2015: Evidence for a wavier jet stream in response to rapid Arctic warming. Environ. Res. Lett, 10, doi:10.1088/1748-9326/10/1/014005.

Francis JA and Skific N, 2015: Evidence linking rapid Arctic warming to mid-latitude weather patterns. Phil. Trans. R. Soc. A 373, doi:10.1098/rsta.2014.0170.

Francis JA, Hunter E, Key JR, and Wang X, 2005: Clues to variability in Arctic minimum sea ice extent. Geophys. Res. Lett, 32, doi:10.1029/2005GL024376.

Giorgi F, 2005: Interdecadal variability of regional climate change: Implications for the development of regional climate change scenarios. J. Meteorol. Atmos. Phys, 89, 1–15, doi:10.1007/s00703-005-0118-y.

Girard L, Weiss J, Molines JM, Barnier B, and Bouillon S, 2009: Evaluation of high resolution sea ice models on the basis of statistical and scaling properties of Arctic sea ice drift and deformation. J. Geophys. Res, 114, 2156–2202, doi:10.1029/2008JC005182.

Gong T, Feldstein SB, and Lee S, 2017: The role of downward infrared radiation in the recent Arctic winter warming trend. J. Climate, doi:10.1175/JCLI-D-16-0180.1.

Good SA, Martin MJ, and Rayner NA, 2013: EN4: quality controlled ocean temperature and salinity profiles and monthly objective analyses with uncertainty estimates. J. Geophys. Res, 118, 6704–6716, doi:10.1002/2013JC009067.

Goss M, Feldstein SB, and Lee S, 2016: Stationary wave interference, and its relation to tropical convection and Arctic warming. J. Climate, 29, 1369–1389, doi:10.1175/JCLI-D-15-0267.1.

NASA Author Manuscript NASA Author Manuscript NASA Author Manuscript

Greene CH, Francis JA, and Monger BC, 2013: Superstorm Sandy: A series of unfortunate events? Oceanography 26, doi://10.5670/oceanog.2013.11.

Hall R, Erdélyi R, Hanna E, Jones JM, and Scaife AA, 2015: Drivers of North Atlantic polar front jet stream variability. Int. J. Climatol, 35, 1697–1720, doi:10.1002/joc.4121.

Handorf D, and Dethloff K, 2012: How well do state-of-the-art atmosphere-ocean general circulation models reproduce atmospheric teleconnection patterns? Tellus A, 64, doi:10.3402/tellusa.v64i0.19777.

Handorf D, Jaiser R, Dethloff K, Rinke A, and Cohen J, 2015: Impacts of Arctic sea ice and continental snow cover changes on atmospheric winter teleconnections. Geophys. Res. Lett, 42, 2367–2377, doi:10.1002/2015GL063203.

Henderson GR, Barrett BS, and LaFleur DM, 2014: Arctic sea ice and the Madden-Julian Oscillation (MJO). Climate Dyn, 43, 2185–2196, doi:10.1007/s00382-013-2043-y.

Hole LR, Bello A, Roberts T, Voss P, and Vihma T, 2016: Atmospheric measurements by controlled meteorological balloons in coastal areas of Antarctica. Antar. Sci, 28, 387–394, doi:10.1017/S0954102016000213.

Holton JR, 1979: An Introduction to Dynamic Meteorology, Second Edition Academic Press, New York, 416 pp.

Honda M, Inoue J, and Yamane S, 2009: Influence of low Arctic sea-ice minima on anomalously cold Eurasian winters. Geophys. Res. Lett, 36, doi:10.1029/2008GL037079.

Hopsch S, Cohen J, and Dethloff K, 2012: Analysis of a link between fall Arctic sea-ice concentration and atmospheric patterns in the following winter. Tellus A, 64, 18624, doi:10.3402/tellusa.v64i0.18624.

Houborg R, Rodell M, Li B, Reichle R, and Zaitchik B, 2012: Drought indicators based on model assimilated GRACE terrestrial water storage observations. Water Resour. Res, 48, doi:10.1029/2011WR011291.

Huang J, et al., 2017: Recently amplified arctic warming has contributed to a continual global warming trend. Nature Climate Change, doi:10.1038/s41558-017-0009-5.

Hunke EC, 2010: Thickness sensitivities in the CICE sea ice model. Ocean Model, 34, 137–149, doi:10.1016/j.ocemod.2010.05.004.

Intrieri JM, Fairall CW, Shupe MD, Persson POG, Andreas EL, Guest PS, and Moritz RE, 2002: An annual cycle of Arctic surface cloud forcing at SHEBA. J. Geophys. Res, 107, doi:10.1029/2000JC000423.

Inoue J, Enomoto T, Miyoshi T, and Yamane S, 2009: Impact of observations from Arctic drifting buoys on the reanalysis of surface fields. Geophys. Res. Lett, 36, doi:10.1029/2009GL037380.

Intrieri JM, de Boer G, Shupe MD, Spackman JR, Wang J, Neiman PJ, Wick GA, Hock TF, and Hood RE, 2014: Global Hawk dropsonde observations of the Arctic atmosphere obtained during the Winter Storms and Pacific Atmospheric Rivers (WISPAR) field campaign. Atmos. Meas. Tech, 7, 3917–3926, doi:10.5194/amt-7-3917-2014.

Jackson K, Wilkinson J, Maksym T, Meldrum D, Beckers J, Haas C, and MacKenzie D, 2013: A novel and low cost sea ice mass balance buoy. J. Atmos. Ocean. Tech, 30, 2676–2688, doi:10.1175/JTECH-D-13-00058.1.

Jaiser R, Dethloff K, Handorf D, Rinke A, and Cohen J, 2012: Impact of sea ice cover changes on the Northern Hemisphere atmospheric winter circulation. Tellus A, 64, doi:10.3402/tellusa.v64i0.11595.

Jaiser R, Nakamura T, Handorf D, Dethloff K, Ukita J, and Yamazaki K, 2016: Atmospheric winter response to Arctic sea ice changes in reanalysis data and model simulations. J. Geophys. Res, 121, 7564–7577, doi:10.1002/2015JD024679.

Jakobson E, Vihma T, Palo T, Jakobson L, Keernik H, and Jaagus J, 2012: Validation of atmospheric reanalyzes over the central Arctic Ocean. Geophys. Res. Lett 39, doi:10.1029/2012GL051591.

Jonassen MO, Tisler P, Altstädter B, Scholtz A, Vihma T, Lampert A, König-Langlo G, and Lüpkes C, 2015: Application of remotely piloted aircraft systems in observing the atmospheric boundary layer over Antarctic sea ice in winter. Polar Res., 34, doi:10.3402/polar.v34.25651.

NASA Author Manuscript NASA Author Manuscript NASA Author Manuscript

Jung T, Hilmer M, Ruprecht E, Kleppek S, Gulev SK, and Zolina O, 2003: Characteristics of the recent eastward shift of interannual NAO variability. J. Climate, 16, 3371–3382, doi: 10.1175/1520-0442(2003)016<3371:COTRES>2.0.CO;2.

Kapcsh M-L, Graversen RG and Tjernstrom M, 2013: Springtime atmospheric energy transport and the control of Arctic summer sea-ice extent. Nature Climate Change, 3,744–748 doi:10.1038/nclimate1884.

Kapsch M-L, Graversen RG, Tjernström M, and Bintanja R, 2016: The effect of downwelling longwave and shortwave radiation on Arctic summer sea ice. J. Climate, 29, 1143–1159, doi: 10.1175/JCLI-D-15-0238.1.

Kay JE, and L'Ecuyer T, 2013: Observational constraints on Arctic ocean clouds and radiative fluxes during the early 21st century. J. Geophys. Res. Atmos, 118, 7219–7236, doi:10.1002/jgrd.50489.

Kim B-M, Son S-W, Min S-K, Jeong J-H, Kim S-J, Zhang X, Shim T, and Yoon J-H, 2014: Weakening of the stratospheric polar vortex by Arctic sea-ice loss. Nat. Comm, 5, doi:10.1038/ncomms5646.

Kim B-M, Hong J-Y, Jun S-Y, Zhang X, Kwon H, Kim S-J, Kim J-H, Kim S-W, and Kim Hyun-Kyung, 2017: Major cause of unprecedented Arctic warming in January 2016: Critical role of an Atlantic windstorm. Scientific Reports, 7, 40051, doi: 10.1038/srep40051. [PubMed: 28051170]

Kinnard C, Zdanowicz CM, Fisher DA, Isaksson E, de Vernal A, and Thompson LG, 2011: Reconstructed changes in Arctic sea ice over the past 1,450 years. Nature, 479, 509–512, doi: 10.1038/nature10581. [PubMed: 22113692]

Kretschmer M, Coumou D, J. Donges J, and Runge J, 2016: Using causal effect networks to analyze different Arctic drivers of midlatitude winter circulation. J. Climate, 29, 4069–81, doi:10.1175/JCLI-D-15-0654.1.

Krikken F, and Hazeleger W, 2015: Arctic energy budget in relation to sea ice variability on monthly-to-annual time scales. J. Climate, 28, 6335–6350, doi:10.1175/JCLI-D-15-0002.1.

Kug J-S, Jeong J-H, Jang Y-S, Kim B-M, Folland CK, Min S-K, and Son S-W, 2015: Two distinct influences of Arctic warming on cold winters over North America and East Asia. Nature Geosci, 8, 759–762, doi:10.1038/ngeo2517.

Kwok R, Cunningham GF, Wensnahan M, Rigor I, Zwally HJ, and Yi D, 2009: Thinning and volume loss of the Arctic Ocean sea ice cover: 2003–2008. J. Geophys. Res,114, doi: 10.1029/2009JC005312.

Laliberte F, and Kushner PJ, 2014: Midlatitude moisture contribution to recent Arctic tropospheric summertime variability. J. Climate, 27, 5693–5706, doi:10.1175/JCLI-D-13-00721.1.

Laloyaux P, Balmaseda M, Dee D, Mogensen K, and Janssen P, 2016: A coupled data assimilation system for climate reanalysis. Quart. J. Roy. Meteorol. Soc, 142, 65–78. doi:10.1002/qj.2629.

Lang A, Yang S, Kass E, 2017: Sea ice thickness and recent Arctic warming. Geophys. Res. Lett, 44, 409–418, doi:10.1002/2016GL071274.

Lee CM, and Coauthors, 2016: Stratified ocean dynamics of the Arctic: Science and experiment plan Technical Report, APL-UW 1601, University of Washington, Seattle, Washington, 46pp, http://www.apl.washington.edu/research/downloads/publications/tr_1601.pdf.

Lee S, Gong TT, Johnson NC, Feldstein SB, and Pollard D, 2011: On the possible link between tropical convection and the Northern Hemisphere Arctic surface air temperature change between 1958–2001. J. Climate, 24, 4350–4367, doi:10.1175/2011JCLI4003.1.

Lee S 2012: Testing of the tropically excited Arctic warming (TEAM) mechanism with traditional El Nino and La Nina. J. Climate, 25, 4015–4022, doi:10.1175/JCLI-D-12-00055.1.

Lee S, 2014: A theory for polar amplification from a general circulation perspective. Asia-Pac. J. Atmos. Sci, 50, 31–43, doi:10.1007/s13143-014-0024-7.

Lee M-Y, Hong C-C, and Hsu H-H, 2015: Compounding effects of warm sea surface temperature and reduced sea ice on the extreme circulation over the extratropical North Pacific and North America during the 2013–2014 boreal winter. Geophys. Res. Lett, 42, 1612–1618, doi: 10.1002/2014GL062956.

Lehmann J, Coumou D, Frieler K, Eliseev AV, and Levermann A, 2014: Future changes in extratropical storm tracks and baroclinicity under climate change. Environ. Res. Lett, 9, doi: 10.1088/1748-9326/9/8/084002.

NASA Author Manuscript NASA Author Manuscript NASA Author Manuscript

Li F, and Wang HJ, 2014: Autumn Eurasian snow depth, autumn Arctic sea ice cover and East Asian winter monsoon. Int. J. Climatol, 34, 3616–3625, doi:10.1002/joc.3936s.

Liptak J, and Strong C, 2014: The winter atmospheric response to sea ice anomalies in the Barents Sea. J. Climate, 27, 914–924, doi:10.1175/JCLI-D-13-00186.1.

Liu C, and Barnes EA, 2015: Extreme moisture transport into the Arctic linked to Rossby wave breaking. J. Geophys. Res, 120, 3774–3788, doi:10.1002/2014JD022796.

Liu JP, Curry JA, Wang H, Song M, and Horton RM, 2012: Impact of declining Arctic sea ice on winter snowfall. Proc. Natl. Acad. Sci, 109, 4074–9, doi:10.1073/pnas.1114910109. [PubMed: 22371563]

Liu Y, and Key JR, 2014: Less winter cloud aids summer 2013 Arctic sea ice return from 2012 minimum. Environ. Res. Lett, 9, doi:10.1088/1748-9326/9/4/044002.

Liu Y, and Key JR, 2016: Assessment of Arctic cloud cover anomalies in atmospheric reanalysis products using satellite data. J. Climate, 29, 6065–6083, doi:10.1175/JCLI-D-15-0861.1.

Liu YY, Dorigo WA, Parinussa RM, de Jeu RAM, Wagner W, McCabe MF, Evans JP, and van Dijk AIJM, 2012: Trend-preserving blending of passive and active microwave soil moisture retrievals. Rem. Sens. Environ, 123, 280–297, doi:10.1016/j.rse.2012.03.014.

Losch M, Menemenlis D, Heimbach P, Campin JM, and Hill C, 2010: On the formulation of sea-ice models. Part 1: Effects of different solver implementations and parameterizations. Ocean Model, 33, 129–144, doi:10.1016/j.ocemod.2009.12.008.

Luo D, Xiao Y, Yao Y, Dai A, Simmonds I, and Franzke CLE, 2016: Impact of Ural blocking on winter warm arctic-cold Eurasian anomalies, Part I: Blocking-induced amplification. J. Climate, 29, 3925–3947, doi:10.1175/JCLI-D-15-0611.1.

Manabe S, and Wetherald RT, 1975: The effects of doubling the CO2 concentration on the climate of a general circulation model. J. Atmos. Sci, 32, 3–15, doi: 10.1175/1520-0469(1975)032<0003:TEODTC>2.0.CO;2.

Marcott SA, Shakun JD, Clark PU, and Mix AC, 2013: A reconstruction of regional and global temperature for the past 11,300 years. Science, 339, 1198–1201, doi:10.1126/science.1228026. [PubMed: 23471405]

Maslowski W, Clement Kinney J, Higgins M, and Roberts A, 2012: The future of Arctic sea ice. Ann. Rev. Earth Planet. Sci, 40, 625–654, doi:10.1146/annurev-earth-042711-105345.

McCusker KE, Fyfe JC, and Sigmond M, 2016: Twenty-five winters of unexpected Eurasian cooling unlikely due to Arctic sea ice loss. Nature Geosci, 9, 838–842, doi:10.1038/ngeo2820.

Messori G, Caballero R, and Gaetani M, 2016: On cold spells in North America and storminess in Western Europe. Geophys. Res. Lett, 43, 6620–6628, doi:10.1002/2016GL069392.

Mori M, Watanabe M, Shiogama H, Inoue J, and Kimoto M, 2014: Robust Arctic sea-ice influence on the frequent Eurasian cold winters in past decades. Nature Geosci, 7, 869–873, doi:10.1038/ngeo2277.

Nakamura N, and Solomon A, 2010: Finite-amplitude wave activity and mean flow adjustments in the atmospheric general circulation. Part I: Quasigeostrophic theory and analysis. J. Atmos. Sci, 67, 3967–3983, doi:10.1175/2010JAS3503.1.

Nakamura T, Yamazaki K, Iwamoto K, Honda M, Miyoshi Y, Ogawa Y, and Ukita J, 2015: A negative phase shift of the winter AO/NAO due to the recent Arctic sea-ice reduction in late autumn. J. Geophys. Res, 120, 3209–3227, doi:10.1002/2014JD022848.

Orsolini Y, Senan R, Benestad RE, and Melsom A, 2012: Autumn atmospheric response to the 2007 low Arctic sea ice extent in coupled ocean-atmosphere hindcasts. Climate Dyn, 38, 2437–2448, doi:10.1007/s00382-011-1169-z.

Overland JE, Walter BA, Curtain TB, and Turet P, 1995: Hierarchy and sea ice mechanics: A case study from the Beaufort Sea. J. Geophys. Res, 100, 4559–4571, doi:10.1029/94JC02502.

Overland JE, Francis JA, Hanna E, and Wang M, 2012: The recent shift in early summer Arctic atmospheric circulation. Geophys. Res. Lett, 39, L19804, doi:10.1029/2012GL053268.

Overland JE, Francis JA, Hall R, Hanna E, Kim S-J, and Vihma T, 2015: The melting Arctic and mid-latitude weather patterns: Are they connected? J. Climate, 28, 7917–7932, doi:10.1175/JCLI-D-14-00822.1.

NASA Author Manuscript NASA Author Manuscript NASA Author Manuscript

Overland JE, Dethloff K, Francis JA, Hall RJ, Hanna E, Kim S-J, Screen JA, Shepherd TG, and Vihma T, 2016: Nonlinear response of mid-latitude weather to the changing Arctic. Nature Climate Change, 6, 992–999, doi:10.1038/NCLIMATE3121.

Park D-S, Lee S, and Feldstein SB 2015: Attribution of the recent winter sea-ice decline over the Atlantic sector of the Arctic Ocean. J. Climate, 28, 4027–4033, doi:10.1175/JCLI-D-15-0042.1.

Park H-S, Lee S, Son S-W, Feldstein SB, and Kosaka Y, 2015a: The impact of poleward moisture and sensible heat flux on Arctic winter sea-ice variability. J. Climate, 28, 5030–5040, doi:10.1175/JCLI-D-15-0074.1.

Park H-S, Lee S, Kosaka Y, Son S-W, and Kim S-W, 2015b: The impact of Arctic winter infrared radiation on early summer sea ice. J. Climate, 28, 6281–6296, doi:10.1175/JCLI-D-14-00773.1.

Peings Y, and Magnusdottir G, 2014: Response of the wintertime Northern Hemisphere atmospheric circulation to current and projected Arctic sea ice decline: A numerical study with CAM5. J. Climate, 27, 244–264, doi:10.1175/JCLI-D-13-00272.1.

Peings Y, Cattiaux J, Vavrus S, and Magnusdottir G, 2017: Late 21st century changes of the mid-latitude atmospheric circulation in the CESM Large Ensemble. J. Climate, doi:10.1175/JCLI-D-16-0340.1.

Perovich DK, and coauthors, 1999: Year on ice gives climate insights. Eos, 80, 481–486, doi:10.1029/EO-080i041p00481-01.

Perovich DK, Richter-Menge JA, Jones KF, and Light B, 2008: Sunlight, water, and ice: Extreme Arctic sea ice melt during the summer of 2007. Geophys. Res. Lett, 35, doi:10.1029/2008gl034007.

Petoukhov V, and Semenov V, 2010: A link between reduced Barents-Kara sea ice and cold winter extremes over northern continents. J. Geophys. Res, 115, doi:10.1029/2009JD013568.

Petrie RE, Shaffrey LC, and Sutton RT, 2015: Atmospheric impact of Arctic sea ice loss in a coupled ocean–atmosphere simulation. J. Climate, 28, 9606–9622, doi:10.1175/JCLI-D-15-0316.1.

Pistone K, Eisenman I, and Ramanathan V, 2014: Observational determination of albedo decrease caused by vanishing Arctic sea ice. Proc. Nat. Acad. Sci, 111, 3322–3326, doi:10.1073/pnas.1318201111. [PubMed: 24550469]

Poli P, and Coauthors, 2016: ERA-20C: An atmospheric reanalysis of the twentieth century. J. Climate, 29, 4083–4097, doi:10.1175/JCLI-D-15-0556.1.

Rigor IG, Wallace M, and Colony R, 2002: Response of sea ice to the Arctic Oscillation. J. Climate, 15, 2648–2663, doi:10.1175/1520-0442(2002)015<2648:ROSITT>2.0.CO;2.

Rohli RV, Wrona KM, and McHugh MJ, 2005: January northern hemisphere circumpolar vortex variability and its relationship with hemispheric temperature and regional teleconnections. Int. J. Climatol, 25, 1421–1436, doi:10.1002/joc.1204.

Romanovsky VE, Drozdov DS, Oberman NG, Malkova GV, Kholodov AL, et al., 2010: Thermal state of permafrost in Russia. Perma. Periglac. Proc, 21, 136–55, doi:10.1002/ppp.683.

Sato K, Inoue J, and Watanabe M, 2014: Influence of the Gulf Stream on the Barents Sea ice retreat and Eurasian coldness during early winter. Environ. Res. Lett, 9, doi:10.1088/1748-9326/9/8/084009.

Screen JA, 2017: Simulated atmospheric response to regional and Pan-Arctic sea-ice loss. J. Climate, doi:10.1175/JC-LI-D-16-0197.1.

Screen JA, Deser C, and Simmonds I, 2012: Local and remote controls on observed Arctic warming. Geophys. Res. Lett 39, doi:10.1029/2012GL051598.

Screen JA, and Simmonds I, 2010: The central role of diminishing sea ice in recent Arctic temperature amplification. Nature, 464, 1334–1337, doi:10.1038/nature09051. [PubMed: 20428168]

Screen JA, Deser C, Simmonds I, and Tomas R, 2014: Atmospheric impacts of Arctic sea-ice loss, 1979–2009: Separating forced change from atmospheric internal variability. Climate Dyn, 43, 333–344, doi:10.1007/s00382-013-1830-9.

Screen JA, Deser C, Smith DM, Zhang X, Blackport R, Kushner PJ, Oudar T, McCusker KE, and Sun L, 2018: Consistency and discrepancy in the atmospheric response to Arctic sea-ice loss across climate models. Nat. Geosci, doi:10.1038/s41561-018-0059-y.

NASA Author Manuscript NASA Author Manuscript NASA Author Manuscript

Semenov VA and Latif M, 2015: Nonlinear winter atmospheric circulation response to Arctic sea ice concentration anomalies for different periods during 1966–2012 Environ. Res. Lett, 10, doi: 10.1088/1748-9326/10/5/054020.

Semmler T, Stulic L, Jung T, Tilinina N, Campos C, Gulev S, and Koracin D, 2016: Seasonal atmospheric responses to reduced Arctic sea ice in an ensemble of coupled model simulations. J. Climate, 29, 5893–5913, doi:10.1175/JCLI-D-15-0586.1.

Sepp M, and Jaagus J, 2011: Changes in the activity and tracks of Arctic cyclones. Climatic Change. 105, 577–595, doi:10.1007/s10584-010-9893-7.

Serreze MC, and Barrett AP, 2008: The summer cyclone maximum over the central Arctic Ocean. J. Climate 21, 1048–1065, doi:10.1175/2007JCLI1810.1.

Shepherd TG, 2016: Effects of Arctic warming. Science, 353, 989–990, doi:10.1126/science.aag2349. [PubMed: 27701102]

Shields CA, and Kiehl JT, 2016: Atmospheric river landfall-latitude changes in future climate simulations. Geophys. Res. Lett, 43, 8775–8782, doi:10.1002/2016GL070470.

Smith DM, Dunstone NJ, Scaife AA, Fiedler EK, Copsey D, and Hardiman SC, 2017: Atmospheric response to Arctic and Antarctic sea ice: the importance of ocean-atmosphere coupling and the background state. J. Climate, doi:10.1175/JCLI-D-16-0564.1.

Smith D, and Coauthors, 2018: The Polar Amplification Model Intercomparison Project (PAMIP) contribution to CMIP6: investigating the causes and consequences of polar amplification. Geosci. Model Dev, submitted.

Sohn B-J, Lee S, Chung E-S, and Song H-J, 2016: The role of the dry static stability for the recent change in the Pacific Walker Circulation. J. Climate, 29, 2765–2779, doi:10.1175/JCLI-D-15-0374.1.

Stevens B, and Bony S, 2013: What are climate models missing? Science, 340, 1053–1054, doi: 10.1126/science.1237554. [PubMed: 23723223]

Stroeve JC, Kattsov V, Barrett A, Serreze M, Pavlova T, Holland M, and Meier WN, 2012: Trends in Arctic sea ice extent from CMIP5, CMIP3 and observations. Geophys. Res. Lett, 39, doi: 10.1029/2012GL052676.

Stroeve JC, Markus T, Boisvert L, Miller J, and Barrett A, 2014: Changes in Arctic melt season and implications for sea ice loss. Geophys. Res. Lett, 41, 1216–1225, doi:10.1002/2013GL058951.

Sun L, Deser C, and Tomas RA, 2015: Mechanisms of stratospheric and tropospheric circulation response to projected Arctic sea ice loss. J. Climate, 28, 7824–7845, doi:10.1175/JCLI-D-15-0169.1.

Sun L, Perlwitz J, and Hoerling M, 2016: What caused the recent “Warm Arctic, Cold Continents” trend pattern in winter temperatures? Geophys. Res. Lett, 43, 5345–5352, doi:10.1002/2016/GL069024.

Tastula E-M, Vihma T, Andreas EL, and Galperin B, 2013: Validation of the diurnal cycles in atmospheric reanalyses over Antarctic sea ice. J. Geophys. Res. Atmos, 118, 4194–4204, doi: 10.1002/jgrd.50336.

Taylor PC, Hegyi BM, and Boeke RC, 2017: The process of amplified Arctic warming: Influence on Arctic-Mid latitude connection in climate models? Workshop on Arctic Change & Its Influence on Mid-latitude Climate and Weather, Poster Presentation, https://usclivar.org/sites/default/files/meetings/2017/arctic-posters/Taylor-Patrick-2017-arctic.pdf.

Taylor PC, Hegyi BM, Boeke RC, and Boisvert LN, 2018: On the increasing importance of air-sea exchanges in a thawing Arctic: A review. Atmos., 9, doi:10.3390/atmos9020041.

Trenary L, DelSole T, Tippett MK, and Doty B, 2016: Extreme eastern US winter of 2015 not symptomatic of climate change. Bull. Amer. Meteor. Soc, 97, 31–35, doi:10.1175/BAMS-D-16-0156.1.

Uttal T, and Coauthors, 2002: Surface heat budget of the Arctic Ocean. Bull. Amer. Meteor. Soc, 83, 255–275, doi:10.1175/1520-0477(2002)083<0255:SHBOTA>2.3.CO;2.

Vaganov EA, Briffa KR, Naurzbaev NM, Schweingruber FH, Shiyatov SG, and Shishov VV, 2000: Long-term climatic changes in the Arctic region of the Northern Hemisphere. Doklady Earth Sci, 375, 1314–1317.

NASA Author Manuscript NASA Author Manuscript NASA Author Manuscript

Vavrus SJ, Wang F, Martin JE, Francis JA, Peings Y, and Cattiaux J, 2017: Changes in North American atmospheric circulation and extreme weather: evidence of an Arctic connection. J. Climate, doi: 10.1175/JCLI-D-16-0762.1.

Villamil-Otero GA, Zhang J, He J, and Zhang X, 2018: Role of extratropical cyclones in the recently observed increase in poleward moisture transport into the Arctic Ocean, Adv. Atmos. Sci, 35, 85–94, doi:10.1007/s00376-017-7116-0.

Walsh JE, Chapman WL, and Fetterer F, 2015: Gridded monthly sea ice extent and concentration, 1850 – onward, Version 1. NSIDC: National Snow and Ice Data Center, Boulder, Colorado, doi: 10.7265/N5833PZ5 Date Accessed 30 March 2017.

Wang S-Y, Lin Y-H, Lee M-Y, Yoon J-H, and Meyer JDD, 2017: Accelerated increase in the Arctic tropospheric warming events surpassing stratospheric warming events during winter. Geophys. Res. Lett, 44, 3806–3815, doi:10.1002/2017GL073012.

Wang Y-H, and Magnusdottir G, 2012: The shift of the northern node of the NAO and cyclonic Rossby wave breaking. J. Climate, 25, 7973–7982, doi:10.1175/JCLI-D-11-00596.1.

Wegmann M, and Coauthors, 2015: Arctic moisture source for Eurasian snow cover variations in autumn. Environ. Res. Lett, 10, doi:10.1088/1748-9326/10/5/054015.

Wegmann M, Orsolini Y, Dutra E, Bulygina O, Sterin A, and Brönnimann S, 2017: Eurasian snow depth in long-term climate reanalyses. Cryosph, 11, 923–935, doi:10.5194/tc-11-923-2017.

Weiss J, and Marsan D, 2004: Scale properties of sea ice deformation and fracturing. Comptes Rendus Phys, 5, 735–751, doi:10.1016/j.crhy.2004.09.005.

Wendisch M, and Coauthors, 2017: Understanding causes and effects of rapid warming in the Arctic. Eos, 98, doi:10.1029/2017EO064803.

Wilks D, 2006: Statistical methods in the atmospheric sciences. Academic Press, San Diego, California, 464 pp., ISBN:9780123850225.

Woods C, and Caballero R, 2016: The role of moist intrusions in winter Arctic warming and sea ice decline. J. Climate, 29, 4473–4485, doi:10.1175/JCLI-D-15-0773.1.

Woollings T, Hannachi A, and Hoskins B, 2010: Variability of the North Atlantic eddy-driven jet stream. Quart. J. Roy. Meteor. Soc, 136, 856–868, doi:10.1002/qj.625.

Wullschleger SD, Hinzman LD, and Wilson CJ, 2011: Planning the next generation of Arctic ecosystem experiments, Eos, 92, 141–148, doi:10.1029/2011EO170006.

Yang W and Magnusdottir G, 2017: Springtime extreme moisture transport into the Arctic and its impact on sea ice concentration. J. Geophys. Res. Atmos, 122, 5516–5329, doi: 10.1002/2016JD026324.

Yang W and Magnusdottir G, 2018: Year-to-year variability in Arctic minimum sea ice extent and its preconditions in observations and the CESM Large Ensemble simulations. Scien. Rep, submitted.

Yin JH, 2005: A consistent poleward shift of the storm tracks in simulations of 21st century climate. Geophys. Res. Lett, 32, L18,701, doi:10.1029/2005GL023684.

Yoo C, Lee S, and Feldstein S, 2012a: Arctic response to an MJO-like tropical heating in an idealized GCM. J. Atmos. Sci, 69, 2379–2393, doi:10.1175/JAS-D-11-0261.1.

Yoo C, Lee S, and Feldstein SB, 2012b: Mechanisms of Arctic surface air temperature change in response to the Madden-Julian Oscillation, J. Climate, 25, 5777–5790, doi:10.1175/JCLI-D-11-00566.1.

Yoo C, Feldstein SB, and Lee S, 2013: The prominence of a tropical convective signal in the wintertime Arctic temperature. Atmos. Sci. Lett, 15, 7–12, doi:10.1002/asl2.455.

Zuo J, Ren HL, Wu B, and Li W, 2016: Predictability of winter temperature in China from previous autumn Arctic sea ice. Climate Dyn, 47, 2331, doi:10.1007/s00382-015-2966-6.

Zhang J, Stegall ST, and Zhang X, 2018: Wind-SST-sea ice relationship in the Chukchi-Beaufort seas during autumn. Environ. Res. Lett, doi:10.1088/1748-9326/aa9adb.

Zhang X, Ikeda M, and Walsh JE, 2003: Arctic sea-ice and freshwater changes driven by the atmospheric leading mode in a coupled sea ice-ocean model. J. Climate, 16, 2159–2177, doi: 10.1175/2758.1.

NASA Author Manuscript

NASA Author Manuscript

NASA Author Manuscript

Zhang X Walsh JE,, Zhang J, Bhatt US, and Ikeda M, 2004: Climatology and interannual variability of arctic cyclone activity: 1948–2002. J. Climate, 17, 2300–2317. doi: 10.1175/1520-0442(2004)017<2300:CAIVOA>2.0.CO;2.

Zhang X, Sorteberg A, Zhang J, Gerdes R, and Comiso JC, 2008: Recent radical shifts in atmospheric circulations and rapid changes in Arctic climate system. Geophys. Res. Lett, 35, doi: 10.1029/2008GL035607.

Zhang X, He J, Zhang J, Polaykov I, Gerdes R, Inoue J, and Wu P, 2013: Enhanced poleward moisture transport and amplified the northern high-latitude wetting trend. Nature Climate Change, 3, 47–51, doi:10.1038/nclimate1631.

NASA Author Manuscript

NASA Author Manuscript

NASA Author Manuscript

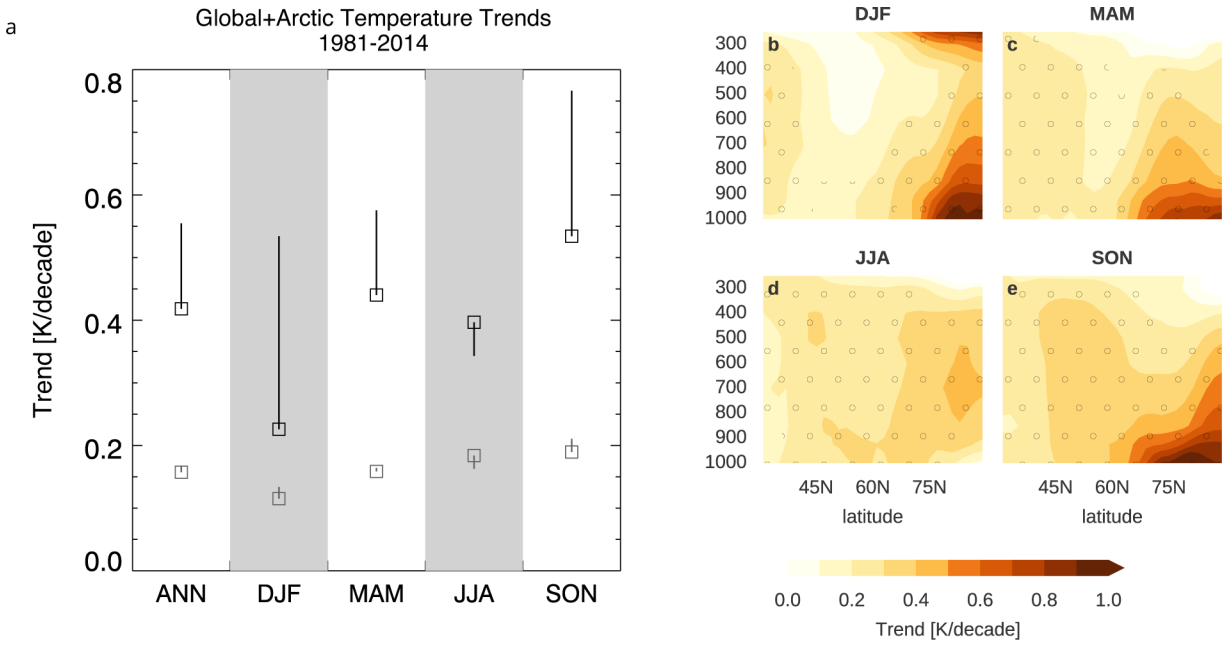

Figure 1.

(a) Annual (ANN) and seasonal (DJF, MAM, JJA, SON) surface air temperature (SAT) trends from 1981 to 2014 in the Arctic (black squares, north of 60°N) and for the whole globe (gray squares) using the average of four observational products (CRU, NOAA, GISS, and BEST) masked in such a way that all four products share a uniform missing data mask over the ocean. The vertical lines show trends for the average of CRU and BEST without applying this uniform mask. This line therefore indicates, in large part, the uncertainty coming from the limited observational temperature record over the Arctic ocean. (b–e) Seasonal and zonal-mean air temperature trends from 1981–2015 for the average of the MERRA, MERRA-2, ERA-Interim, JRA-55, and CFSR reanalysis products. Stippling indicates trends significant with a $p < 0.05$ after the false discovery rate was applied (Wilks 2006).

NASA Author Manuscript

NASA Author Manuscript

NASA Author Manuscript

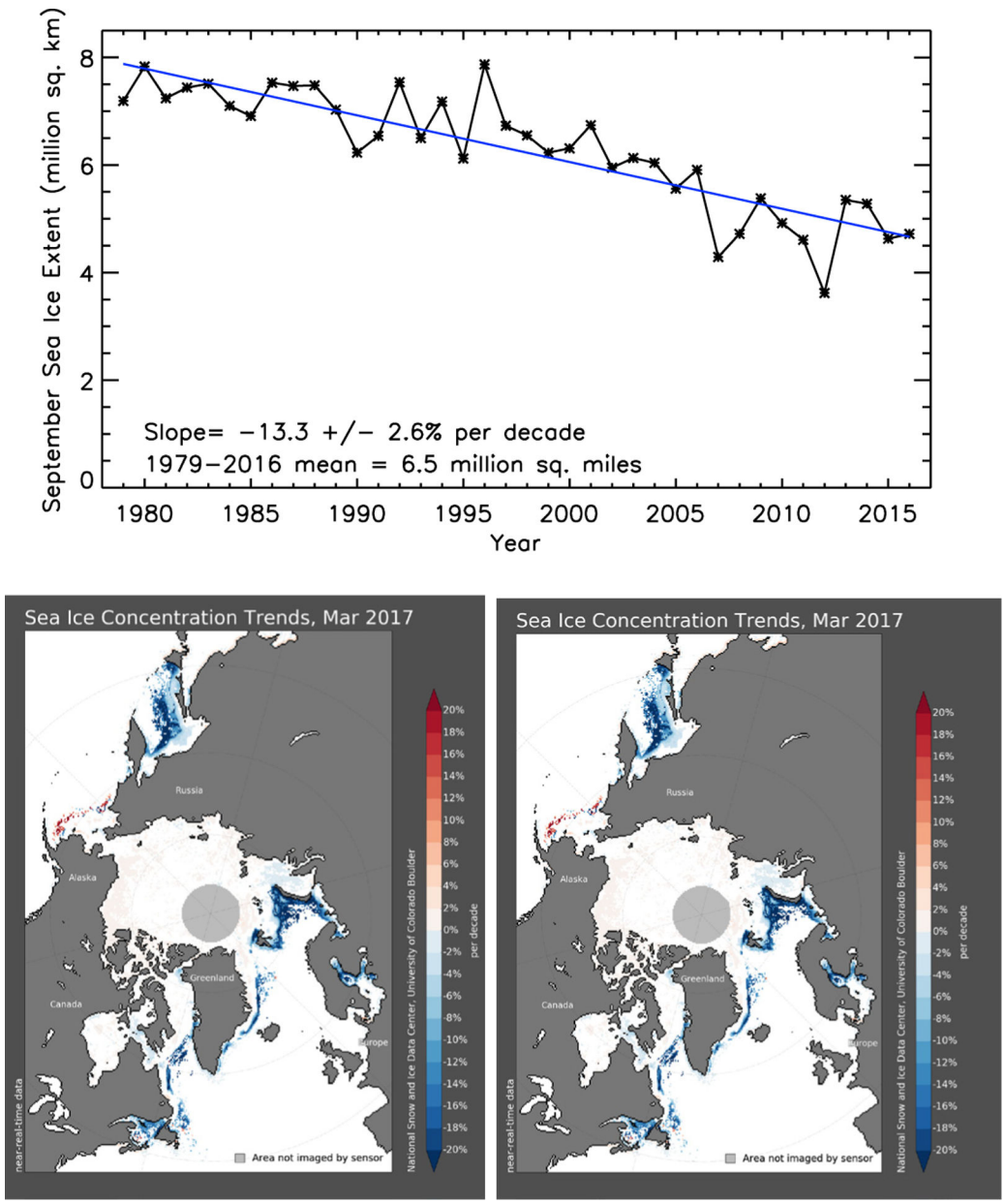

Figure 2.

Satellite-era Arctic sea ice trends from 1979–2016 are shown for (top) September areal extent (courtesy Patrick Taylor, NASA) and (bottom) March and September regional ice concentration trends (units: % per decade; courtesy of Julienne Stroeve, NSIDC).

NASA Author Manuscript

NASA Author Manuscript

NASA Author Manuscript

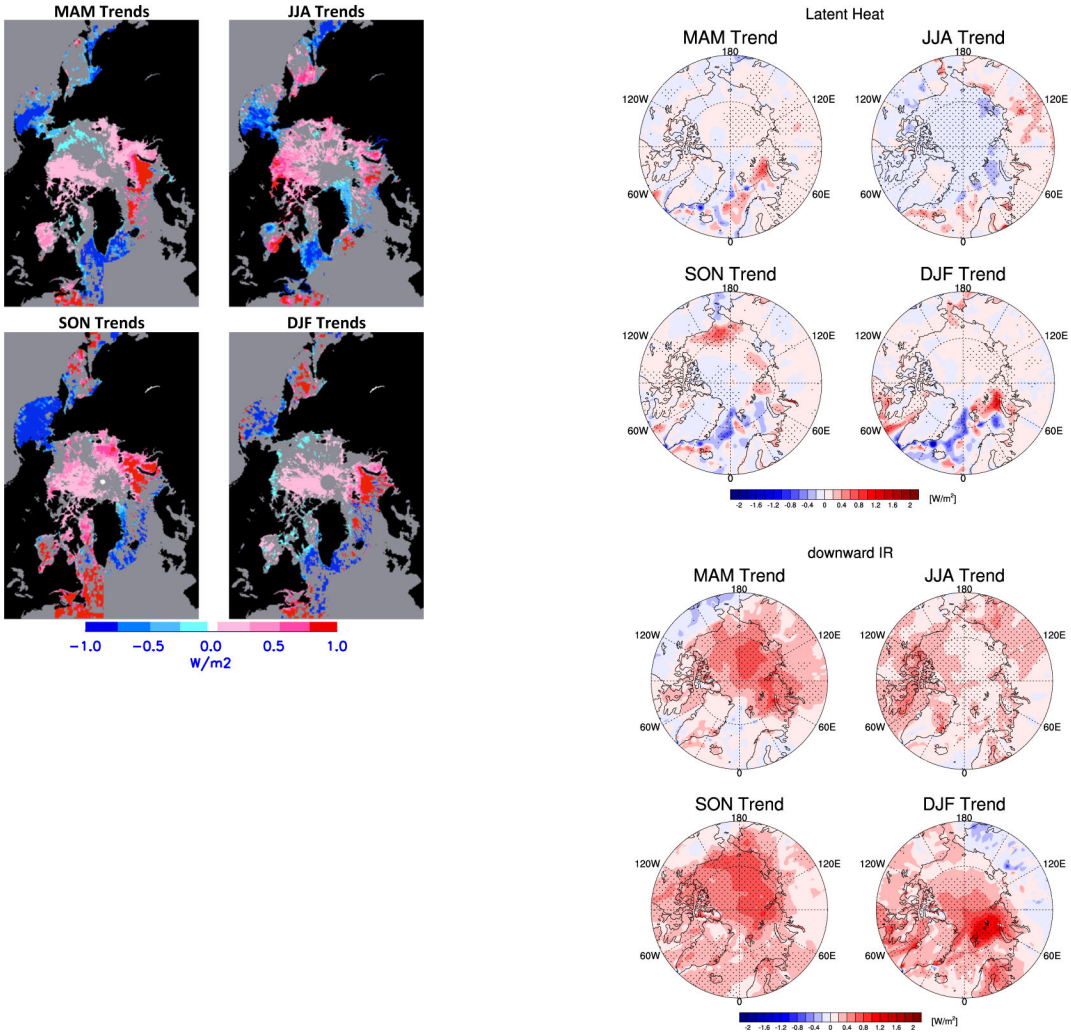

Figure 3.

Trends in selected components of the Arctic surface energy budget: (top left) Atmospheric Infrared Sounder (AIRS)-based observational surface latent heat flux trends constrained from 2002–2016 (W m^{-2} yr^{-1}; adapted by Linette Boisvert, U. Maryland, from Boisvert and Stroeve 2015); (top right) ERA-I surface latent heat flux trends for 1979–2016 (W m^{-2} yr^{-1}; courtesy of Tingting Gong, Qingdao National Lab. for Marine Science and Technology); and (bottom) ERA-I surface downwelling longwave radiation from 1979–2016 (courtesy Tingting Gong). Positive latent heat fluxes are defined as surface to atmosphere, whereas positive surface downwelling longwave trends are from atmosphere to surface.

NASA Author Manuscript

NASA Author Manuscript

NASA Author Manuscript

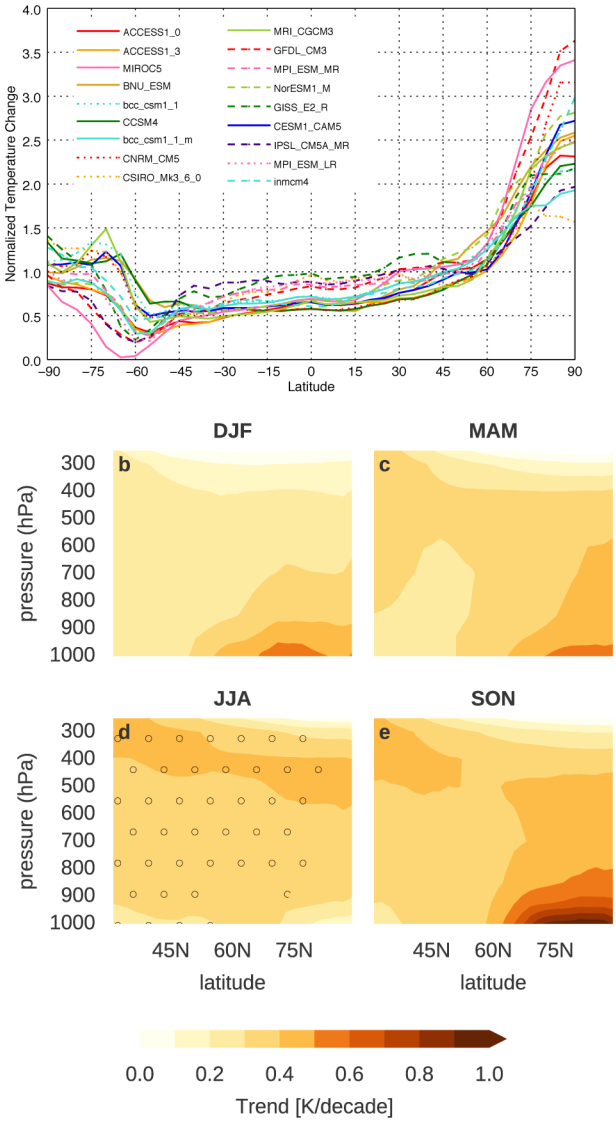

Figure 4.

CMIP5 models simulations of (a) zonal-mean temperature changes normalized by the global mean change (2080–2100 minus 2005–2025) and (b–e) same as Figure 1b–e but for the CMIP5 multi-model mean historical + RCP8.5 for 1981–2015. Stippling indicates trends significant with a $p < 0.05$ after the false discovery rate was applied (Wilks 2006).

NASA Author Manuscript

NASA Author Manuscript

NASA Author Manuscript

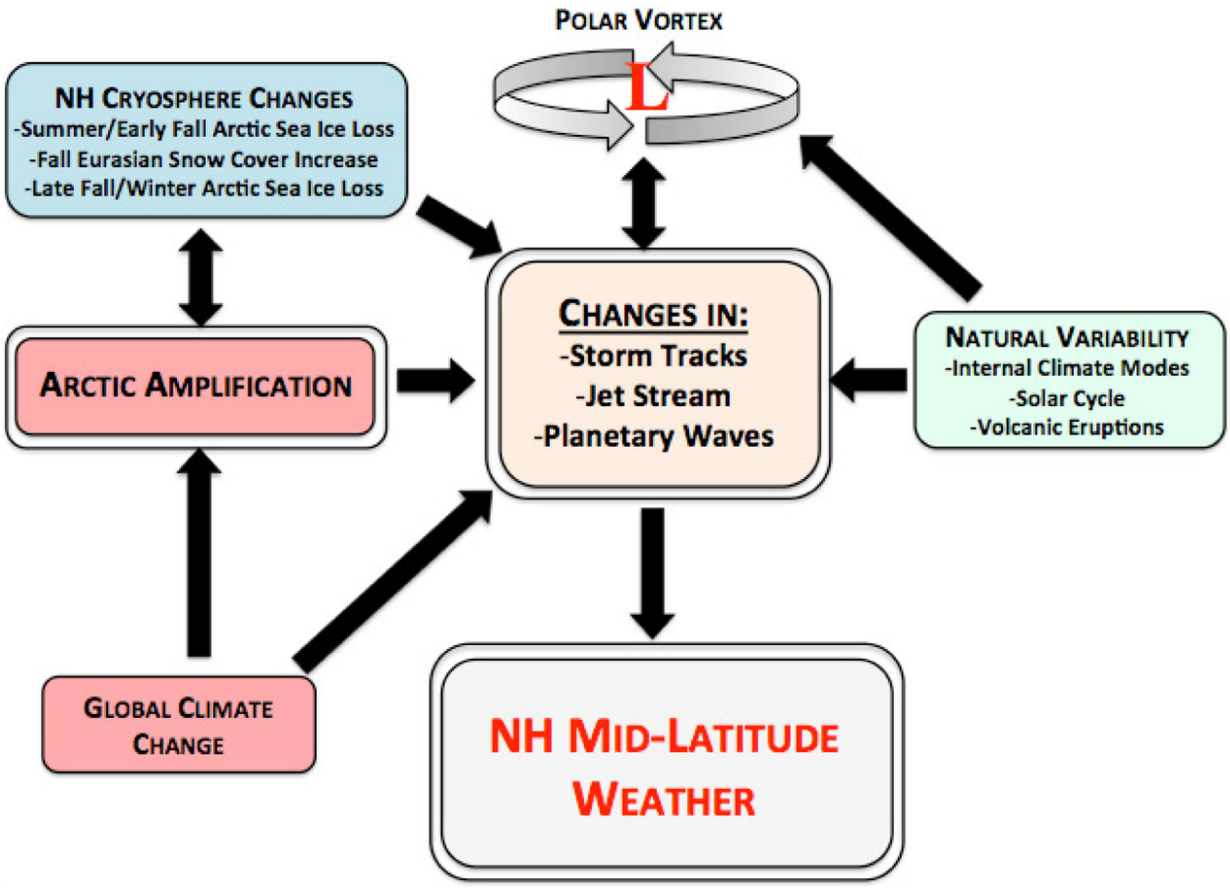

Figure 5.
Complexity of linkage pathways. (Figure from Cohen et al. 2014).

NASA Author Manuscript

NASA Author Manuscript

NASA Author Manuscript

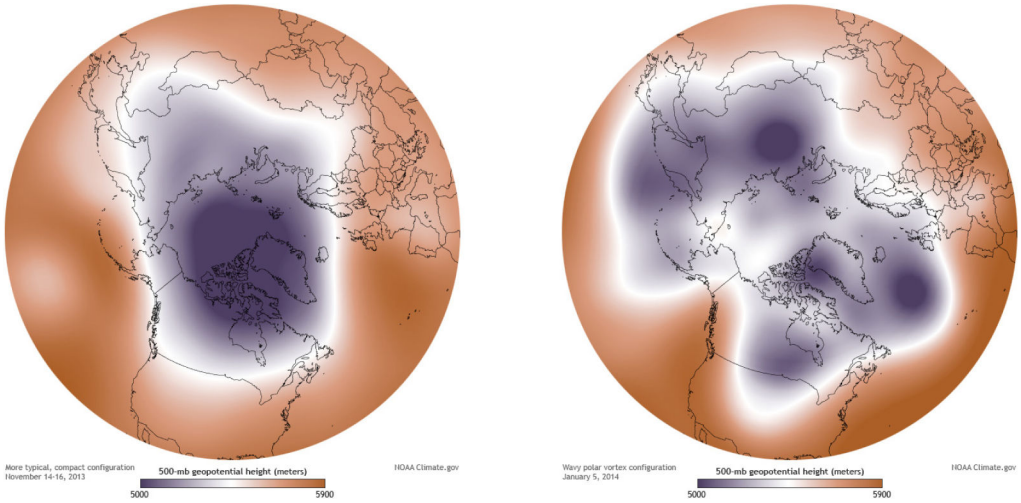

Figure 6.

Sample geopotential height fields for 500 hPa with lower values in purple and the jet stream in white. (a) Contrasts a single, more zonal path encircling the tropospheric polar vortex versus a wavier configuration (b) with multiple low centers. (Figure from NOAA Climate.gov).

NASA Author Manuscript

NASA Author Manuscript

NASA Author Manuscript

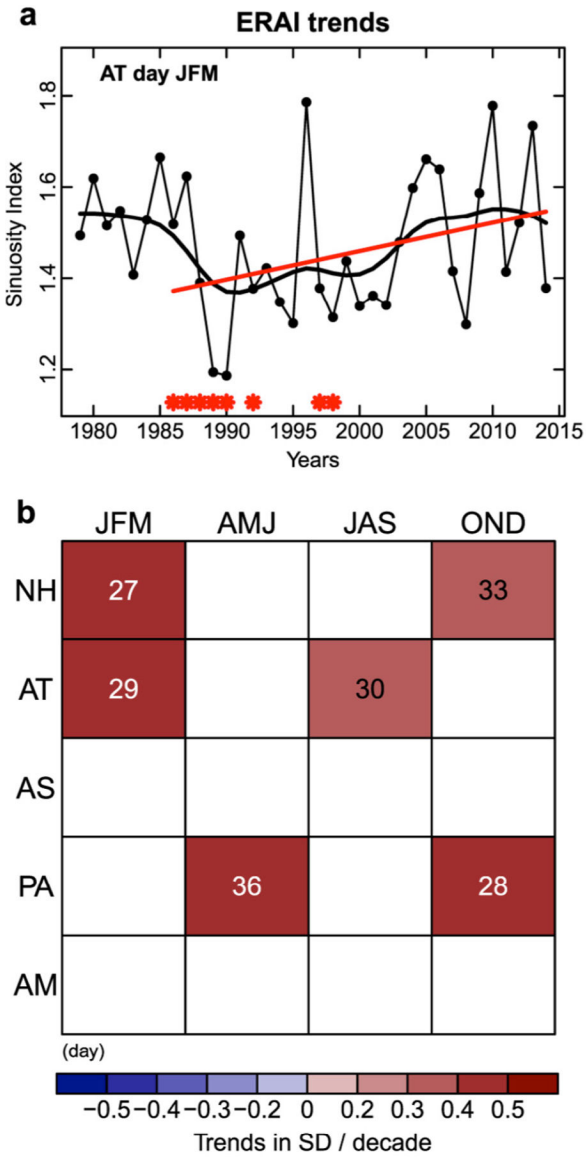

Figure 7.

ERA-Interim recent trends in sinuosity. a) Time series of Atlantic JFM sinuosity, with a 5-year spline smoothing, and b) longest significant trends in sinuosity for all geographic domains (rows) and seasons (columns). Colors represent trends in standard deviation (SD) per decade. (Figure from Cattiaux et al. 2016).

NASA Author Manuscript

NASA Author Manuscript

NASA Author Manuscript

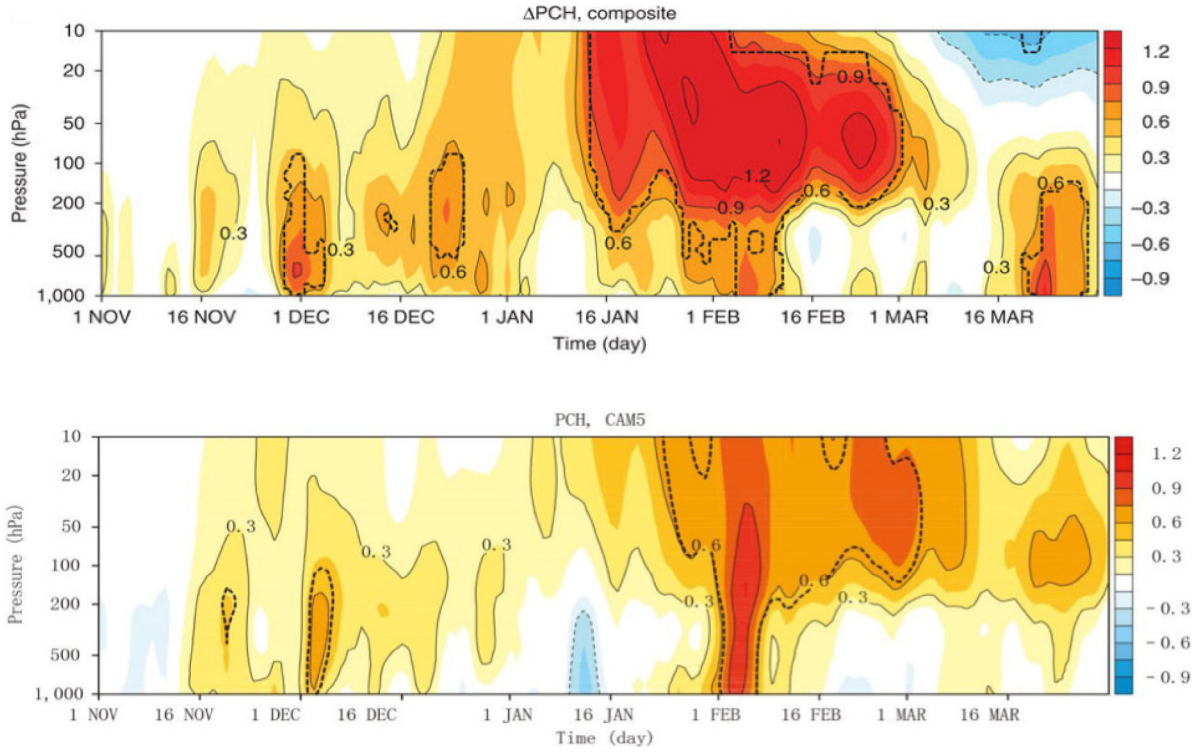

Figure 8.

Observed (top) and modeled (bottom) ensemble-mean responses to reduced sea ice over Barents-Kara seas for the subseasonal evolution of the polar cap height anomaly (PCH; shading is standard deviation) as a function of pressure (hPa; Figure from Kim et al. 2014).

NASA Author Manuscript

NASA Author Manuscript

NASA Author Manuscript

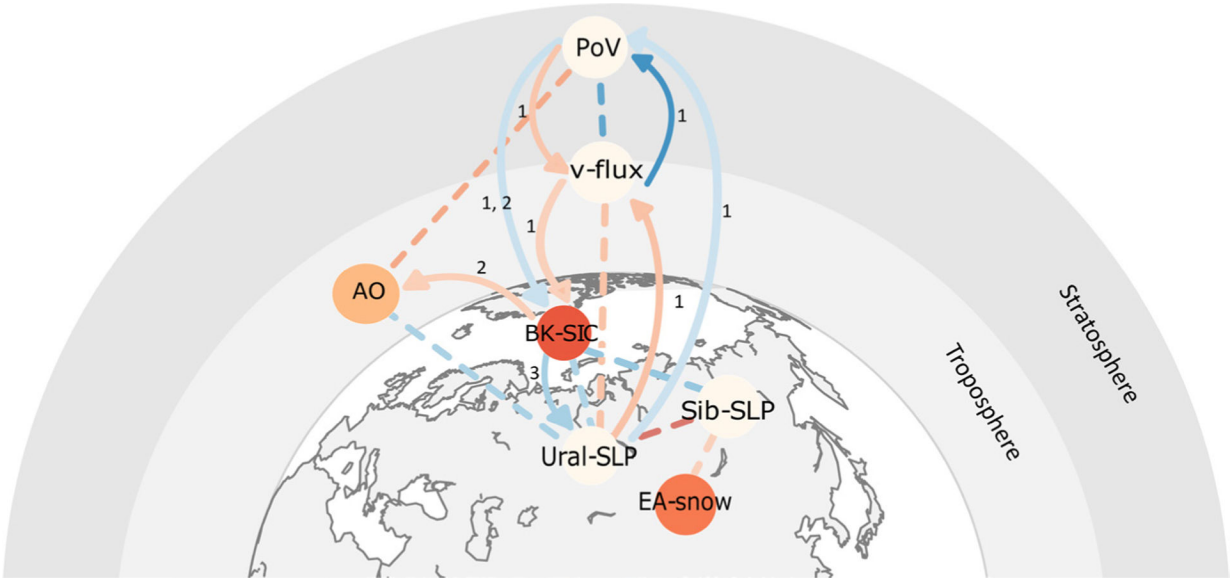

Figure 9.

Causal pathways between different Arctic actors extracted from observations. Blue arrows indicate a negative causal influence, red arrows a positive causal influence, and the number next to the arrows indicates the lag in months. The regional actors, Barents-Kara sea ice concentration (BK-SIC), Ural region sea level pressure (Ural-SLP), Siberian sea level pressure (Sib-SLP), and East Asia snow cover (EA-snow), are presented according to their approximate geographical location. The hemispheric actors (Arctic Oscillation (AO), upward wave propagation (v-flux), and polar vortex (PoV)), are presented according to their approximate latitude and pressure levels. (Figure from Kretschmer et al. 2016).

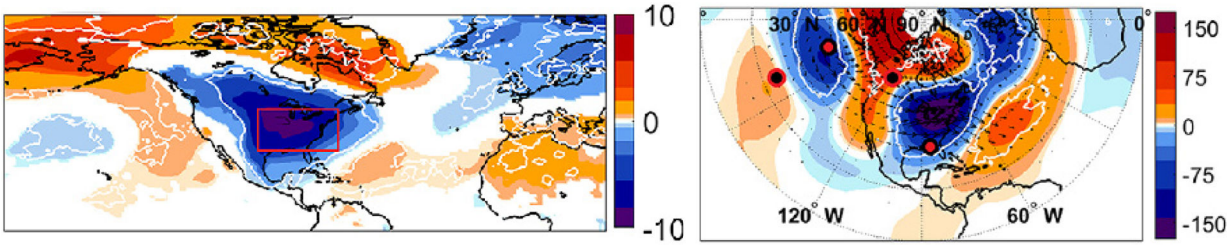

Figure 10.

(left) Surface temperature anomalies (K) and (right) 250 hPa geopotential height anomalies (m, shading) during North American cold spells as determined in the red box region. Only anomalies exceeding the 95% confidence level derived from a random Monte Carlo sampling procedure are shown. The data covers ERA-20C DJFs over the period 1900–2010. (Figure from Messori et al. 2016).

NASA Author Manuscript NASA Author Manuscript NASA Author Manuscript

NASA Author Manuscript

NASA Author Manuscript

NASA Author Manuscript

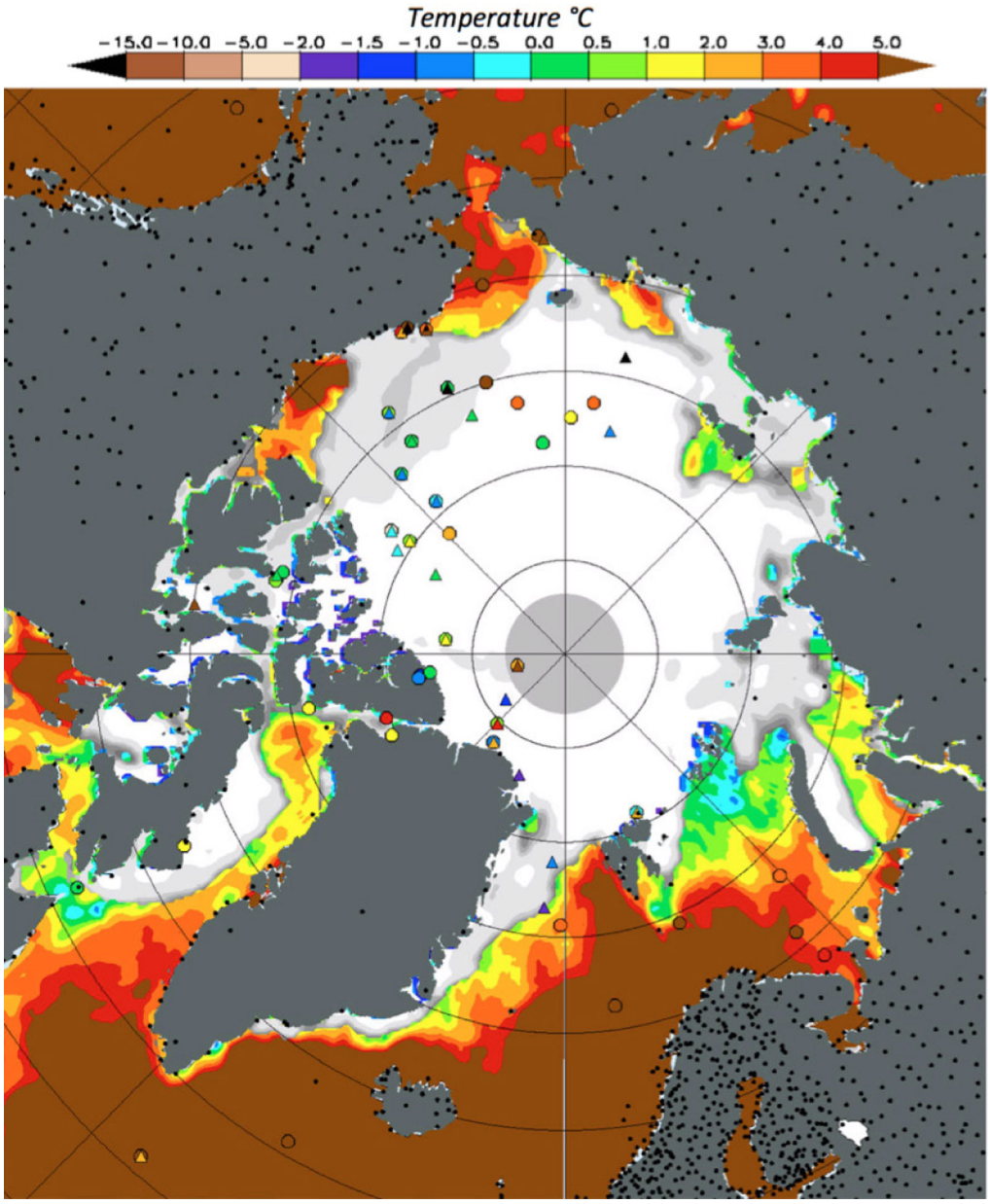

Figure 11.

Map of *in situ* observations on June 28, 2017 of surface temperature (colored circles) and air temperature (colored triangles) from the International Arctic Buoy Programme (IABP); analyses of SST from NOAA OISST; and ice concentration from NSIDC Daily Polar Gridded Sea Ice Concentration. Also shown are the positions of land stations (black dots; courtesy of Wendy Ermold, University of Washington).

NASA Author Manuscript

NASA Author Manuscript

NASA Author Manuscript

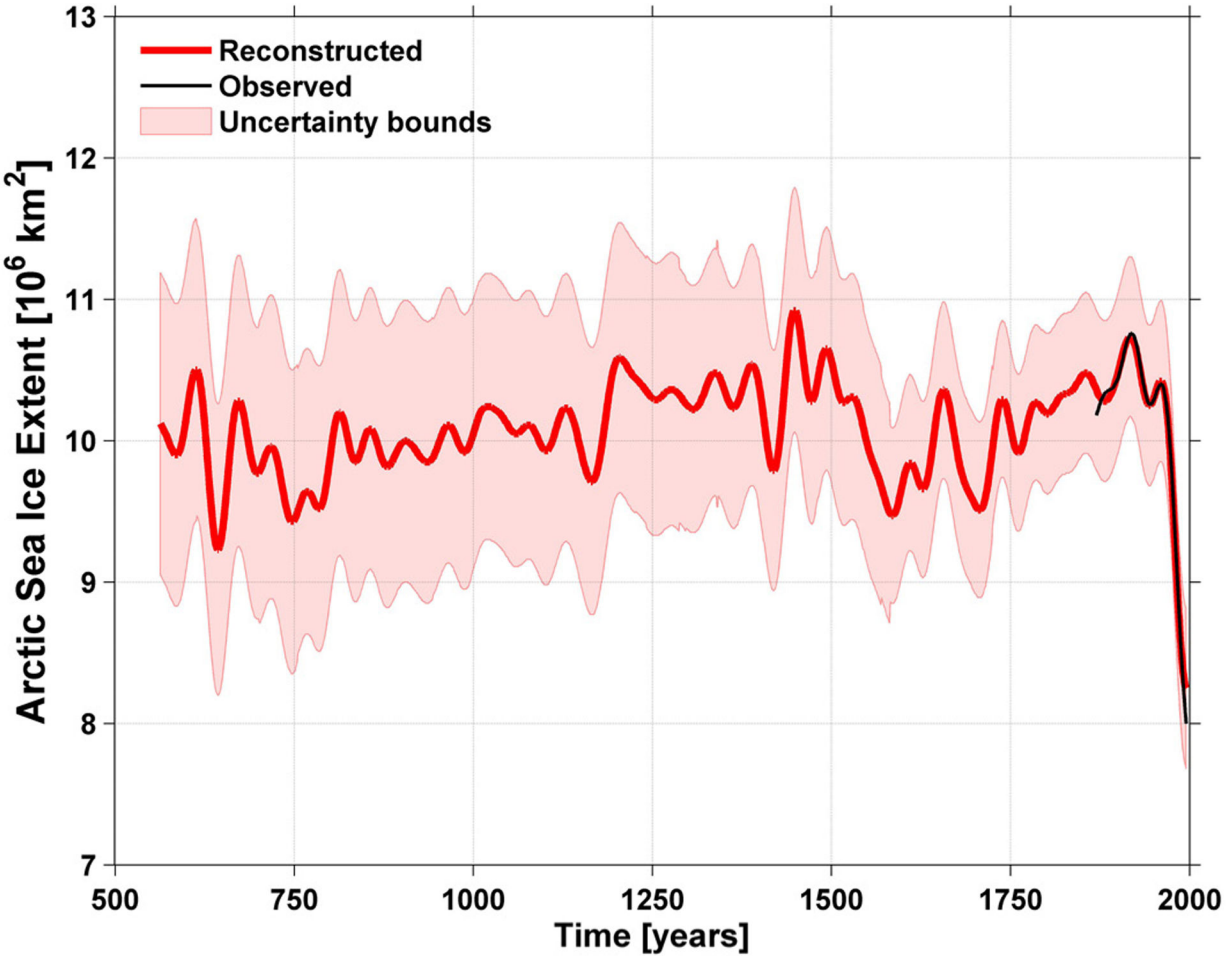

Figure 12.

Fourty-years of smoothed reconstructed late summer Arctic sea ice extent with 95% confidence interval (red line) and modern observations (black line) from 800 to present. (Figure from Kinnard et al. 2011).

NASA Author Manuscript

NASA Author Manuscript

NASA Author Manuscript

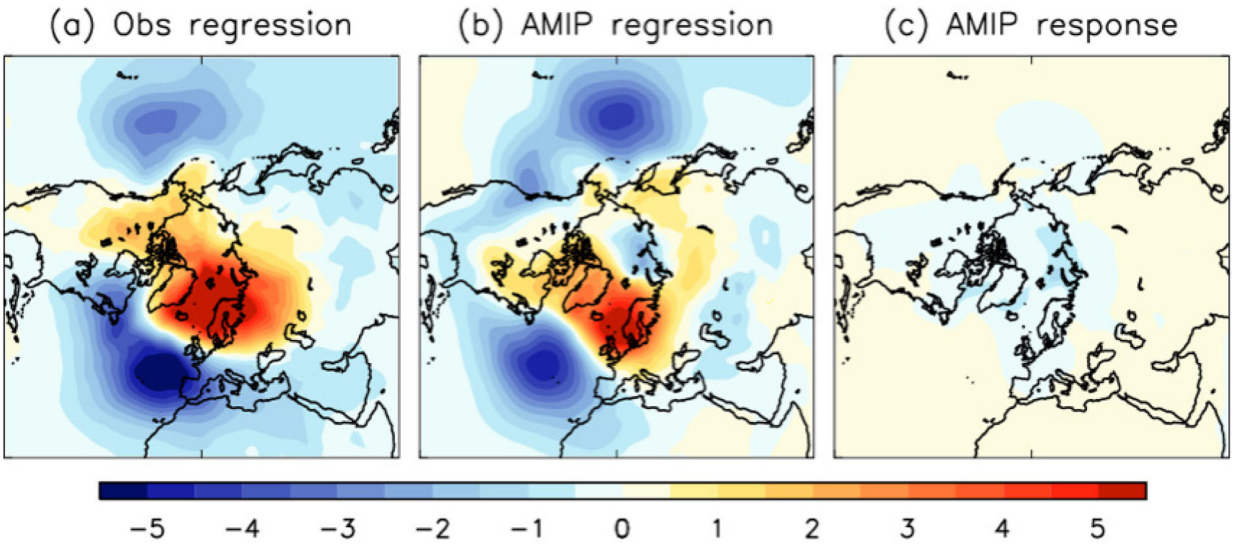

Figure 13.

Linear regression between autumn (September-November) Arctic sea ice extent and winter (December-February) mean sea level pressure (reversed sign) in (a) observations and (b) atmosphere model experiments forced by observed sea ice and sea surface temperatures following the Atmosphere Model Intercomparison Project (AMIP) protocol. All time series were linearly detrended and cover the period December 1979 to November 2009. (c) Winter mean sea level response to reduced sea ice in atmospheric model experiments (scaled by the average autumn sea ice extent reduction). Units are hPa per million km^2. (Figure from Smith et al. 2017).

NASA Author Manuscript NASA Author Manuscript NASA Author Manuscript

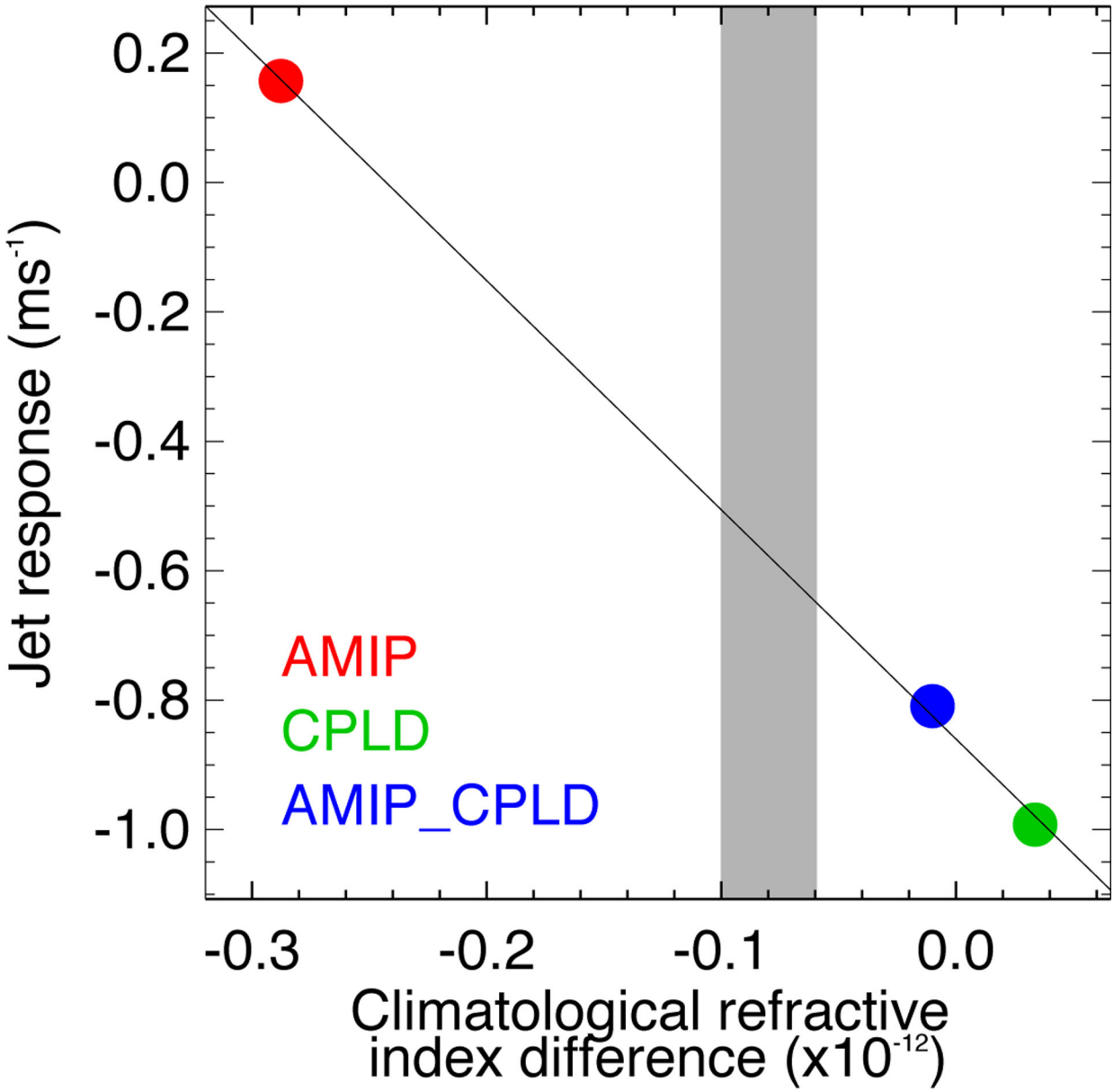

Figure 14.

Dependence of Atlantic jet response on the background climatological refractive index difference between mid (25–35oN) and high (60–80oN) latitudes at 200 hPa. Grey shading shows the observed range from the ERA-Interim and NCEP II reanalyses. The Atlantic jet response is defined as the difference in zonal mean zonal wind at 200 hPa over the region 60–0oW, 50–60oN between model experiments with reduced and climatological Arctic sea ice. Experiments were performed with the same model but with three different configurations: atmosphere only (AMIP); fully coupled (CPLD); and atmosphere only but with SST biases from the coupled model (AMIP_CPLD). An “emergent constraint” is obtained where the observed refractive index difference (grey shading) intersects the

simulated response (black line), suggesting a modest weakening of the Atlantic jet in response to reduced Arctic sea ice (Figure from Smith et al. 2017).

NASA Author Manuscript
NASA Author Manuscript
NASA Author Manuscript

NASA Author Manuscript

NASA Author Manuscript

NASA Author Manuscript

Table 1.

Atmospheric and oceanic reanalysis datasets covering at least 100 years.

Name	Resolution	Coverage	Reference
20CR (V2c) (Atmosphere)	2° × 2°	1850 – 2014 (V2: 1971–2010)	Compo et al. (2011)
ERA-20C (Atmosphere)	1° × 1°	1900 – 2010	Poli et al. (2016)
CERA-20C (Atmosphere + Ocean)	1° × 1°	1900 – 2010	Laloyaux et al. (2016)
EN.4.2.0 (Ocean)	1° × 1°	1900 – up to date	Good et al. (2013)
SODA2.2.4 (Ocean)	0.25° × 0.25°	1871 – 2008	Carton and Giese (2008)

NASA Author Manuscript

NASA Author Manuscript

NASA Author Manuscript

Table 2.

Proposed Coordinated Multi-Model Experiments: Polar Amplification Multi-model Intercomparison Project (PAMIP)

Experiment - Time Slice			Forcing
1. AMIP *	Control		Present-day climatological SST and sea ice (SIC)
	SST	pi	Pre-industry SST
		2 degree	Future 2 degree warming SST
	Arctic SIC	pi	Pre-industry SIC
		2 degree	Future 2 degree warming SIC
	Antarctic SIC	pi	Pre-industry SIC
		2 degree	Future 2 degree warming SIC
2. Coupled	Control		Constrained by present-day climatological SIC
	Arctic SIC	pi	Constrained by pre-industry SIC
		2 degree	Constrained by future 2 degree warming SIC
	Antarctic SIC	pi	Constrained by pre-industry SIC
		2 degree	Constrained by future 2 degree warming SIC
3. AMIP-Reg **	Arctic SIC - Pacific	2 degree	Future 2 degree warming SIC in the Pacific Arctic
	Arctic SIC - Atlantic	2 degree	Future 2 degree warming SIC in the Atlantic Arctic
4. AMIP-BKGD ***	Arctic SIC	present-day	Present-day SIC
	Arctic SIC	2 degree	Future 2 degree warming SIC
5. AMIP	SIC	1979–2014	Climatological SST and transient SIC
	SST	1979–2014	Transient SST and climatological SIC
6. Coupled	SIC	present-day	Constrained by present-day SIC
	SIC	2 degree	Constrained by 2 degree warming SIC

* Experiment “SST”, “Arctic SIC”, and “Antarctic SIC” are designed the same as “Control” except the specified forcing of “SST” or “SIC”.

** The same as Experiment “Arctic SIC” but SIC is prescribed in the Pacific or Atlantic Arctic seas.

*** SST in both experiments are from experiment “Coupled Control” above, instead of observation.

ResearchGate

See discussions, stats, and author profiles for this publication at: https://www.researchgate.net/publication/281375803

Two distinct influences of Arctic warming on cold winters over North America and East Asia

Article *in* Nature Geoscience · August 2015

DOI: 10.1038/NGEO2517

CITATIONS
167

READS
521

7 authors, including:

J.-S. Kug
Pohang University of Science and Technology
209 PUBLICATIONS **7,479** CITATIONS
SEE PROFILE

Jee-Hoon Jeong
Chonnam National University
68 PUBLICATIONS **2,158** CITATIONS
SEE PROFILE

Yeon-Soo Jang
Pohang University of Science and Technology
5 PUBLICATIONS **229** CITATIONS
SEE PROFILE

Baek Min Kim
Korea Polar Research Institute
93 PUBLICATIONS **1,523** CITATIONS
SEE PROFILE

Some of the authors of this publication are also working on these related projects:

Dynamics, impacts, and predictability of primary climate variability modes View project

Winter North Atlantic Oscillation prediction View project

All content following this page was uploaded by Chris K. Folland on 31 August 2015.

The user has requested enhancement of the downloaded file.

nature geoscience

REVIEW ARTICLE

PUBLISHED ONLINE: 17 AUGUST 2014 | DOI: 10.1038/NGEO2234

Recent Arctic amplification and extreme mid-latitude weather

Judah Cohen[1]*, James A. Screen[2], Jason C. Furtado[1], Mathew Barlow[3,4], David Whittleston[5], Dim Coumou[6], Jennifer Francis[7], Klaus Dethloff[8], Dara Entekhabi[5], James Overland[9] and Justin Jones[1]

The Arctic region has warmed more than twice as fast as the global average — a phenomenon known as Arctic amplification. The rapid Arctic warming has contributed to dramatic melting of Arctic sea ice and spring snow cover, at a pace greater than that simulated by climate models. These profound changes to the Arctic system have coincided with a period of ostensibly more frequent extreme weather events across the Northern Hemisphere mid-latitudes, including severe winters. The possibility of a link between Arctic change and mid-latitude weather has spurred research activities that reveal three potential dynamical pathways linking Arctic amplification to mid-latitude weather: changes in storm tracks, the jet stream, and planetary waves and their associated energy propagation. Through changes in these key atmospheric features, it is possible, in principle, for sea ice and snow cover to jointly influence mid-latitude weather. However, because of incomplete knowledge of how high-latitude climate change influences these phenomena, combined with sparse and short data records, and imperfect models, large uncertainties regarding the magnitude of such an influence remain. We conclude that improved process understanding, sustained and additional Arctic observations, and better coordinated modelling studies will be needed to advance our understanding of the influences on mid-latitude weather and extreme events.

The Arctic cryosphere is an integral part of Earth's climate system and has undergone unprecedented changes within the past few decades. Rapid warming and sea-ice loss has had significant impacts locally, particularly in late summer and early autumn. September sea ice has declined at a rate of 12.4% per decade since 1979 (ref. 1), so that by summer 2012, nearly half of the areal coverage had disappeared. This decrease in ice extent has been accompanied by an approximately 1.8 m (40%) decrease in mean winter ice thickness since 1980 (ref. 2) and a 75–80% loss in volume[3].

Though sea-ice loss has received most of the research and media attention, snow cover in spring and summer has decreased at an even greater rate than sea ice. June snow cover alone has decreased at nearly double the rate of September sea ice[4]. The decrease in spring snow cover has contributed to both the rise in warm season surface temperatures over the Northern Hemisphere extratropical landmasses and the decrease in summer Arctic sea ice[5]. The combined rapid loss of sea ice and snow cover in the spring and summer has played a role in amplifying Arctic warming. However, snow cover and sea-ice trends diverge in the autumn and winter with sea ice decreasing in all months while snow cover has exhibited a neutral to positive trend in autumn and winter[6].

Climate change and Arctic amplification

While the global-mean surface temperature has unequivocally risen over the instrumental record[7], spatial heterogeneity of this warming plays an important role in the resulting climate impacts. In particular, the near-surface of the Northern Hemisphere high latitudes are warming at rates double that of lower latitudes[8–10]. This observed phenomenon (Figs 1 and 2a,b) is termed polar or Arctic amplification. Arctic amplification occurs in all seasons, but is strongest in autumn and winter. It is also a consistent feature in coupled climate model simulations of the recent past and future projections forced with increased greenhouse-gas concentrations[11,12]. Several processes are thought to contribute to Arctic amplification, including local radiative effects from increased greenhouse-gas forcing[12,13], changes in the snow- and ice-albedo feedback induced by a diminishing cryosphere[14–16], aerosol concentration changes and deposits of black carbon on snow and ice surfaces[17], changes in Arctic cloud cover and water vapour content[18,19], and a relatively smaller increase in emission of longwave radiation to space in the Arctic compared with the tropics for the same temperature increase[20]. In addition to these local drivers of Arctic amplification, Arctic temperature change is sensitive to variations in the poleward transport of heat and moisture into the Arctic from lower latitudes[16,21].

Rapid Arctic warming has been accompanied by extensive loss of sea ice[9]. Arctic sea ice strongly modulates near-surface conditions at high latitudes, which then influences regional and, potentially, remote climate. Because open water has a much lower albedo than ice, more sunlight is absorbed at the ocean surface, where sea ice has recently receded in the Arctic. More absorbed energy has resulted in 4–5 °C sea surface temperature anomalies in these newly ice-free regions[22]. However, during autumn when the air cools to temperatures lower than the ocean surface, the excess heat absorbed during summer is transferred from the ocean to the atmosphere via radiative and turbulent fluxes, which strongly warms the lower Arctic troposphere. The additional heat in the system slows the formation

[1]Atmospheric and Environmental Research, Inc., Lexington, Massachusetts 02421, USA, [2]College of Engineering, Mathematics and Physical Sciences, University of Exeter, Exeter, Devon EX4 4QF, UK, [3]Department of Environmental, Earth, and Atmospheric Sciences, University of Massachusetts Lowell, Lowell, Massachusetts 01854, USA, [4]The Climate Change Initiative, University of Massachusetts Lowell, Lowell, Massachusetts 01854, USA, [5]Department of Civil and Environmental Engineering, Massachusetts Institute of Technology, Cambridge, Massachusetts, 02139, USA, [6]Potsdam Institute for Climate Impact Research — Earth System Analysis, 14412 Potsdam, Germany, [7]Institute for Marine and Coastal Sciences, Rutgers University, New Brunswick, New Jersey 08901, USA, [8]Alfred Wegener Institute, Helmholtz Centre for Polar and Marine Research, AWI Potsdam 14473, Germany, [9]Pacific Marine Environmental Laboratory, Seattle, Washington 98115, USA. *e-mail: jcohen@aer.com

© 2014 Macmillan Publishers Limited. All rights reserved

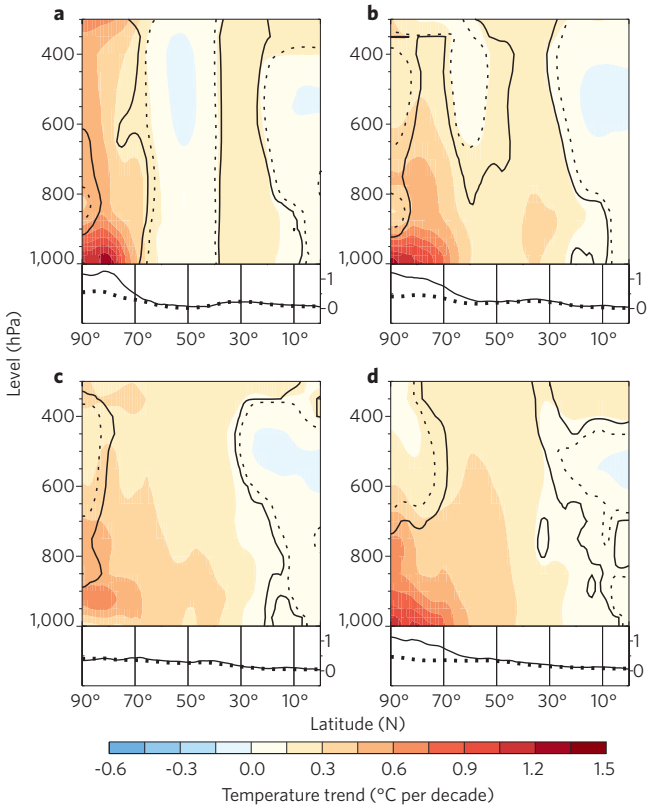

Figure 1 | Polar amplification of temperature trends, 1979–2014. Zonally averaged temperature trends averaged around circles of latitude for **a**, winter (December–February), **b**, spring (March–May), **c**, summer (June–August) and **d**, autumn (September–November). Trends are based on ERA-Interim reanalysis data[95] from March 1979 to February 2014. The black contours indicate where trends differ significantly from zero at the 99% (solid lines) and 95% (dotted lines) confidence levels. The line graphs show trends (same units as in colour plots) averaged over the lower part of the atmosphere (950–1,000 hPa; solid lines) and over the entire atmospheric column (300–1,000 hPa; dotted lines)[9].

of sea ice through winter, both in extent and, especially, thickness[23,24]. Hence, winter sea ice has thinned[2], enabling easier melting, fracturing and/or mobility of the ice cover. The increased fraction of open water in winter generates warmer, moister air masses over the Arctic Ocean and nearby continents[15,25], weakening the meridional near-surface temperature gradient. Therefore, these feedbacks indicate that observed Arctic sea-ice loss acts as both a response to and a driver of Arctic amplification.

Mid-latitude extreme weather

A large number of extreme heat and rainfall events have been reported over the past decade, especially in the Northern Hemisphere mid-latitudes[26–31]. Figure 3 illustrates that several standard extreme temperature and precipitation indices have increased in frequency and intensity over mid-latitude land areas (20–50° N) with especially rapid changes since the 1990s. For example, the amount of precipitation on very wet days (exceeding the 95th percentile) has increased from 160 to 185 mm, and the percentage of warm days (exceeding the 90th percentile) has increased from 10% before 1980 to 16% at present[32].

Extreme weather has not been limited to heavy rainfall and warm temperatures and recently has included cold extremes as well. Winter temperatures have generally warmed since 1960 (Fig. 2a), and the frequency of anomalously cold winter days has decreased over mid-to-high latitudes, but primarily north of 50° N, since 1979 in response to mean warming and decreased variability[33]. However, also evident in Fig. 3d,f is that the number of days continuously below freezing has increased and the minimum temperatures have decreased since 1990. Figure 3h also indicates that the frequency of unusually cold winter months (colder than two standard deviations below the 1951–1980 mean[30]) had reversed its longer-term downward trend by the end of the 1990s. This trend reversal in cold extremes has coincided with an acceleration in the rate of warming at high latitudes relative to the rest of the Northern Hemisphere starting approximately in 1990 (Fig. 2b). As seen in Fig. 2c, continental winter temperature trends since 1990 exhibit cooling over the mid-latitudes, replacing the warming trends observed over the longer period since 1960 (Fig. 2a). The winter temperature trends shown in Fig. 2c start in 1990 but are not sensitive to the exact start date. However, on average, daily winter cold extremes were less severe over this period than they have been historically[33]. The rapid Arctic warming implies that cold air outbreaks, when Arctic air moves south into the mid-latitudes, are becoming less severe[33].

The seven years between 2007 and 2013 have exhibited the lowest minimum sea-ice extents recorded in September since satellite observations began, with an all-time record low in 2007 followed by another in 2012, when sea-ice extent fell below 4 million km^2 for the first time in the observational record. Several of these seven winters following the low sea-ice minima have been unusually cold across the Northern Hemisphere extratropical landmasses[34–38]. The recent winter of 2013–2014 was characterized by record cold and widespread snowstorms across the eastern United States and Canada with the most intense cold-air outbreak in decades associated with the weakening of the polar vortex[39]. The persistent and harsh cold resulted in all-time record cold winters around the Great Lakes of the United States since record keeping began in the 1870s.

The media and public have been quick to make the connection between global, and in particular Arctic, warming and extreme weather[40]. While global warming theory is consistent with record warm temperatures and more intense precipitation events, it does not directly explain cold extremes. Coupled models project boreal winter amplification under greenhouse-gas forcing, where the Northern Hemisphere landmasses would warm faster in winter relative to the other seasons[11,41]. Warming in the Arctic has continued unabated since at least 1960. Longer-term observed temperature trends in mid-latitudes are consistent with these projections, while shorter-term trends are not. This highlights that results are sensitive to the spatial extent of the analysis, the exact definition used and especially the duration of an extreme, as extremes of differing durations may be driven by different physical processes.

While cold extremes may be mostly due to natural variability, a growing number of recent studies argue that recent extreme winter weather is related to Arctic amplification. Three possible dynamical pathways through which Arctic amplification may influence mid-latitude weather, including extreme weather, are summarized below. We focus our discussion on Arctic linkages to mid-latitude weather in the winter season for two reasons. First, most studies that have linked Arctic amplification to mid-latitude weather have focused on winter (a brief discussion of proposed linkages in other seasons, mainly summer, is provided in the Supplementary Information). Second, winter is the season in which mid-latitude temperature trends have diverged most notably from both model projections and from the other seasons[42]. To provide a focused review, we limit our consideration to the literature concerning recent past (mid-twentieth century onwards) and present-day climate variability and trends. The implications of projected future Arctic amplification (for example, at the end of the twenty-first century) are likely large and wide ranging, but are not considered here.

Arctic amplification influences and uncertainties

Whether to attribute severe winter weather to Arctic amplification or natural variability has emerged as a major debate among

© 2014 Macmillan Publishers Limited. All rights reserved

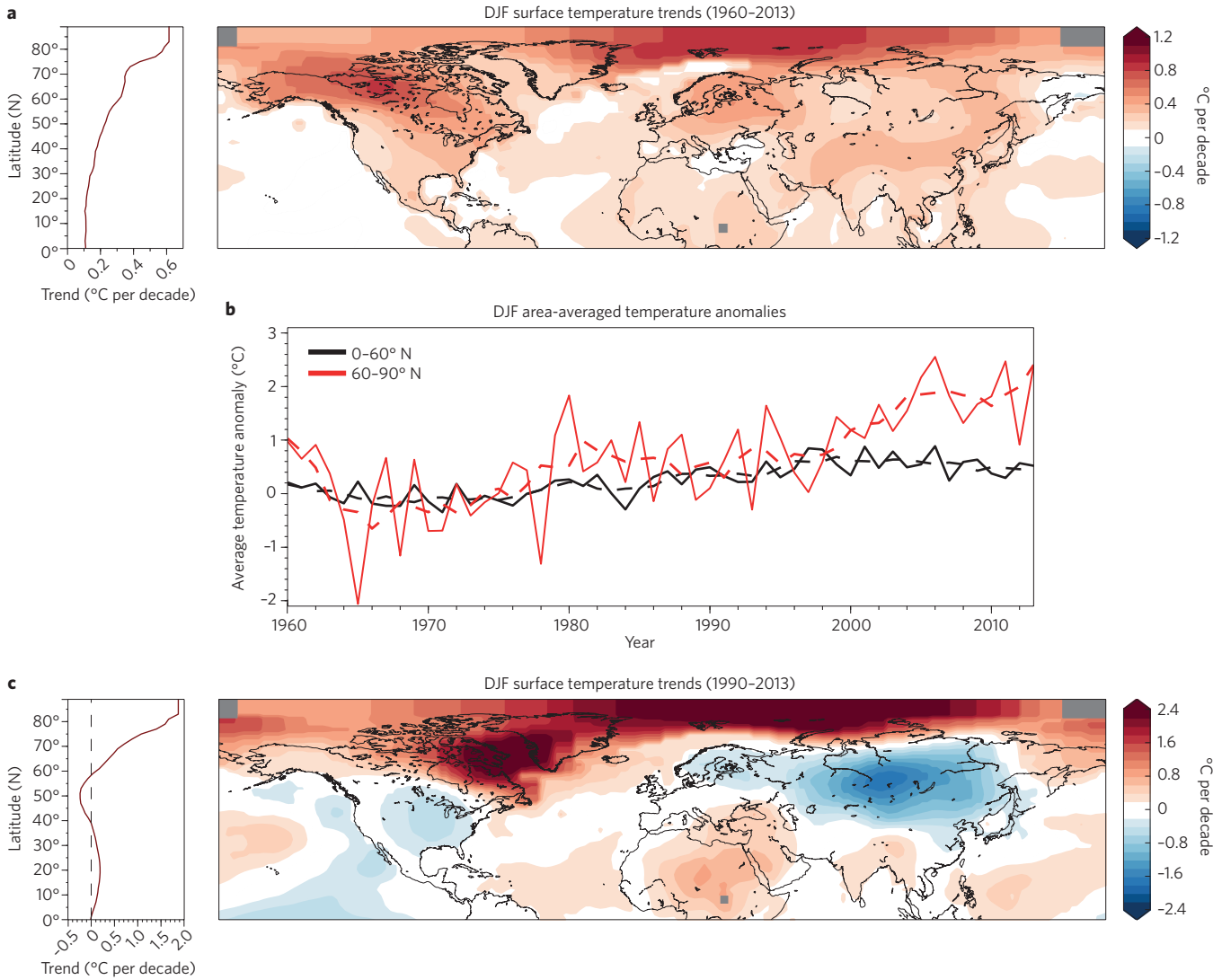

Figure 2 | Winter temperature trends since 1960 and over the most recent period from 1990. a, Right: linear trend (°C per 10 years) in December–February (DJF) mean surface air temperatures from 1960–1961 to 2013–2014. Shading interval every 0.1 °C per 10 years. Dark grey indicates points with insufficient samples to calculate a trend. Left: The zonally averaged linear trend (°C per 10 years). **b**, Area-average surface temperature anomalies (°C) from 0° to 60° N (solid black line) and 60° to 90° N (solid red line) along with five-year smoothing (dashed black and red lines, respectively). **c**, As in panel **a** but from 1960–1961 to 2013–2014. Shading interval every 0.2 °C per 10 years. Also note different scales between **a** and **c**. Data from the National Aeronautics and Space Administration Goddard Institute for Space Studies temperature analysis (http://data.giss.nasa.gov/gistemp)[96].

scientists[43–45]. In the observations, Arctic amplification has separated from the noise of natural variability only in the past approximately two decades (Fig. 2b), presenting a challenge for the detection of robust atmospheric responses to Arctic amplification, including mid-latitude weather, over such a short time period. In addition to the relatively short length of the observational record, the Arctic is poorly sampled. A major caveat of any observational study is that correlation alone cannot demonstrate a causal link. Cause and effect can be established through sensitivity or perturbation studies using climate models, but models are subject to their own deficiencies. Known model errors include sea-ice–atmosphere coupling[46,47], energy fluxes and cloud properties[47]. Furthermore, modelling studies of the effects of sea-ice loss on large-scale atmospheric circulation have produced conflicting results that make interpretation difficult. Finally, our understanding of fundamental driving forces of mid-latitude weather is incomplete[48].

Given these sources of uncertainty, a consensus on whether and how Arctic amplification is influencing mid-latitude weather is lacking. To facilitate advancement on this important issue, therefore, we synthesize key findings that argue for and against a significant link between Arctic amplification and mid-latitude weather. All studies agree that the first order impact of sea-ice melt is to modify the boundary layer in the Arctic[15,25]. However, if and how that signal propagates out of the Arctic to mid-latitudes differs and can be loosely grouped under three broad dynamical frameworks: (1) changes in storm tracks mainly in the North Atlantic sector; (2) changes in the characteristics of the jet stream; and (3) regional changes in the tropospheric circulation that trigger anomalous planetary wave configurations. In Fig. 4, we show the known primary influences on mid-latitude weather, including the three dynamical pathways introduced above and described in more detail in the following sections. We recognize that these three pathways are not distinct as they involve dynamical features of the atmospheric circulation that are highly interconnected. Whilst imperfect, our choice of this separation reflects the different dynamical frameworks that are commonly used — if not explicitly acknowledged — to study the dynamics of mid-latitude weather.

© 2014 Macmillan Publishers Limited. All rights reserved

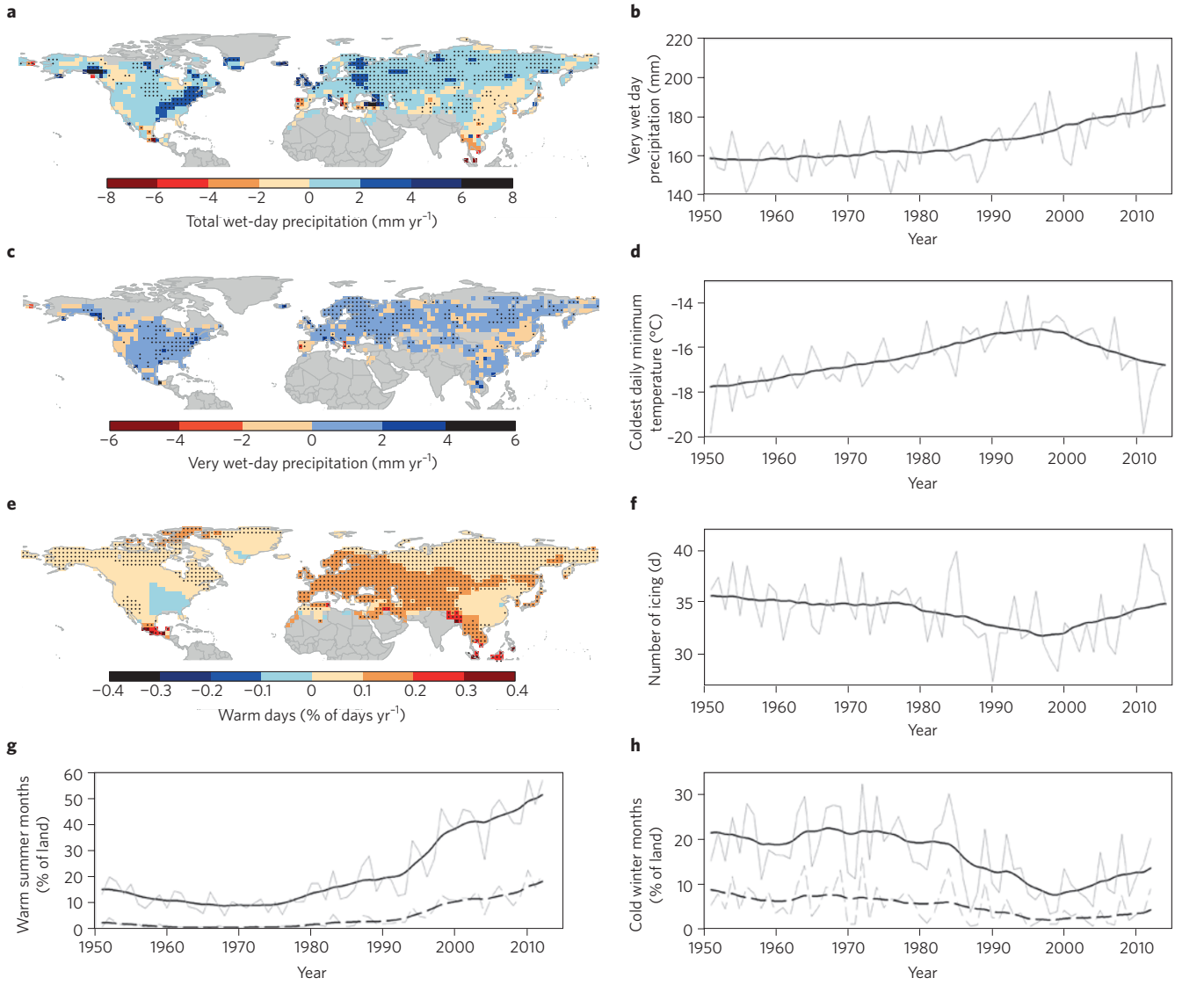

Figure 3 | Temperature and precipitation extremes. Extreme indices in the mid-latitudes: trend maps for the 1951–2013 period and time series averaged over the land area from 20° to 50° N. **a**, Trend in annual total wet-day precipitation. **b**, Annual very wet-day precipitation (that is, precipitation during days exceeding the 95th percentile). **c**, Trend in annual very wet-day precipitation (that is, precipitation during days exceeding the 95th percentile). **d**, Coldest daily minimum temperature. **e**, Trend in annual warm days (that is, percentage of days with temperatures exceeding the 90th percentile). **f**, Annual number of icing days (days with maximum temperature <0 °C). **g**, Percentage of land with summer months warmer than one standard deviation (solid) and two standard deviations (dashed) above the 1951–1980 mean. **h**, Percentage of land with winter months colder than one standard deviation (solid) and two standard deviations (dashed) below the 1951–1980 mean[30]. Stippling in the trend maps indicates significance at 95% confidence. The time series plot yearly values (thin grey curves) and the long-term nonlinear trend (thick black curves). Panels **a**–**f** were created using the GHCNDEX global land gridded dataset of climate extremes[32] and definition of the extreme indices[32].

Storm tracks

Large-scale and low-frequency variability in the extratropical atmosphere is dominated by shifts in storm tracks, often expressed by changes in large-scale atmospheric modes[49]. The dominant atmospheric or climate mode that explains the greatest percentage of the mid- to high-latitude atmospheric variability, including changes in the storm tracks, is the North Atlantic Oscillation/Arctic Oscillation (NAO/AO). Changes in the storm tracks associated with the NAO/AO have a strong influence on the surface temperature and precipitation variability in the North Atlantic sector[50]. When the NAO/AO is in its positive phase, the storm tracks shift poleward and winters are predominately mild across northern Eurasia and the eastern United States but cold in the Arctic. When the NAO/AO is in its negative phase, the storm tracks shift equatorward and winters are predominantly more severe across northern Eurasia and the eastern United States, but relatively mild in the Arctic. This temperature pattern is sometimes referred to as the 'warm Arctic–cold continents' pattern[51]. Recent observed wintertime temperature trends across the Northern Hemisphere continents (Fig. 2c) project strongly on this temperature-anomaly pattern[37], reflecting a negative trend in the NAO/AO over the past two decades[37]. Given that climate models forced by regional and latitudinal variations in atmospheric heating also exhibit changes in the NAO/AO[50,52], it is plausible that variability in sea ice and/or snow cover can influence the phase and amplitude of the NAO/AO, and consequently the storm tracks.

The temperature pattern associated with variations in Eurasian snow cover projects strongly onto the temperature pattern associated with the NAO/AO and recent temperature trends[34,37,53]. October snow cover anomalies across Eurasia have been proposed as a skilful

© 2014 Macmillan Publishers Limited. All rights reserved

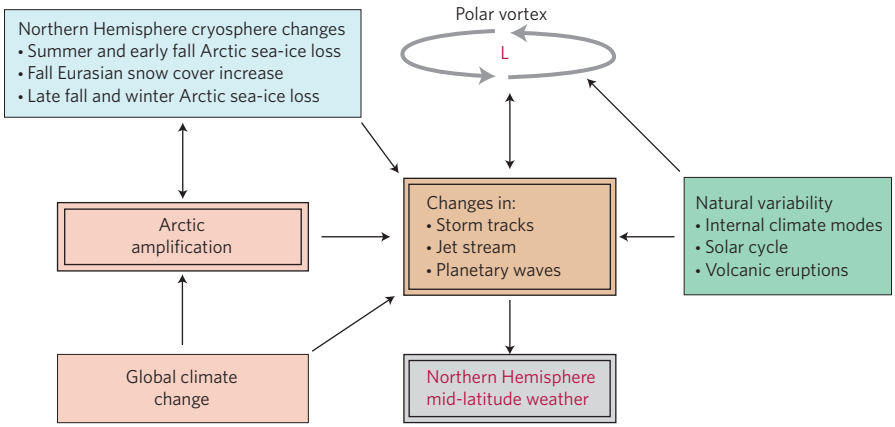

Figure 4 | Schematic of ways to influence Northern Hemisphere mid-latitude weather. Three major dynamical features for changing Northern Hemisphere mid-latitude weather — changes in the storm tracks, the position and structure of the jet stream, and planetary wave activity — can be altered in several ways. The pathway on the left and highlighted by double boxes is reviewed in this manuscript. Arctic amplification directly (by changing the meridional temperature gradient) and/or indirectly (through feedbacks with changes in the cryosphere) alters tropospheric wave activity and the jet stream in the mid- and high latitudes. Two other causes of changes in the storm tracks, jet stream and wave activity that do not involve Arctic amplification are also presented: (1) natural modes of variability and (2) the direct influence of global climate change (that is, including influences outside the Arctic) on the general circulation. The last two causes together present the current null hypothesis in the state of the science against which the influence of Arctic amplification on mid-latitude weather is tested in both observational and modelling studies. Bidirectional arrows in the figure denote feedbacks (positive or negative) between adjacent elements. Stratospheric polar vortex is represented by 'L' with anticlockwise flow.

predictor of the winter NAO/AO[54,55], where extensive snow cover is associated with the negative phase of the NAO/AO, though the relationship may lack stationarity[56]. Satellite-based data indicate a positive trend in Eurasian snow cover during October over the past two to three decades[6,37], though the veracity of these satellite-based increases has recently been questioned[57]. A proposed physical mechanism to explain increased snow cover is that a warmer Arctic atmosphere can hold more water vapour, which enhances precipitation over the Eurasian continent. Additionally, the loss of sea ice — and thus the increase in open water — has increased moisture fluxes to the atmosphere[9]. If near-surface atmospheric temperatures remain sufficiently cold — as is the case in Siberia during autumn and winter — any additional precipitation will likely occur as snow[58,59]. Therefore, increasing October Eurasian snow cover may have contributed to the recent tendency towards a negative NAO/AO and cold Northern Hemisphere winters[37]. However, given that the NAO/AO has considerable internal variability on multiple timescales, the recent negative trend may be predominantly internally driven.

The strong decline in sea ice during recent decades has intensified interest in the interactions between sea-ice conditions and the atmosphere[47,60]. Most sea-ice–atmosphere coupled studies have discussed the atmospheric response in the context of NAO/AO variability. Observational analyses have shown significant correlation between reduced Arctic sea-ice cover and the negative phase of the winter NAO/AO[35,37,61–64], although it is unclear whether late summer and early autumn[35] or late autumn and early winter[38] sea-ice anomalies are more skilful at predicting the winter weather patterns.

Modelling studies have also examined the NAO/AO response to variations in Arctic sea ice[35,65–74], by running simulations forced by past sea-ice trends or case studies of years with large sea-ice anomalies. These studies have shown a full spectrum of NAO/AO responses to reduced sea ice, from shifts toward the positive phase[68,71,73], the negative phase[35,65,74] or no significant change[73].

Furthermore, attributing NAO/AO changes and associated shifts in storm tracks to Arctic forcing has proved very difficult. The simulated atmospheric circulation response to sea-ice loss is sensitive to differences in model physics, background atmospheric and oceanic states, and the spatial patterns and magnitude of sea-ice anomalies. Additionally, it has proven difficult to separate forced change due to sea-ice loss from internal model variability. Large numbers of model runs or ensembles are likely required to achieve statistically significant responses to forced sea-ice changes[73]. While these disparities between studies preclude definitive conclusions, two general results emerge. First, there are more studies that show a negative NAO/AO response than a positive NAO/AO response. Second, the simulated NAO/AO response to sea-ice loss is relatively small compared with natural variability. This is consistent with the view that changes in the NAO/AO are predominately internally driven and do not necessarily require remote forcing[75].

Jet stream

The second proposed dynamical pathway linking Arctic amplification to increased weather extremes is through its effects on the behaviour of the polar jet stream. The difference in temperature between the Arctic and mid-latitudes is a fundamental driver of the polar jet stream; therefore, a reduced poleward temperature difference could result in a weaker zonal jet with larger meanders. A weaker and more meandering flow may cause weather systems to travel eastward more slowly and thus, all other things being equal, Arctic amplification could lead to more persistent weather patterns[76]. Furthermore, Arctic amplification causes the thickness of atmospheric layers to increase more to the north, such that the peaks of atmospheric ridges may elongate northward and, thus, increase the north–south amplitude of the flow[76]. Weather extremes frequently occur when atmospheric circulation patterns are persistent, which tends to occur with a strong meridional wind component[77,78].

Some aspects of this hypothesized linkage are supported by observations and model simulations. A significant decrease in zonal-mean zonal wind at 500 hPa during autumn is observed regionally[76,79]. This may be understood through the thermal wind relationship, which states that vertical wind shear is proportional to the meridional temperature gradient. Assuming that the winds do not increase at the surface, the zonal wind at the jet-stream level should slacken with a weaker meridional temperature gradient. In other seasons when Arctic amplification is weaker, no significant trend in zonal-mean zonal wind is observed.

© 2014 Macmillan Publishers Limited. All rights reserved

However, challenges remain in linking Arctic amplification directly to changes in the speed and structure of the jet stream. For example, other factors besides the near-surface meridional temperature gradient influence the zonal jet, including feedbacks from synoptic eddies or storms and the upper-level meridional temperature gradient. Indeed, although Arctic amplification has weakened the near-surface meridional temperature gradient, the temperature gradient between the tropics and mid-latitudes at higher altitudes has strengthened[80], which would increase jet stream-level winds. Another challenge is identifying how much of the Arctic

Box 1 | Jet-related dynamics.

The different components of a generalized mid-latitude jet are illustrated in Fig. B1a. The proposed dynamical pathways linking Arctic amplification to increased weather extremes are through the highly nonlinear interaction between the jet stream, the planetary waves and the storm tracks (Fig. 4). The wintertime extratropical climate variability is affected by a complex set of interactions and feedbacks between components, such as natural variability modes, diabatic heating anomalies due to variations in sea ice and snow cover, and atmospheric and oceanic heat transport from tropical and subtropical latitudes. However, recently it has been proposed that air–sea interaction in the Arctic could be forcing teleconnection patterns and influencing weather patterns remotely in the mid-latitudes by heating the Arctic relative to the rest of the globe[36,76].

A change in the meridional temperature gradient, which projects onto the thermally driven component of the jet may or may not result in a significant change in the jet depending on how the eddy-driven part of the jet varies. Complex interactions between the mid-latitude wind jets, the planetary waves and baroclinic weather systems is a nonlinear two-way feedback process, where diabatic heating and cooling, orographic forcing and eddy wave breakings drive the jets and teleconnection patterns. The yellow arrow denotes the final influence, which is of synoptic variability (jet eddies) on mid-latitude weather. The dynamical mechanisms associated with each green arrow are as follows:

A. The temperature gradient, in this definition, influences the thermally driven jet (black solid circle) via the thermal-wind balance (in combination with boundary conditions).

B. The temperature gradient influences the eddy-driven jet (black dashed circle) via changes in baroclinicity. The eddy-driven jet influences the temperature gradient via horizontal heat fluxes.

C. The eddy-driven jet affects stratospheric winds (black U shape) via vertical wave propagation. Stratospheric winds affect the eddy-driven jet by altering the vertical wave-guide.

D. The thermally driven jet affects stratospheric winds via generation of orographically forced waves. Stratospheric winds affect the thermally driven jet by altering the vertical wave guide.

E. The thermally driven jet affects the eddy-driven jet by acting as a wave guide (the role of baroclinicity here directly associated with the temperature gradient). The eddy-driven jet affects the thermally driven jet via energy fluxes.

As can be seen from the figure, there are many feedbacks and interactions involving mid-latitude jets, with the temperature gradient being just one of them. Therefore a weakening in the temperature gradient may or may not result in a slowing down of the jet depending on the net effect of other factors.

The North Atlantic Oscillation/Arctic Oscillation (NAO/AO) may be considered a paradigm for the debate within the climate community. Shown in Fig. B1b are the changes in the atmospheric circulation associated with the negative phase of the NAO/AO. Positive (negative) zonal wind anomalies associated with the negative NAO/AO are superimposed on the jet shown by a green solid (dashed) line. Also shown are the temperature changes with warmer temperatures in the Arctic (red) and colder temperatures in the mid-latitudes (blue), increased high-latitude blocking (represented by clockwise flow around a high) and a southward shift in the storm tracks (represented by a anticlockwise flow around a low), and increased meridional flow. All these dynamical changes are observed as the NAO/AO shifts from its positive phase to the negative phase. However, external forcing, such as a reduced thermal gradient due to Arctic amplification, will project onto these dynamical patterns associated with the negative NAO/AO: an equatorward shift in the zonal jet, increased meridional flow, high-latitude blocking and a southward shift in storm tracks. The yellow broken arrow denotes uncertainty whether a change in the meridional temperature gradient can force all the other changes depicted in the figure. Attributing observed changes in mid-latitude weather to either Arctic amplification or internal variability has proven challenging to date.

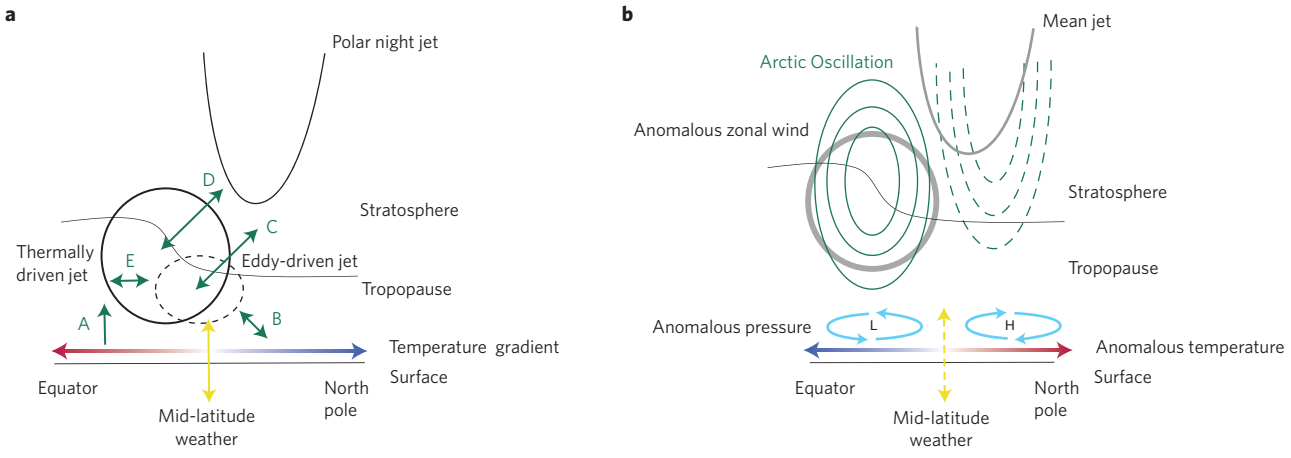

Figure B1 | Schematic view of jet-related and negative North Atlantic Oscillation/Arctic Oscillation dynamics. a, Here, the tropospheric jet is divided into two parts, a thermally driven part and an eddy-driven part. **b**, Changes in the atmospheric circulation associated with the negative phase of the North Atlantic Oscillation/Arctic Oscillation. See Box text for detailed explanation.

© 2014 Macmillan Publishers Limited. All rights reserved

amplification is driven by local changes compared with remote changes[16]. This distinction is highly relevant to the current debate on possible Arctic–mid-latitude linkages, because if a significant portion of Arctic amplification is driven remotely, then Arctic amplification may be partly viewed as a response to rather than a forcing of mid-latitude weather. This highlights the importance of

Box 2 | Synthesis of cryospheric forcings.

As a summary of the studies presented, in Fig. B2 we synthesize some common ideas about the atmospheric response to sea-ice and snow cover variability that have until now been treated independently. All sea-ice studies agree that sea-ice loss heats and moistens the boundary layer of the Arctic atmosphere. It has also been shown that a surface heat source in the extratropics induces downward descent of air over the heat source, warming the atmospheric column and raising heights in the mid-troposphere, while a trough develops downstream inducing an equatorward flow of cold air[97]. This is consistent with the result that reduced sea ice favours an increase in mid-tropospheric heights in the Barents and Kara seas region in winter[51,88,92] with downstream troughing over Eurasia. Studies also agree that increased snow cover cools the boundary layer[54]. Therefore a snow-induced surface cooling can lower heights in the mid-troposphere, inducing enhanced ridging upstream.

In September and October, sea-ice loss has been most pronounced in the Chukchi and East Siberian seas. Warming of the atmosphere due to increased heating from newly ice-free ocean causes geopotential heights to increase in the mid-troposphere, which suppresses the jet stream southward over east Siberia. This pattern, referred to as the Arctic Dipole, has strengthened during the era of sea-ice loss[61]. A southward shift in the storm tracks over East Asia allows for a more rapid advance of Eurasian snow cover in October. Enlarged areas of open water north of Siberia also provide increased moisture flux to the atmosphere, which precipitates as snow as the air mass is advected southward over Siberia[58,71] (left globe in Fig. B2).

In October, a more extensive snow cover cools the surface leading to lower heights and a trough in the mid-troposphere. Increased troughing over East Asia favours upstream ridging near the Barents and Kara seas and the Urals. Concurrently, the large sea-ice deficits and the associated strong surface heating anomalies migrate from the Chukchi and East Siberian seas in September and October to the Barents and Kara seas in November and December. This favours mid-tropospheric ridging in the Barents and Kara seas region with downstream troughing over East Asia. Therefore, the extensive snow cover over Siberia in October and November and the sea-ice loss over the Barents and Kara seas in November and December produce same-signed mid-tropospheric geopotential height patterns over Eurasia. This planetary wave configuration is favourable for increased vertical propagation of Rossby waves from the troposphere into the stratosphere[98–100] (middle globe in Fig. B2).

Increased vertical propagation of Rossby wave energy from the troposphere to the stratosphere weakens the polar vortex, resulting in a stratospheric warming event. Circulation anomalies associated with the warming event appear first in the stratosphere and subsequently appear in the troposphere in January and February. These circulation anomalies resemble those associated with the negative phase of the NAO/AO; that is, ridging over the Arctic especially near Greenland, and a weaker, equatorward-shifted polar jet stream. As a result, warmer conditions prevail in the Arctic regions, but colder and more severe winter weather occurs across the mid-latitude continents with a greater likelihood of snowstorms in the population centres of the Northern Hemisphere mid-latitudes (right globe in Fig. B2).

We propose a chain of events where less sea ice and increased open water in the Arctic (that heats the atmosphere) and more snow cover (that cools the atmosphere) both force the same pattern, which results in a weakened polar vortex. Because the heating anomalies are displaced longitudinally, extensive Eurasian snow cover and reduced Arctic sea ice can constructively interfere to weaken the polar vortex and hence influence surface weather.

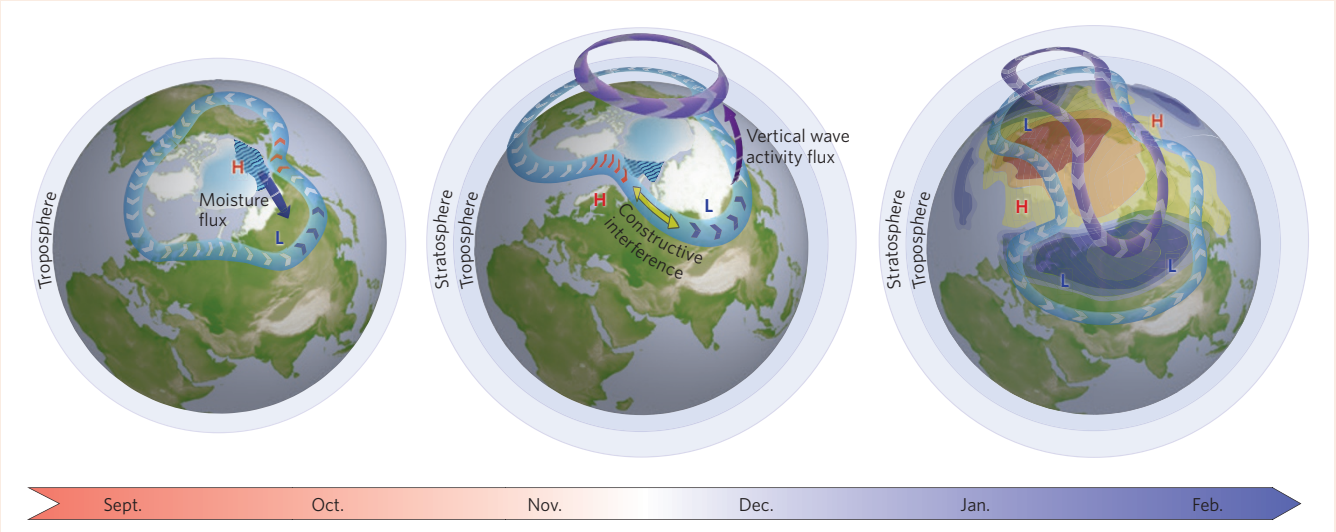

Figure B2 | Synthesis of proposed cryospheric forcings. The schematic highlights a proposed way in which Arctic sea-ice loss in late summer through early winter may work in concert with extensive Eurasian snow cover in the autumn to force the negative phase of the NAO/AO in winter. Snow is shown in white, sea ice in white tinged with blue, sea-ice melt with blue waves, high and low geopotential heights with red 'H' (red represents anomalous warmth) and blue 'L' (blue represents anomalous cold) respectively, tropospheric jet stream in light blue with arrows, and stratospheric jet or polar vortex shown in purple with arrows. On the right globe, cold (warm) surface temperature anomalies associated with the negative phase of the winter NAO/AO are shown in blue (brown). See Box text for detailed explanation.

© 2014 Macmillan Publishers Limited. All rights reserved

considering the many ways in which mid-latitude jets are influenced, including the meridional temperature gradient, which are shown schematically in Fig. B1 in Box 1.

Observational support for the follow-on impacts of the hypothesis related to a weakening zonal component of the jet[76] is even less strong — namely, whether Arctic amplification leads to larger amplitude waves, slower wave propagation speeds and more persistent weather patterns. Statistically robust evidence of increasing north–south wave amplitude and slower propagation speed has not been established[79,81]. This is not surprising given the recent emergence of Arctic amplification and the large natural variability of the atmosphere. Recent studies provide tentative evidence for increasing amplitude in summer and autumn for some definitions of wave amplitude, but not for others[81]. A significant reduction in 500 hPa wave speeds during autumn was reported[79], but the response was not apparent in higher-level winds. The frequency of blocking-high patterns is metric, region and time dependent, but as a whole the observations do not support a significant increase in blocking occurrence over recent decades[82].

The theory that Arctic amplification is resulting in a slower zonal jet, increased meridional flow, amplified waves and more persistent extreme weather has received a lot of attention from the media, policymakers and climate sceintists[83]. In part due to the high profile, this hypothesis has been scrutinized in the scientific literature more extensively than other hypotheses linking Arctic climate change to mid-latitude weather. However, it is worth noting that other studies on related topics, especially other observational studies, share some of the same shortcomings[35,37,38,61–64] (lack of statistical significance, causality unclear, incomplete mechanistic understanding, and so on).

Planetary waves

Modification to large-scale Rossby waves over Eurasia is the third proposed dynamical pathway linking Arctic amplification to mid-latitude weather. Both observational analyses and modelling experiments link more extensive snow cover across Eurasia, especially in October, to changes in wave structure at high latitudes. Extensive snow cover may lead to larger planetary waves that increase the vertical propagation of wave energy into the stratosphere, favouring a warmer and weakened stratospheric polar vortex[84–87]. It is proposed that the atmospheric response lags the snow cover changes by a few months because of the response time of the stratospheric circulation and subsequent feedback to the troposphere.

Observed reductions in autumn–winter Arctic sea ice, especially in the Barents and Kara seas, are also correlated with strengthened anticyclonic circulation anomalies over the Arctic Ocean, which tend to induce easterly flow and cold air advection over northern Europe[38,88–90], a link that may be sensitive to the timing of the sea-ice anomalies. Winter anomalies trigger an immediate, local and direct atmospheric response forced by increased turbulent heat fluxes locally over the Barents and Kara seas, which in turn changes the baroclinicity and affects large-scale planetary or Rossby waves in the atmosphere. Alternatively autumn sea-ice anomalies may force a delayed, remote and indirect atmospheric response through increased Eurasian snow cover[46] or through altered baroclinicity and high pressure over the Barents and Kara seas that force upward propagating planetary waves into the stratosphere. Sufficient wave breaking in the polar stratosphere weakens the stratospheric polar vortex and can trigger a stratospheric warming event. The circulation anomalies associated with a stratospheric warming event propagate back down to the surface in subsequent weeks, contributing to a persistent negative NAO/AO and cold continental conditions[90,91].

Several modelling studies have used prescribed Barents and Kara sea-ice reductions to examine how the atmosphere responds. Horizontal downstream propagation of the energy away from anomalous, sea-ice-induced high pressure over the Barents and Kara seas leads to the formation of a trough over Eurasia and subsequent cold continental temperatures[92]. Such model experiments have thus far only included the impact of sea-ice changes and not the full extent of Arctic amplification.

The proposed response of planetary waves to reductions in both snow cover and sea ice has inherent shortcomings. Free-running (that is, without prescribed forcing) climate models do not simulate well observations of the amplitude or the timing of wave changes to more extensive snow cover[86], resulting in a simulated weak relationship found between October Eurasian snow cover and the winter NAO/AO[93]. Regarding the response to sea-ice loss, caution is urged, because strong trends in the sea-ice extent have made analyses of the co-variability between sea ice and the atmosphere difficult to interpret[46]. Furthermore the proposed atmospheric response to sea-ice forcing is not robust and has yet to achieve statistical significance[46], in part due to the shortness of the data record.

To conclude, variability in both sea ice and snow cover have been hypothesized to independently force anomalously high geopotential heights in the Barents and Kara seas. In Fig. B2 in Box 2, we provide a complementary perspective by proposing a synthesis of how extensive snow cover and reduced sea ice in the autumn and early winter can force local changes that constructively interfere to force the same response in the planetary waves, which could influence winter weather patterns.

Synthesis of Arctic and mid-latitude linkages

Dramatic changes are occurring in the Arctic climate system, and at the same time, the frequency of mid-latitude extreme weather events appears to have increased. The potential link between Arctic amplification and changes in extreme weather is a critical one, especially as Arctic amplification is robustly predicted to continue over the coming decades. The climate dynamics literature concerning Arctic–mid-latitude linkages is currently inconclusive, which may help explain the media portrayal of a polarized view among scientists[81]. Furthermore, the severe winter of 2013–2014 across eastern North America focused the debate of whether extreme cold events are attributable to climate change, including Arctic amplification, or natural variability[43,44]. Cold winters such as the one experienced in 2013–2014 have occurred before and are expected as part of normal weather variability even on a warmer planet[94]. Preliminary evidence for a link between Arctic amplification and continental weather has been presented, along with a range of dynamical hypotheses for such a link. However, evidence demonstrating no robust statistical or dynamical link between Arctic amplification and mid-latitude climate variability has also been presented.

Nevertheless, dramatic changes to high-latitude sea ice and snow cover have occurred, along with profound impacts at least locally in the Arctic. The most robust atmospheric response to these changes is an altered near-surface climate in the Arctic region. There is consensus that sea-ice loss enhances local warming, which weakens near-surface meridional temperature gradients, moistens the boundary layer and decreases the near-surface static stability. A growing body of observational, modelling and theoretical evidence suggests that the impact of high-latitude surface heating increases upper-level geopotential heights, which affects the large-scale atmospheric circulation beyond the Arctic.

To the first order, amplified warming in the Arctic and a decrease in the meridional temperature gradient should favour a weaker zonal jet. However, whether weaker upper-level zonal winds causes amplified and slower-moving planetary waves remains unclear. Further evidence from modelling studies suggests that cryospheric anomalies can alter the stratospheric polar vortex, storm tracks and jet stream — all of which are key drivers of mid-latitude weather and extremes. These changes appear to be more likely in winter than other seasons owing to the large Arctic amplification signal and divergence of winter temperature trends from the other seasons.

© 2014 Macmillan Publishers Limited. All rights reserved

The link between reduced Arctic sea ice and cold continental winters is currently the most studied and arguably the best-supported link between Arctic amplification and mid-latitude extreme weather patterns.

Based on the research conducted to date, we offer a brief perspective on the challenges and research opportunities in the near future (a more detailed list is included in the Supplementary Information). Understanding the relative importance of different forcings mechanisms, and how they interact with internally generated variability, remains a key challenge. More and better observations (for example, of ocean–ice–atmosphere energy exchange, cloud cover and troposphere–stratosphere coupling) would not only improve our understanding of the Arctic and its climate, but also help to elucidate the mechanisms of atmospheric response to Arctic amplification and better constrain the models. Better standardization of metrics (extremes, blocking, wave amplitude, and so on) and coordination of modelling experiments would allow results to be more directly compared and the current disparities to be better understood. Finally, testing hypotheses in a hierarchy of models of increasing complexity, from simple dynamical models to state-of-the-art Earth system models, would help to further our understanding and better equip us to untangle the complexity of Arctic–mid-latitude linkages.

Methods

For Fig. 1, we used the monthly mean fields from the ERA-Interim reanalysis[95] to compute seasonal means for the period March 1979 to February 2014. These data were averaged around circles of latitude (at 1.5° resolution). Standard seasonal means were computed and used. We estimated trends using least-squares linear regression. The statistical significances of the regressions were calculated from a two-tailed *t*-test.

Surface temperature anomalies for Fig. 2 were taken from the NASA Goddard Institute for Space Studies temperature record[96]. The decadal linear trends in surface air temperature anomalies in Fig. 2a are based on a least-squares regression of the December–February (DJF) mean of monthly mean temperature anomalies from 1960–1961 to 2013–2014. The corresponding time series of DJF temperatures anomalies (Fig. 2b) was constructed by weighting the anomalies by the cosine of latitude. The same convention is used for Fig. 2c except that the linear trends were calculated based on DJF values during the period 1990–1991 to 2013–2014.

Figure 3a–f was created using the GHCNDEX global land gridded dataset of climate extremes[32] available at www.climdex.org. The online data-visualization tool was used to create linear trend maps and time series (over the period 1951–2014) for different extreme indices provided in the GHCNDEX global land gridded dataset. Time series are area-weighted averages of land regions within the latitudinal belt from 20° to 50° N. Figure 3g,h shows the percentage of land in the mid-latitudes with unusually warm summer months or unusually cold winter months[30]. For this, we used monthly gridded data from the NASA Goddard Institute for Space Studies surface temperature dataset with a base period of 1951–1980. First, we determined the local standard deviation due to natural variability at each grid point in the latitudinal belt from 20° to 50° N for each calendar month of the boreal winter (December–January–February) and boreal summer (June–July–August) seasons. To do so, we applied a singular spectrum analysis to extract the long-term (periods of 30 years or greater) nonlinear trend over the twentieth century. Next, we detrended the original time series by subtracting the long-term trend, which gives the year-to-year variability. From this detrended signal, monthly standard deviations were calculated using the 1951–2010 period, which were then seasonally averaged. For boreal summer, we determined the percentage of land with temperatures warmer than one and two standard deviations beyond the mean (Fig. 3g). For boreal winter, we determined the percentage of land with temperatures colder than one and two standard deviations below the mean (Fig. 3h).

Received 3 March 2014; accepted 22 July 2014;
published online 17 August 2014

References

1. Stroeve, J. C. *et al.* Sea ice response to an extreme negative phase of the Arctic Oscillation during winter 2009/2010. *Geophys. Res. Lett.* **38,** L02502 (2011).
2. Kwok, R. & Rothrock, D. A. Decline in Arctic sea ice thickness from submarine and ICESat records: 1958–2008. *Geophys. Res. Lett.* **36,** L15501 (2009).
3. Overland, J. E., Wang, M., Walsh, J. E. & Stroeve, J. C. Future Arctic climate changes: adaptation and mitigation timescales. *Earth's Future* **2,** 68–74 (2014).
4. Derksen, C. & Brown, R. Spring snow cover extent reductions in the 2008–2012 period exceeding climate model projections. *Geophys. Res. Lett.* **39,** L19504 (2012).
5. Matsumura, S., Zhang, X. & Yamazaki, K. Summer Arctic atmospheric circulation response to spring Eurasian snow cover and its possible linkage to accelerated sea ice decrease. *J. Clim.* http://dx.doi.org/10.1175/JCLI-D-13-00549.1 (2014).
6. Mudryk, L. R., Kushner, P. J. & Derksen, C. Interpreting observed Northern Hemisphere snow trends with large ensembles of climate simulations. *Clim. Dynam.* **43,** 345–359 (2013).
7. IPCC Summary for Policymakers in *Climate Change 2013: The Physical Science Basis* (eds Stocker, T. F. *et al.*) 3–29 (Cambridge Univ, Press, 2013).
8. Serreze, M. C., Barrett, A. P., Stroeve, J. C., Kindig, D. M. & Holland, M. M. The emergence of surface-based Arctic amplification. *Cryosphere* **3,** 11–19 (2009).
9. Screen, J. A. & Simmonds, I. The central role of diminishing sea ice in recent Arctic temperature amplification. *Nature* **464,** 1334–1337 (2010).
10. Cowtan, K. & Way, R. G. Coverage bias in the HadCRUT4 temperature series and its impact on recent temperature trends. *Q. J. R. Meteorol. Soc.* **133,** 459–77 (2013).
11. Holland, M. M. & Bitz, C. M. Polar amplification of climate change in coupled models. *Clim. Dynam.* **21,** 221–232 (2003).
12. Stroeve, J. C. *et al.* The Arctic's rapidly shrinking sea ice cover: a research synthesis. *Climatic Change* **110,** 1005–1027 (2012).
13. Gillett, N. P. *et al.* Attribution of polar warming to human influence. *Nature Geosci.* **1,** 750–754 (2008).
14. Winton, M. Amplified Arctic climate change: What does surface albedo feedback have to do with it? *Geophys. Res. Lett.* **33,** L03701 (2006).
15. Serreze, M. C. & Barry, R. G. Processes and impacts of Arctic amplification: a research synthesis. *Glob. Planet. Change* **77,** 85–96 (2011).
16. Screen, J. A., Deser, C. & Simmonds, I. Local and remote controls on observed Arctic warming. *Geophys. Res Lett.* **39,** L10709 (2012).
17. Shindell, D. & Faluvegi, G. Climate response to regional radiative forcing during the twentieth century. *Nature Geosci.* **2,** 294–300 (2009).
18. Francis, J. A. & Hunter, E. New insight into the disappearing Arctic sea ice. *EOS Trans. Am. Geophys. Union* **87,** 509–511 (2006).
19. Graverson, R. G. & Wang, M. Polar amplification in a coupled climate model with locked albedo. *Clim. Dynam.* **33,** 629–643 (2009).
20. Pithan, F. & Mauritsen, T. Arctic amplification dominated by temperature feedbacks in contemporary climate models. *Nature Geosci.* **7,** 181–184 (2014).
21. Graversen, R. G., Mauritsen, T., Tjernstrom, M., Kallen, E. & Svensson, G. Vertical structure of recent Arctic warming. *Nature* **451,** 53–56 (2008).
22. Wood, K. R. *et al.* Is there a "new normal" climate in the Beaufort Sea? *Polar Res.* **32,** 19552 (2013).
23. Steele, M., Ermold, W. & Zhang, J. Arctic Ocean surface warming trends over the past 100 years. *Geophys. Res. Lett.* **35,** L19715 (2008).
24. Inoue, J. & Hori, M. E. Arctic cyclogenesis at the marginal ice zone: A contributory mechanism for the temperature amplification? *Geophys. Res. Lett.* **38,** L12502 (2011).
25. Screen, J. A. & Simmonds, I. Increasing fall-winter energy loss from the Arctic Ocean and its role in Arctic amplification. *Geophys. Res. Lett.* **37,** L16707 (2010).
26. Min, S. K., Zhang, X., Zwiers, F. W. & Hegerl, G. C. Human contribution to more-intense precipitation extremes. *Nature* **470,** 378–381 (2011).
27. Coumou, D. & Rahmstorf, S. A decade of weather extremes. *Nature Clim. Change* **2,** 491–496 (2012).
28. Westra, S., Alexander, L. V. & Zwiers, F. W. Global increasing trends in annual maximum daily precipitation. *J. Clim.* **26,** 3904–3918 (2013).
29. Coumou, D. & Robinson, A. Historic and future increase in the global land area affected by monthly heat extremes. *Environ. Res. Lett.* **8,** 034018 (2013).
30. Coumou, D., Robinson, A. & Rahmstorf, S. Global increase in record-breaking monthly-mean temperatures. *Climatic Change* **118,** 771–782 (2013).
31. Seneviratne, S. I., Donat, M. G., Mueller, B. & Alexander, L. V. No pause in the increase of hot temperature extremes. *Nature Clim. Change* **4,** 161–163 (2014).
32. Donat, M. G. *et al.* Global land-based datasets for monitoring climatic extremes. *Bull. Am. Meteorol. Soc.* **94,** 997–1006 (2013).
33. Screen, J. A. Arctic amplification decreases temperature variance in northern mid- to high-latitudes. *Nature Clim. Change* **4,** 577–582 (2014).
34. Cohen, J., Barlow, M. & Saito, K. Decadal fluctuations in planetary wave forcing modulate global warming in late boreal winter. *J. Clim.* **22,** 4418–4426 (2009).
35. Liu, J., Curry, J. A., Wang, H., Song, M. & Horton, R. Impact of declining Arctic sea ice on winter snow. *Proc. Natl Acad. Sci. USA* **109,** 4074–4079 (2012).
36. Greene, C. H. & Monger, B. C. An Arctic wild card in the weather. *Oceanography* **25,** 7–9 (2012).

© 2014 Macmillan Publishers Limited. All rights reserved

37. Cohen, J., Furtado, J., Barlow, J. M., Alexeev, V. & Cherry, J. Arctic warming, increasing fall snow cover and widespread boreal winter cooling. *Environ. Res. Lett.* **7,** 014007 (2012).
38. Tang, Q., Zhang, X., Yang, X. & Francis, J. A. Cold winter extremes in northern continents linked to Arctic sea ice loss. *Environ. Res. Lett.* **8,** 014036 (2013).
39. Tollefson, J. US cold snap fuels climate debate. *Nature* http://dx.doi.org/10.1038/nature.2014.14485 (2014).
40. Hamilton, L. C. & Lemcke-Stampone, M. Arctic warming and your weather: public belief in the connection. *Int. J. Climatol.* **34,** 1723–1728 (2013).
41. Alexeev, V. A., Langen, P. L. & Bates, J. R. Polar amplification of surface warming on an aquaplanet in "ghost forcing" experiments without sea ice feedbacks. *Clim. Dynam.* **24,** 655–666 (2005).
42. Cohen, J., Furtado, J., Barlow, M., Alexeev, V. &. Cherry, J. Asymmetric seasonal temperature trends. *Geophys. Res. Lett.* **39,** L04705 (2012).
43. Wallace, J. M., Held, I. M., Thompson, D. W. J., Trenberth, K. E. & Walsh, J. E. Global warming and winter weather. *Science* **343,** 729–730 (2014).
44. Palmer, T. Record-breaking winters and global climate change. *Science* **344,** 803–804 (2014).
45. Fischer, E. M. & Knutti, R. Heated debate on cold weather. *Nature Clim. Change* **4,** 577–582 (2014).
46. Cohen, J., Jones, J., Furtado, J. C. &. Tziperman, E. Warm Arctic, cold continents: a common pattern related to Arctic sea ice melt, snow advance, and extreme winter weather. *Oceanography* **26,** 150–160 (2013).
47. Vihma, T. Effects of Arctic sea ice decline on weather and climate: a review. *Surv. Geophys.* http://dx.doi.org/10.1007/s10712-014-9284-0 (2014).
48. Hoskins, B. The potential for skill across the range of the seamless weather-climate prediction problem: a stimulus for our science. *Q. J. R. Meteorol. Soc.* **139,** 573–584 (2013).
49. Woollings, T. & Blackburn, M. The North Atlantic jet stream under climate change and its relation to the NAO and EA patterns. *J. Clim.* **25,** 886–902 (2012).
50. Bader, J. *et al.* A review on Northern Hemisphere sea-ice, storminess and the North Atlantic Oscillation: observations and projected changes. *Atmos. Res.* **101,** 809–834 (2011).
51. Overland, J. E., Wood, K. R. & Wang, M. Warm Arctic–cold continents: impacts of the newly open Arctic Sea. *Polar Res.* **30,** 15787 (2011).
52. Wu, A., Hsieh, W. W., Boer, G. J. & Zwiers, F. W. Changes in the Arctic Oscillation under increased atmospheric greenhouse gases. *Geophys. Res. Lett.* **34,** L12701 (2007).
53. Mote, T. & Kutney, E. Regions of autumn Eurasian snow cover and associations with North American winter temperatures. *Int. J. Climatol.* **32,** 1164–1177 (2012).
54. Cohen, J. & Entekhabi, D. Eurasian snow cover variability and Northern Hemisphere climate predictability. *Geophys. Res. Lett.* **26,** 345–348 (1999).
55. Cohen, J. & Jones, J. A new index for more accurate winter predictions. *Geophys. Res. Lett.* **38,** L21701 (2011).
56. Peings, Y., Brun, E., Mauvais, V. & Douville, H. How stationary is the relationship between Siberian snow and Arctic Oscillation over the 20th century? *Geophys. Res. Lett.* **40,** 183–188 (2013).
57. Brown, R. D. & Derksen, C. Is Eurasian October snow cover extent increasing? *Environ. Res. Lett.* **8,** 024006 (2013).
58. Ghatak, D., Frei, A., Gong, G., Stroeve, J. & Robinson, D. On the emergence of an Arctic amplification signal in terrestrial Arctic snow extent. *J. Geophys. Res.* **115,** D24105 (2010).
59. Ghatak, D. *et al.* Simulated Siberian snow cover response to observed Arctic sea ice loss, 1979–2008. *J. Geophys. Res.* **117,** D23108 (2012).
60. Budikova, D. Role of Arctic sea ice in global atmospheric circulation. *Glob. Planet. Change* **68,** 149–163 (2009).
61. Francis, J. A., Chan, W., Leathers, D. J., Miller, J. R. & Veron, D. E. Winter Northern Hemisphere weather patterns remember summer Arctic sea-ice extent. *Geophys. Res. Lett.* **36,** L07503 (2009).
62. Overland, J. E. & Wang, M. Large-scale atmospheric circulation changes are associated with the recent loss of Arctic sea ice. *Tellus A* **62,** 1–9 (2010).
63. Strong, C., Magnusdottir, G. & Stern, H. Observed feedback between winter sea ice and the North Atlantic Oscillation. *J. Clim.* **22,** 6021–6032 (2009).
64. Hopsch, S., Cohen, J. & Dethloff, K. Analysis of a link between fall Arctic sea ice concentration and atmospheric patterns in the following winter. *Tellus A* **64,** 18624 (2012).
65. Magnusdottir, G., Deser, C. & Saravanan, R. The effects of North Atlantic SST and sea-ice anomalies on the winter circulation in CCM3. Part I: Main features and storm track characteristics of the response. *J. Clim.* **17,** 857–876 (2004).
66. Deser, C., Magnusdottir, G., Saravanan, R. & Phillips, A. The effects of North Atlantic SST and sea-ice anomalies on the winter circulation in CCM3. Part II: Direct and indirect components of the response. *J. Clim.* **17,** 877–889 (2004).
67. Alexander, M. A. *et al.* The atmospheric response to realistic Arctic sea ice anomalies in an AGCM during winter. *J. Clim.* **17,** 890–905 (2004).
68. Strey, S. T., Chapman, W. L. & Walsh, J. E. The 2007 sea ice minimum: impacts on the Northern Hemisphere atmosphere in late autumn and early winter. *J. Geophys. Res.* **115,** D23103 (2010).
69. Porter, D. F., Cassano, J. J. & Serreze, M. C. Local and large-scale atmospheric responses to reduced Arctic sea ice and ocean warming in the WRF model. *J. Geophys. Res.* **117,** D11115 (2012).
70. Bluthgen, J., Gerdes, R. & Werner, M. Atmospheric response to the extreme Arctic sea ice conditions in 2007. *Geophys. Res. Lett.* **39,** L02707 (2012).
71. Orsolini, Y., Senan, R., Benestad, R. & Melsom, A. Autumn atmospheric response to the 2007 low Arctic sea ice extent in coupled ocean–atmosphere hindcasts. *Clim. Dynam.* **38,** 2437–2448 (2012).
72. Singarayer, J. S., Valdes, P. J. & Bamber, J. L. The atmospheric impact of uncertainties in recent Arctic sea-ice reconstructions. *J. Clim.* **18,** 3996–4012 (2005).
73. Screen, J. A., Deser, C., Simmonds, I. & Tomas, R. Atmospheric impacts of Arctic sea-ice loss, 1979–2009: separating forced change from atmospheric internal variability. *Clim. Dynam.* **43,** 333–344 (2013).
74. Peings, Y. & Magnusdottir, G. Response of the wintertime Northern Hemispheric atmospheric circulation to current and projected Arctic sea ice decline: a numerical study with CAM5. *J. Clim.* **27,** 244–264 (2014).
75. Tanaka, H. L. & Seki, S. Development of a three-dimensional spectral linear baroclinic model and its application to the baroclinic instability associated with positive and negative Arctic Oscillation indices. *J. Meteorol. Soc. Jpn* **91,** 193–213 (2013).
76. Francis, J. A. & Vavrus, S. J. Evidence linking Arctic amplification to extreme weather in mid-latitudes. *Geophys. Res. Lett.* **39,** L06801 (2012).
77. Petoukhov, V., Rahmstorf, S., Petri, S. & Schellnhuber, H. J. Quasiresonant amplification of planetary waves and recent Northern Hemisphere weather extremes. *Proc. Natl Acad. Sci. USA* **110,** 5336–5341 (2013).
78. Screen, J. A. & Simmonds, I. Amplified mid-latitude planetary waves favour particular regional weather extremes. *Nature Clim. Change* http://dx.doi.org/10.1038/nclimate2271 (2014).
79. Barnes, E. A. Revisiting the evidence linking Arctic amplification to extreme weather in midlatitudes. *Geophys. Res. Lett.* **40,** 1–6 (2013).
80. Allen, R. J. & Sherwood, S. C. Warming maximum in the tropical upper troposphere deduced from thermal winds. *Nature Geosci.* **1,** 399–403 (2008).
81. Screen, J. A. & Simmonds, I. Exploring links between Arctic amplification and mid-latitude weather. *Geophys. Res. Lett.* **40,** 959–964 (2013).
82. Barnes, E. A., Dunn-Sigouin, E., Masato, G. & Woollings, T. Exploring recent trends in Northern Hemisphere blocking. *Geophys. Res. Lett.* **41,** 638–644 (2014).
83. Kintisch, E. Into the maelstrom. *Science* **344,** 250–253 (2014).
84. Fletcher, C., Hardiman, S. C., Kushner, P. J. & Cohen, J. The dynamical response to snow cover perturbations in a large ensemble of atmospheric GCM integrations. *J. Clim.* **22,** 1208–1222 (2009).
85. Allen, R. J. & Zender, C. S. Forcing of the Arctic Oscillation by Eurasian snow cover. *J. Clim.* **24,** 6528–6539 (2011).
86. Cohen, J., Furtado, J. C., Jones, J., Barlow, M., Whittleston, D. & Entekhabi, D. Linking Siberian snow cover to precursors of stratospheric variability. *J. Clim.* **27,** 5422–5432 (2014).
87. Peings Y., Saint-Martin, D. & Douville, H. A numerical sensitivity study of the influence of Siberian snow on the northern annular mode. *J. Clim.* **25,** 592–607 (2012).
88. Petoukhov, V. & Semenov, V. A. A link between reduced Barents-Kara sea ice and cold winter extremes over northern continents. *J. Geophys. Res.* **115,** D21111 (2010).
89. Inoue, J., Hori, M. E. & Takaya, K. The role of Barents Sea ice in the wintertime cyclone track and emergence of a warm-Arctic cold-Siberian anomaly. *J. Clim.* **25,** 2561–2568 (2012).
90. Jaiser, R., Dethloff, K., Handorf, D., Rinke, A. & Cohen, J. Impact of sea ice cover changes on the Northern Hemisphere atmospheric winter circulation. *Tellus A* **64,** 11595 (2012).
91. Jaiser, R., Dethloff, K. & Handorf, D. Stratospheric response to Arctic sea ice retreat and associated planetary wave propagation changes. *Tellus A* **65,** 19375 (2013).
92. Honda, M., Inue, J. & Yamane, S. Influence of low Arctic sea-ice minima on anomalously cold Eurasian winters. *Geophys. Res. Lett.* **36,** L08707 (2009).
93. Hardiman, S. C., Kushner, P. J. & Cohen, J. Investigating the ability of general circulation models to capture the effects of Eurasian snow cover on winter climate. *J. Geophys. Res.* **113,** D21123 (2008).
94. Martin, S. & Diffenbaugh, N. S. Transient twenty-first century changes in daily-scale temperature extremes in the United States. *Clim. Dynam.* **42,** 1383–1404 (2014).
95. Dee, D. P. *et al.* The ERA-Interim reanalysis: configuration and performance of the data assimilation system. *Q. J. R. Meteorol. Soc.* **137,** 553–597 (2011).
96. Hansen, J. E. & Lebedeff, S. Global trends of measured surface air temperature. *J. Geophys. Res.* **92,** 13345–13372 (1987).

© 2014 Macmillan Publishers Limited. All rights reserved

97. Hoskins, B. J. & Karoly, D. J. The steady linear response of a spherical atmosphere to thermal and orographic forcing. *J. Atmos. Sci.* **38,** 1179–1196 (1981).
98. Garfinkel, C. I., Hartmann, D. L. & Sassi, F. Tropospheric precursors of anomalous Northern Hemisphere stratospheric polar cortices. *J. Clim.* **23,** 3282–3299 (2010).
99. Kolstad, E. W. & Charlton-Perez, A. J. Observed and simulated precursors of stratospheric polar vortex anomalies in the Northern Hemisphere. *Clim. Dynam.* **37,** 1443–1456 (2010).
100. Cohen, J. & Jones, J. Tropospheric precursors and stratospheric warmings. *J. Clim.* **24,** 6562–6572 (2011).

Acknowledgements

We are grateful to E. Barnes for many helpful discussions and suggested revisions to the manuscript. J.C. is supported by the National Science Foundation grants BCS-1060323 and AGS-1303647. J.S. is funded by Natural Environment Research Council grant NE/J019585/1. M.B. received support from National Science Foundation grant ARC-0909272 and NASA NNX13AN36G. J.O. receives support from the Arctic Research Project of the National Oceanic and Atmospheric Administration Climate Program Office and the Office of Naval Research, Code 322.

Author contributions

J.C. proposed and was the main author of the manuscript. All co-authors contributed to the writing of the manuscript. J.S. created Fig. 1, J.F. Figs 2 & 4, D.C. Fig. 3, J.F. and J.C. Fig. 4, M.B. and J.C. Fig. B1, and D.W. and J.C. Fig. B2.

Additional information

Supplementary information accompanies this paper on www.nature.com/ngeo.
Reprints and permissions information is available online at www.nature.com/reprints.
Correspondence and requests for materials should be addressed to J.C.

Competing financial interests

The authors declare no competing financial interests.

© 2014 Macmillan Publishers Limited. All rights reserved

nature geoscience

LETTERS

PUBLISHED ONLINE: 31 AUGUST 2015 | DOI: 10.1038/NGEO2517

Two distinct influences of Arctic warming on cold winters over North America and East Asia

Jong-Seong Kug[1], Jee-Hoon Jeong[2*], Yeon-Soo Jang[1], Baek-Min Kim[3], Chris K. Folland[4,5], Seung-Ki Min[1] and Seok-Woo Son[6]

Arctic warming has sparked a growing interest because of its possible impacts on mid-latitude climate[1–5]. A number of unusually harsh cold winters have occurred in many parts of East Asia and North America in the past few years[2,6,7], and observational and modelling studies have suggested that atmospheric variability linked to Arctic warming might have played a central role[1,3,4,8–11]. Here we identify two distinct influences of Arctic warming which may lead to cold winters over East Asia or North America, based on observational analyses and extensive climate model results. We find that severe winters across East Asia are associated with anomalous warmth in the Barents–Kara Sea region, whereas severe winters over North America are related to anomalous warmth in the East Siberian–Chukchi Sea region. Each regional warming over the Arctic Ocean is accompanied by the local development of an anomalous anticyclone and the downstream development of a mid-latitude trough. The resulting northerly flow of cold air provides favourable conditions for severe winters in East Asia or North America. These links between Arctic and mid-latitude weather are also robustly found in idealized climate model experiments and CMIP5 multi-model simulations. We suggest that our results may help improve seasonal prediction of winter weather and extreme events in these regions.

One of the clearest manifestations of recent climate change is Arctic amplification—that is, surface warming over the Arctic being faster than that at other latitudes under greenhouse warming[12]. Such amplification has accelerated in recent decades and the Arctic has warmed approximately twice as rapidly as the Northern Hemisphere (NH) as a whole[5]. This clearly indicates that the Arctic is very susceptible to climate change, a phenomenon evident in both observations and climate projections[12,13].

Although greenhouse gas concentrations have increased continuously over the past half-century, extratropical NH winter temperature trends have exhibited considerable interdecadal variation (Fig. 1), partly because of natural climate variability. For example, between 1979 and 1997, when global-mean surface air temperature (SAT) increase was fastest, the winter warming trend was clear over Europe, East Asia and the USA (Fig. 1a), whereas the Arctic exhibited little trend or even slight cooling in places. However, between 1998 and 2013, the pattern of winter SAT trends in these regions became conspicuously different from that in 1979–1997. First, Arctic surface warming has progressed rapidly since 1998 (Fig. 1b), with stronger warming trends over the Barents–Kara and East Siberian–Chukchi sea regions where marked reductions in sea-ice concentration have occurred[12]. By contrast, strong cooling trends are evident over parts of the extratropical northern continents[3,14]. In addition to these cooling trends, many parts of the northern continents have experienced frequent cold extremes, especially in recent years[2,6,7].

A key feature of Fig. 1 is the generally opposite sign of SAT trends between the Arctic and extratropics in the two epochs; in the earlier epoch the Arctic was actually cooling slightly whereas in the later epoch it was warming rapidly. Many recent studies have suggested that recent cold winters in northern continents are related to Arctic warming[5,8–11,15–18]. However, it remains debatable whether the trend to colder winters is due to Arctic amplification or internal variability[2,5,19–21] because the underlying dynamical mechanisms are not fully understood. Several studies have argued that sea-ice loss over the Barents–Kara Sea region in autumn plays a critical role in influencing atmospheric circulation in the following

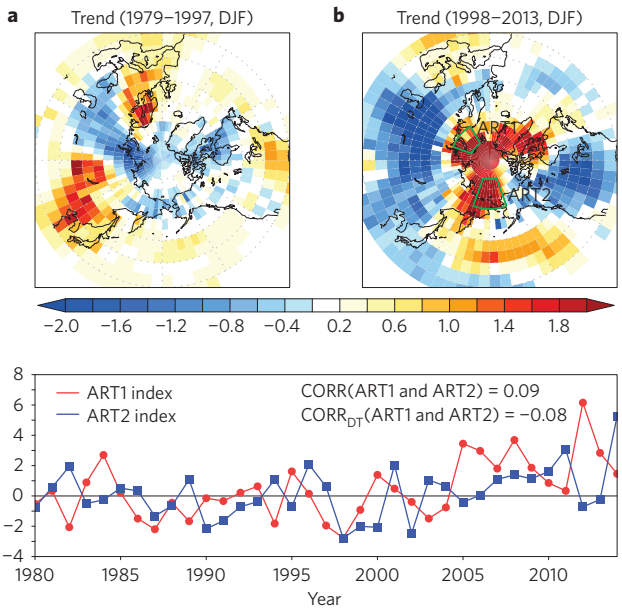

Figure 1 | SAT trends and Arctic temperature (ART) indices. a,**b**, The linear trend in surface air temperature during December–February for the periods 1979/1980–1997/1998 (**a**) and 1997/1998–2013/2014 (**b**) from the observed data[32]. Green boxes denote the region for ART indices in **b**. **c**, Time series of seasonal-mean ART1 and ART2 during December–February for the period 1979/1980–2013/2014. DT denotes the de-trended state.

[1]School of Environmental Science and Engineering, Pohang University of Science and Technology (POSTECH), 37673 Pohang, Korea. [2]Department of Oceanography, Chonnam National University, 61186 Gwangju, Korea. [3]Korea Polar Research Institute, 21990 Incheon, Korea. [4]Met Office Hadley Centre, Exeter EX1 3PB, UK. [5]Department of Earth Sciences, University of Gothenburg, 405 30 Gothenburg, Sweden. [6]School of Earth and Environmental Sciences, Seoul National University, 00826 Seoul, Korea. *e-mail: jjeehoon@jnu.ac.kr

© 2015 Macmillan Publishers Limited. All rights reserved

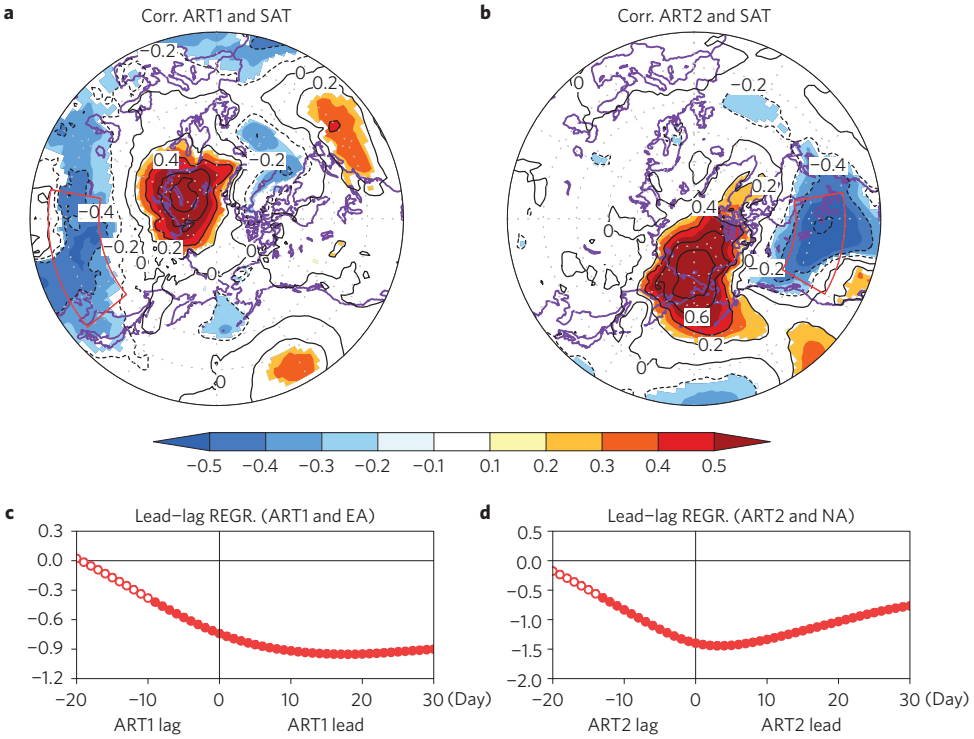

Figure 2 | Relationships between Arctic temperature and SAT over the NH extratropics. a,**b**, Correlation coefficients of SAT anomalies with respect to de-trended monthly ART1 (**a**) and ART2 indices (**b**) during December–February for the period 1979/1980–2013/2014 from the reanalysis data. Shading denotes significant values at the 95% confidence level based on a Student's *t*-test. **c**,**d**, Lead–lag regression coefficients of a moving 31-day-mean SAT over East Asia (80°–130° E, 35°–50° N) with respect to the normalized ART1 index (**c**), and over North America (80°–120° W, 40°–55° N) with respect to the normalized ART2 index (**d**). Correlation coefficients that are statistically significant at the 95% confidence level are indicated with filled circles.

winter[11,17,18,22–24]. A reduction of autumn sea ice is generally followed by warm Arctic SAT in winter (Supplementary Figs 3 and 4). This often leads to the so-called 'warm Arctic–cold continent' pattern[23] forced via stationary Rossby waves[11]. It is further suggested that more frequent and persistent episodes of atmospheric blocking occur[10,15,17], with downstream responses of enhanced cyclonic activity[9,18] and possibly weakening of the polar vortex due to an enhanced upward propagation of planetary waves[8]. Accordingly, Arctic sea-ice information may be useful for improving climate prediction in NH extratropical regions[25]. However, atmospheric responses to Arctic sea-ice variations are complex, depending on background atmospheric states and seasons[9,22], which may weaken statistical relationships with extratropical climate variations. Furthermore, it has recently been recognized that extratropical impacts depend highly on the regional structure of the anomalous Arctic climate state[16,26].

In high latitudes, surface heat flux forcing and low-level baroclinicity associated with sea-ice loss and other anomalous Arctic climate states are important for modulating the slow-varying atmospheric circulation[8,18,22]. Modelling studies showed that these sea-ice variations are related to regional SAT patterns[17,21,22] that are easy to observe and have relatively high predictability. To investigate the observed connections between Arctic warming and regional extratropical cold winters, we define two Arctic temperature (ART) indices: ART1, which averages SAT over the Barents–Kara Sea region (30°–70° E, 70°–80° N), and ART2, which averages SAT over the East Siberian–Chukchi Sea region (160° E–160° W, 65°–80° N). These two regions exhibit the strongest warming trends since 1998 (Fig. 1b), but de-trended correlations between the two indices are almost zero (Fig. 1c).

Figure 2 shows correlations between the de-trended monthly ART indices and SAT from 1979 to 2014. Both indices exhibit strong positive correlations over their own regions, but show different correlation patterns in much of the NH extratropics. For ART1, negative correlations prevail over most of Eurasia (Fig. 2a), and are particularly strong over East Asia. This indicates that when the Arctic SAT gets warmer over the Barents–Kara Sea region, East Asia experiences cold winters, consistent with previous studies[9,11,18].

On the other hand, the ART2 index is negatively correlated with SAT anomalies over North America (Fig. 2b). The negative correlation is strongest over most of Canada and the central and eastern parts of the United States. The correlation coefficient between monthly ART2 and North American SAT in the region shown in Fig. 2b is close to −0.65, suggesting that North American winter SAT anomalies are strongly negatively correlated with SAT anomalies in the East Siberian–Chukchi Sea region. These relationships are fairly robust even for long-term historical data (Supplementary Fig. 2).

Figure 2c,d shows lead–lag relationships between the ART indices and East Asian and North American SAT calculated from a moving 31-day-mean ERA-Interim data set[27]. As shown in Fig. 2c,d, ART1 tends to precede the maximum East Asian SAT response by about 15 days, and ART2 shows the strongest relationship with North America SAT, about 5 days ahead. These results imply that the atmospheric circulation anomalies associated with the continental cooling over both regions are related to the regional Arctic warming in the upstream regions, suggesting that regional patterns of Arctic warming/cooling may be crucial for understanding extratropical NH winter climate variability.

Figure 3 shows the atmospheric circulation anomalies associated with regional Arctic warming. Warm conditions over the Barents–Kara Sea region (ART1) are associated with negative sea-level pressure (SLP) anomalies over the central Arctic and strong positive anomalies over western Russia (Fig. 3a). The positive SLP anomalies over western Russia develop from the coastal regions of the Barents–Kara Sea, slightly southward of the ART1 centre, to the central Eurasian continent. Once the anomalous anticyclonic

© 2015 Macmillan Publishers Limited. All rights reserved

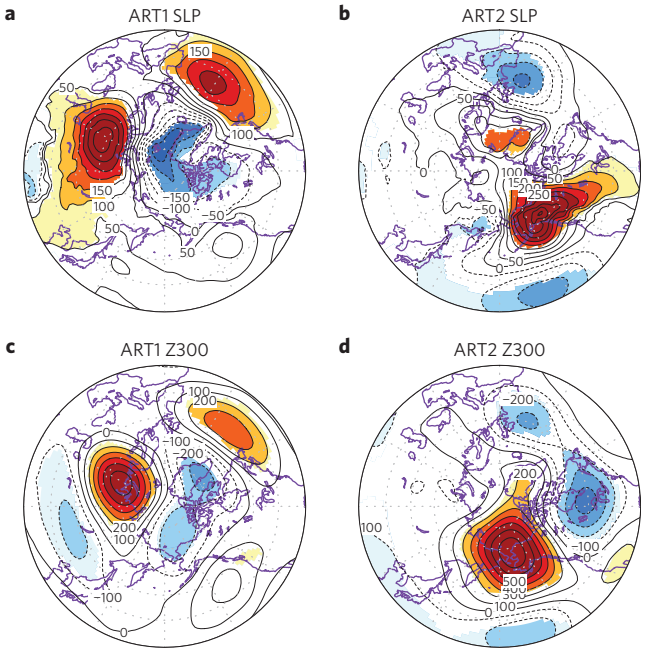

Figure 3 | Atmospheric circulation anomalies linked to Arctic temperature. Linear regression of sea-level pressure (Pa) (**a**,**b**) and 300 hPa geopotential height (m) (**c**,**d**) with respect to de-trended monthly ART1 (**a**,**c**) and ART2 indices (**b**,**d**) during December–February for the period of 1979/1980–2013/2014. Shading denotes significant values at 95% confidence level based on a Student's *t*-test.

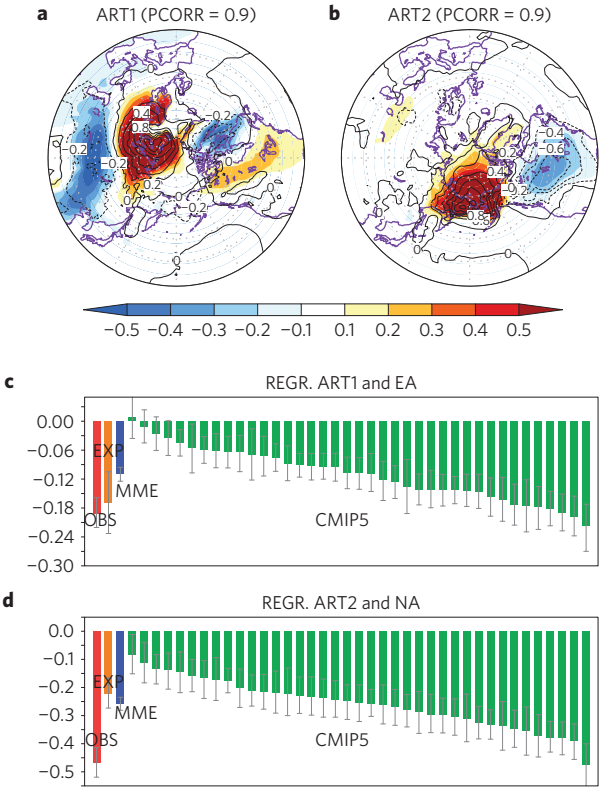

Figure 4 | Modelling support on the relationships between Arctic temperature and SAT over the NH extratropics. a,**b**, SAT anomalies regressed on de-trended monthly ART1 (**a**) and ART2 indices (**b**) during December–February for the period 1979/1980–2012/13 from observation (contour) and CM2.1 model experiments (shaded). The pattern correlation coefficients between the observation and the model experiments over 30°–90° N are denoted in the upper right side of the figure. **c**,**d**, Regression coefficients of SAT over the East Asia region on the ART1 index (**c**) and SAT over the North America region on the ART2 index (**d**) during December–February in the 39 CMIP5 simulations. Red and orange bars show the coefficients from the observation and the CM2.1 model experiments, respectively. Green bars show the coefficients from the CMIP5 models, and blue bars denote the multi-model ensemble mean. The scale bars represent a range of 95% confidence levels from internal variability using a Monte Carlo approach.

flow is established, it develops further and expands to the east owing to anomalous cold advection at the climatologically cold surface[28]. The eastward expansion of the anomalous west-Russian anticyclone is linked to an intensified Siberian High, leading to cold advection and frequent occurrence of cold events over East Asia[28,29]. It is noteworthy from Fig. 3a,c that significant positive anomalies appear over the North Atlantic, centred near 40° N, upstream of the ART1 region. Likewise, significant negative anomalies are evident over the subtropical North Pacific, upstream of the ART2 region. These statistical results suggest that regional Arctic warming and their downstream teleconnection patterns could be influenced by such upstream disturbances[30]. The role of the upstream disturbances in the Arctic-to-extratropical connections needs further study (for example, Supplementary Fig. 5).

The upper-level circulation shows that the anomalous west-Russian anticyclone is quasi-equivalent barotropic, and accompanies anomalous cyclonic flow in the downstream region of far eastern Siberia (Fig. 3c). This cyclonic anomaly can be explained by Rossby wave propagation from the upstream anticyclonic anomaly. Such an upper cyclonic anomaly implies an intensified and westward-shifted Asian trough, closely related to a stronger East Asian winter monsoon with more frequent cold extreme events[29].

Circulation patterns associated with ART2 are seemingly different from those with ART1. For example, the SLP responses over the Arctic are opposite. However, there is great dynamical similarity, particularly in the downstream regions. There is an anomalous equivalent barotropic anticyclone near the Arctic warming area and anomalous cyclonic flow in the downstream regions (Fig. 3b,d). The anomalous anticyclone implies a weakened Aleutian Low and more frequent North Pacific blocking events[31]. Associated northerly winds bring cold Arctic air into northern North America.

The above results clearly indicate that regional warming over the Arctic Ocean can affect extratropical climate in the downstream region by inducing a downstream teleconnection pattern. To substantiate the Arctic-to-extratropical connections in the observations, idealized model experiments were carried out using a coupled global climate model (GCM). In the six model experiments, sea surface temperature (SST) in the Arctic region was restored to the historical SST but the model was fully coupled with the oceans in other regions (see Methods). The sea-ice concentration simulated in the model mostly follows the observational evolution, indicating that sea ice quickly adjusts to the SST evolution.

For these model simulations, a similar correlation analysis of de-trended ART1 and ART2 with SAT is performed (Fig. 4a,b). Figure 4a shows that, for ART1, the model gives a similar pattern of negative correlation of SAT over the Eurasian continent, the negative correlation being again strong over East Asia. The pattern correlation between the observations and the model simulation is 0.90, indicating high similarity between model responses and the observations. More importantly, the model quantitatively reproduces the regression coefficient of the observations (compare red and orange bars in Fig. 4c). For ART2, the model simulation also captures the overall negative SAT correlation over northern North America well. The pattern correlation between the observation and model simulation is very high at 0.90, although regression coefficient is underestimated (Fig. 4d). In addition to the SAT pattern,

© 2015 Macmillan Publishers Limited. All rights reserved

the model also simulates the observed downstream atmospheric teleconnection patterns reasonably well (Supplementary Fig. 6). Because only the high-latitude SST is restored to the observed SST in the model experiments, these results strongly support two separate Arctic influences on NH extratropical winter climate.

These results are further supported by an extensive multi-model analysis. Simulations from 39 CMIP5 (Coupled Model Intercomparison Project phase 5) models are analysed to examine the relationships between their own de-trended monthly ART indices and East Asian and North American SAT (Fig. 4c,d and also see Supplementary Figs 7 and 8). In general, the CMIP5 models reproduce the observed circulation anomalies associated with ART indices reasonably well (Supplementary Fig. 9). It is found that 36 out of 39 models show statistically significant negative regressions between the ART1 index and East Asian SAT, supporting the idea that warming over the Barents–Kara Sea region is connected to cooling over East Asia. However, most CMIP5 models underestimate the observed regression coefficients. For ART2, all CMIP5 models show statistically significant negative regressions, although most models again show smaller regression coefficients than observations (Fig. 4d). Although the most models consistently simulate the negative regression coefficients of SAT, there is a large inter-model diversity in their magnitude.

This study shows that there are two key Arctic regions where regional warming can induce distinguishable cold winters over northern continents. Warming over the Barents–Kara Sea region is likely to lead to East Asian cooling, whereas northern North America cooling is closely related to warming over the East Siberian–Chukchi Sea region. These results suggest that the regional distribution of Arctic warming may provide additional predictability for intra-seasonal to seasonal forecasts in the NH extratropics. These results may also provide guidance for assessing the potential risk of extreme events over regions where current seasonal prediction skill is often poor. In particular, this study suggests that the recent increased frequency of severe winters over East Asia and North America may be partly caused by recent rapid Arctic warming.

Methods

Methods and any associated references are available in the online version of the paper.

Received 16 February 2015; accepted 23 July 2015; published online 31 August 2015

References

1. Francis, J. A. & Vavrus, S. J. Evidence for a wavier jet stream in response to rapid Arctic warming. *Environ. Res. Lett.* **10,** 014005 (2015).
2. Wallace, J. M., Held, I. M., Thompson, D. W., Trenberth, K. E. & Walsh, J. E. Global warming and winter weather. *Science* **343,** 729–730 (2014).
3. Outten, S. D. & Esau, I. A link between Arctic sea ice and recent cooling trends over Eurasia. *Climatic Change* **110,** 1069–1075 (2012).
4. Screen, J. A. & Simmonds, I. Amplified mid-latitude planetary waves favour particular regional weather extremes. *Nature Clim. Change* **4,** 704–709 (2014).
5. Cohen, J. *et al.* Recent Arctic amplification and extreme mid-latitude weather. *Nature Geosci.* **7,** 627–637 (2014).
6. Van Oldenborgh, G. J., Haarsma, R., De Vries, H. & Allen, M. R. Cold extremes in North America vs. mild weather in Europe: The winter of 2013–14 in the context of a warming world. *Bull. Am. Meteorol. Soc.* **96,** 707–714 (2015).
7. Wang, L. & Chen, W. The East Asian winter monsoon: Re-amplification in the mid-2000s. *Chin. Sci. Bull.* **59,** 430–436 (2014).
8. Kim, B. M. *et al.* Weakening of the stratospheric polar vortex by Arctic sea-ice loss. *Nature Commun.* **5,** 4646 (2014).
9. Tang, Q. H., Zhang, X. J., Yang, X. H. & Francis, J. A. Cold winter extremes in northern continents linked to Arctic sea ice loss. *Environ. Res. Lett.* **8,** 014036 (2013).
10. Screen, J. A. & Simmonds, I. Exploring links between Arctic amplification and mid-latitude weather. *Geophys. Res. Lett.* **40,** 959–964 (2013).
11. Honda, M., Inoue, J. & Yamane, S. Influence of low Arctic sea-ice minima on anomalously cold Eurasian winters. *Geophys. Res. Lett.* **36,** L08707 (2009).
12. Hartmann, D. L. *et al.* in *Climate Change 2013: The Physical Science Basis* (eds Stocker, T. F. *et al.*) 159–254 (IPCC, Cambridge Univ. Press, 2013).
13. Simmonds, I. Comparing and contrasting the behaviour of Arctic and Antarctic sea ice over the 35-year period 1979–2013. *Ann. Glaciol.* **56,** 18–28 (2015).
14. Cohen, J. L., Furtado, J. C., Barlow, M., Alexeev, V. A. & Cherry, J. E. Asymmetric seasonal temperature trends. *Geophys. Res. Lett.* **39,** L04705 (2012).
15. Francis, J. A. & Vavrus, S. J. Evidence linking Arctic amplification to extreme weather in mid-latitudes. *Geophys. Res. Lett.* **39,** L06801 (2012).
16. Petoukhov, V. & Semenov, V. A. A link between reduced Barents–Kara sea ice and cold winter extremes over northern continents. *J. Geophys. Res.* **115,** D21111 (2010).
17. Liu, J., Curry, J. A., Wang, H., Song, M. & Horton, R. M. Impact of declining Arctic sea ice on winter snowfall. *Proc. Natl Acad. Sci. USA* **109,** 4074–4079 (2012).
18. Inoue, J., Hori, M. E. & Takaya, K. The Role of Barents Sea ice in the wintertime cyclone track and emergence of a warm-Arctic cold-Siberian anomaly. *J. Clim.* **25,** 2561–2568 (2012).
19. Screen, J. A., Deser, C., Simmonds, I. & Tomas, R. Atmospheric impacts of Arctic sea-ice loss, 1979–2009: Separating forced change from atmospheric internal variability. *Clim. Dynam.* **43,** 333–344 (2013).
20. Fischer, E. M. & Knutti, R. Heated debate on cold weather. *Nature Clim. Change* **4,** 537–538 (2014).
21. Mori, M., Watanabe, M., Shiogama, H., Inoue, J. & Kimoto, M. Robust Arctic sea-ice influence on the frequent Eurasian cold winters in past decades. *Nature Geosci.* **7,** 869–873 (2014).
22. Deser, C., Tomas, R., Alexander, M. & Lawrence, D. The seasonal atmospheric response to projected Arctic Sea ice loss in the late twenty-first century. *J. Clim.* **23,** 333–351 (2010).
23. Overland, J. E., Wood, K. R. & Wang, M. Y. Warm Arctic-cold continents: Climate impacts of the newly open Arctic Sea. *Polar Res.* **30,** 15787 (2011).
24. Hopsch, S., Cohen, J. & Dethloff, K. Analysis of a link between fall Arctic sea ice concentration and atmospheric patterns in the following winter. *Tellus A* **64,** 18624 (2012).
25. Scaife, A. A. *et al.* Skillful long-range prediction of European and North American winters. *Geophys. Res. Lett.* **41,** 2514–2519 (2014).
26. Budikova, D. Role of Arctic sea ice in global atmospheric circulation: A review. *Glob. Planet. Change* **68,** 149–163 (2009).
27. Dee, D. P. *et al.* The ERA-Interim reanalysis: Configuration and performance of the data assimilation system. *Q. J. R. Meteorol. Soc.* **137,** 553–597 (2011).
28. Takaya, K. & Nakamura, H. Geographical dependence of upper-level blocking formation associated with intraseasonal amplification of the Siberian high. *J. Atmos. Sci.* **62,** 4441–4449 (2005).
29. Zhang, Y., Sperber, K. R. & Boyle, J. S. Climatology and interannual variation of the East Asian Winter Monsoon: Results from the 1979–95 NCEP/NCAR Reanalysis. *Mon. Weath. Rev.* **125,** 2605–2619 (1997).
30. Sato, K., Inoue, J. & Watanabe, M. Influence of the Gulf Stream on the Barents Sea ice retreat and Eurasian coldness during early winter. *Environ. Res. Lett.* **9,** 084009 (2014).
31. Renwick, J. A. & Wallace, J. M. Relationships between North Pacific wintertime blocking, El Nino, and the PNA pattern. *Mon. Weath. Rev.* **124,** 2071–2076 (1996).
32. Cowtan, K. & Way, R. G. Coverage bias in the HadCRUT4 temperature series and its impact on recent temperature trends. *Q. J. R. Meteorol. Soc.* **140,** 1935–1944 (2014).

Acknowledgements

J.-S.K. was supported by National Research Foundation (NRF-2014R1A2A2A01003827). J.-H.J. was supported by Korea Polar Research Institute project (PE15010). B.-M.K. was supported by Korea Meteorological Administration Research and Development Program (KMIPA2015-2093). C.K.F. was supported by the Joint UK DECC/Defra Met Office Hadley Centre Climate Programme (GA01101).

Author contributions

J.-S.K. and J.-H.J. designed the research, conducted analyses, and wrote the majority of the manuscript content. B.-M.K., C.K.F., S.-K.M. and S.-W.S. conducted the analysis and report-writing tasks. Y.-S.J. conducted analyses, numerical experiments and prepared figures. All the authors discussed the study results and reviewed the manuscript.

Additional information

Supplementary information is available in the online version of the paper. Reprints and permissions information is available online at www.nature.com/reprints. Correspondence and requests for materials should be addressed to J.-H.J.

Competing financial interests

The authors declare no competing financial interests.

© 2015 Macmillan Publishers Limited. All rights reserved

Methods

Data and statistics. The linear trends of SAT, as shown in Fig. 1, are calculated from interpolated median version HadCRUT4 data (http://www.metoffice.gov.uk/hadobs/hadcrut4/data/current/download.html), hybridized with the University of Alabama in Huntsville (UAH) satellite data[32] (http://www-users.york.ac.uk/~kdc3/papers/coverage2013/series.html) for the period 1979 to 2014. The monthly- and daily-mean SAT, wind, geopotential height and SLP from 1979 to 2014 are obtained from the ERA-Interim Reanalysis[27] (http://apps.ecmwf.int/datasets/data/interim_full_daily). All analyses in Figs 2–4 are conducted after removing linear trends. The significance test used in this study is based on a standard two-tailed t-test in Figs 2, 3 and Supplementary Figures, with the number of degrees of freedom estimated by calculating autocorrelations. We also use a Monte Carlo approach using a bootstrap method to estimate internal variability in Fig. 4. For each model simulation, we randomly select 100 years from the historical simulation, calculate the regression coefficient using the selected 100 years, and finally compute the distribution of the regression coefficients by repeating this process 1,000 times. For MME, 39 regression coefficients are randomly selected from the 39 models, and their average is computed. By repeating this process 1,000 times, the distribution of MME is computed.

Model experiments. The GFDL CM2.1 model is used for the idealized coupled GCM experiment, developed by the Geophysical Fluid Dynamics Laboratory. To examine the impact of Arctic warming/cooling, SST in high latitudes (north of 70° N) is restored to the historical observed SST for 1950–2013, with a five-day restoring timescale, whereas the model is fully coupled over the other regions. ERSST v3 (http://www.esrl.noaa.gov/psd/data/gridded/data.noaa.ersst.html) is used for the observed SST. A total of six ensemble simulations with different initial conditions are carried out. The initial conditions were randomly chosen from long-term climate simulations under present-day climate conditions.

Analysis of CMIP5 data. We analyse the 39 CGCM simulations from the historical runs available in the CMIP5 archives (http://cmip-pcmdi.llnl.gov/cmip5/data_portal.html), reflecting transient climate conditions which include observed atmospheric composition due to both anthropogenic and natural sources. For a fair comparison, we used only one ensemble member from each model. Model references, details of the institutions where the models were run, and integration periods are summarized in Supplementary Table 1.

Code availability. We have opted not to make the computer code associated with this paper available because all the codes are for well-known statistical calculations.

View publication stats

© 2015 Macmillan Publishers Limited. All rights reserved